Measuring Nonlinear Viscoelasticity of Cheese Using Oscillatory Shear

by

Salman Tariq

A thesis submitted in partial fulfillment of
the requirements for the degree of

Master of Science
(Mechanical Engineering)

at the

University of Wisconsin-Madison

1998

To my mother, Seema Tariq,
and
in loving memory of my father, Tariq Anwar

MEASURING NONLINEAR VISCOELASTICITY OF CHEESE USING OSCILLATORY SHEAR

Salman Tariq
Under the Supervision of Professor A. Jeffrey Giacomin
Department of Mechanical Engineering and Rheology Research Center
University of Wisconsin-Madison

ABSTRACT

Cheese viscoelasticity is commonly measured using steady uniaxial compression, steady uniaxial extension, shear and compressive creep, and stress relaxation in shear and compression. Viscoelastic properties for many cheeses have also been studied using small amplitude oscillatory shear. However, these tests measure *linear* viscoelastic properties, while several real-life cheese processes are *nonlinear*. The large deformation test usually conducted on cheese to study nonlinear viscoelasticity is uniaxial compression, but in this test the cheese hardly departs from linear behavior. Therefore, this research aimed to measure the *nonlinear* viscoelastic properties of cheese using *large amplitude* oscillatory shear. A sliding plate rheometer incorporating a shear stress transducer was used. The data were evaluated using spectral analysis and the results are presented mainly in the form of shear stress *versus* shear rate loops. Four cheese varieties were studied, and the effects of temperature, age, and fat content were evaluated. Comparisons were also made to the Lodge rubberlike liquid theory to establish the amounts of nonlinearity.

MESURE DE LA VISCOÉLASTICITÉ NON-LINÉAIRE DU FROMAGE EN CISAILLEMENT OSCILLATOIRE

Salman Tariq

Dirigé par le Professeur A. Jeffrey Giacomin

RÉSUMÉ

La viscoélasticité du fromage à l'état solide et fondu est normalement mesurée en élongation pure, soit en traction ou en compression, en utilisant une déformation à contrainte constante ou la relaxation de contrainte après un déformation subite. En cisaillement simple, les propriétés viscoélastiques de plusieurs fromages ont été étudiées en mode oscillatoire à faible amplitude. Cependant, ces mesures reflètent les propriétés viscoélastiques linéaires, tandis que, dans les procédés, le fromage subit normalement des déformations non-linéaires. L'expérience en grande déformation normalement employéer pour étudier la viscoélasticité non-linéaire du fromage est la compression pure, mais celle-ci ne provoque que de faibles écarts à son comportement linéaire. Par conséquence, ce travail vise à mesurer les propriétés viscoélastiques non-linéaires du fromage en utilisant le cisaillement oscillatoire à large amplitude. Nous avons employé un rhéomètre à plaques parallèles, incorporant une sonde de contrainte de cisaillement. Les mesures ont été évaluées avec une analyse spectrale et les résultats sont présentés principalement sous forme de boucles de contrainte de cisaillement en fonction du taux de cisaillement. Quatre fromages ont été étudiés, et les effets de la température, de l'âge, et de la teneur en gras ont été évalués. Des comparaisons ont aussi été faites avec la loi de Lodge pour établir l'importance de la non-linéarité.

PANEER KI LAYAAB - DAR KHICHAYI KA ANDAZA THAR-THARANE WALEY CHAKU KE ISTAMAL SEY

Salman Tariq

Zaire Nigrani Professor A. Jeffrey Giacomin

KHALASA

Paneer ki iyaab – dar khichayi aam taur par yak tarfa dabaoo, yak tarfa khichayo yah garmai ke assar key phailaoo sey napa jata hai. Bahot kissam ke paneer ki layaab – dar khichayi aam taur par harkat karney waley chaku say napi jati hai. Tahaam yeh tarika seraf *linear* layaab – dari ka khichayo napnee main madad deita hai, jabkey bahot sarey aam kessam key paneer lambaee key khichayo main nahi attey. Bareey shakal badal ney wale tajarbey jo paneer par kiyay jatey hain, voou yak tarfa dabao sey phailaoo ko naptey hain, laiken yeh tajarbey bhi lambai waley khichao sey zeadah mukhta lif nahee. Lehaza ish tajarbay ka maqsad paneer ke mukhtalif phailao (*nonlinear*) ko napnee key liyay lambey harkat karne waley, thar tharane chaku ke istamal sey hai. Ish key liye layaab – dar mada napne wali *sliding plate* key sath dabao dalney wala *shear stress transducer* istamal kiya qaya hai. Natijah zahir honey waley addad-o-shumar sey akhaz kiya gaya hai, khas taur par dabao bil – muqabalah *shear rate loops*. Yeh tajarba char mukhtalif keesam key paneer par kiya gaya hai, un par hararat ka assar, omar, aur chiknai ki miqdar ka andaza lagaya gaya hai. Ish tajarba ka muqabalah *Lodge rubberlike liquid theory* sey bhi kiya gaya hai takey *nonlinearity* ka andaza lagaya ja sakey.

ACKNOWLEDGMENT

I would like to acknowledge Professor Giacomin for his guidance and encouragement throughout my graduate years. His knowledge and advice were indispensable, and have contributed significantly to my development both as an engineer and a researcher.

I would like to thank Seon-Keat Lan for his help with the sliding plate rheometer. Things would have been so much more difficult without him around. Also, I am ever so grateful to Won Yoon for his help with the dynamic tests. We all know how tight and precious his schedule is. The help of Ya-Chun Wang with the samples and cheese literature is also greatly appreciated. I would also like to acknowledge Professors Sundaram Gunasekaran and Norman F. Olson for their suggestions and interest in this research, and Professor Bruno Vergnes of Ecole des Mines de Paris for proofing the French abstract.

Most importantly, I would like to thank my mother and sister for their support and encouragement throughout my college years; and special thanks to Attiya, my wife and best friend, whose “A kobokos” and “Fajr wake-up calls” played a vital role in the successful completion of this research.

My sincere thanks to all my friends at the Islamic Center, who made my stay in Madison so wonderful. I’ll miss you.

Special recognition goes to the Rheology Research Center for providing the weekly seminar series. It was an honor to be part of such a distinguished group.

Finally, I would like to thank the Wisconsin Center for Dairy Research and the Biological Systems Engineering Department for funding this research.

TABLE TITLES

FIGURE CAPTIONS

NOMENCLATURE

A	AREA
$B_{ij}(t,t')$	FINGER TENSOR
D	DIAMETER
De	DEBORAH NUMBER
$E(t)$	STRESS RELAXATION MODULUS
F	APPLIED FORCE
f	FREQUENCY, HZ
f_o	FUNDAMENTAL (TEST) FREQUENCY, HZ
$G(t)$	SHEAR RELAXATION MODULUS
$G'(\omega)$	STORAGE MODULUS
$G''(\omega)$	LOSS MODULUS
$G^*(\omega)$	COMPLEX MODULUS
G_d	DYNAMIC MODULUS
G_i	DISCRETE RELAXATION MODULUS
G_o	INITIAL SHEAR MODULUS
h	SAMPLE THICKNESS
$J(t)$	CREEP COMPLIANCE
j	$\sqrt{-1}$
K_e	ELASTIC CONSTANT
K_v	VISCOUS CONSTANT
L	LENGTH
$m(t-t')$	MEMORY FUNCTION
N_1	FIRST NORMAL STRESS DIFFERENCE
N_2	SECOND NORMAL STRESS DIFFERENCE
n	ANY INTEGER

R	RADIUS
s	$t - t'$
t	TIME/ CURRENT TIME
t'	PAST TIME
t_{proc}	PROCESS TIME
V	PLATE VELOCITY
We	WEISSENBERG NUMBER
X	DISPLACEMENT
X_o	DISPLACEMENT AMPLITUDE
δ	MECHANICAL LOSS ANGLE (OR PHASE ANGLE)
δ_m	PHASE ANGLE OF m^{th} STRESS HARMONIC
δ_γ	PHASE ANGLE OF SHEAR STRAIN
$\delta\gamma(t_i)$	SHEAR STEP-STRAIN AT TIME t_i
η	VISCOSITY
γ	SHEAR STRAIN
γ_o	SHEAR STRAIN AMPLITUDE
$\dot{\gamma}$	SHEAR RATE
$\dot{\gamma}_o$	SHEAR RATE AMPLITUDE
λ	CHARACTERISTIC (OR RELAXATION) TIME
ω	ANGULAR FREQUENCY
σ	STRESS
τ	SHEAR STRESS
τ_m	AMPLITUDE OF m^{th} SHEAR STRESS HARMONIC
τ_o	SHEAR STRESS AMPLITUDE
Ω	ANGULAR VELOCITY
$\Psi_1(\dot{\gamma})$	FIRST NORMAL STRESS COEFFICIENT
$\Psi_2(\dot{\gamma})$	SECOND NORMAL STRESS COEFFICIENT

CONTENTS

CHAPTER 1 Introduction

The rheological properties of dairy products have been studied for over half a century. Cheese is the most diverse group of dairy products, and is considered to be the most academically interesting and challenging. Unlike many dairy products which are biologically, biochemically, and chemically stable, cheeses are biologically and biochemically dynamic, and consequently, inherently *unstable* (Fox, 1993). The process of cheesemaking is fascinating, both in itself and to rheologists, considering that a nearly Newtonian raw material (milk) produces such a diversity of mostly *viscoelastic* products. Up to 2000 cheese varieties have been developed, of which 700 have been described, with no two alike (Holsinger *et al.*, 1995; Olson, 1995). Therefore, the rheology of each cheese variety is unique.

1.1 Reasons for Investigation

The most common fundamental rheological tests used in the study of cheese viscoelasticity are: steady uniaxial compression, steady uniaxial extension, shear and compressive creep, and stress relaxation in shear and compression. Viscoelastic properties for many cheeses have also been studied using *small amplitude oscillatory shear*. However, these tests measure *linear* viscoelastic properties, while several real-life cheese processes are *nonlinear*. For example, mastication and swallowing are only accomplished with large deformations, necessitating nonlinear testing. The large deformation test usually conducted on cheese to study nonlinear viscoelasticity is uniaxial compression, but in this test the cheese

hardly departs from linear behavior (Olson, 1997). The theoretical complexity associated with nonlinear viscoelasticity also challenges rheologists.

Therefore, the goal of this research project was to measure the *nonlinear* viscoelastic properties of cheese using *large amplitude oscillatory shear* (LAOS). In LAOS, the strain magnitude, time scale, and temperature can be varied independently, allowing a wide range of test conditions. This provides a good approach to studying the melt and flow properties of cheese in a way relevant to real-life processes. The results from LAOS are best evaluated with spectral analysis. The stress wave generated can be represented by a Fourier series and summarized by the amplitudes and phase angles of the Fourier components. A discrete Fourier transform (DFT) of LAOS data determines the amplitudes and phase angles, which are then used to characterize the cheese at the given test conditions. Results from LAOS are best presented as stress *versus* shear rate loops, and an amplitude spectrum showing the different harmonics provides an excellent means of comparing cheese rheologies.

The *sliding plate rheometer* developed by Giacomin *et al.* (1989) was used for the tests. Unlike classical shear rheometers, such as rotational rheometers, the sliding plate rheometer generates a homogeneous flow field except near the sample edges. The shear stress is measured locally, using a *shear stress transducer*, in the area of uniform deformation away from the free boundaries. This eliminates error due to flow heterogeneity near the sample edges, a problem primarily associated with rotational rheometers.

Four cheese varieties were studied: 1) natural mozzarella, 2) natural pizza cheese, 3) natural cheddar, and 4) process mozzarella. The effects of temperature, age, and fat content

were evaluated, and comparisons were made to the Lodge rubberlike liquid theory to establish the amount of nonlinearity.

1.2 Why Cheese Rheology Matters

Rheological measurements on cheese using mechanical instruments are performed (1) for quality control by cheese makers and (2) for scientists to study cheese texture (Tunick and Nolan, 1992). The textural properties of cheese can be as important as flavor, and comprise a significant part of the total sensory score awarded by cheese graders (Farkye and Fox, 1990). For example, texture is a major determinant of quality in cheddar (Ma *et al.*, 1996), followed by flavor and appearance. Therefore, an objective instrumental method of measuring cheese rheological properties would be valuable, especially when used in conjunction with cheese chemical properties. For example, the effects of pH on cheese during manufacturing and maturation are well recognized, and the most demonstrable effect of pH is to impart brittleness when pH falls below 5 in hard cheeses (Olson *et al.*, 1996). Attributes such as softness and meltability of most cheeses are also affected by pH. The amounts of fat, moisture, protein, and salt in cheese also affect texture, resulting in profound differences between cheese types (Olson *et al.*, 1996; Tunick and Nolan, 1992). Therefore, research into the origins of cheese texture is an important dairy science. The ultimate goal of cheese rheologists is to correlate the results of various instrumental tests to each other and to subjective evaluations by sensory panels and consumers (Tunick and Nolan, 1992).

1.3 Cheesemaking

Cheesemaking is thousands of years old. By modern industrial standards, cheesemaking is complicated, combining art and science (Cheese Links). The primary stages of cheesemaking are shown in Fig. 1. Milk is the main ingredient, and milks from different species of mammals can be used, such as cow, goat, sheep, and buffalo. This leads to variations in cheese quality. For example, milk containing high total solids (sheep milk) increases cheese yields, whereas milk high in fat (buffalo milk) produces softer cheeses, and improves the mouth-feel. Therefore, cheesemaking must accommodate the milk type.

Cheesemaking capitalizes on milk curdling (Cheese Links). The milk must not contain antibiotics or agents that could harm the process; therefore, it is first pasteurized (heated) at a given temperature for a short period to destroy harmful bacteria. Next, special starter cultures are added to the warm milk. These cultures convert small amounts of milk sugar into lactic acid, and this acidifies the milk more rapidly. Rennet (mainly chymosin) is then added and, shortly, a curd is produced. This curd is then cut into small cubes, and heated to start a shrinking process, which, with the steady production of lactic acid from the starter cultures, converts the curd to small rice-sized grains. At a carefully chosen point, the curd grains are allowed to fall to the bottom of the cheese vat, through the remaining liquid (now called whey) consisting of water, milk sugar, and albumen. The whey is then drained and the curd grains mat to form large slabs of curd.

The slabs are then milled, and salt is added to flavor and preserve the cheese. Later, the cheese is pressed, and then packed in containers (or vacuum packed in oxygen and water impermeable plastic bags) for maturation. This is the basic method for making what are

called hard-pressed cheeses. The manufacturing processes for specific cheese varieties will differ depending on the cheese type. For example, in the manufacture of mozzarella, the fresh curd goes through a special plasticizing and kneading process in hot water that is typical of the pasta filata family of cheeses.

1.4 Mozzarella, Pizza Cheese, and Cheddar

Mozzarella and Pizza Cheese

Mozzarella is a prominent member of the pasta filata, or stretched curd, cheese varieties that originated in Italy. It is a soft, white curd cheese often melted in cookery. *Mozzarella* is the Italian dimunitive of *mozza*, meaning to slice, as in "sliced cheese," and from *mozzare*, to cut off; or perhaps from Latin *mutilare*, meaning to mutilate, or from *mutilus*, to cut short. Pasta filata cheeses are distinguished by their characteristic fibrous structure and melting and stretching properties. This unique fibrous structure is obtained by mixing and molding the cheese curd in hot water at a pH of approximately 5.2 using open discharge single screw extrusion. Mozzarella is primarily used as an ingredient in prepared foods such as pizza and lasagna. This requires it to have good shredding, stringing, and melting properties, the correct chewing characteristics, and good browning properties when grilled (Kindstedt, 1991).

In the United States, mozzarella is categorized four ways based on moisture and fat contents (Kindstedt, 1993). Whole milk and part-skim mozzarella are high in water and rarely used in pizzas due to their poor shredding and clumping properties and limited shelf life. In contrast, low-moisture and low-moisture part-skim mozzarella have firmer body,

good shredding properties, and longer shelf life. Thus, they are primarily used on pizza, lasagna, or other foods where mozzarella is grilled.

Pizza cheese is *unstretched* mozzarella. During manufacture, instead of processing the curd in hot water by the usual mixing and molding, the curd is steamed to a semi-plastic state and then pressed into blocks to produce what is called pizza cheese (Kindstedt, 1993). While mozzarella has a well defined fiber orientation, pizza cheese is isotropic.

Cheddar

Cheddar is one of the most popular cheese varieties, with most of its production concentrated in the former British colonies (Olson, 1995). It is used in several food products, such as burgers and sandwiches. During cheddar manufacture, the curd handling after whey drainage is unique. In traditional manufacturing, the curd particles are allowed to fuse into a contiguous mass as the whey is drained. The mass of fused curd is then cut into smaller blocks which are turned and piled manually (cheddaring). The blocks are then cut into smaller pieces (milling), and salt is added, followed by pressing, packaging, and ripening (Olson, 1995; Lawrence *et al.*, 1993).

Current manufacturing processes for cheddar are highly mechanized. Mechanized equipment is used to drain the whey, fuse the curd, convey the curd during cheddaring, apply salt, fuse the salted curd in towers, remove blocks of fused cheese, and package the cheese. In the United States, a system called stirred-curd cheddar is now popular (Olson, 1995). This procedure is more efficient and less capital intensive. It resembles the traditional method,

except that the pieces of curd are stirred mechanically and prevented from fusing during whey drainage. The fused blocks of cheese are then subjected to vacuum to eliminate voids.

1.5 Process Cheese Products

Process cheese products are considered a major alternative to natural cheeses produced directly from milk. They are produced by blending shredded natural cheeses differing in type and degree of maturity with emulsifying agents (primarily phosphates and citrates), and by heating the blend under partial vacuum with constant agitation until homogeneous (Caric and Kalab, 1993). Heat treatment destroys dangerous microorganisms and destroys any phosphates in cheese made from unpasteurized milk. It also arrests curing and acts as a preservative (Zehren and Nusbaum, 1992).

Hence, a diversity of process cheese products can be made to satisfy consumer and food ingredient demands. These can range from those that closely simulate moisture and fat contents of natural cheeses to products that contain virtually no fat, higher moisture contents, and added ingredients to impart desired functionalities (Olson, 1995). The first step in processing cheese is the selection of a blend of natural cheeses to obtain the desired composition, flavor, and physical properties. This is followed by adding emulsifying salts to disperse and hydrate cheese proteins. Other ingredients such as milk solids, gums, sweetening agents, mold inhibitors, and selected foods such as vegetables and meats might also be added to certain process cheese products (Olson, 1995). Process cheese products are popular because of their uniform properties and their stability achieved by heat treatment.

CHAPTER 2 Literature on Cheese Rheology

Several tests have been developed to measure cheese consistency. Textural properties such as firmness (hardness), meltability, stretchability, springiness, adhesiveness, cohesiveness, chewiness, sliceability, and fracturability have been measured using empirical or semi-empirical methods (Olson *et al.*, 1996; Steffe, 1996). However, most such tests cannot provide fundamental rheological parameters (Rao, 1992). Also, most of the *viscoelastic* properties measured are in the linear viscoelastic range, while many real-life processes involving cheese are nonlinear. This has been due to instrument limitations and to the theoretical complexity of nonlinear viscoelasticity (Steffe, 1996; Dealy and Wissbrun, 1990). Therefore, research is needed in the nonlinear viscoelasticity of cheese.

2.1 History of Rheological Measurements on Cheese

Food texture measurements are classified as (Scott Blair, 1958): empirical, imitative, or fundamental. Empirical tests measure parameters that experience indicates are related to texture (Tunick and Nolan, 1992). The first rheological measurements of cheese were empirical: the cheese graders would press into the cheese surface with their thumbs to judge firmness and elasticity. Gradually, simple instruments followed such as the ball compressor and the penetrometer. The former presses a hemisphere into the cheese surface, and measures the resulting compression depth and its recovery with time. The latter measures force as a needle is pushed into the cheese. Other tests include the resistance to a wire cutting through a cheese block, the penetration rate of a standard borer under a standard load, and the

indentation rate caused by an increasing load on a sphere (Scott Blair and Baron, 1949). However, the main drawback of all these methods is that several measurements must be taken over the sample surface to get an accurate average. Also, these instruments are not always useful for rigorous theoretical studies due to arbitrary test conditions (Tunick and Nolan, 1992).

Imitative tests help us correlate sensory perception with test procedures that mimic cheese use. For instance, in the Schreiber test for meltability, a cheese disk is placed on a flat surface in an oven at 292^{o}C for five minutes and its spread is measured (Olson *et al.*, 1996). This mimics cheese baking in pizza or lasagna. In the 1930's, the first instrument to study texture by imitating human chewing was developed. A wedge, imitating teeth on the upper jaw, was brought down toward a second wedge, thereby exerting a biting and squeezing action on the cheese (Volodkevich, 1938; Tunick and Nolan, 1992). This was followed by the MIT denture tenderometer in the mid 1950's and the more advanced General Foods texturometer in the early 1960's. The latter compresses a bite size-sized sample to 25% of its original height, releases, and repeats, thus imitating jaw motion. Its strain gauges and a strip chart produce a force-time curve from which a texture profile analysis (TPA) can be derived (Tunick and Nolan, 1992) (see Section 2.3 for more on TPA). Later, Bourne (1968 and 1978) adapted the Instron Universal Testing Machine for TPA studies. Despite duplicating real-life cheese processes, imitative tests cannot yield material properties (Olson *et al.*, 1996).

Fundamental tests measure rheological properties such as dynamic moduli which can be related to basic rheological models. In these tests, the sample shape and size and the nature of the deformation are controlled. The earliest fundamental tests on cheese were

performed in the late 1930's, in which cylinders of cheese were compressed uniaxially under constant load (Davis, 1937). These tests are the forerunners of recent serious cheese rheology research. Scott Blair and coworkers also conducted fundamental work on cheese, emphasizing viscoelastic properties, which led to an increase in applications of rheological theory to cheese analysis (Bagley and Christianson, 1987; Tunick and Nolan, 1992). However, the main drawback with fundamental tests is that they primarily measure linear viscoelastic properties, while many real-life cheese processes are nonlinear. The usual large deformation test conducted on cheese to measure nonlinear viscoelastic properties is uniaxial compression, but in this test the cheese hardly departs from linear behavior (Olson, 1997). Hence, improved methods of studying nonlinear viscoelasticity are needed.

2.2 Fundamental Tests

This section describes fundamental experiments for measuring certain rheological properties of cheese. As mentioned earlier, most of these tests do not provide much information regarding nonlinear behavior.

2.2.1 Uniaxial Compression and Extension

For solid cheeses, uniaxial compression is a useful test that provides many important mechanical properties. This test is usually performed using an Instron-type testing machine. Cheese samples of a defined size, shape, and temperature are compressed uniaxially between parallel plates to produce stress-strain curves. The local maximum stress is then correlated with firmness or hardness, and this is the most useful information obtained from such a test

with respect to consumer and sensory perception (Lee *et al.*, 1978; Olson *et al.*, 1996). However, this definition of firmness is controversial because different cheeses could reach the same local maximum through different paths; in some cases, the local maximum is hard to identify or depends on the strain rate (Olson *et al.*, 1996). The slope of the stress-strain curve gives the stiffness (or modulus), another useful property, but again, different values can be obtained due to nonlinearity. Thus, uniaxial compression data should be studied cautiously. Friction at the plate-sample interface can also significantly affect the results of a compression test. To minimize frictional effects, the specimen must be either firmly bonded to the contact surfaces or sufficiently lubricated (Casiraghi *et al.*, 1985).

For melted cheeses, a tensile test such as uniaxial extension can be used to measure elongational properties such as stretchability and springiness. Ak (1993) used the Instron testing machine to study mozzarella in tension. Barbell-shaped samples were immersed horizontally in mineral or corn oil to avoid sagging and drying, and the tests were conducted at several temperatures to measure stretchability (fracture strain) and springiness (strain recovery of a portion of stretched sample). In another tensile test, a barbell-shaped cheese sample is suspended vertically in a hot oil bath. As the sample is heated, it sags under its weight or added weights, and the stretching rate and force response are recorded to calculate its elongational viscosity (Olson *et al.*, 1996).

2.2.2 Creep and Stress Relaxation

Transient tests are used to study *creep* and *stress relaxation*. In creep, a constant stress (τ) is applied instantaneously at time zero and the resulting deformation response is

measured versus time, $\gamma(t)$. The data are usually presented as creep compliances, $J(t) = \gamma(t)/\tau$, and the corresponding plot is called a creep curve. When the force is removed, the strain decreases, producing recovery called recoil.

In a stress relaxation test, a constant, instantaneous strain (γ_o) is applied at time zero and the changing *stress* is measured versus time, $\tau(t)$. The results are usually presented as stress relaxation moduli, $E(t) = \gamma_o / \tau(t)$ (see also Section 3.4.1). The creep compliance and relaxation moduli are related by $E(t)J(t) \leq 1$, and for a perfectly elastic solid, $E(t)J(t) = 1$ (Olson *et al.*, 1996).

Mechanical models using springs and dashpots can describe material behavior in creep and stress relaxation. For example, Chang *et al.* (1986) used a four-element model to adequately represent cheese behavior in creep. Also, in linear viscoelasticity, knowing one transient function, either $E(t)$, $J(t)$ or $G'(\omega)$, $G''(\omega)$, over wide enough ranges of time or frequency enables calculation of the others (Olson *et al.*, 1996). This is detailed in Chapter 3 under Linear Viscoelasticity. Ak (1993) calculated $G'(\omega)$ for mozzarella using relaxation data and found good agreement with relaxation measurements.

2.2.3 Steady Simple Shear

A rotational or sliding plate rheometer can be used for *steady simple shear* tests on cheese. *Simple shear* is the flow generated between two parallel plates with a constant gap. More on this type of flow can be found in Chapter 3 (Section 3.1). *Steady simple shear* is simple shear carried out at a constant shear rate long enough for the stresses to become steady. Thus, transient stresses disappear during steady shear and the steady stresses will

depend only on shear rate, $\dot{\gamma}$. A shear rate dependent viscosity function can be defined by analogy with the Newtonian viscosity, $\eta(\dot{\gamma}) = \tau_{xy} / \dot{\gamma}$; and two new functions, the first and second normal stress *coefficients*, are defined by: $\Psi_1(\dot{\gamma}) \equiv N_1 / \dot{\gamma}^2$ and $\Psi_2(\dot{\gamma}) \equiv N_2 / \dot{\gamma}^2$; where N_1 and N_2 are the first and second normal stress *differences* (Dealy and Wissbrun, 1990). Together, these three functions completely describe the stress in steady simple shear and are called the viscometric functions. Special instrumentation must be used to measure N_1 and N_2, while the viscosity function $\eta(\dot{\gamma})$ is determined directly from the steady simple shear measurements.

In a rotational rheometer, the fixture holding the cheese may be two parallel disks (Fig. 13), a cone and plate, or two concentric cylinders (Tunick and Nolan, 1992). One part of the fixture is fixed, while the other (the lower plate, the cone, or a cylinder) rotates at a constant angular velocity. In a sliding plate rheometer, the sample is between two rectangular plates. One plate is fixed while the other moves at a constant velocity parallel to the fixed plate (Giacomin, 1987). In both instruments, the specimen resistance to steady shear is measured with transducers. Parallel disk and sliding plate geometries allow samples of different thicknesses to be tested, and are also useful for studying slip. Cone and plate fixtures provide a constant shear rate throughout the sample. Concentric cylinders are best used for low viscosity materials, such as cheese spreads (Tunick and Nolan, 1992).

2.2.4 Dynamic Testing

Dynamic tests are usually performed using a parallel disk rotational rheometer (see Section 4.2), but a sliding plate rheometer can also be used. The physical configuration of

these rheometers was described in Section 2.2.3. In dynamic testing, the moving plate oscillates imparting a *sinusoidal* strain. These tests are usually conducted at small strains within the material's linear viscoelastic range; thus, they are called *small amplitude oscillatory shear* (SAOS) tests. In SAOS, the shear stress is also sinusoidal but leads the strain by a phase angle δ, called the mechanical loss angle. The theory behind SAOS is detailed in Chapter 3 under Linear Viscoelasticity.

Dynamic testing of cheese, however, has several limitations (Olson *et al.*, 1996). Since cheese is neither homogeneous nor isotropic, it is hard to get samples representative of the whole cheese. Also, it is hard to get a sample with the desired geometry such as discs with flat edges. Sample slip at the interfaces becomes a problem at high temperatures, which can lead to errors.

In dynamic testing, the viscoelastic properties measured are the dynamic moduli, G', G'' and $\tan\delta$, where δ is the mechanical loss angle. G' reflects the energy stored and subsequently released, G'' the energy dissipated per cycle of deformation, and $\tan\delta$ of the dynamic character of the protein-protein bonds in a gel network (Olson *et al.*, 1996). These properties, over ranges of strain amplitudes (strain sweeps) and frequencies (frequency sweeps) provide information regarding the robustness of the network (Olson *et al.*, 1996). These properties have been reported for many cheeses at many temperatures. In general, the moduli decrease with the moisture-in-nonfat-portion and with temperature, G'' increases with fat content, and G' decreases with age due to proteolysis in mozzarella (Olson *et al.*, 1996). Ma *et al.* (1996) studied the effects of lecithin on G' and G'' for reduced-fat and full-fat cheddars, and reported that the moduli of reduced-fat cheddar with lecithin exceed those

of reduced-fat cheddar without; but the moduli of reduced-fat cheddar with lecithin fall below those of full-fat cheddar.

2.3 Texture Profile Analysis

Texture is the human sensation of food derived from its rheological behavior during mastication and swallowing (Steffe, 1996). However, it is hard to get a quantitative description of texture because no equipment can duplicate human capabilities. The mouth is complicated as it crushes, wets, enzymatically degrades, pressurizes, heats or cools, pumps, chemically samples for taste, and senses force and temperature (Steffe, 1996). Therefore, it is almost impossible to develop an instrument that incorporates all these attributes. This explains the slow progress in correlating fundamental rheological properties to the human perception of texture.

Overall, there are two methods to evaluate food texture (Steffe, 1996) (1) sensory and (2) instrumental. The sensory method uses human taste panels to develop texture profiles. This is obviously the ultimate test, but as mentioned earlier, cannot be completely duplicated by any instrumental procedure. Instrumental methods on the other hand are much less time consuming and less costly than sensory tests. They correlate certain critical sensory attributes, such as hardness and chewiness, which helps predict consumer preferences. Results from these instruments can then be combined with sensory panels. The process of generating and interpreting texture profile information, with instrumental or sensory means, is called texture profile analysis (TPA). The General Foods Texturometer was the first

instrument to produce texture profiles for foods, and this technique was later extended to the Instron Universal Testing Machine (Bourne, 1968).

In the General Foods Texturometer, a plunger descends onto a sample on a flat plate (or a shallow dish if the sample is a liquid). The plunger decelerates as it compresses, stops, and then accelerates upwards. This produces a sinusoidal deformation which closely approximates the action of the human jaw (Tunick and Nolan, 1992). A force-time curve is produced. In the Instron machine, a crosshead descends, causing a flat plate to compress cheese on the lower plate. The Instron ends its compression stroke at full speed, stops abruptly, and then rises at full speed, producing sharper peaks than the Texturometer (Tunick and Nolan, 1992). Both force-time and force-distance curves are produced. The work done is then calculated from the force-distance integral.

Various textural parameters can be determined from the force-time curve. The description of some texture related terms, some of which were also mentioned previously, follow (Szczesniak, 1983; Ak, 1993):

Hardness: the force to attain a given deformation.

Cohesiveness: the strength of the internal bonds making up the body of the product.

Textural Viscosity: the flow rate per unit force.

Springiness (Elasticity): the rate at which a deformed material returns toward its undeformed condition after the deforming force is removed.

Fracturability (Brittleness): the force at which the material fractures.

Chewiness: the energy required to masticate a solid food product to a steady state ready for swallowing.

Gumminess: the energy required to disintegrate a semisolid food to a state ready for swallowing.

Chen *et al.* (1979) ran TPA on eleven cheeses, and concluded that the protein content dominates hardness. Lee *et al.* (1978) used the correlation between a sensory panel and measurements by the Instron machine to determine important textural characteristics of several cheeses. They found that hardness, springiness, and adhesiveness correlated well with the instrumental results, and concluded that hardness was most important.

2.4 Use of the Weissenberg Effect

An important manifestation of viscoelasticity is the tendency of a viscoelastic fluid to climb a rotating rod. This fascinating phenomenon is associated with the normal stress differences and is called the Weissenberg effect. A fluid climbing a rod has flow lines circling the rod. When the rod rotates, shearing occurs across these lines producing forces both perpendicular and parallel to the rod, caused by the normal stress differences (Weissenberg, 1947). These forces create pressure differences across flow lines due to the elasticity of the fluid trying to recoil. The more elastic the material, the higher it climbs. This technique has been used to evaluate the viscoelasticity of foods such as “string” honey, aged sweet condensed milk, cake batter, wheat flour dough, and malt extract (Nelson *et al.*, 1983).

Nelson *et al.* (1983) evaluated the viscoelasticity of molten mozzarella by applying the Weissenberg effect. They used an electronically controlled rotating rod in a container of molten cheese. A traveling microscope was employed, and the cheese was evaluated on the

basis of (1) climb height, (2) fracture time, (3) place of fracture, and (4) texture as it climbed the rod. The tests were conducted on natural mozzarella and three mozzarella substitutes. These samples were also evaluated for the sensory properties of meltability, stringiness, and eating texture on cheese pizzas for correlation with the four criteria. One of the problems encountered was the release of excessive free oil from the cheese upon melting, causing slip at the rod, container, and sample interfaces. To overcome this, filter paper was taped to the rod and container surfaces to absorb the free oil.

The most meaningful criterion, climb height, indicated cheese *elasticity*. The higher it climbed, the more elastic the cheese. The second criterion, fracture time, also reflected cheese elasticity. Samples with short fracture times were called tough or rubbery; intermediate fracture times were considered desirable with the cheese having good stringing properties and slightly chewy texture; and long fracture times reflected low elasticity and the texture was described as soft and tender. The third criterion, place of fracture, provided similar information as the previous criteria. Different fracture points were related to cheese elasticity and correlated with toughness, stringiness, and softness. The fourth criterion, cheese texture as it climbed the rod, indicated cheese meltability. A smooth texture indicated that the cheese had good melting and stringing properties, while a rough texture indicated poor meltability with the cheese having a rough, rubbery texture.

Nelson *et al.* (1983) concluded that the Weissenberg test adequately measured elasticity of melted and imitation mozzarella cheeses. Besides measuring elasticity, they found that the test also gave a general evaluation of the meltability and texture of cheese when eaten on pizzas. They found good correlation of the four test criteria with the sensory

evaluation of cheese pizzas. However, as mentioned earlier, this technique did not provide fundamental rheological parameters and did not measure true material properties. Thus, its use has been limited and it does not hold much promise.

CHAPTER 3 Oscillatory Shear

Oscillatory shear is a *simple shear* test widely used in the measurement of viscoelastic properties of polymeric materials. It is useful, since it allows the strain amplitude and frequency to be varied independently, allowing a wide range of test conditions to be attained. *Linear* viscoelastic properties are typically measured using *small amplitude* oscillatory shear (SAOS) by tests commonly called dynamic tests. *Nonlinear* viscoelastic properties can be measured using *large amplitude* oscillatory shear (LAOS). Since oscillatory shear does not involve sudden jumps in speed or position, it is a relatively easy flow to generate, and error analysis for this strain history is straightforward (Giacomin and Dealy, 1993).

There is a unifying theory that describes linear viscoelasticity, which makes SAOS especially useful to polymer scientists. Currently, no unifying constitutive theory exists for nonlinear viscoelasticity. Therefore, LAOS, together with SAOS, is of interest for studying *nonlinear* viscoelasticity in polymeric materials such as cheese.

3.1 Simple Shear

Simple shear is the flow generated between two parallel plates with a constant gap. One plate is fixed, and the other moves in its own plane subject to a force F acting in the plane (Fig. 2). This deformation causes a change in shape without change in volume. The applied force F produces a shear stress:

$$\tau = \frac{F}{\mathrm{A}} \tag{3. 1}$$

where A is the contact area. At steady state, this stress is uniform throughout the material. This can be seen by making a force balance on any horizontal slice of fluid, one surface of which contacts the upper plate.

The *shear strain* is the tangent of the angle of deformation:

$$\gamma = \frac{\Delta x}{\Delta y} = \frac{X_o}{\mathrm{h}} \tag{3. 2}$$

and the *shear rate,* defined as the time rate of change of the shear strain, is:

$$\dot{\gamma} = \frac{\mathrm{d}\gamma}{\mathrm{dt}} = \frac{\mathrm{d}}{\mathrm{dt}}\left(\frac{X_o}{\mathrm{h}}\right) = \frac{V}{\mathrm{h}} \tag{3. 3}$$

From above, the rate of deformation tensor will have only one independent nonzero component:

$$\dot{\gamma}_{ij} = \begin{bmatrix} 0 & \dot{\gamma} & 0 \\ \dot{\gamma} & 0 & 0 \\ 0 & 0 & 0 \end{bmatrix} \tag{3. 4}$$

For uniform fluid properties and in the absence of fluid inertia, it can be shown that this nonzero component is uniform throughout the fluid. This is called a homogeneous flow field. Because of the unique relation between stress and deformation, the resulting nonzero components of the stress tensor are also uniform throughout. This contrasts with other configurations for determining rheological properties, such as tube flow viscometers, in which the flow field is heterogeneous (Darby, 1976).

In simple shear, one usually describes the state of stress from a *rheological* point of view by specifying the shear stress, τ, and the *first* and *second normal stress differences*:

$$N_1 = \tau_{11} - \tau_{22} \tag{3. 5}$$

$$N_2 = \tau_{22} - \tau_{33} \tag{3. 6}$$

3.2 Oscillatory Shear

Oscillatory shear is a uniform simple shear deformation in which the shear strain varies harmonically:

$$\gamma(t) = \gamma_o \sin 2\pi f_o t = \gamma_o \sin \omega t \tag{3. 7}$$

where γ_o is the shear strain amplitude and ω is the angular frequency, $\omega = 2\pi f_o$.

The shear rate is found by differentiating Eq. (3. 7):

$$\dot{\gamma}(t) = \gamma_o \omega \cos \omega t = \dot{\gamma}_o \cos \omega t \tag{3. 8}$$

where $\dot{\gamma}_o$ is the shear rate amplitude. In controlled rate experiments such as LAOS, the strain amplitude and frequency are fixed (assigned) variables, and the shear stress is the dependent (measured) variable. Thus, by varying γ_o and ω independently, a wide range of test conditions can be attained, making oscillatory shear ideal for replicating various real-life processes.

3.3 The Pipkin Diagram

A useful diagram showing the various regimes of behavior that can be exhibited at various combinations of strain amplitude and frequency is shown in Fig. 3. Pipkin (1972) proposed a plot of strain amplitude (γ_o) *versus* frequency (ω) as a basis for such a diagram. Tanner (1985) later improved this to strain rate amplitude ($\dot{\gamma}_o$) *versus* ω and called it the

Pipkin diagram. The Pipkin diagram in Fig. 4 shows the shape of the shear stress *versus* shear rate (or shear strain) loops for the different regimes in oscillatory shear.

At low frequencies, the deformation approaches that of steady simple shear, because the shear rate varies slowly with time. Thus, on the left side of the diagram, the flow will be governed by the viscometric functions. If the shear rate amplitude is also small, the flow will be Newtonian, as shown near the origin.

As frequency increases, the material exhibits viscoelasticity. Identifying the region of *linear* viscoelastic response is of special interest here. It has been shown, using basic concepts of continuum mechanics, that at low frequencies it is the *strain rate* amplitude that governs departures from linearity, while at higher frequencies it is the *strain* amplitude that governs the onset of nonlinear behavior (Astarita and Jongschaap, 1977-78; Dealy and Wissbrun, 1990). On the Pipkin diagram, γ_o is constant along straight lines through the origin, and one such line is shown in Fig. 3 as the limit of linear viscoelastic behavior at higher frequencies.

At high frequencies, the behavior becomes more elastic, and there is a zone on the right side of the diagram that gives nondissipative (purely elastic) responses. Increasing γ_o in this nondissipative region causes nonlinear elasticity.

For polymer melts, it has been suggested that at some critical stress amplitude, slip will occur at the plate surfaces causing the stress response to become erratic (Hatzikiriakos and Dealy, 1991). When this occurs, the effects of slip and nonlinear viscoelasticity can be hard to distinguish.

3.4 Linear Viscoelasticity

Linear viscoelasticity is the simplest type of viscoelastic behavior. It is observed when the total deformation is small or when the deformation occurs slowly, as in steady simple shear at low shear rates (Fig. 5). In both cases, the molecules are hardly perturbed from their equilibrium configuration and entanglement state. This is because relaxation processes due to Brownian motion return the molecules to their equilibrium states, and if the deformation is slow, this relaxation mechanism can keep up with the deformation (Dealy and Wissbrun, 1990). Hence, there is no significant deviation from equilibrium. In oscillatory shear testing, therefore, linear viscoelasticity will be observed at small strain amplitudes (SAOS). The actual range of γ_o for linear behavior will depend on the material and test conditions.

3.4.1 Relaxation Modulus and Boltzmann Superposition Principle

Consider the simple shear set up in Fig. 2. Suppose at time $t = 0$, the sample is suddenly deformed by a shear strain γ_o. The resulting shear stress can now be measured versus time, $\tau(t)$. This is called *stress relaxation*, and the results are reported in terms of the *shear relaxation modulus, G*:

$$G(t, \gamma_o) \equiv \frac{\tau(t)}{\gamma_o} \tag{3. 9}$$

In general, the relaxation modulus is a function of the shear strain amplitude γ_o. However, at low strain amplitudes, it will not depend on strain and the relationship between the stress and relaxation modulus will be linear:

$$\tau(t) = G(t)\gamma_o \tag{3.10}$$

Hence, the term *linear* viscoelasticity for small strain behavior.

The *Boltzmann superposition principle* provides a general equation that describes all types of linear viscoelastic behavior. This equation can be derived by considering a sequence of small shear step-strains $\delta\gamma(t_1)$, $\delta\gamma(t_2)$, $\delta\gamma(t_3)$, … $\delta\gamma(t_N)$ occuring at times t_1, t_2, t_3, … t_N (Dealy and Wissbrun, 1990). Thus, from Eq. (3.10), for the shear strain $\delta\gamma(t_1)$ introduced at time t_1:

$$\tau(t) = G(t - t_1)\delta\gamma(t_1) \tag{3.11}$$

For the shear strain $\delta\gamma(t_2)$, the stress can be calculated by assuming that the incremental response of the material to this second step strain is independent of the strain introduced at time t_1. Therefore, the stress resulting from $\delta\gamma(t_2)$ can be *superposed* or added to the right side of Eq. (3.11); and in general, for N combinations of infinitesimal strains:

$$\tau(t) = \sum_{i=1}^{N} G(t - t_i)\delta\gamma(t_i) \tag{3.12}$$

For a smooth strain history, Eq. (3.12) can be written in terms of an integral:

$$\tau(t) = \int_{-\infty}^{t} G(t - t')\mathrm{d}\gamma(t') \tag{3.13}$$

or

$$\tau(t) = \int_{-\infty}^{t} G(t - t')\dot{\gamma}(t')\mathrm{d}t' \tag{3.14}$$

Equations (3.13) and (3.14) represent the Boltzmann superposition principle for shearing deformations.

3.4.2 Stress Response in SAOS and the Complex Modulus

In SAOS, the shear stress can be calculated using Boltzmann superposition. Thus, by substituting the shear rate, Eq. (3. 8), into Eq. (3.14), it can be shown that the shear stress is also sinusoidal and has the same frequency as the strain:

$$\tau(t) = \tau_o \sin(\omega t + \delta) \tag{3.15}$$

where τ_o is the shear stress amplitude and the phase angle δ is called the *mechanical loss angle*. The *dynamic modulus* G_d is defined by the amplitude ratio:

$$G_d \equiv \frac{\tau_o}{\gamma_o} \tag{3.16}$$

In the region of linear viscoelasticity, δ and G_d will be functions of frequency alone, and independent of the strain amplitude. Also, a plot of shear stress *versus* shear rate will always give an ellipse (Fig. 4).

A trigonometric identity is used to expand Eq. (3.15):

$$\tau(t) = \gamma_o \left[G'(\omega) \sin \omega t + G''(\omega) \cos \omega t \right] \tag{3.17}$$

This introduces $G'(\omega)$ and $G''(\omega)$, called the *storage modulus* and the *loss modulus* respectively. They are both functions of frequency and can be calculated from:

$$G'(\omega) = G_d \cos \delta \tag{3.18}$$

$$G''(\omega) = G_d \sin \delta \tag{3.19}$$

$G'(\omega)$ and $G''(\omega)$ provide a useful means of interpreting linear behavior in terms of *energy* storage and loss respectively. For example, a Hookean solid in SAOS will have zero phase angle and $G''(\omega)$ will be zero, since there is no viscous dissipation (loss) in a purely elastic

material. A Newtonian fluid, on the other hand, will have a 90° phase angle, and in this case $G'(\omega)$ will be zero, because there is no energy storage in a purely viscous material. A viscoelastic material will therefore exhibit both viscous dissipation and energy storage, and its phase angle will lie between 0 and 90°.

A useful way of expressing $G'(\omega)$ and $G''(\omega)$ is in terms of a *complex modulus*, $G^*(\omega)$, defined as:

$$G^*(\omega) = G'(\omega) + jG''(\omega) \tag{3.20}$$

where $j = \sqrt{-1}$. The amplitude ratio, G_d, is thus the magnitude of $G^*(\omega)$:

$$G_d \equiv \frac{\tau_o}{\gamma_o} = \left|G^*\right| = \sqrt{(G')^2 + (G'')^2} \tag{3.21}$$

Since the Boltzmann superposition principle describes all types of linear viscoelastic behavior, one can relate SAOS response to the linear relaxation modulus. Therefore, it can be shown that $G'(\omega)$ and $G''(\omega)$ are the Fourier sine and cosine transforms of the relaxation modulus $G(t)$ (Dealy and Wissbrun, 1990):

$$G'(\omega) = \omega \int_0^\infty G(s) \sin \omega s \, ds \tag{3.22}$$

$$G''(\omega) = \omega \int_0^\infty G(s) \cos \omega s \, ds \tag{3.23}$$

3.4.3 The Lodge Rubberlike Liquid

Using the Finger tensor as a finite measure of strain, the Boltzmann superposition principle can be generalized to formulate a *finite* theory of linear viscoelasticity:

$$\tau_{ij}(t) = \int_{-\infty}^{t} m(t-t')B_{ij}(t,t')\mathrm{d}t' \tag{3.24}$$

where $m(t-t')$ is a memory function and the Finger tensor, $B_{ij}(t,t')$, in simple shear is:

$$B_{ij}(t,t') = \begin{bmatrix} 1+[\gamma(t)-\gamma(t')]^2 & [\gamma(t)-\gamma(t')] & 0 \\ [\gamma(t)-\gamma(t')] & 1 & 0 \\ 0 & 0 & 1 \end{bmatrix} \tag{3.25}$$

t is the current time and is the time at which the material element is in its reference configuration, and t' is the past time and is the time at which the strain is evaluated, relative to the configuration at time t. Eq. (3.24) is called the Lodge *rubberlike* liquid model (Lodge, 1964).

In his kinetic network theory, Lodge (1964) assumed that the strong interactions between polymer molecules in a melt could be seen as forming a network in which the entanglements act as temporary crosslinks, and that these network junctions are continuously being created and destroyed. The memory function that arises from this network theory is:

$$m(t-t') = \sum_{i=1}^{N} \frac{G_i}{\lambda_i} e^{-\frac{(t-t')}{\lambda_i}} \tag{3.26}$$

It can be shown that the relaxation modulus corresponding to Eq. (3.26) is the same as that of the generalized Maxwell model (Dealy and Wissbrun, 1990). Since Lodge's network theory looks at the melt as a collection of network strands rather than molecules, parameters such as chain length and friction coefficient do not appear. Also, the theory does not predict the relaxation spectrum and effects of molecular structure on rheological properties.

In oscillatory shear, the Lodge rubberlike liquid model predicts a sinusoidal shear stress given by Eq. (3.15). However, it also predicts a *sinusoidal* first normal stress difference that has a frequency of 2ω and a nonzero offset or average value equal to $\gamma_o^2 G'(\omega)$ (Lodge, 1964; Giacomin and Dealy, 1993). The second normal stress difference is predicted to be zero. In LAOS, N_1 and N_2 are expected to contain higher harmonics at multiples of ω just like the shear stress (see Section 3.5.1).

Although the Lodge rubberlike liquid model does not predict nonlinearity in the stress response in oscillatory shear, it does predict a nonzero first normal stress difference, and any material response that deviates from the model's prediction reflects nonlinear behavior.

3.4.4 Generalized Maxwell Model and Discrete Relaxation Spectrum

Mechanical analog models can simulate a material's response (Ferry, 1980). These models can be constructed by some suitable combination of springs (obeying Hooke's law) and viscous dashpots (obeying Newton's law). One of the most common mechanical analogs used in modeling linear behavior is the Maxwell element shown in Fig. 6. This is a *fluid* model, since the force *F* will cause continuous deformation of the assembly due to the unrestrained extension of the dashpot (assuming the dashpot has infinite length).
The constitutive equation for the Maxwell element is:

$$\tau_{ij}(t) = \int_{-\infty}^{t} G_o e^{-\frac{1}{\lambda}(t-t')} \dot{\gamma}_{ij}(t')\mathrm{d}t' \tag{3.27}$$

where G_o and λ are the *initial* shear modulus and *relaxation time* of the polymeric material. To simulate actual relaxation processes, more than one exponential function is usually

required (Ferry, 1980; Dealy and Wissbrun, 1990). Greater flexibility can be achieved by placing several Maxwell elements in parallel as shown in Fig. 7. The forces in each element are additive, and the resulting constitutive equation is known as the *generalized* Maxwell model:

$$\tau_{ij}(t) = \int_{-\infty}^{t} \sum_{k} G_k e^{-\frac{1}{\lambda_k}(t-t')} \dot{\gamma}_{ij}(t')\mathrm{d}t' \tag{3.28}$$

where G_k and λ_k are the initial modulus and relaxation time for each Maxwell element. Thus, the relaxation modulus for the generalized Maxwell model is:

$$G(t) = \sum_{i=1}^{N} G_i e^{-\frac{t}{\lambda_i}} \tag{3.29}$$

Using enough elements, Eq. (3.29) can describe almost any experimental $G(t)$ behavior. Usually five to ten (G_i, λ_i) pairs are sufficient to fit experimental data reasonably (Dealy and Wissbrun, 1990). The (G_i, λ_i) set is called the *discrete relaxation spectrum* of the material.

Using Eq. (3.29) to represent the relaxation modulus, the functions defined in Equations (3.22) and (3.23) can now be represented in terms of G_i, λ_i (Dealy and Wissbrun, 1990):

$$G'(\omega) = \sum_{i=1}^{N} \frac{G_i(\omega\lambda_i)^2}{\left[1+(\omega\lambda_i)^2\right]} \tag{3.30}$$

$$G''(\omega) = \sum_{i=1}^{N} \frac{G_i(\omega\lambda_i)}{\left[1+(\omega\lambda_i)^2\right]} \tag{3.31}$$

Section 3.4.6 describes a method for obtaining the discrete relaxation spectrum, (G_i, λ_i), from experimental data. Once the set of (G_i, λ_i) pairs for a material are known, Equations

(3.30) and (3.31) can be used to compute the storage and loss moduli, $G'(\omega)$ and $G''(\omega)$, at any given test frequency, provided the frequency is within the experimental range of (G_i, λ_i).

3.4.5 The Deborah and Weissenberg Numbers

An important dimensionless parameter, the Deborah number, can be defined as follows:

$$De \equiv \frac{\lambda}{t_{proc}} = \lambda\omega \tag{3.32}$$

where t_{proc} is the characteristic time of the process (related to the time scale of the deformation) and λ is the relaxation time of the material. The Deborah number reflects the extent to which elastic or memory effects will play a role in the material's response (Dealy and Wissbrun, 1990). At large Deborah numbers ($De > 1$), elastic behavior is observed while low Deborah numbers ($De << 1$) depict viscous behavior. Viscoelasticity is observed at moderate values of the Deborah number. In oscillatory shear testing, the process time t_{proc} is inversely proportional to the frequency; therefore, as frequency increases, *De* increases causing the material to exhibit more solid-like characteristics.

Another dimensionless parameter, the Weissenberg number, can be defined as follows:

$$We \equiv \lambda\dot{\gamma} \tag{3.33}$$

It is a measure of the extent to which nonlinearity (anisotropy) will be exhibited in the fluid's response (Dealy and Wissbrun, 1990). Large Weissenberg numbers depict nonlinear behavior while low Weissenberg numbers depict linear behavior.

The Pipkin diagram can thus be represented in terms of dimensionless variables by replacing $\omega\gamma_o$ and ω with *We* and *De*, as shown in Fig. 4. As mentioned earlier, LAOS is one of the few simple tests in which these two groups can be varied independently.

3.4.6 Parsimonious Spectrum and IRIS

(G_i, λ_i) pairs for a material are determined from experimental data. By using a step-strain experiment, the relaxation modulus $G(t)$ may be measured directly. However, a more advanced method is to use SAOS. An SAOS frequency sweep (see Section 4.2) gives $G'(\omega)$ and $G''(\omega)$ for a range of select frequencies. (G_i, λ_i) pairs are then determined by fitting Equations (3.30) and (3.31) to these experimental values.

Several different methods have been proposed for obtaining an accurate fit of experimental $G'(\omega)$, $G''(\omega)$ data (Ferry, 1980; Friedrich and Hoffman, 1983). One of the most commonly used techniques is nonlinear regression, but this method can give multiple solutions. Baumgaertel and Winter (1989) developed a robust numerical technique that converts SAOS data from the frequency domain to the time domain and calculates the discrete relaxation spectrum (G_i, λ_i) (Winter *et al.*, 1993). The method is called *parsimonious modeling*, since it finds the spectrum with the *smallest number of relaxation modes* which still represent the data within experimental error (Baumgaertel *et al.*, 1987-97). The resulting spectrum is termed *parsimonious spectrum*. Fewer parameters avoid the difficulties associated with curve fitting techniques such as nonlinear regression and also help in simplifying the calculations. This makes parsimonious modeling efficient.

The *Innovative Rheological Interface Software* (IRIS), developed by Baumgaertel *et al.* (1987-97), uses parsimonious modeling to determine the discrete relaxation spectrum (G_i, λ_i) for a polymeric material. Required are input data from SAOS, $G'(\omega)$ and $G''(\omega)$, within a finite frequency window. The algorithm automatically selects a suitable set of initial values $G_{i,o}$, $\lambda_{i,o}$. The number of relaxation times reduces during the iterative calculations depending on the needs for improved fit (Baumgaertel *et al.*, 1987-97).

3.5 Nonlinear Viscoelasticity

Nonlinear viscoelasticity is much more complicated than the linear viscoelastic case. It is observed when the deformation is neither slow nor small, as shown in Fig. 5. The response to an imposed deformation now depends on the size, rate, and kinematics of the deformation. This means that to duplicate responses in a particular type of deformation, the rate, magnitude, and kinematics of the deformation must match. Hence, the Boltzmann superposition principle is no longer valid, and the material functions $G'(\omega)$ and $G''(\omega)$ cannot describe a material's response. The threshold γ_o for nonlinear behavior will depend on the material and test temperature.

3.5.1 Stress Response in LAOS and Nonlinear Viscoelastic Phenomena

For most polymeric materials, the stress response in LAOS is *not* sinusoidal. After a few cycles, the shear stress becomes a standing wave that can be represented by a Fourier

series of *odd* harmonics (for more on the Fourier series and LAOS stress response, see Chapter 5):

$$\tau(t) = \sum_{m=1,odd}^{M} \tau_m \sin(\, m\omega t + \delta_m) \tag{3.34}$$

where $\tau_m(\omega, \gamma_o)$ and $\delta_m(\omega, \gamma_o)$ are the amplitudes and phase angles of the *odd* harmonics. They depend upon both the strain amplitude and frequency, and since only odd valued harmonics are observed, a plot of shear stress *versus* shear rate will always give a two-fold symmetric loop (Fig. 4). Fig. 8 explains the definition of two-fold symmetry. The existence of higher harmonics makes the property definitions $|G^*|$ and δ meaningless for a nonlinear viscoelastic response.

An interesting feature of the stress response in LAOS is the energy dissipation per cycle per unit volume, W_L, given by the cyclic integral of the shear stress with respect to the shear strain (Onogi and Matsumotu, 1981):

$$W_L = \oint \tau \, d\gamma = \pi \tau_1 \gamma_o \sin \delta_1 \tag{3.35}$$

Thus, all the energy dissipation is in the first harmonic. From the second law of thermodynamics, $W_L \geq 0$. Combining this with Eq. (3.35), the following inequality is obtained:

$$\sin \delta_1 \geq 0 \tag{3.36}$$

giving:

$$0 \leq \delta_1 \leq \pi \tag{3.37}$$

Measured values of the phase angle for the first harmonic are always in the first quadrant, $0 \le \delta_1 \le \pi/2$, and by convention, higher harmonics lie between 0 and 2π radians (see Chapter 5).

Many important rheological phenomena are completely absent from the predictions of linear viscoelastic theory. These important effects are observed even in the simplest flow types such as simple shear, with linear behavior observed only at low shear rates. The predominant nonlinear phenomena are the nonzero first normal stress difference (N_1) and the dependence of the viscosity on the shear rate (Dealy and Wissbrun, 1990). N_1 gives rise to the *Weissenberg effect*, discussed earlier in Chapter 2. The Weissenberg effect is the tendency of the free surface of an elastic liquid to rise near a partially immersed rotating rod. Another nonlinear effect is the dependence of the relaxation modulus on the strain magnitude.

Although these effects seem interesting and give rise to fascinating phenomena, they complicate representation of nonlinear data. Additional parameters such as shear strain or shear rate must be introduced, and in other cases entirely new material functions must be defined (Dealy and Wissbrun, 1990).

3.5.2 Theories and Constitutive Equations

As the Boltzmann superposition principle provides a basis for describing linear viscoelastic behavior, there is no universal theory for interpreting nonlinear behavior. Several approaches have been taken to develop a theory of nonlinear viscoelasticity, but none has led to a general, unifying theory. Two of the most popular approaches have been

continuum mechanics and *molecular theory* (Dealy and Wissbrun, 1990). The former establishes an initial model based on certain general hypotheses, and then uses experimental results to further develop the model. More on the continuum mechanics approach can be found in the texts by Tanner (1985) and Larson (1988). The latter starts from a model for molecular behavior and uses statistical mechanics to derive a constitutive equation, but this approach is mathematically complex. More on molecular theory can be found in the text by Bird *et al.* (1987).

Despite the drawbacks of modeling nonlinear behavior, the results from these techniques find use as follows (Dealy and Wissbrun, 1990):

- They provide criteria for the appearance of nonlinear effects.
- They predict the nature of the first departures from linear behavior.
- They suggest methods for representing experimental results.

As a result, several constitutive equations have been developed to describe nonlinear behavior of polymer melts in LAOS. Examples of some of these constitutive equations include the upper convected Maxwell (UCM), the Bernstein-Kearsley-Zappas (BKZ), and the Phan Thien-Tanner (PTT) models, the Doi Edwards theory, and the Lodge rubberlike liquid model (Baird and Collias, 1995; Giacomin and Dealy, 1993). The Lodge rubberlike liquid model discussed in Section 3.4.3 is a kinetic network theory that predicts the main features of the response just beyond the region of linear viscoelasticity.

3.6 Experimental Errors

In oscillatory shear testing, experimental errors may be caused by fluid inertia or viscous heating. Throughout the discussion so far, the effects of fluid inertia and viscous dissipation have been neglected, but if either of these matter, they can significantly corrupt the stress response.

If fluid inertia matters, it can cause flow field heterogeneity. In SAOS, the gap between the plates must be small enough to minimize inertial effects (Giacomin and Dealy, 1993). In LAOS, on the other hand, there is no general design equation for minimizing inertial effects since there is no unifying theory for nonlinear viscoelasticity. Therefore, the effects of fluid inertia must be experimentally verified by comparing the stress waveforms for two different gaps. For fluid inertia to be insignificant, these stress waveforms should match and thus not depend on gap.

Viscous dissipation is the temperature rise of a fluid when it is deformed, and the effects of viscous dissipation must also be minimized, since rheological properties are strong functions of temperature. It has been found that viscous heating will cause the shear stress amplitude τ_o to go through a maximum with strain amplitude γ_o, and when γ_o exceeds this value, the melt temperature will increase indefinitely (Schapery and Cantey, 1966; Giacomin and Dealy, 1993). This is called *thermal runaway*. However, reasonably accurate measurements can still be made before the onset of thermal runaway. Schapery (1966) showed that the time till thermal runaway is proportional to:

$$t \propto \left(\frac{h}{\tau_o} \right)^2 \tag{3.38}$$

where *h* is the gap and τ_o is the shear stress amplitude. In practice, viscous dissipation causes the fundamental stress amplitude $\tau_1(\omega, \gamma_o)$ to decrease with increasing number of oscillations. Also, if the sample is too thick, erroneously low values of $\tau_1(\omega, \gamma_o)$ will be observed (Giacomin and Dealy, 1993).

CHAPTER 4 Method

To measure the nonlinear viscoelastic properties of a polymeric material such as cheese, one must use an instrument that can generates large, uniform, transient deformations involving high shear rates. Classical shear rheometers such as rotational or sliding plate (measuring total force) cannot produce such deformations. At high strains and shear rates, these instruments generate heterogeneous flow fields near the sample edges, which is highly undesirable. These edge effects cause significant errors when total force or total torque measurements are used to infer material properties. Table 1 compares different rheometers used for nonlinear measurements on polymeric materials using LAOS. Problems with each geometry are tabulated along with their advantages and disadvantages.

In this research, the sliding plate *true shear* rheometer was used to measure the nonlinear viscoelastic properties of cheese using LAOS. Linear viscoelastic properties were measured using a parallel disk rheometer.

4.1 The Sliding Plate Rheometer

To avoid the nonuniform flow field of capillary viscometers and the flow irregularities associated with rotational rheometers, Giacomin *et al.* (1989) developed a novel rheometer called the sliding plate rheometer (SPR). Unlike other geometries, the SPR generates a homogeneous, simple shear flow field (Fig. 2) except near the sample edges. The shear stress is measured locally in the region of uniform deformation, away from the free boundaries, using a Dealy (1984) *shear stress transducer* (SST). The SST is flush mounted

on the fixed plate and touches the sample. This is how flow heterogeneity error is eliminated. Another advantage of the SPR is that sample life is prolonged, since degradation at the exposed edges does not affect the stress response until it reaches the sample center.

The SPR was commercialized by Interlaken Technology Corporation (ITC), Eden Prairie, Minnesota. Figures 9 and 10 show a schematic of the Interlaken rheometer, designed for use with molten polymers, fiber reinforced materials, concentrated solutions, raw elastomers, food products, and other viscoelastic or thixotropic materials. It can generate shear rates from $0.02\,s^{-1}$ to $200\,s^{-1}$, shear strains up to 500, and can measure both linear and nonlinear viscoelastic properties. The heart of the system is the patented SST, which uses a capacitance proximeter (Capacitec) that consists of two essential components: a circular beam and the proximeter, which act as capacitor plates. A schematic of the SST is shown in Fig. 11. In this configuration, the system produces a signal proportional to the beam deflection. Thus, when the shear stress exerted by the polymer deflects the beam, the signal changes, and this change is converted to a digital stress signal. The maximum operating temperature of the SST is 800^{o}C and the proximeter signal is conditioned by a Capacitec 4100-CM3 amplifier.

The entire rheometer and SST are in a forced convection oven mounted on an ITC Series 3300 test frame. The maximum operating temperature is 300^{o}C, controlled by an ITC Series 3260 Temperature Controller. The plate displacement is generated by a servohydraulic linear actuator (MTS Systems Inc., Minneapolis). The actuator is equipped with precision servovalves and powered by a heavy-duty hydraulic pump, providing great flexibility in shear history and high performance. Both the moving and fixed plates consist of type-420 stainless

steel and the gap between the plates is set using high precision shims (Fig. 10). The gap is usually set between 0.23 and 1 mm.

The rheometer also comes with a full application software package called QuikTest, designed to measure a wide range of linear and nonlinear viscoelastic properties. The package includes test setup, data acquisition, results analysis, reports, and plots. It provides complete control of the test environment by enabling users to monitor and run tests from one screen. Its main features include powerful waveform generation, continuous amplitude control, and integrated data acquisition. The application program for oscillatory shear is included in these features. QuikTest also offers over 20 commands for creating customized application software programs, for tests such as exponential shear, interrupted shear, and step-strain. QuikTest runs on a desktop 486 Zeos Pantera personal computer.

4.1.1 Shear Stress Transducer Calibration

The SST must be accurately calibrated. The routine procedures for proximeter setup and SST calibration are provided by the manufacturer (ITC) and described in Appendix A. ITC also provides the calibration constant required for calibrating the SST. For the rheometer used in the experiments, it was determined that the calibration constant provided by ITC was inaccurate (Lan, 1997). The actual calibration constant was measured to be 150.0 kPa/kg[*], higher than the 130.2 kPa/kg value provided by ITC. Thus, 150.0 kPa/kg was used for calibration.

[*] kPa/kg means kPa of measured shear stress per kg of hung mass during static calibration.

The new calibration constant was measured using the McGill method, which is described in Appendix B. The calibration results are given in Table 2 and a sample calculation is in Appendix B. Normally, the calibration constant for the SST must be measured only once, since it does not vary with time or temperature.

4.1.1.1 Calibration Constant Verification

Lan (1997) further verified the calibration constant by comparing data from the SPR with published results. He conducted steady shear experiments on both Dowlex 2045 and IUPAC X resins using a triangular waveform and plotted the results as power law viscosity curves. He found good agreement, within 10%, between the experimental and published viscosity curves for both polymers.

4.1.2 Sample Preparation

Natural Cheese

Fresh reduced-fat mozzarella, full-fat and reduced-fat pizza cheese, and reduced-fat cheddar blocks were obtained from the University of Wisconsin dairy plant and refrigerated at 4^{o}C until sample preparation. The blocks were vacuum packed to prevent moisture loss and contamination. Table 3 shows the average cheese compositions.

A couple of days before each experiment, a small slab was cut from the main block to make the samples. First, a food slicer (Model No. 1042, Rival Company, Kansas City, MO) sliced the cheese into samples with the desired thickness (approximately 1.2 mm); mozzarella was sliced in the direction of fiber orientation (Fig. 12). A laboratory knife was then used to

trim the edges. The samples were cut to approximately $50 \times 80 \times 1.2$ mm dimensions. However, the thickness was hard to control and varied considerably depending on the cheese. Each sample was then carefully wrapped in plastic and placed in an airtight zipper bag to maintain freshness. The remaining cheese block was again vacuum packed and refrigerated for future use.

Process Cheese

Kraft™ *fat-free* process mozzarella singles were obtained from a grocery store and refrigerated at 4°C until sample preparation. Each slice came individually wrapped in plastic film and measured $80 \times 80 \times 1.5$ mm. Before testing, the square slices were cut into rectangles measuring approximately $50 \times 80 \times 1.5$ mm using a laboratory knife. The sample thickness was already at the desired value.

4.1.3 Testing

Before beginning each test, the rheometer plates and SST were thoroughly cleaned using a common sodium hydroxide based household oven cleaner (Easy Off™) and degreaser (Pro 409™) to remove residue from previous experiments. The plates and SST were then wiped with a damp cloth to remove all traces of cleaner. Next, the right pair of shims were installed to obtain the desired gap, h. Since it was difficult to obtain the same thickness for all the cheese samples, 0.36 or 0.5 mm gap shims were used depending on the initial sample thickness. After the rheometer was clean and the right pair of shims installed, the oven was heated to the test temperature.

At the test temperature, the SST was calibrated using Interlaken's method (Appendix A). After calibration, the hydraulics were turned on and the sliding plate centered at the zero position. The sample was then placed on the fixed plate with the active face centered on the sample. It was carefully flattened to prevent air bubble entrapment. The oven door was then closed and the rheometer heated back to the test temperature along with the sample.

The shear strain in oscillatory shear is given by Eq. (3.7), and since the gap h is known, the shear strain amplitude γ_o is specified in terms of the plate displacement X_o (Fig. 2). For example, for a sinusoidal shear strain $\gamma_o = 2$ and gap $h = 0.5\,\text{mm}$, from Eq. (3.2), the applied maximum plate displacement will be $X_o = 1\,\text{mm}$. Tables 4 and 5 show the range of strain amplitudes used for the LAOS tests.

Large plate displacements can cause errors in the stress reading. This happens when the sample edges approach the SST, thereby imparting an irregular shearing force to the transducer. To avoid this, Giacomin (1987) suggests the following relation for the maximum plate displacement:

$$X_{\max} < \Phi_c (L - D) \tag{4. 1}$$

where $X_{\max}$ is the maximum allowable plate displacement without edge effects, L is the sample length, D is the active face diameter, and Φ_c is 0.2. This relation gives $X_{\max} \approx 14$ mm for an 80 mm sample length, which is well above the maximum plate displacement of 5 mm used in the experiments.

The tests on process cheese were conducted at two temperatures: 30°C and 35°C, and at a test frequency of 0.25 Hz. The tests on natural cheese were conducted over 12 weeks at

the following intervals from the manufacture date: 1 week, 4 weeks, 6 weeks, and 12 weeks. Two temperatures were studied: 40°C at which the cheeses were solid, and 60°C at which the cheeses had melted. Mozzarella was sheared in the direction of fiber orientation as shown in Fig. 12. The test frequency for both temperatures was 0.4 Hz, aimed to approximate real-life chewing frequency. A fresh sample was used for each new strain magnitude, and the tests were repeated using the same sample to check for repeatability. The SST was thoroughly cleaned after every third sample to remove cheese from the gap between the SST beam and housing, and then it was re-calibrated.

4.2 The Parallel Disk Rheometer

A rotational rheometer such as the parallel disk rheometer can be used to measure linear viscoelastic properties of cheese using SAOS. A schematic of the parallel disk geometry is shown in Fig. 13. In rotational rheometers, the shear stress is determined based on the torque response of the system.

The Bohlin-CVO Melt Rheometer (Bohlin Instruments Inc., Cranbury, NJ) was used to conduct SAOS strain sweep and frequency sweep tests on six week old reduced-fat mozzarella and cheddar (40°C and 60°C), and fat-free process mozzarella (30°C and 35°C). The rheometer was fitted with a 95.234 g-cm torque element using parallel disk geometry and the temperature was controlled using a water bath (Bohlin Instruments Inc., Cranbury, NJ).

4.2.1 Sample Preparation and Testing

Disk-shaped samples were prepared using a borer and slicer (Model No. 1042, Rival Company, Kansas City, MO). During testing, a sample was placed on the lower plate and the upper plate was brought into contact with the sample. The sample was held five minutes for temperature equilibrium and its perimeter was brushed with mineral oil to minimize drying. Fiber orientation in reduced-fat mozzarella was perpendicular to the rotation axis, as shown in Fig. 14.

The linear viscoelastic range for the different cheeses was determined by measuring dynamic properties using SAOS strain sweep tests. Once the linear range was known, SAOS frequency sweep measurements were made, and the storage and loss moduli, $G'(\omega)$ and $G''(\omega)$, reported. These experimental moduli were then used to calculate the discrete relaxation spectrum for the respective cheeses (see Section 3.4.6).

CHAPTER 5 Spectral Analysis of LAOS Test Results

There are several methods of analyzing LAOS experimental results, but the most precise way is to use the discrete Fourier transform (DFT) (Giacomin, 1987). The DFT is a spectral analysis tool derived from Fourier theory. It operates on time series, and transforms them to a series of frequency domain samples. In LAOS, these results are then used to characterize the material at the given test conditions. Therefore, the DFT provides a useful means of evaluating nonlinear behavior.

This chapter presents some background on Fourier theory, followed by development of the DFT with reference to the stress signal from the sliding plate rheometer. Determination of material properties and useful material characterization techniques are then described.

5.1 The Fourier Series and Fourier Integral

A periodic waveform can be approximated with a Fourier series (Lathi, 1992):

$$x(t) = a_o + \sum_{n=1}^{\infty} (a_n \cos 2\pi n f_o t + b_n \sin 2\pi n f_o t) \tag{5. 1}$$

or in more compact form:

$$x(t) = \sum_{n=-\infty}^{\infty} c_n e^{j2\pi n f_o t} \tag{5. 2}$$

The coefficients of the Fourier series are:

$$a_o = \frac{1}{T}\int_0^T x(t)dt \tag{5. 3}$$

$$a_n = \frac{2}{T}\int_0^T x(t)\cos 2\pi nf_o tdt \tag{5. 4}$$

$$b_n = \frac{2}{T}\int_0^T x(t)\sin 2\pi nf_o tdt \tag{5. 5}$$

$$c_n = \frac{1}{T}\int_{-T/2}^{T/2} x(t)e^{-i2\pi nf_0 t}dt \tag{5. 6}$$

From the exponential form, Eq. (5. 2), it can be deduced that:

- If an analytical expression for $x(t)$ is known, c_n can be evaluated analytically.
- For each *n*, c_n gives the magnitude and phase of the harmonic component of $x(t)$ having frequency nf_o.
- Each harmonic is separated by $\Delta f = 1/T$.

The *Fourier series* therefore yields *discrete* (or line) spectra for *periodic* waveforms, and each Fourier coefficient occurs at an integer multiple of the fundamental frequency f_o.

Real-life waveforms, however, are aperiodic (i.e. they have an infinite period), and the tool used to investigate the frequency spectra of *aperiodic* waveforms is the *Fourier integral*. The Fourier integral can be developed from the Fourier series by expressing Eq. (5. 2) into a form that involves taking the limit as Δf goes to zero (period T, approaches infinity) (Ramirez, 1985):

$$x(t) = \lim_{\Delta f \to 0} \sum_{-\infty}^{\infty} X(nf_o)e^{j2\pi nf_o t}\Delta f \tag{5. 7}$$

Thus, from Eq. (5. 7), as Δf goes to zero, the Fourier series for an aperiodic waveform reduces to:

$$x(t) = \int_{-\infty}^{\infty} X(f) e^{j2\pi ft} df \tag{5. 8}$$

If an analytic expression for $x(t)$ is known, the Fourier coefficients $X(f)$ can be obtained from the integral:

$$X(f) = \int_{-\infty}^{\infty} x(t) e^{-j2\pi ft} dt \tag{5. 9}$$

Here, f is a continuous frequency variable and $X(f)$ represents the *continuous* frequency spectrum of $x(t)$. Together, these two integrals are called the *Fourier transform pair*. The former, Eq. (5. 8), is called the *inverse Fourier transform* or *Fourier integral* and Eq. (5. 9) the *Fourier transform* (Ramirez, 1985).

As implied by its development, the Fourier transform only exists for aperiodic waveforms. In addition, $x(t)$ must satisfy the following Dirichlet conditions (Ramirez, 1985):

1. For $-\infty \le t \le \infty$, $x(t)$ must contain a finite number of maxima and minima.
2. If $x(t)$ contains discontinuities, they must be finite in number over $-\infty \le t \le \infty$.
3. $x(t)$ must be integrable such that $\int_{-\infty}^{\infty} |x(t)| dt < \infty$.

The Fourier series and Fourier integral are important experimental tools, since they allow time domain signals to be analyzed in the frequency domain in terms of their spectral

components. To further understand applications of these two powerful tools, “periodic” and “aperiodic” must be clearly defined.

Strictly, periodic means *repeating in time from minus infinity to plus infinity*, and aperiodic means *a transient* or *pulse occurring only once over infinite time*. Normally, any physically generated waveform that repeats itself, such as a sine wave, is called periodic and the *Fourier series* is used for analysis. Only one complete cycle of the waveform is needed for the Fourier series approach.

On the other hand, if one were to “window” a periodic signal by simply selecting an interval of the waveform and zeroing everything outside, then the aperiodic definition can be taken and the *Fourier integral* used for analysis. For example, to transform a sine wave, any integer of cycles of the waveform can be selected and the Fourier integral applied over the interval to obtain its frequency spectrum. In other words, the Fourier transform of a periodic waveform *can* be calculated using the concept of *windowing*. However, the spectrum associated with a strictly periodic waveform and a windowed version of the same signal will differ. The periodic signal will have a discrete spectrum, Eq. (5. 6), and the aperiodic or windowed signal will have a continuous spectrum, Eq. (5. 9).

The shear stress signal from the sliding plate rheometer is analyzed similarly. Part of the stress response is windowed as described above, and the *discrete* Fourier transform applied over the windowed waveform to determine its spectral components. Development of the discrete Fourier transform is shown in Section 5.3.

5.2 The Stress Response in LAOS

After reaching steady state, the stress response in LAOS becomes a standing wave that is not sinusoidal. This waveform is continuous and for practical purposes will be considered periodic.

Section 5.1 showed that periodic waveforms can be approximated by a Fourier series, Eq. (5. 2). In polar form, this equation can be written as a sum of cosinusoids. Therefore, the stress response in LAOS can be represented by:

$$\tau(t) = \sum_{m=1}^{\infty} \tau_m \cos(2\pi m f_o t + \delta_m) \tag{5.10}$$

The variable $x(t)$ in Eq. (5. 2) has now been replaced by the shear stress $\tau(t)$. Thus, a Fourier series can also be defined as the sum of harmonically related cosinusoids that best approximates a time series.

It has been proven that in LAOS, for an isotropic liquid with fading memory, this series has odd terms only (Graham, 1995):

$$\tau(t) = \sum_{m=1,odd}^{M} \tau_m \cos(2\pi m f_o t + \delta_m) \tag{5.11}$$

Although in theory M is infinity, components of $\tau(t)$ where $m > 7$ are hard to resolve (see Section 5.5).

The amplitudes, $\tau_m(f_o, \gamma_o)$, and phase angles, $\delta_m(f_o, \gamma_o)$, are material properties that provide an excellent means of evaluating and comparing nonlinear viscoelastic behavior. They can be determined from the DFT of the stress and strain signals from the sliding plate rheometer, as shown in the following sections.

5.3 The Discrete Fourier Transform

The shear stress signal from the sliding plate rheometer is sampled digitally and gives a time series $\tau(n\Delta t)$. This series is a *discrete* set of values separated by equal time intervals Δt. As illustrated earlier in Section 5.1, Equations (5. 6) and (5. 9) are only useful when an analytical expression for $\tau(t)$ is known. But $\tau(n\Delta t)$ can be transformed to the frequency domain by applying the *Fourier integral* over the *window* interval which contains the sampled shear stress wave (Ramirez, 1985).

After the above transform has been performed, and with some further mathematical manipulation, the *discrete Fourier transform* (DFT) is obtained:

$$\tau_d(k\Delta f_o) = \frac{1}{N}\sum_{n=0}^{N-1}\tau(n\Delta t)\frac{\cos 2\pi kn}{N} - j\tau(n\Delta t)\frac{\sin 2\pi kn}{N} \qquad (5.12)$$

where N is the number of samples and n is the time sample index with values 0, 1, 2,…, $N-1$. Δf is the sample interval in the frequency domain, $\Delta f = 1/N\Delta t$, and k is the discrete frequency component index with values 0, 1, 2,…, $N-1$.

Some important properties of the DFT are:

- The DC (direct current) term, $\tau_d(0)$, is the arithmetic mean of the time series.
- The highest frequency component occurs at $k = N/2$ and is called the Nyquist frequency. Its magnitude is $1/2\Delta t$. This means that only $N/2$ points of $\tau_d(k\Delta f_o)$ are physically meaningful.
- The spectral components (or harmonics) occur at multiples of the number of cycles from the DC point; for example, if 4 cycles are analyzed, then for m =1, 3, 7, …, M the *odd* spectral components will lie at k =1(4), 3(4), 7(4), …, $M(4)$.

- Obtaining $\tau_d(k\Delta f_o)$ requires $N \times N$ major operations.

The DFT yields a set of complex numbers, the amplitudes and phase contents of which are:

$$\left|\tau_d(k\Delta f_o)\right| = \sqrt{\mathrm{Re}^2\left[\tau_d(k\Delta f_o)\right] + \mathrm{Im}^2\left[\tau_d(k\Delta f_o)\right]} \tag{5.13}$$

$$\delta_d(k\Delta f_o) = \tan^{-1}\left[\frac{\mathrm{Im}\left[\tau_d(k\Delta f_o)\right]}{\mathrm{Re}\left[\tau_d(k\Delta f_o)\right]}\right] \tag{5.14}$$

where Im and Re mean the imaginary and real parts.

Another algorithm, the fast Fourier transform (FFT), is sometimes employed to accurately approximate the DFT of large time series. The number of operations required for an FFT are $N\mathrm{Log}_2 N$, which is fewer than the N^2 operations required for the DFT. Therefore, the FFT is a more efficient way of computing the DFT. However, with advances in modern computer technology, the DFT can be computed as efficiently as the FFT.

5.3.1 Determining Material Properties

The material property, τ_m, defined in Eq. (5.11) can therefore be inferred from the amplitudes of $\tau_d(k\Delta f_o)$ as follows:

$$\tau_m = 2\left|\tau_d(k\Delta f_o)\right|; \qquad k = mC \tag{5.15}$$

where $\left|\tau_d(k\Delta f_o)\right|$ is given by Eq. (5.13) and C is the integer of cycles analyzed. m =1 denotes the fundamental harmonic and occurs at the test frequency f_o.

The phase angles, δ_m, are obtained by a more complicated procedure. The command shear strain wave prescribed to the sliding plate rheometer gives a nearly perfect, slightly displaced sinusoid. Hence, the command and actual shear strain will be slightly out of phase

depending on the frequency response of the servo-hydraulic system (Giacomin, 1987). The actual shear strain will be:

$$\gamma(t) = \gamma_o \cos(2\pi f_o t + \delta_\gamma) \tag{5.16}$$

where δ_γ is its phase content. The phase spectra for the shear stress signal must be corrected with δ_γ before the material properties δ_m can be determined. Therefore, a DFT must also be applied to the shear strain signal to determine δ_γ. For a proper LAOS test, the fundamental harmonic (m =1) should be the only significant peak in the shear strain amplitude spectrum (Giacomin, 1987).

Once δ_γ is known, the phase angles, δ_m, defined in Eq. (5.11), can be computed from (Giacomin and Dealy, 1993):

$$\delta_m(f_o) = \delta_d(k\Delta f_o) - m\delta_\gamma \tag{5.17}$$

where $\delta_d(k\Delta f_o)$ is given by Eq. (5.14) for $k = mC$.

Hence, for example, the first three odd harmonics will be:

$$\delta_1 = \delta_d(f_o) - \delta_\gamma \tag{5.17a}$$

$$\delta_3 = \delta_d(3f_o) - 3\delta_\gamma \tag{5.17b}$$

and

$$\delta_5 = \delta_d(5f_o) - 5\delta_\gamma \tag{5.17c}$$

This procedure of determining the phase angles is called frequency modulation. By convention, reported phase angles lie between 0 and 2π radians.

5.3.2 The Amplitude Spectrum

The left side of Eq. (5.13) can be plotted against frequency to give an *amplitude spectrum* of the stress response in oscillatory shear. Figures 15 and 16 are amplitude spectra for process mozzarella at two strain amplitudes. In Fig. 15, for γ_o = 0.27, only the first (or fundamental) harmonic is detectable, and occurs at the test frequency f_o. However, at a higher strain amplitude of γ_o = 1.38 in Fig. 16, the first, third, and fifth harmonics are all clearly detectable, and occur at multiples of the test frequency f_o. Higher harmonics indicate deviations from linearity, with the linear case defined by Fig. 15, where only the fundamental harmonic matters. This is unsurprising, since the strain amplitude in the first case, Fig. 15, was much smaller than the second, Fig. 16.

Therefore, a useful way to evaluate and compare nonlinear viscoelastic behavior is to plot the amplitude spectrum for increasing strain amplitudes in three dimension (τ, f, γ_o). Fig. 17 shows a 3D amplitude spectrum for process fat-free mozzarella at 30°C. Clearly the higher, odd harmonics exceed the signal noise with increasing strain amplitude. Low strain amplitudes create a flat bed, while higher values create peaks and valleys, the peaks being the odd harmonics. Plots like this can therefore be used to approximate the conditions at which the stress response will no longer be sinusoidal, and the degree of nonlinearity with respect to the strain amplitude. Another useful plot is the effect of strain amplitude on $\tau_m(f_o, \gamma_o)$ and $\delta_m(f_o, \gamma_o)$ as shown in Figures 18 and 19.

The smaller peaks occuring as even harmonics are caused by mechanical interference. The DFT thus proves to be an extremely useful tool in distinguishing and eliminating undesired spectral components from the stress response.

5.3.3 Frequency Matching

Before conducting LAOS tests, the sampling rate and number of samples must be carefully selected to give the desired frequency range and resolution. The time series should be collected so that components of the DFT occur exactly at multiples of the test frequency f_o. Spectral lines between adjacent DFT components can give incorrect amplitudes, or may not even appear in the DFT due to poor frequency resolution (Giacomin, 1987). Also, the sampling interval must be small enough so that the highest frequency of interest is below the Nyquist frequency.

This procedure of adapting the time series to the DFT is known as frequency matching, and the following guidelines have been developed by Giacomin (1987) to accomplish this.

1. Select the desired test frequency f_o.

   Avoid mechanical resonant frequencies of the rheometer and principal harmonics of 60 Hz.

2. Decide how many higher harmonics are needed, H.

   For LAOS, a value between 8-10 is recommended. Fewer can be used for SAOS.

3. Compute desired Nyquist frequency, $N_{QD} = \frac{3Hf_o}{2}$.

4. Select number of samples, N.

   N is chosen such that computer memory is not exceeded and so that a practical computation time will result.

5. Compute desired sampling interval, $\Delta t_D = \frac{1}{2N_{QD}}$.

6. Choose available clock speed, Δt, closest to Δt_D.

   If the desired sampling rate is unavailable on the data acquisition system, then the nearest value below Δt_D is chosen.

7. Compute Nyquist frequency, $N_Q = \frac{1}{2\Delta t}$; where $N_Q \geq N_{QD}$.

8. Compute required test period, $T = N\Delta T$.

9. Compute frequency resolution, $\Delta f_o = \frac{1}{N\Delta t}$.

10. Compute upper limit for test frequency.

    The maximum allowable test frequency which can provide a frequency-matched frequency spectrum is $f_{\max} = \frac{2N_Q}{3H}$. The adjusted test frequency must satisfy $f_o \le \frac{2N_Q}{3H}$.

11. Compute required integer of cycles, C.

    C must satisfy $(Tf_o - 1) < C \le Tf_o$. C is the highest integer below Tf_o.

12. Adjust test frequency to collect C cycles.

    Hence, the "matched" test frequency will be $f_m = \frac{C}{T}$. If the matched frequency differs significantly from the desired frequency then a larger number of samples must be chosen.

5.4 Material Characterization Loops

The DFT provides a complete mathematical description of the nonlinear viscoelastic response to LAOS. However, these results are more complex than the linear viscoelastic case, where $G'(\omega)$ and $G''(\omega)$ can be used. They now consist of amplitudes and phase angles for as many harmonics as can be identified in the response.

Therefore, an extremely useful technique to characterize material response in LAOS is with stress *versus* strain, or stress *versus* shear rate loops (Dealy and Wissbrun, 1990). For the linear viscoelastic case these loops are ellipses, but with higher harmonics, the loops distort. Fig. 20 shows stress *versus* strain loops for four week old pizza cheese at 40°C. For liquids, the stress *versus* shear rate loops have been found to be more distinctive than the stress *versus* strain loops (Tee and Dealy, 1975), as shown in Fig. 21. The nonlinearities of the response can be clearly identified by the distortion of the two-fold symmetric loops. Although the higher harmonics might not exceed 5% of the fundamental, they profoundly affect the loop shape (Giacomin and Dealy, 1993).

The stress *versus* shear rate loop requires differentiation of the strain. Since the frequency spectra provide analytical expressions for the stress and strain, computation of this derivative from the DFT results is mathematically trivial. This technique of computing the derivative is called pseudodifferentiation (Giacomin, 1987).

5.5 Computer Code for Spectral Analysis

A FORTRAN computer code was developed for spectral analysis of LAOS test results using the DFT. This program computes the material properties $\tau_m(f_o,\gamma_o)$ and $\delta_m(f_o,\gamma_o)$ from the stress and strain signals (time series), and plots the results as stress *versus* strain and stress *versus* shear rate loops. A flowchart for the program is shown in Fig. 22 and the code is in Appendix C.

The program gives users the option of selecting the maximum number of harmonics to be included in the stress response. In theory, all the odd harmonics are material properties, but sometimes the amplitude spectrum shows higher harmonics that might appear to be material properties, but in reality are just noise. Including them in the stress response can be highly misleading. Therefore, to ensure accuracy, the program overlays the experimental (time series) stress-strain plot with the computed DFT results. If the fit is good, the harmonics selected are material properties, but if it is poor, the user has to go back and select the next lower harmonic. This process can be seen more clearly on the flowchart in Fig. 22. For cheese, the highest harmonic selected does not normally exceed five.

5.5.1 Numerical Differentiation

The shear rate can also be determined by numerical differentiation of the strain time series using a least squares method. Giacomin (1987) proposed using the method of Whitaker and Pigford (1960). However, numerical techniques should be avoided whenever possible, since the data are empirical and subject to various experimental errors such as noise. Errors can strongly affect the numerical derivative; noise is amplified. However, if the data is reasonably smooth and error free, numerical differentiation methods can accurately approximate the shear rate.

A FORTRAN code was developed to compute the numerical derivative of a time series using the *parabolic* least squares method (Perry, 1997) (see Appendix D).

CHAPTER 6 Results

6.1 Start-up Behavior

The stress response during start-up of LAOS was studied for the different cheeses. Figures 23 and 24 show the time trace of the shear stress response for reduced-fat mozzarella and pizza cheese at 60^{o}C. The stress waves reach steady state within four cycles. The peak stresses first increase, then level off. In general, all the natural cheeses reached steady state within four cycles at 60^{o}C, irrespective of their ages. Similar behavior was observed at 40^{o}C, as shown in Fig. 25 for reduced-fat cheddar. However, unlike at 60^{o}C, the peak stresses at 40^{o}C decrease as they steady, and then continue to decline over time, signifying cheese structure damage (Fig. 25). Fat-free process mozzarella also reached steady state within four cycles at both test temperatures.

6.2 Shear Stress *versus* Shear Rate Loops

Shear stress *versus* shear rate loops for mozzarella, cheddar, and pizza cheese for two test temperatures and four ages are shown in Figures 28 to 75. 3D amplitude spectra at 4 weeks and the effects of age are also included for both temperatures. The results are for a constant test frequency of 0.4 Hz.

Figures 76 and 77 show shear stress *versus* shear rate loops for fat-free *process* mozzarella at the two test temperatures, and Figures 17 and 78 show their 3D amplitude spectra. The results are for a constant test frequency of 0.25 Hz.

6.2.1 Effect of Strain Amplitude and Temperature

Figures 28 to 31 show shear stress *versus* shear rate loops for reduced-fat mozzarella at 40°C. Mozzarella was sheared in the direction of fiber orientation. At 1 week, the loops are elliptical up to a strain amplitude of 0.75, after which they become two-fold symmetric as higher harmonics matter (Fig. 33). As mozzarella ages, the elliptical range extends to a strain amplitude of 1. However, it was not possible to exceed strains of 3 due to slip. This was attributed to the entrapped fat globules in the casein network, which began to agglomerate at high shear rates. When this happened at the plate-sample interface, it caused slip. Fig. 34 shows 4 week mozzarella tests repeated using the same samples. The stresses are much lower than those in Fig. 29. Thus, the cheese structure is permanently damaged after repeated shearing at 40°C. This was also observed in the start-up behavior of mozzarella (Section 6.1). Figures 35 to 38 show shear stress *versus* shear rate loops for reduced-fat mozzarella at 60°C. The loops are elliptical at all strain amplitudes, meaning only the fundamental components of the stress response matter (Fig. 40). The melted cheese has a strong structure that adheres well to the plate surfaces and does not slip. As a result, strains up to 10 were reached. Mozzarella also exhibited good repeatability at 60°C, as shown in Figures 41 and 42, with slightly higher stresses compared to Figures 35 and 37. Melted mozzarella therefore has good shearing properties at 60°C, meaning it does not fracture easily at high shear rates. However, as mozzarella aged to 12 weeks, repeatability worsened as its structure weakened (Fig. 43).

Similar behavior was observed for reduced-fat cheddar at both test temperatures, as shown in Figures 44 to 58. At 40°C, the loops are elliptical up to a strain amplitude of 0.75,

after which they become two-fold symmetric. As with mozzarella, it was not possible to exceed strains of 2.5 without slip. Cheddar, however, exhibited relatively good repeatability at 4 weeks (Fig. 50), but not at 12 weeks (Fig. 51). At 60°C, the loops are elliptical at all strain amplitudes (Figures 52 to 55), with reduced-fat cheddar having a strong structure with good shearing properties.

Figures 59 to 72 show shear stress *versus* shear rate loops for pizza cheese at 40°C. The results resemble mozzarella and cheddar. The loops are elliptical up to strain amplitudes of 0.75 for reduced-fat pizza cheese, and 1 for full-fat pizza cheese. At both fat contents, it was not possible to exceed strains of 2.5 without causing slip. An interesting feature with full-fat pizza cheese was twisting of the loops upon slip (Fig. 65). Fig. 26 shows the time trace of the shear stress response for full-fat pizza cheese at a strain amplitude of 4. The irregular stress wave is caused by slip. The corresponding shear stress *versus* shear rate loop in Fig. 27 demonstrates the twisting. At 60°C, the loops become elliptical at all strain amplitudes, as shown in Figures 67 to 72. However, slip was still a problem with full-fat pizza cheese at 60°C, and strains of 4 could not be exceeded. At 12 weeks, tests could not be conducted because pizza cheese softened and dripped down the plates. Pizza cheese exhibited poor repeatability with significant structure damage at both test temperatures and fat contents.

Figures 76 and 77 show shear stress *versus* shear rate loops for fat-free process mozzarella at 30°C and 35°C. At 30°C, the cheese is extremely soft and slips at strains greater than 1. Slip is caused by fracture of the cheese structure at high shear rates, and this is seen by loop twisting at a strain amplitude of 1.4 (Fig. 76). As the cheese melts at 35°C,

higher strains are reached without slip (Fig. 77), and the loops are concentric in contrast to the behavior at 30°C. At both temperatures, higher harmonics matter at strains above 0.5 (Figures 17 and 78), making the loops two-fold symmetric. Repeatability on same samples was poor for fat-free process mozzarella at both test temperatures due to its weak structure.

6.2.2 Effect of Age on Natural Cheeses

Mozzarella, cheddar, and pizza cheese softened with age due to proteolysis. Figures 32 and 39 show the effect of age on shear stress *versus* shear rate loops for reduced-fat mozzarella at 40°C and 60°C. The stresses decrease with age, and the loop areas reduce. Similar results were obtained for reduced-fat cheddar (Fig. 48) and reduced-fat and full-fat pizza cheese. In general, the cheese structure weakens with age due to proteolytic changes, thus improving flow characteristics and cheese meltability.

6.2.3 Comparing the Natural Cheeses

Mozzarella, cheddar, and pizza cheese behaved similarly at both test temperatures. At 40°C, the loops were elliptical up to strain amplitudes of about 0.75, after which they became two-fold symmetric. 3D amplitude spectra at 40°C showed the higher, odd harmonics rising with increasing strain amplitude (Figures 33, 49, and 63). Strain amplitudes above 2.5 caused agglomeration of the fat globules, which led to sample slip, and this was more pronounced in full-fat pizza cheese. Repeating the tests at 40°C caused structure damage for all three cheeses. At 60°C, the loops were elliptical at all strain amplitudes and strains up to 10 were reached, and unlike at 40°C, the loops were intersecting. 3D amplitude spectra at

60°C (Figures 40, 56, and 70) showed only the fundamental harmonic at the test frequency being significant. Mozzarella and cheddar had good repeatability at 60°C, but pizza cheese did not. In general, all three cheeses exhibited good shearing properties at 60°C with a stronger structure compared to 40°C.

Figures 74 and 75 compare shear stress *versus* shear rate loops for 4 week old reduced-fat mozzarella, cheddar, and pizza cheese at 40°C and 60°C. Mozzarella and cheddar have similar shapes and stresses, while pizza cheese is much softer with significantly lower stresses. Similar results were obtained at the other ages. Pizza cheese therefore has better melt and flow properties. Since pizza cheese is *unstretched* mozzarella (Section 1.4), the difference between the two cheeses can be attributed to the fiber orientation in mozzarella.

6.2.4 Effect of Fat Content in Pizza cheese

Fig. 73 shows the effect of fat content on shear stress *versus* shear rate loops for pizza cheese at 40°C and 60°C. Full-fat pizza cheese is much softer, with approximately half the stresses of reduced-fat pizza cheese. Therefore, it will flow more easily.

6.3 Fourier Analysis

Figures 79, 81, and 83 show the effect of strain amplitude on the first three odd harmonics of shear stress for reduced-fat mozzarella, cheddar, and pizza cheese at 4 weeks and 40°C. Mozzarella is linear up to a strain amplitude of 1 (i.e. τ_1 is proportional to γ_o and

shear stress *versus* shear rate loops are elliptical), after which the higher harmonics, τ_3 and τ_5, emerge (Fig. 79). Similarly, cheddar and pizza cheese are linear up to strain amplitudes of about 0.75 (Figures 81 and 83). These results agree with the findings in Section 6.2.1. However, unlike mozzarella and cheddar, pizza cheese also appears to exhibit a yield stress since τ_1 *versus* γ_o does not extend through the origin (Fig. 83). Figures 80, 82, and 84 show the effect of strain amplitude on the phase angles of the principal harmonics of shear stress for the three natural cheeses. δ_1 increases with increasing strain amplitude for all three cheeses, while δ_3 and δ_5 behave irregularly. Figures 85, 86, and 87 compare δ_1, δ_3, and δ_5 for the three cheeses at 40°C. In Fig. 85, δ_1 rises from an average value of 0.3 radians to about 0.65 radians for the three cheeses. Similarly, in Figures 86 and 87, δ_3 and δ_5 have similar shapes for the three cheeses, with δ_5 for mozzarella and cheddar almost overlapping at $\gamma_o / \gamma_{max} \geq 0.4$. In summary, the behavior of all three cheeses was similar at 40°C, with mozzarella and cheddar being the closest.

For the natural cheeses at 60°C, only the fundamental harmonic of the shear stress is significant (Figures 40, 56, and 70). Figures 88 to 96 show the effect of strain amplitude on τ_1 and δ_1 for reduced-fat mozzarella, cheddar, and pizza cheese at 60°C. The results are for 1, 4, and 6 weeks. τ_1 for mozzarella is linear up to a strain amplitude of 8 at 1 week (Fig. 88), and stays linear up to strain amplitudes of about 7 at weeks 4 and 6 (Figures 89 and 90). The linear ranges of τ_1 for cheddar and pizza cheese do not extend to such high strain amplitudes, and pizza cheese again exhibits a yield stress (Figures 95 and 96). Probably the most interesting feature at 60°C is that δ_1 for all three cheeses does not depend on strain

amplitude. Also, τ_1 at 60°C exceeds τ_1 at 40°C for the three cheeses. Fig. 97 compares the effect of age on the average fundamental phase angles $<\delta_1>$ for the three cheeses at 60°C. $<\delta_1>$ increases with age for all three cheeses, with pizza cheese having the highest value. $<\delta_1>$ for mozzarella and cheddar nearly overlap at weeks 1 and 4, but not at week 6. $<\delta_1>$ for mozzarella and pizza cheese run parallel to each other, pizza cheese having the higher value. $\tan\delta_1$ has been found to serve as an indicator of cheese meltability (Ruegg *et al.*, 1991; Olson *et al.*, 1996). Therefore, since pizza cheese has a higher $\tan\delta_1$, it will have better melting characteristics than mozzarella. This agrees with the results in Section 6.2.3.

Figures 18 and 19 show the effect of strain amplitudes and phase angles of the principle harmonics of shear stress for fat-free process mozzarella at 30°C. The linear range of τ_1 is narrow, extending only to a strain amplitude of 0.4, after which the higher harmonics matter (Fig. 17). The phase angles follow trends similar to reduced-fat natural mozzarella at 40°C. δ_1 increases with increasing strain amplitude, while the higher harmonics, δ_3 and δ_5, are irregular with shapes similar to natural mozzarella (Figures 19 and 80).

6.4 Comparisons to the Lodge Rubberlike Liquid

The discrete relaxation spectrum for select cheeses was calculated from dynamic (SAOS) data using parsimonious modeling (Section 3.4.6). The departures from linearity were then studied by normalizing the shear stress with the Lodge rubberlike liquid prediction:

$$\frac{\tau(t)}{\tau_o} = \frac{\tau(t)}{\gamma_o\sqrt{(G')^2 + (G'')^2}} \tag{6.1}$$

Figures 98 to 101 show the discrete relaxation spectrum for 6 week old reduced-fat mozzarella and cheddar at 40°C and 60°C. Four to six (G_i, λ_i) pairs sufficed to fit the experimental data reasonably. Fig. 102 compares the Lodge rubberlike liquid to LAOS results for reduced-fat cheddar at 40°C. There is reasonable agreement. Figures 105 and 106 show the departures from linearity for reduced-fat cheddar at 40°C and 60°C. Cheddar is almost linear at 40°C, though it slightly over predicts the stresses; but at 60°C it is highly nonlinear, predicting only 4-5% of the linear stresses. Figures 103 and 104 show the departures from linearity for reduced-fat mozzarella at 40°C and 60°C. Unlike cheddar, mozzarella is nonlinear at 40°C, predicting 24-40% of the linear stresses (Fig. 103). At 60°C, mozzarella becomes highly nonlinear, predicting only 8-12% of the linear stresses (Fig. 104). Therefore, although the shear stress *versus* shear rate loops for both cheeses are elliptical at 60°C, they are still highly nonlinear. There is no known constitutive equation that predicts nonlinearity without loop distortion.

Figures 107 and 108 show the discrete relaxation spectrum for fat-free process mozzarella at 30°C and 35°C. Five to nine (G_i, λ_i) pairs sufficed to fit the experimental data reasonably. Figures 109 and 110 show the corresponding normalized shear stress *versus* shear rate loops. Fat-free process mozzarella is highly nonlinear at both test temperatures, and this behavior resembles reduced-fat natural mozzarella.

CHAPTER 7 Conclusion

LAOS adequately measured the nonlinear viscoelasticity of cheese, and spectral analysis proved useful in characterizing and comparing the different cheese types. Natural mozzarella, pizza cheese, and cheddar demonstrated similar behavior in both the melted and solid states. They exhibited a strong structure with good shearing properties at 60°C, but not at 40°C. The loops were elliptical at all strain amplitudes at 60°C, but highly nonlinear when compared to the Lodge rubberlike liquid. Pizza cheese was softer than mozzarella, with better melt and flow properties. The difference between the two cheeses was attributed to fiber orientation in mozzarella. All three natural cheeses softened with age due to proteolysis, thus weakening the structure and improving flow properties. Process fat-free mozzarella was much softer compared to the natural cheeses, and highly nonlinear. Fat reduction in pizza cheese roughly doubled the stress amplitudes. This underscores the contemporary industrial challenge of formulating reduced-fat pizza cheese while matching its texture to full-fat pizza cheese.

LAOS was therefore extremely useful in evaluating and comparing cheese rheologies. However, work is needed in overcoming slip at 40°C, so that large strain behavior can be studied. More work is also needed in understanding how nonlinear viscoelasticity affects cheese texture. Other constitutive theories should also be evaluated to gain a better understanding of the nature of cheese in relation to its chemical and physical structure. There are no known constitutive equations that predict intersecting loops, and none that predict nonlinearity without loop distortion.

Mozzarella mixing during manufacture employs open discharge single screw extrusion, and classical screw design requires only the steady shear viscosity curve (Baird and Collias, 1995). In the plastics industry, the Cox-Merz rule is frequently used to obtain the steady shear viscosity:

$$\eta(\dot{\gamma}) = |\eta^*(\omega)|; \qquad \omega = \dot{\gamma} \tag{7.1}$$

where $|\eta^*(\omega)|$ is the complex viscosity. In future work, the Cox-Merz rule should therefore be experimentally verified for mozzarella.

Tables

Table 1 Comparing geometries used for LAOS measurements. Extracted from Giacomin and Dealy (1993).

Geometry	Advantages	Disadvantages	Literature
Cone-plate	1. Homogeneous flow field 2. Suitable for strain amplitudes less than one	1. Large strains cause sample outflow, degradation, and fracture at edges 2. Normal stress effects distort free boundary	MacSporran and Spiers (1984) Pearson and Rochefort (1982)
Parallel-disk	1. Suitable for small strain measurements in the linear viscoelastic region	1. Heterogeneous flow field 2. Sample outflow and degradation at edges leading to fracture 3. Normal stress effects distort free boundary	MacSporran and Spiers (1984) Powell and Schwarz (1979) Spiers (1977)
Concentric Cylinder	1. Nearly homogeneous flow field at small strains	1. Weissenberg effect causes severe distortion of free boundary at strains greater than 10	Onogi and coworkers (1970; 1973; 1981) Dealy and coworkers (1975; 1973)
Sliding Cylinder	1. Nearly homogeneous flow field at small strains	1. Large strains cause sample outflow and degradation at edges	Tsai and Soong (1985) McCarthy (1978) Hibberd and coworkers (1966; 1975)
Sliding-plate (total force measurement)	1. Nearly homogeneous flow field at small strains	1. Edge effects at large strains 2. Error due to friction in guide mechanisms	Liu *et al.* (1983; 1984) Sivashinsky *et al.* (1984)
Sliding-plate true shear rheometer (shear-stress transducer)	1. Homogeneous flow field 2. Can neglect flow heterogeneity near sample edges 3. Prolonged sample life	1. Limited displacement of sliding plate	Giacomin *et al.* (1989) Giacomin (1987) Giacomin and Dealy (1986)

Table 2 Shear stress transducer calibration data (Lan, 1997).

Stress Range (kPa)	30	30
Mass Used (kg)	0.1	0.202
Calculated Stress (kPa)	13.105	26.329
Computer Stress Readout (kPa)	11.2	22.9
Ideal Calibration Constant (kPa/kg)	130.2	130.2
New Calibration Constant (kPa/kg)	$130.2 \times (13.105/11.2)$ =**152**	$130.2 \times (13.105/11.2)$ =**150**

Stress Range (kPa)	300	300
Mass Used (kg)	1.009	1.515
Calculated Stress (kPa)	131.51	197.41
Computer Stress Readout (kPa)	114.80	171.00
Ideal Calibration Constant (kPa/kg)	130.2	130.2
New Calibration Constant (kPa/kg)	$130.2 \times (131.51/114.8)$ =**149**	$130.2 \times (197.41/171.0)$ =**150**

Table 3 Composition of the *natural* cheeses.

1 week							
Cheese Type	% Fat	% Moisture	% MNFP[1]	% FDM[2]	% Salt	% S/M[3]	pH
RF Pizza[4]	12.4	53.2	60.7	26.7	1.95	3.67	5.48
FF Pizza	21.1	51.4	6501	43.4	2.01	3.91	5.39
RF Ched	13.0	46.4	53.3	24.3	1.66	3.58	5.15
RF Mozza	10.2	52.2	58.1	21.3	1.32	2.53	5.39
4 weeks							
RF Pizza	12.8	53.1	60.9	27.3	1.89	3.56	5.44
FF Pizza	21.6	51.2	65.3	44.3	1.94	3.79	5.33
RF Ched	11.8	46.8	53.1	22.2	1.74	3.72	5.10
RF Mozza	7.5	52.4	56.6	15.8	1.27	2.42	5.31
6 weeks							
RF Pizza	11.5	52.9	59.8	24.4	1.56	2.95	5.41
FF Pizza	18.0	51.6	62.9	37.2	1.78	3.45	5.29
RF Ched	9.5	46.5	51.4	17.8	1.51	3.25	5.00
RF Mozza	9.9	52.3	58.0	20.8	1.44	2.75	5.25
12 weeks							
RF Pizza	11.3	53.0	59.8	24.0	2.07	3.90	5.34
FF Pizza	20.3	49.9	62.6	40.5	1.39	2.79	5.21
RF Ched	10.3	47.2	52.6	19.5	1.63	3.45	5.00
RF Mozza	8.25	52.4	55.3	17.3	1.32	2.52	5.07

[1] moisture-in-the-nonfat-portion

[2] fat in the dry matter

[3] salt/moisture

[4] **FF** ≡ full fat, **RF** ≡ Reduced fat, **Pizza** ≡ Pizza cheese, **Ched** ≡ Cheddar, and **Mozza** ≡ Mozzarella

Table 4 *Natural* mozzarella, pizza cheese, and cheddar test schedule.

Strain Amplitude, γ_o	**Plate Displacement (mm)**		**Frequency (Hz)**
	0.36mm gap	*0.5mm gap*	
0.10	0.036	0.050	0.4
0.50	0.180	0.250	0.4
0.75	0.270	0.375	0.4
1.00	0.360	0.500	0.4
1.50	0.540	0.750	0.4
2.00	0.720	1.000	0.4
2.50	0.900	1.250	0.4
3.00	1.080	1.500	0.4
4.00	1.440	2.000	0.4
6.00	2.160	3.000	0.4
8.00	2.880	4.000	0.4
10.00	3.600	5.000	0.4

Table 5 *Process* mozzarella test schedule.

Strain Amplitude, γ_o	**Plate Displacement (mm)** *0.36mm gap*	**Frequency (Hz)**
0.28	0.10	0.25
0.42	0.15	0.25
0.56	0.20	0.25
0.69	0.25	0.25
0.83	0.30	0.25
1.11	0.40	0.25
1.39	0.50	0.25
2.78	1.00	0.25
4.17	1.50	0.25
5.56	2.00	0.25
6.94	2.50	0.25
8.33	3.00	0.25
9.72	3.50	0.25
11.11	4.00	0.25
13.89	5.00	0.25

Figures

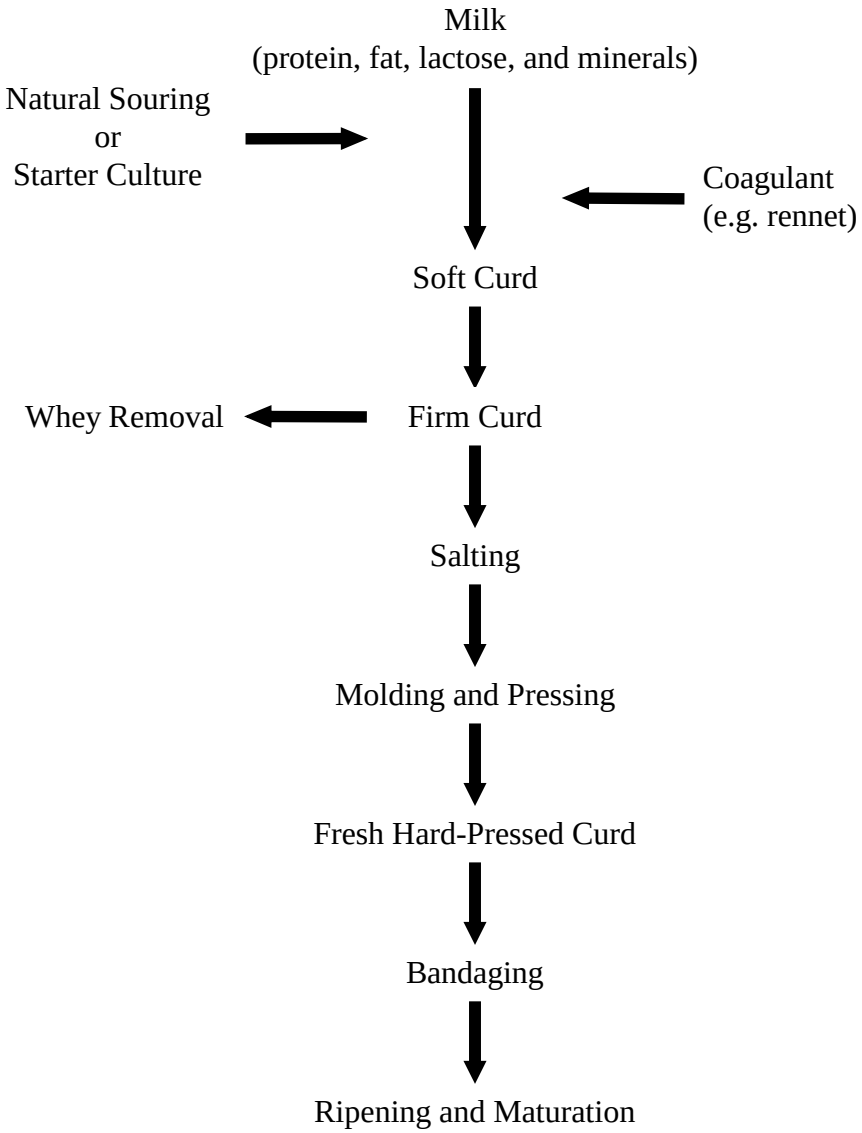

Figure 1 Basic stages of cheesemaking.

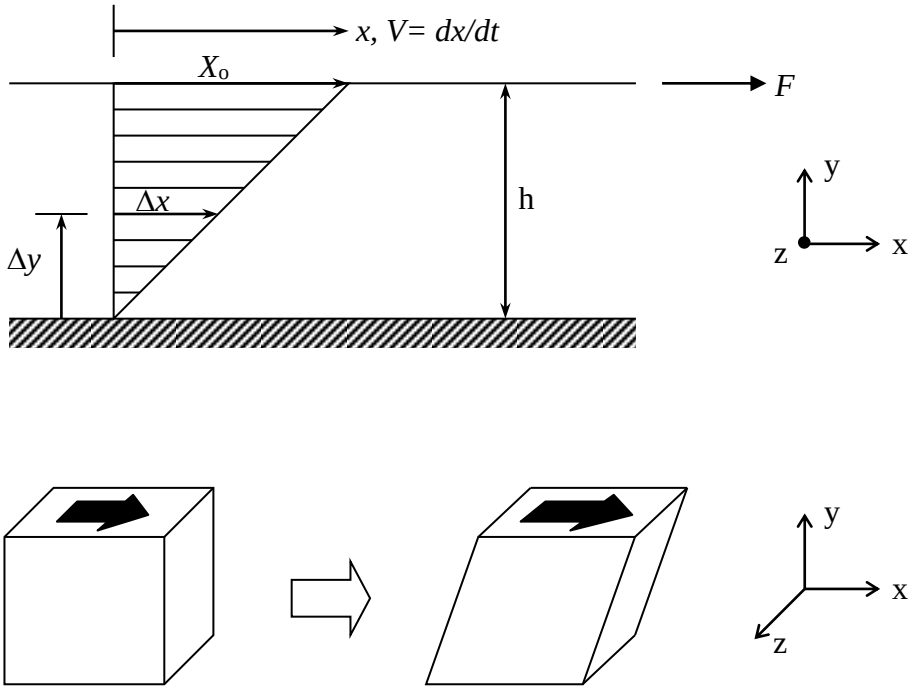

Figure 2 Simple shear

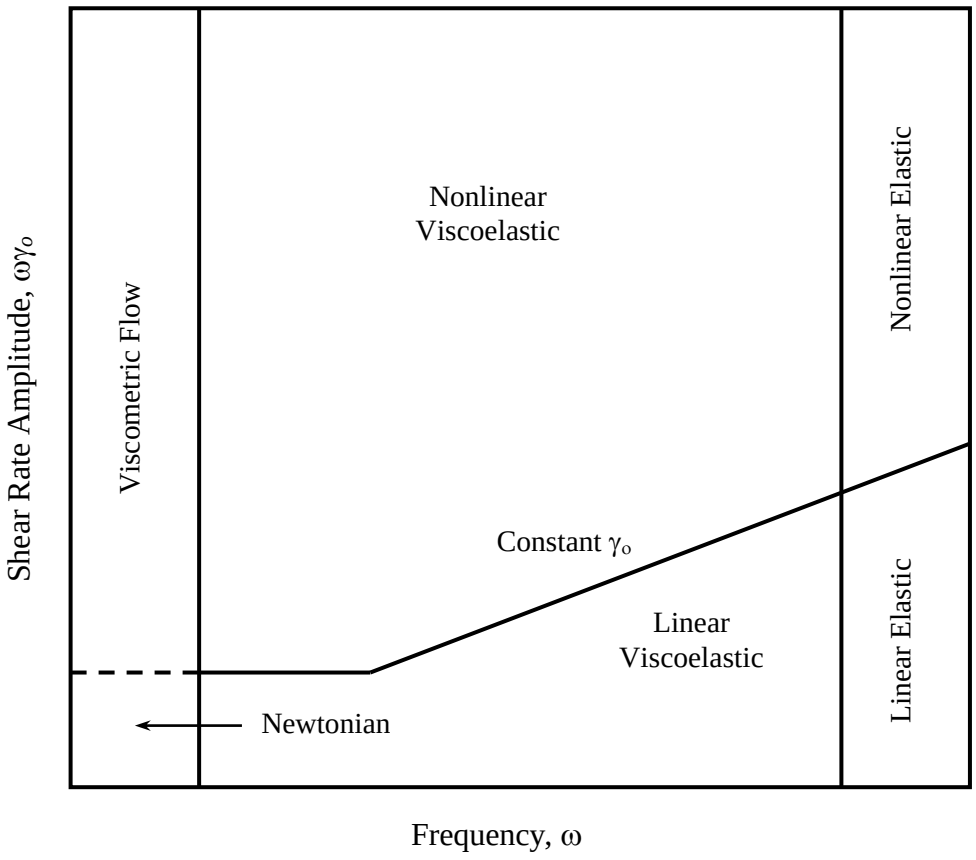

Figure 3 Pipkin diagram showing regimes of behavior for oscillatory shear. (Not to scale; viscometric flow and linear viscoelasticity zones are actually much narrower). Adapted from Dealy and Wissbrun (1990).

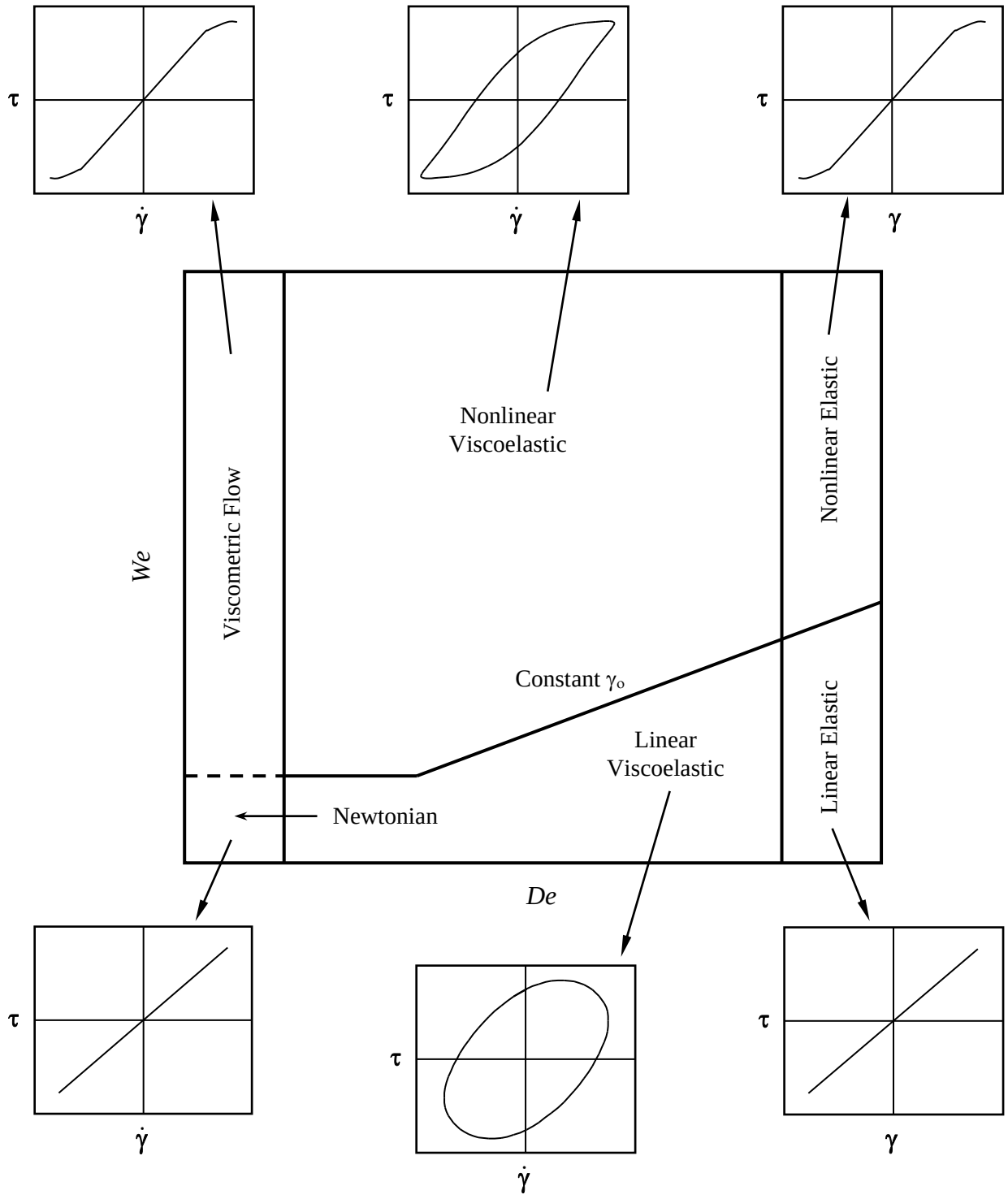

Figure 4 Pipkin diagram showing shear stress *versus* shear rate or *versus* shear strain loops for the regimes in oscillatory shear.

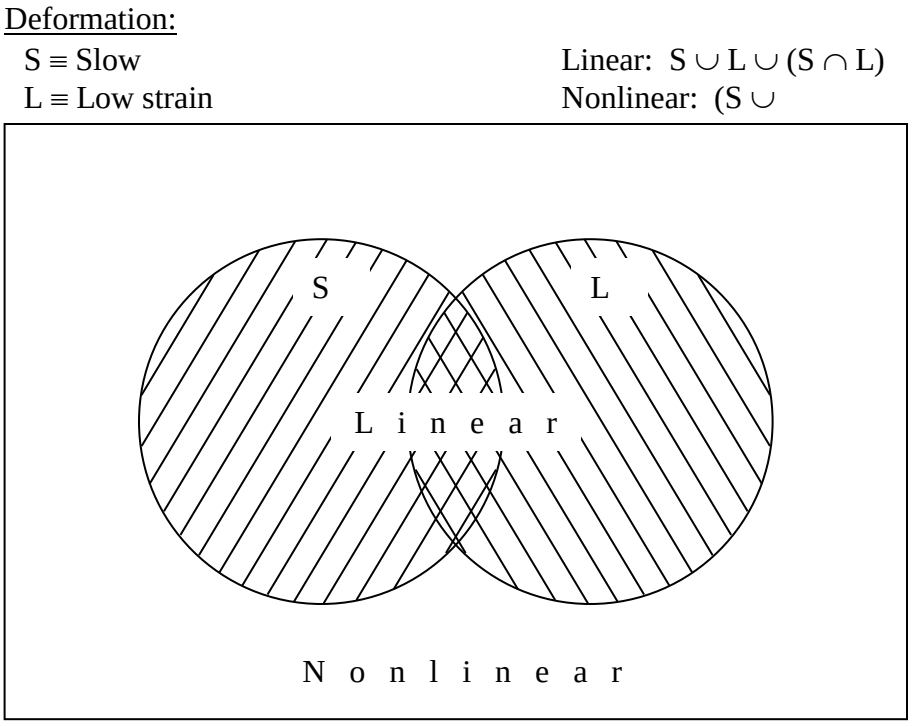

Figure 5 Venn diagram distinguishing linear and nonlinear viscoelastic behavior.

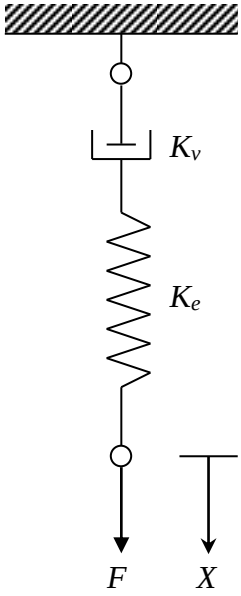

Figure 6 Maxwell element analog of a viscoelastic material.

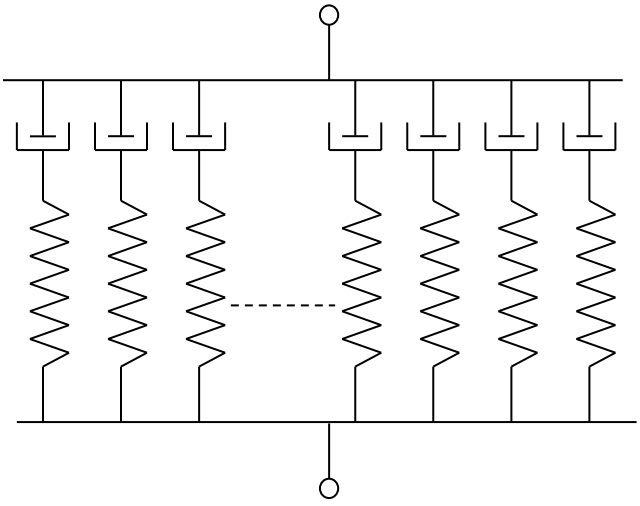

Figure 7 Mechanical analog of the generalized Maxwell model.

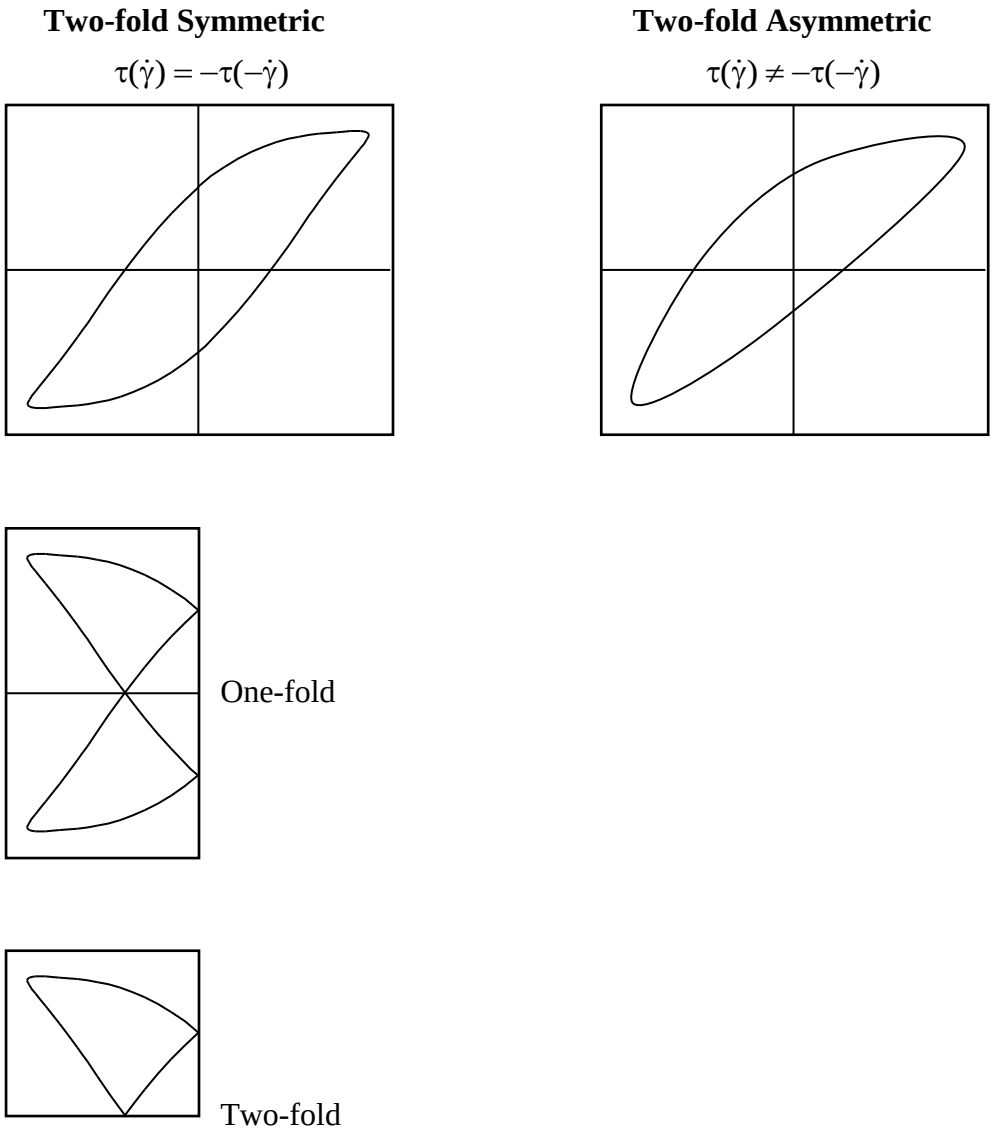

Figure 8 Two-fold symmetry

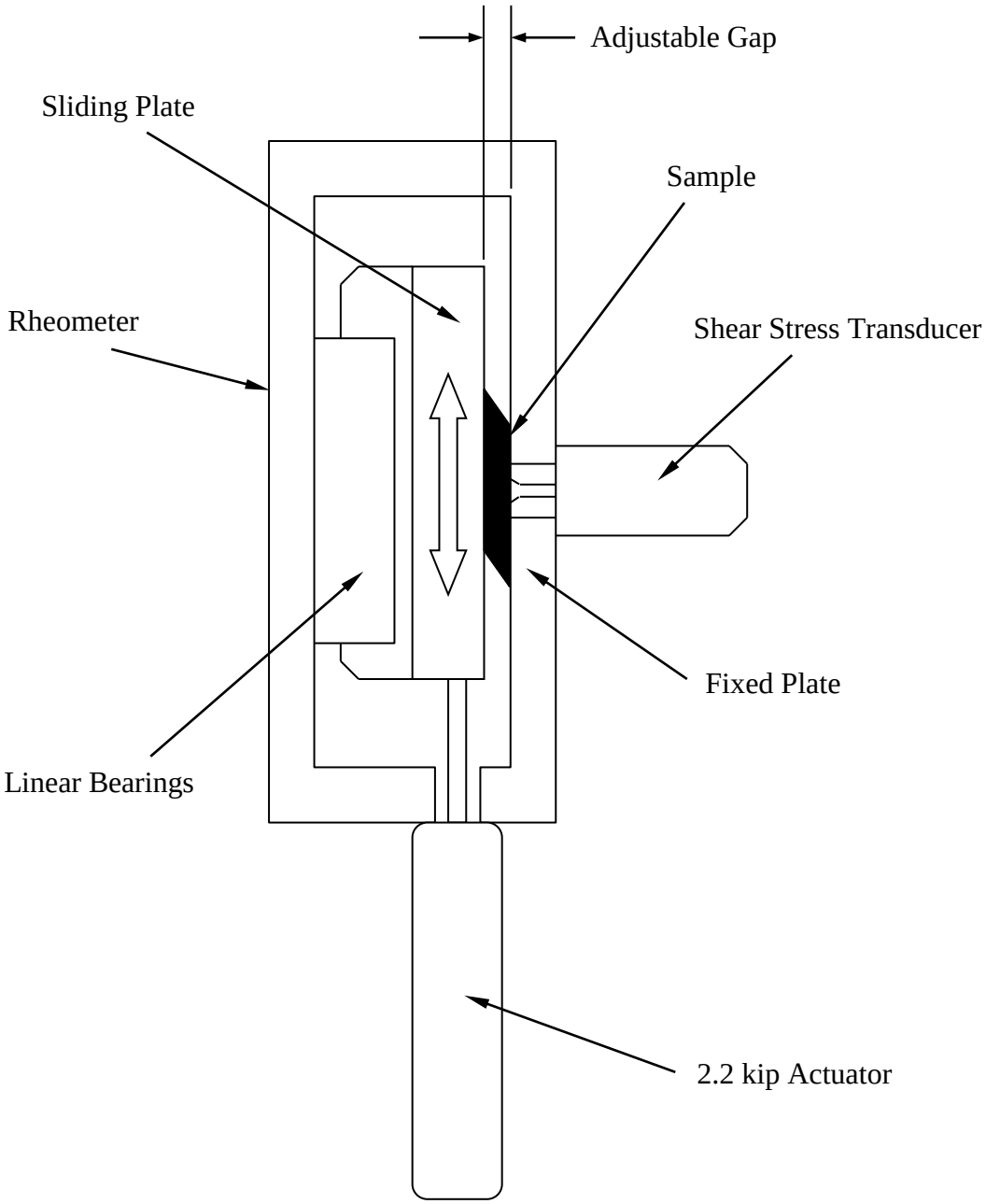

Figure 9 Interlaken sliding plate rheometer incorporating Dealy shear stress transducer (not to scale). Adapted from ITC rheometer manual.

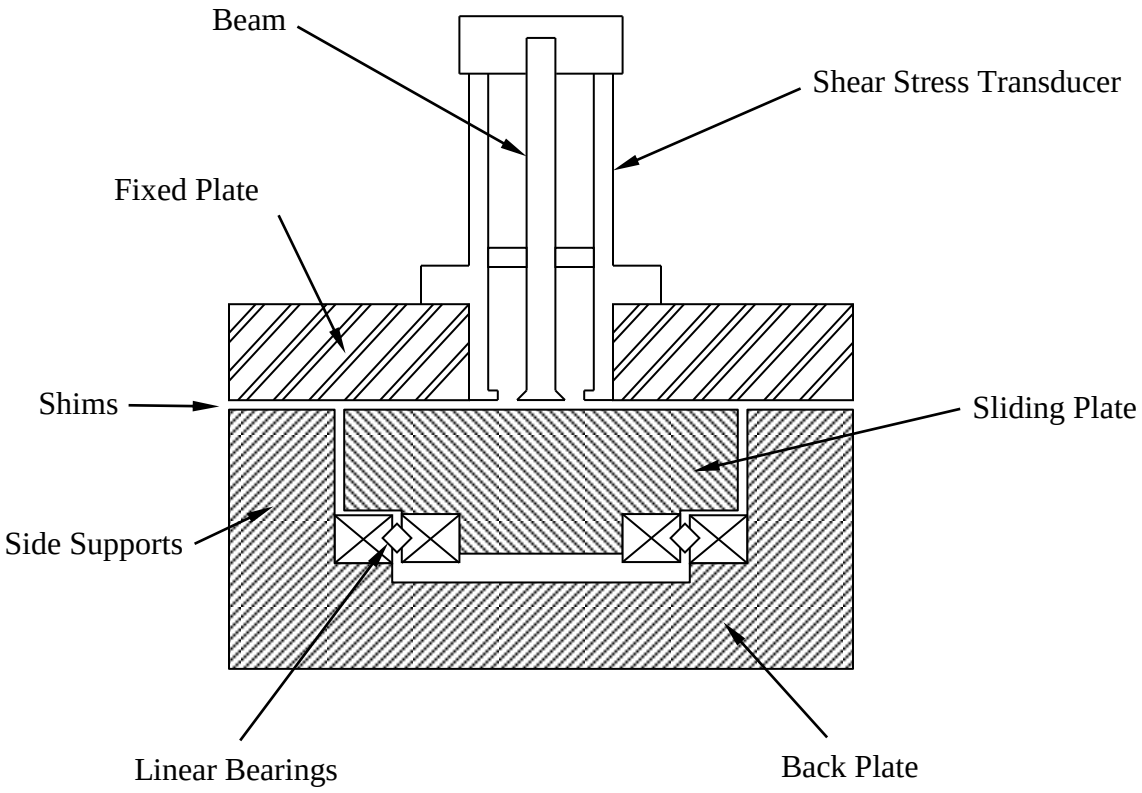

Figure 10 Top-view cross section of the sliding plate rheometer (not to scale). Sliding plate moves in and out of the plane of the paper. Adapted from Giacomin *et al.* (1989).

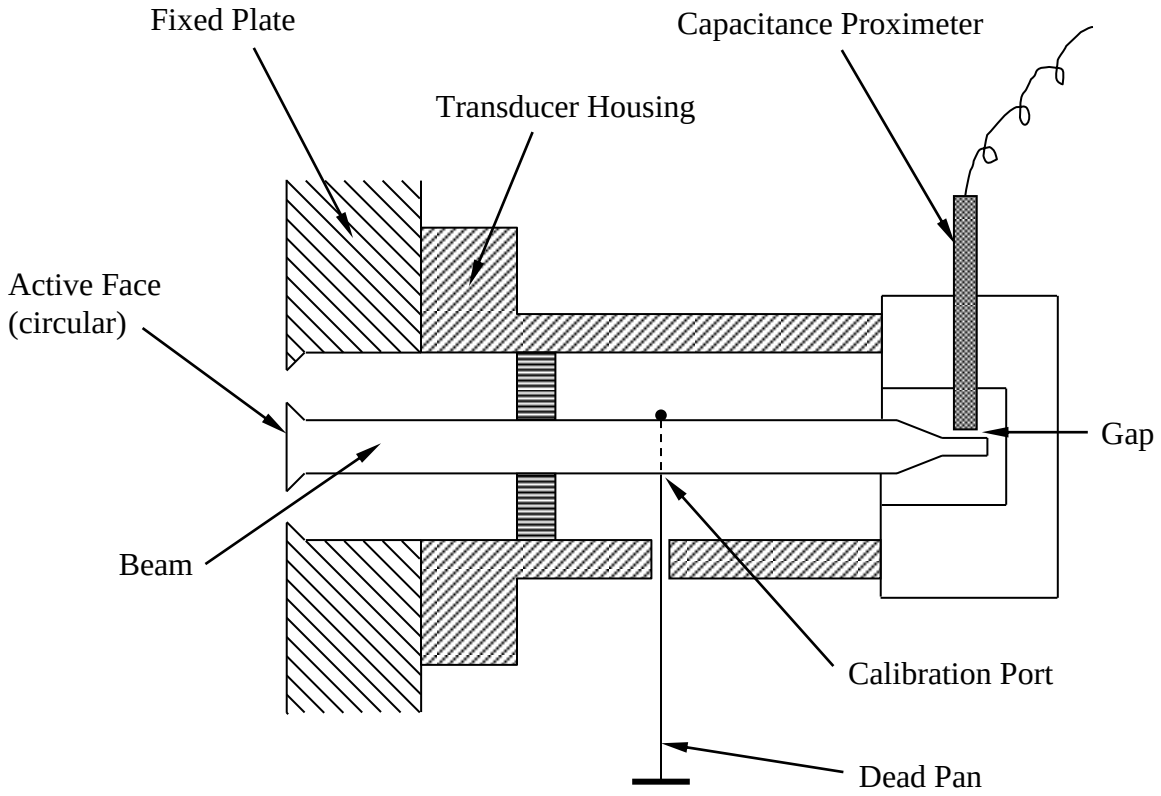

Figure 11 Side view cross section of SST showing beam and capacitance proximeter (not to scale).

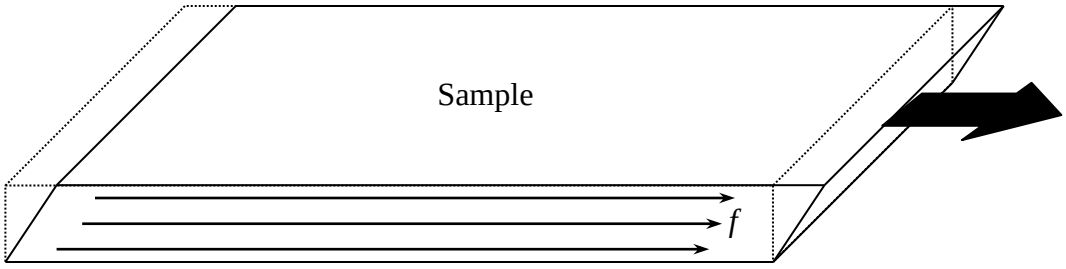

Figure 12 Rectangular mozzarella sample showing fiber orientation *f*.

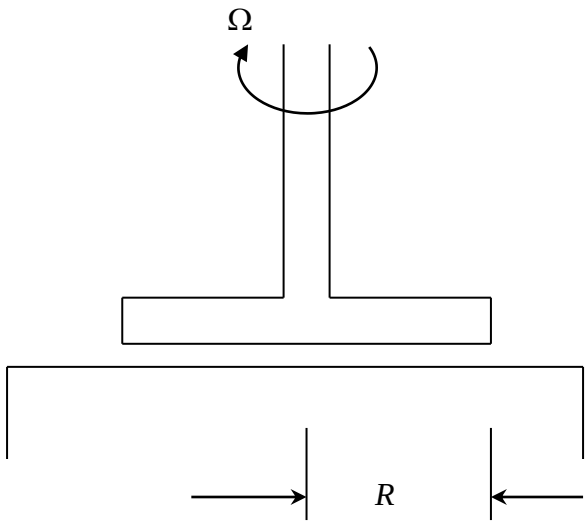

Figure 13 Parallel disk geometry

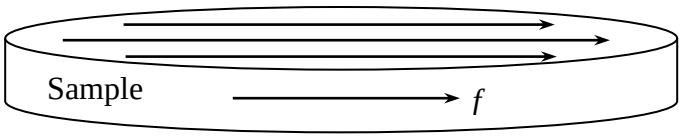

Figure 14 Disk-shaped mozzarella sample showing fiber orientation *f*.

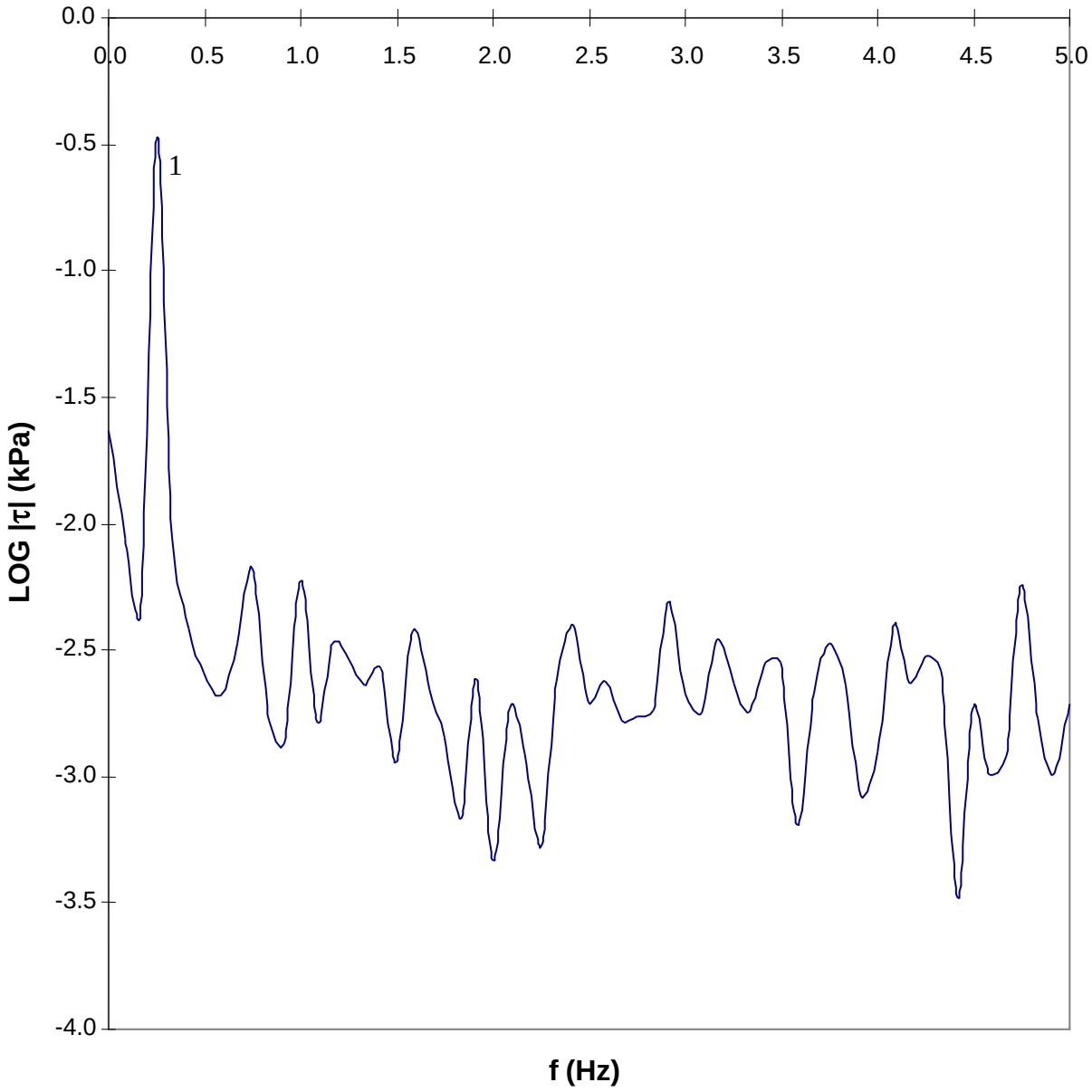

Figure 15 Amplitude spectrum for fat-free process mozzarella at 30°C and test frequency of 0.25 Hz. Only the fundamental harmonic is detectable at a low strain amplitude of $\gamma_o = 0.27$.

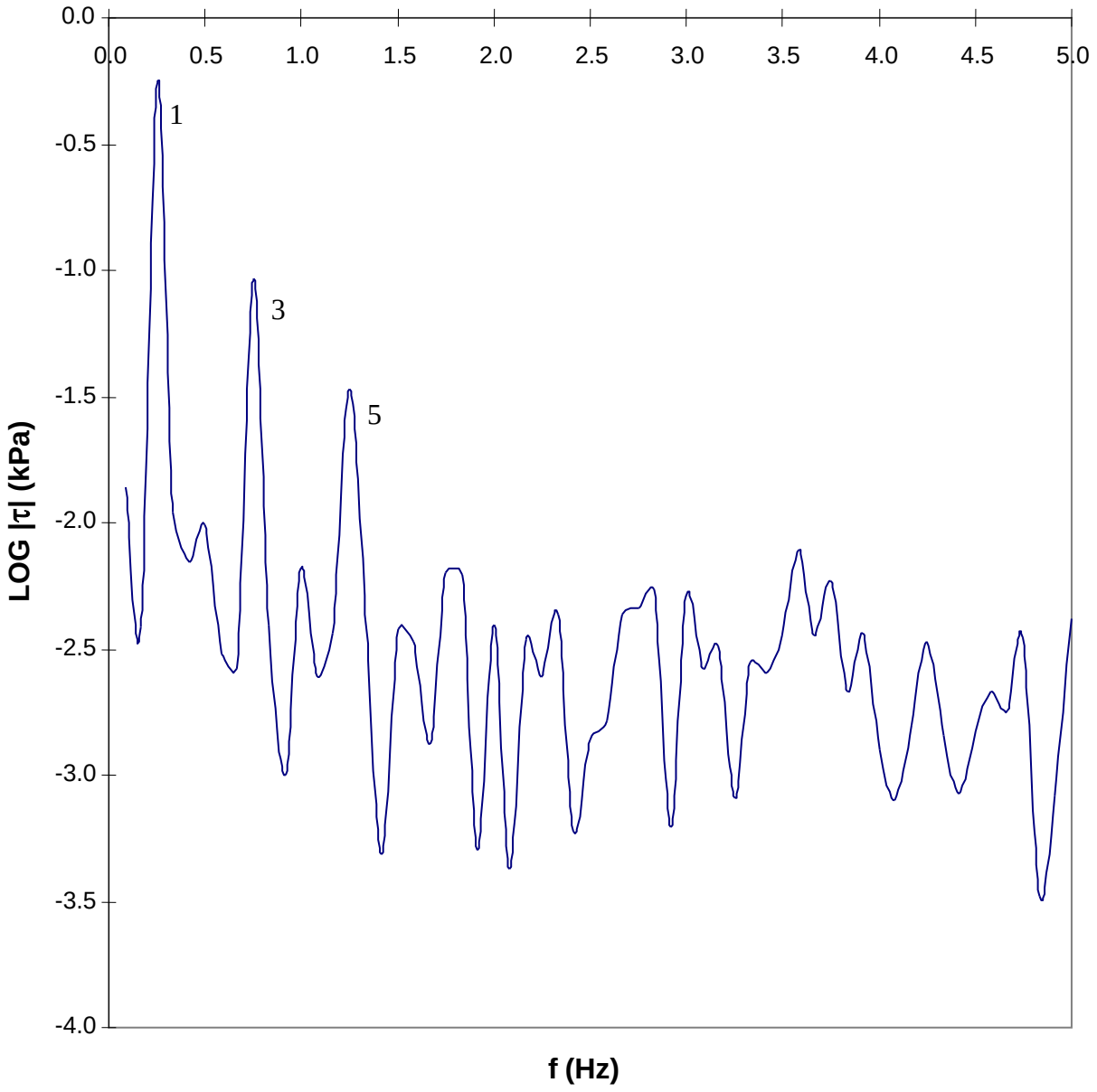

Figure 16 Amplitude spectrum for fat-free process mozzarella at 30°C and at a test frequency of 0.25 Hz. First three *odd* harmonics are now detectable at a higher strain amplitude of $\gamma_o = 1.38$.

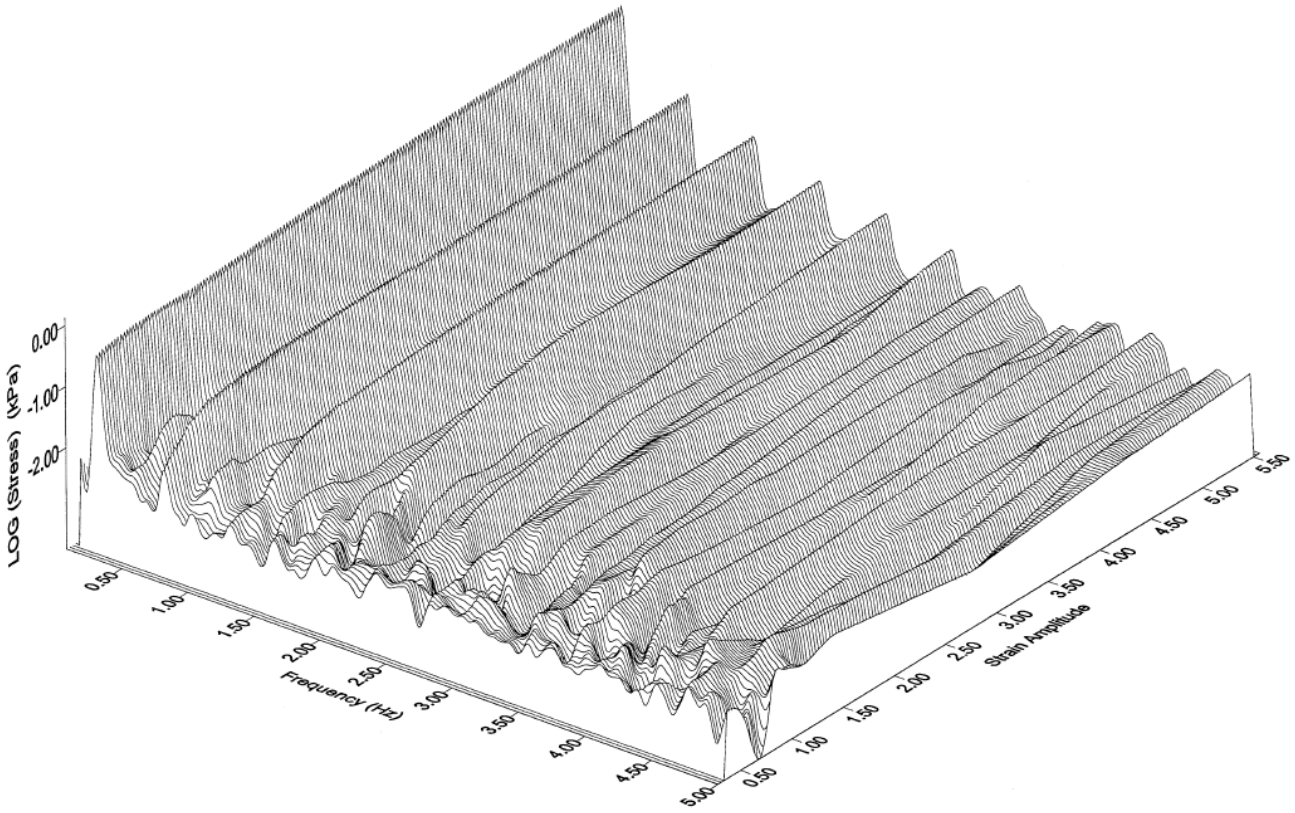

Figure 17 3D Amplitude spectrum for fat-free process mozzarella at 30ºC and test frequency of 0.25 Hz. The higher, odd harmonics rise with strain amplitude.

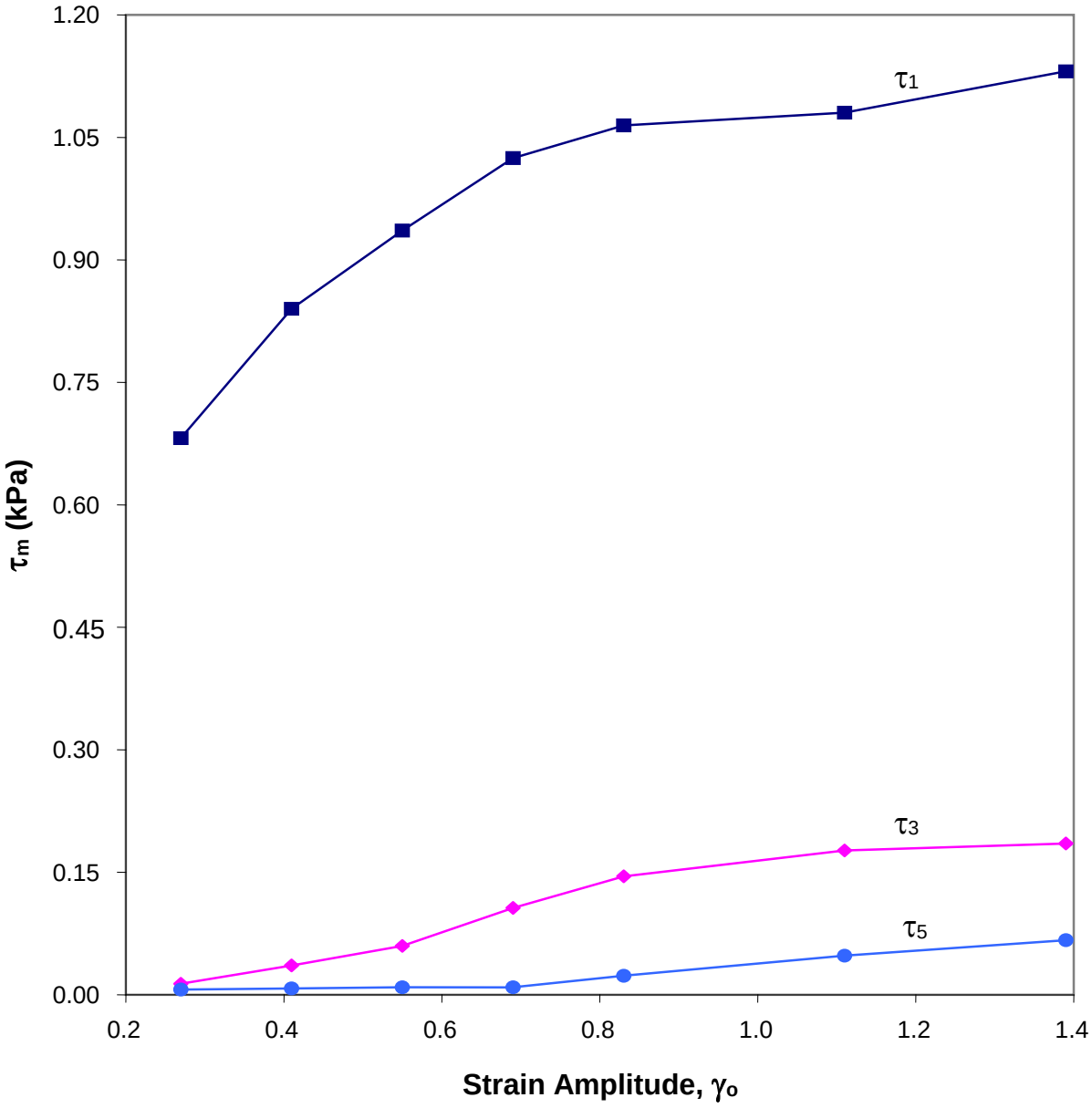

Figure 18 Effect of γ_o on fundamental, third, and fifth harmonics of shear stress for fat-free process mozzarella at 30°C and test frequency of 0.25 Hz. The higher, odd harmonics rise with γ_o.

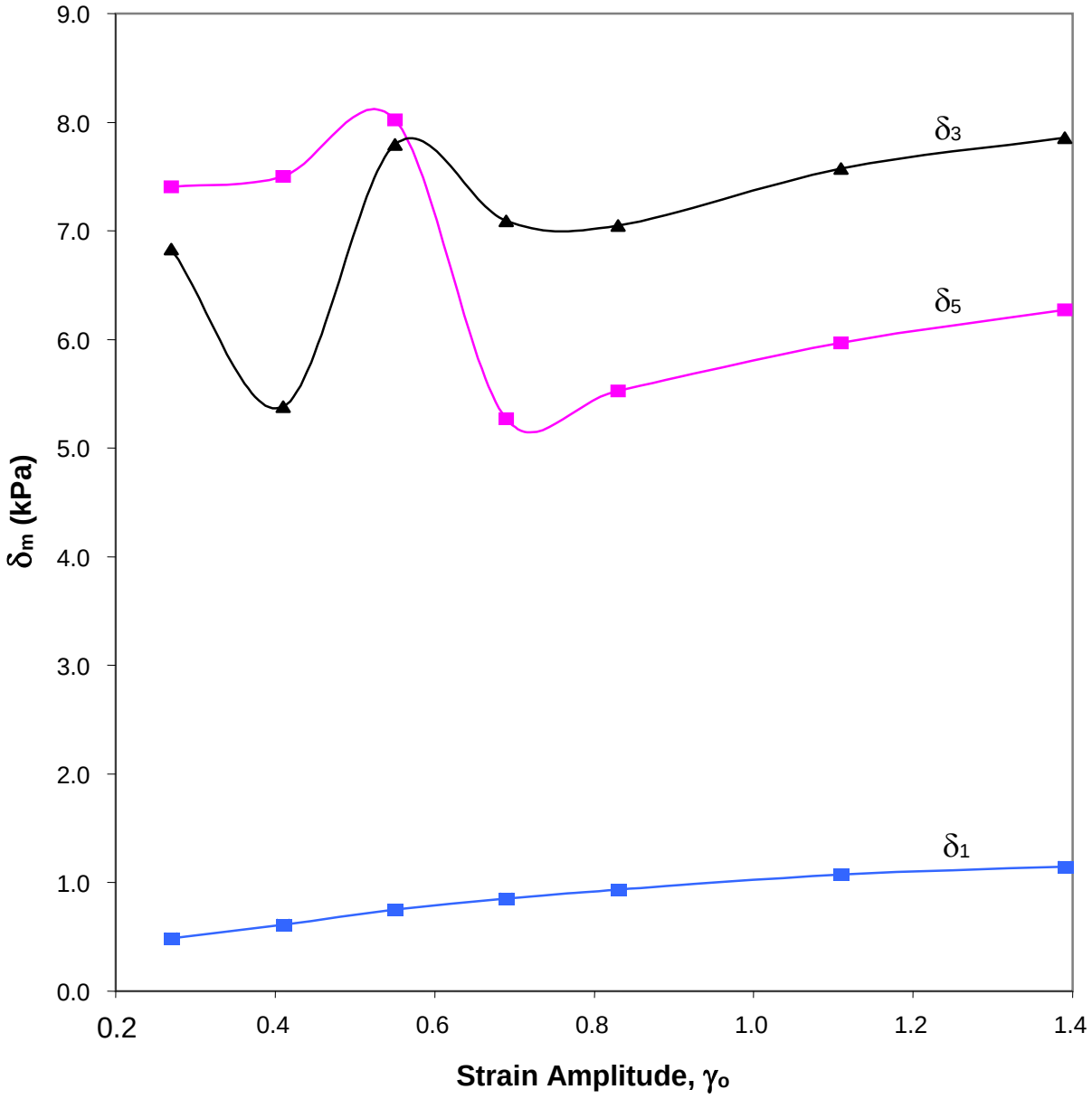

Figure 19 Effect of γ_o on the phase angles of the principal harmonics of shear stress for fat-free process mozzarella at 30°C and test frequency of 0.25 Hz. δ_1 rises with γ_o, while δ_3 and δ_5 are not monotonic with γ_o.

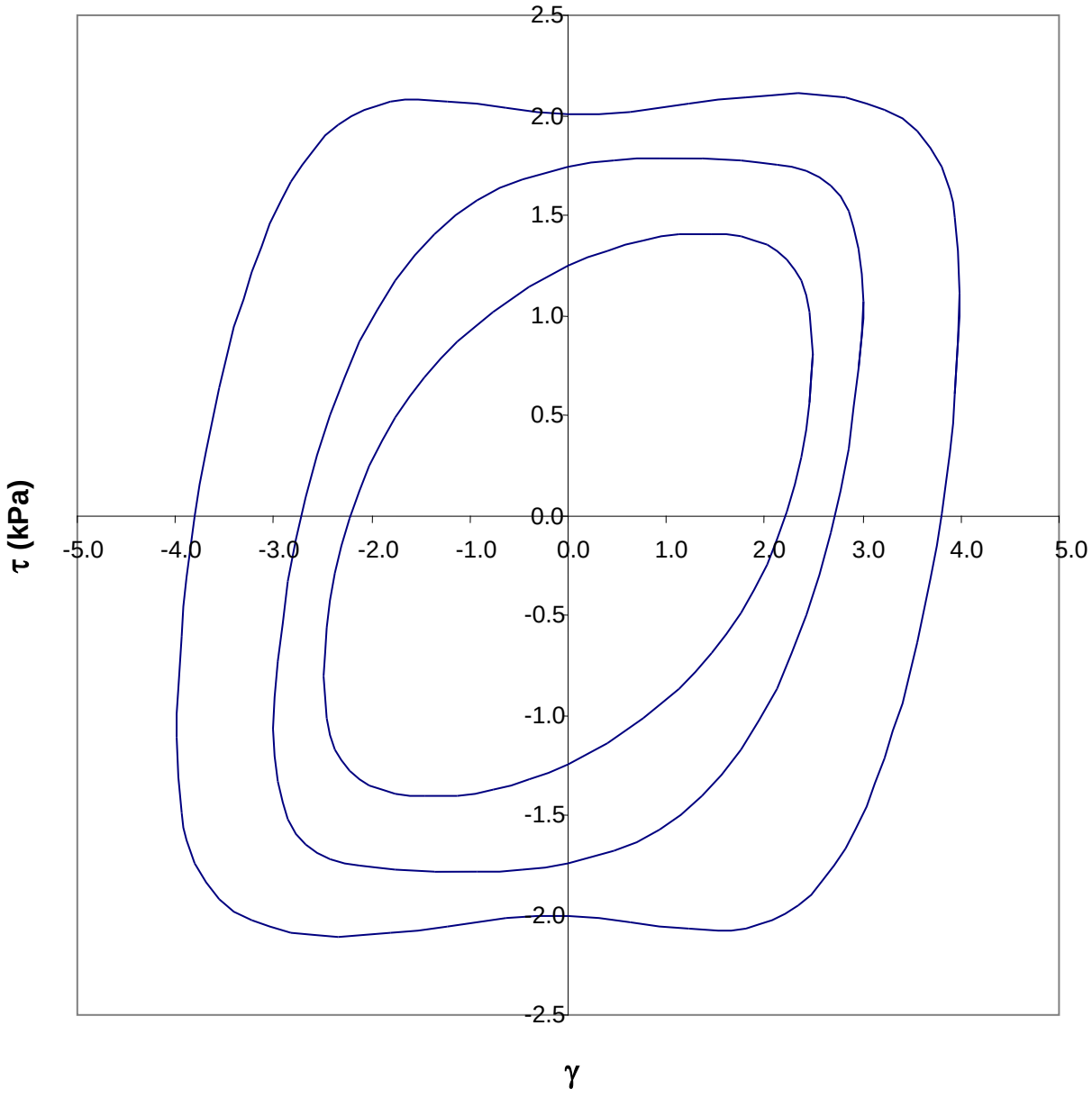

Figure 20 Shear stress *versus* shear strain loops for 4 week old full-fat pizza cheese at 40^{o}C and test frequency of 0.4 Hz. Strain amplitudes are 2.5, 3, and 4. Nonlinearities are distinguishable in this plot.

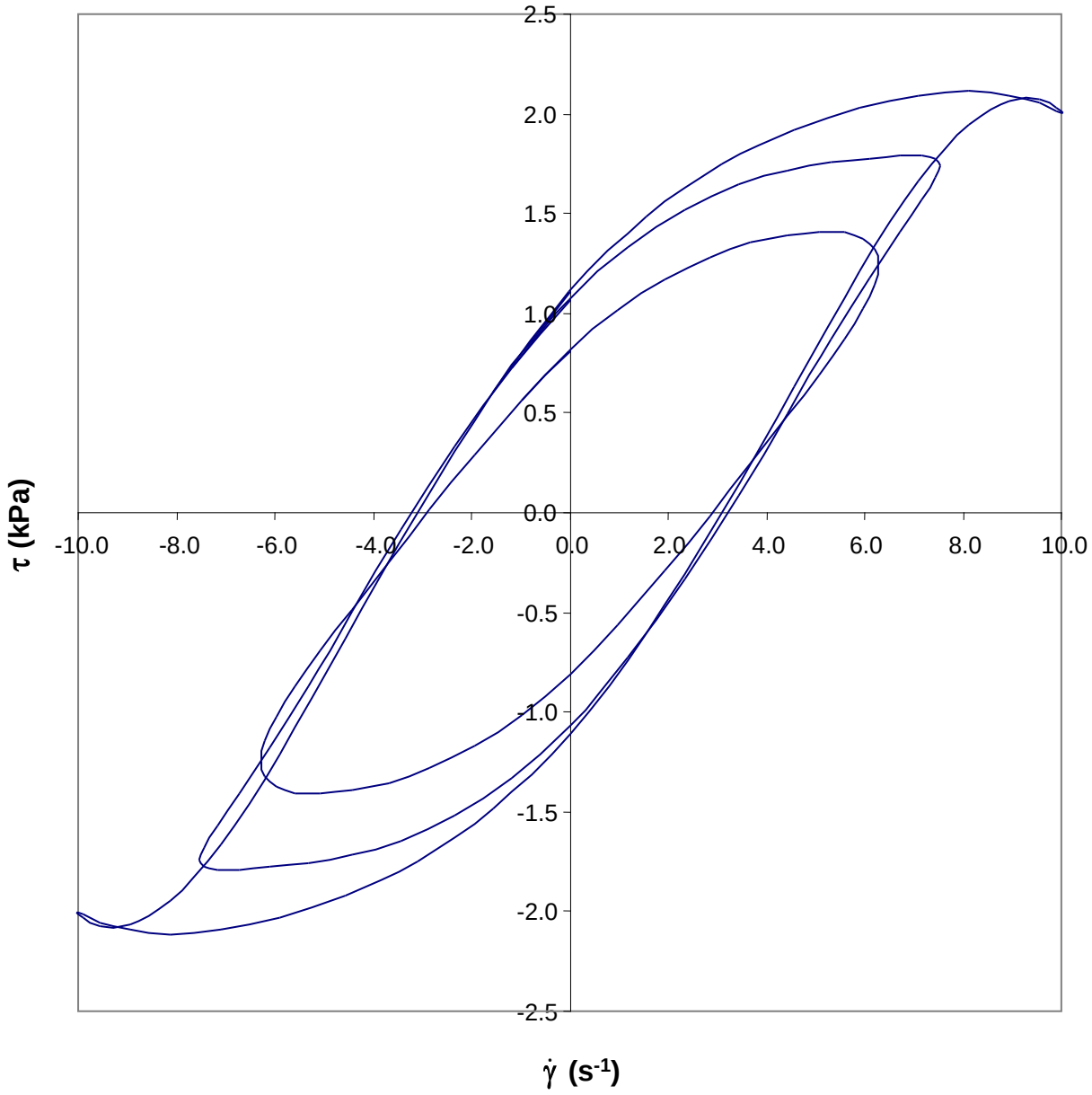

Figure 21 Shear stress *versus* shear rate loops for 4 week old full-fat pizza cheese at 40°C and test frequency of 0.4 Hz. Strain amplitudes are 2.5, 3, and 4. Nonlinearities are distinctive in this plot.

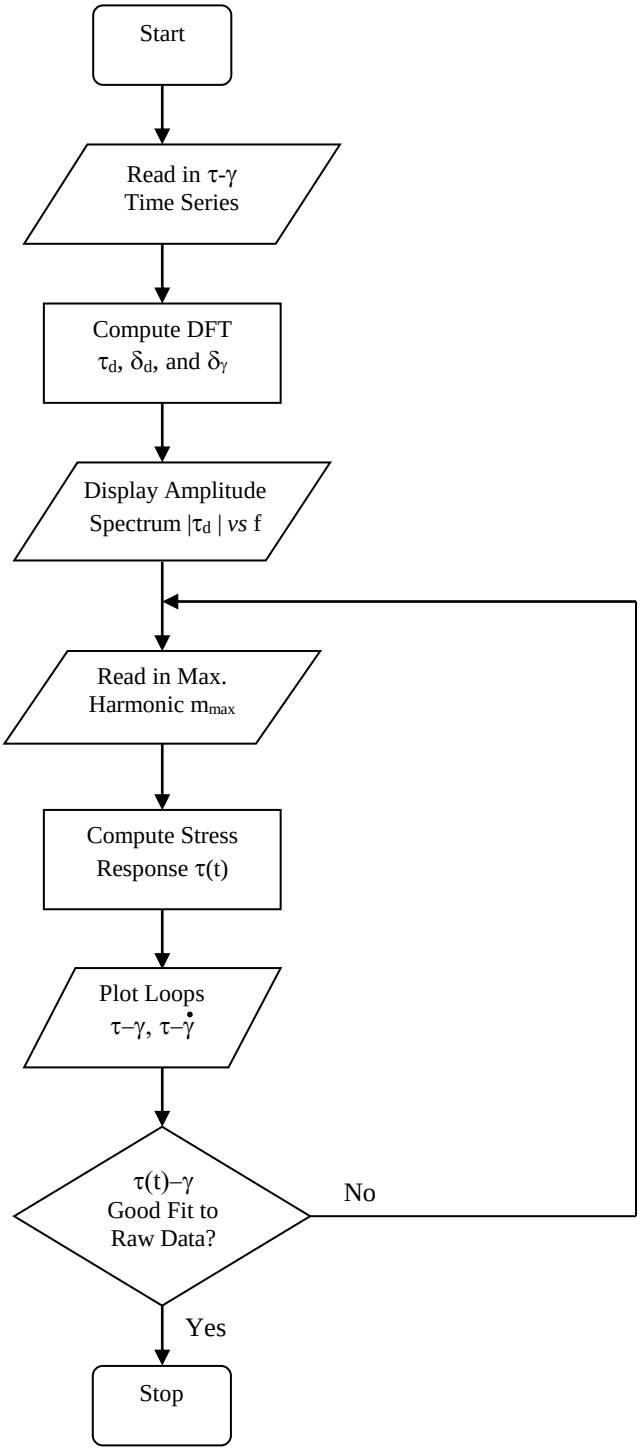

Figure 22 Flowchart for spectral analysis (Appendix C).

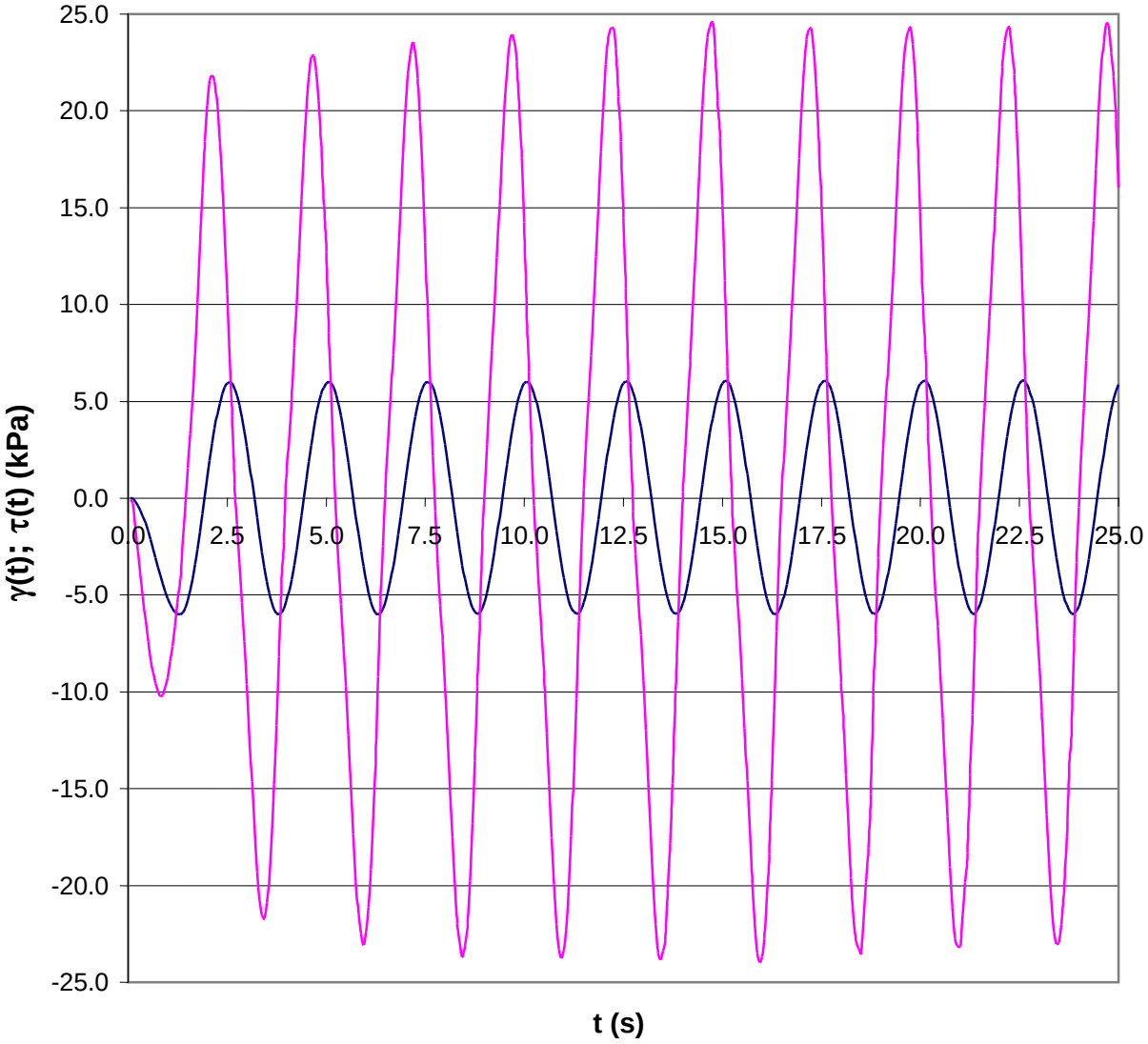

Figure 23 Time trace of shear stress response to strain amplitude, γ_o = 6, for 1 week old reduced-fat mozzarella at 60°C with f_o = 0.4 Hz. The stress wave reaches steady-state within four cycles.

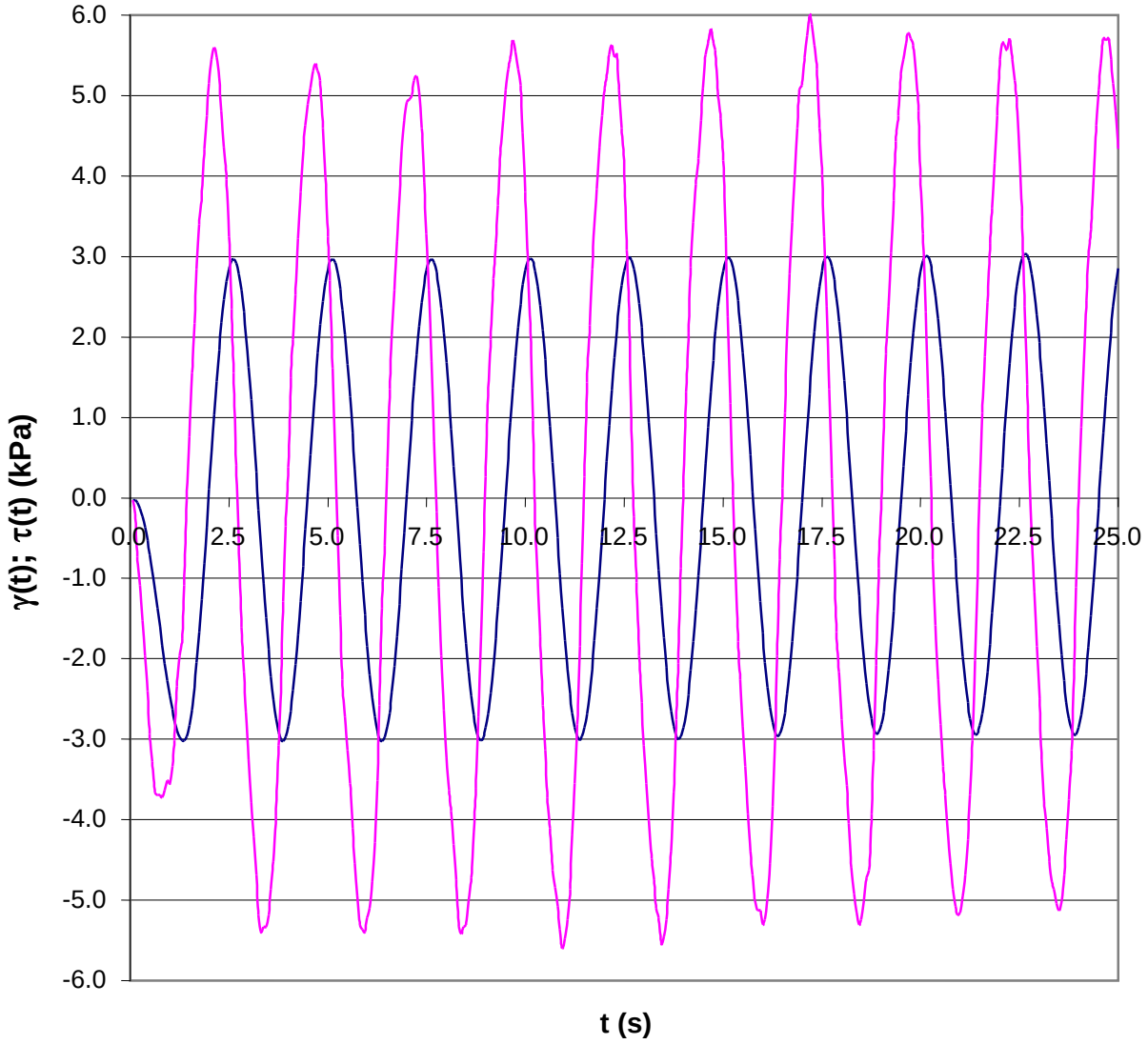

Figure 24 Time trace of shear stress response to strain amplitude, γ_o = 3, for 1 week old reduced-fat pizza cheese at 60°C with f_o = 0.4 Hz. The stress wave reaches steady-state within four cycles. Cycle-to-cycle differences are due to background noise.

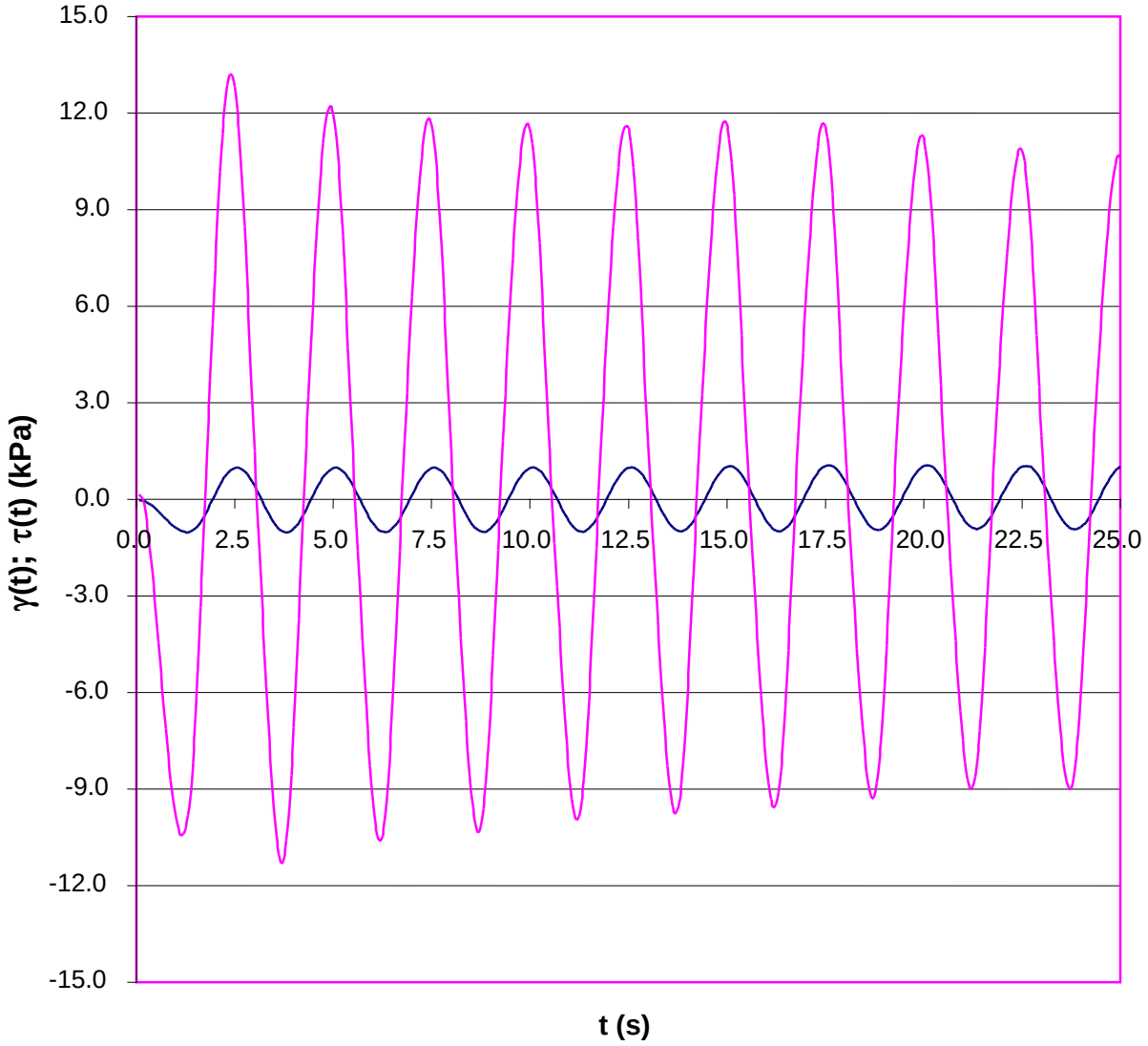

Figure 25 Time trace of shear stress response to strain amplitude, γ_o = 1, for 4 week old reduced-fat cheddar at 40°C with f_o = 0.4 Hz. The stress wave reaches steady-state within three cycles. Decrease in peak stress toward the end of waveform is due to structure damage.

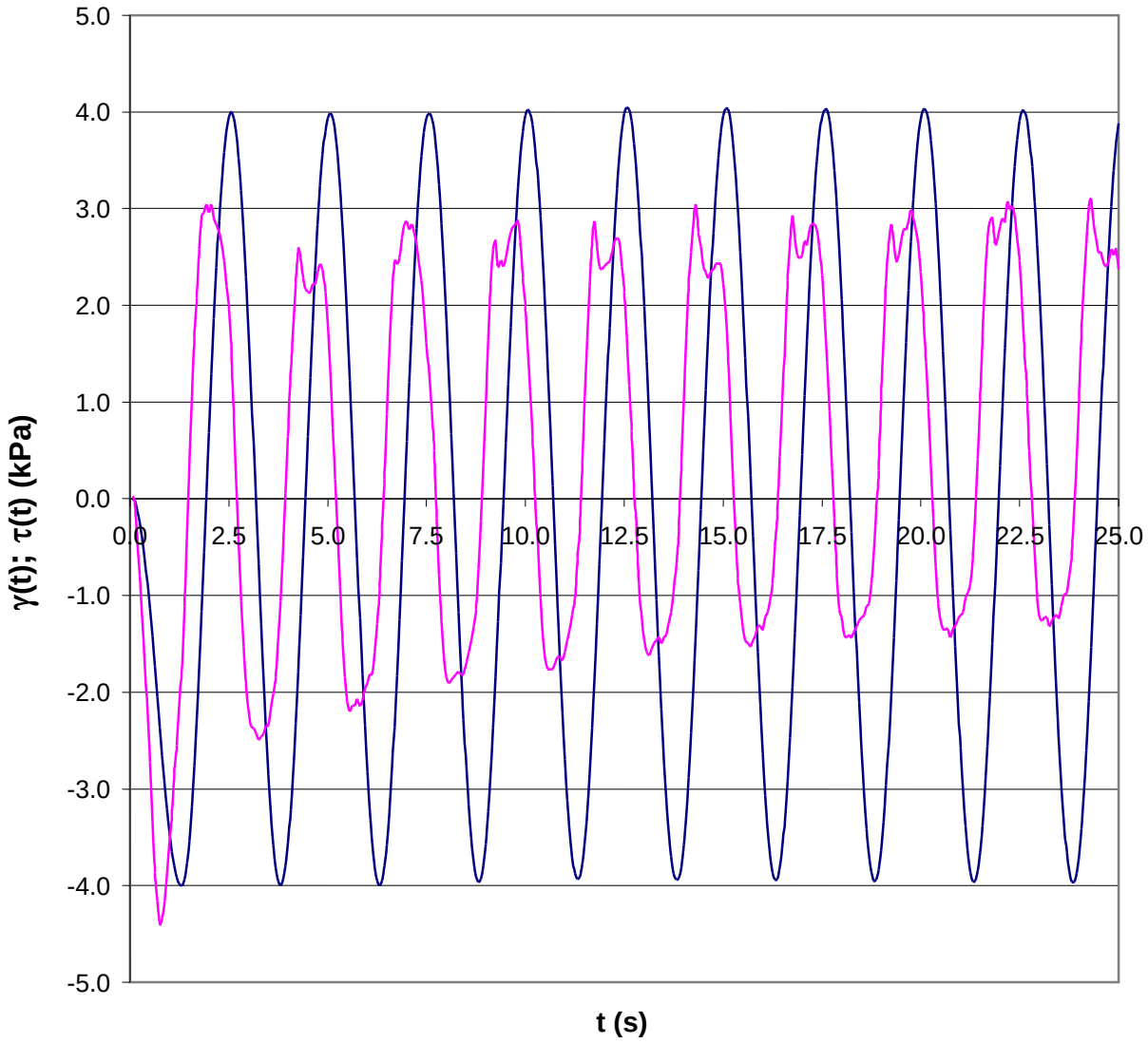

Figure 26 Time trace of shear stress response to strain amplitude, γ_o = 4, for 6 week old full-fat pizza cheese at 40°C with f_o = 0.4 Hz. The irregular stress response is caused by slip.

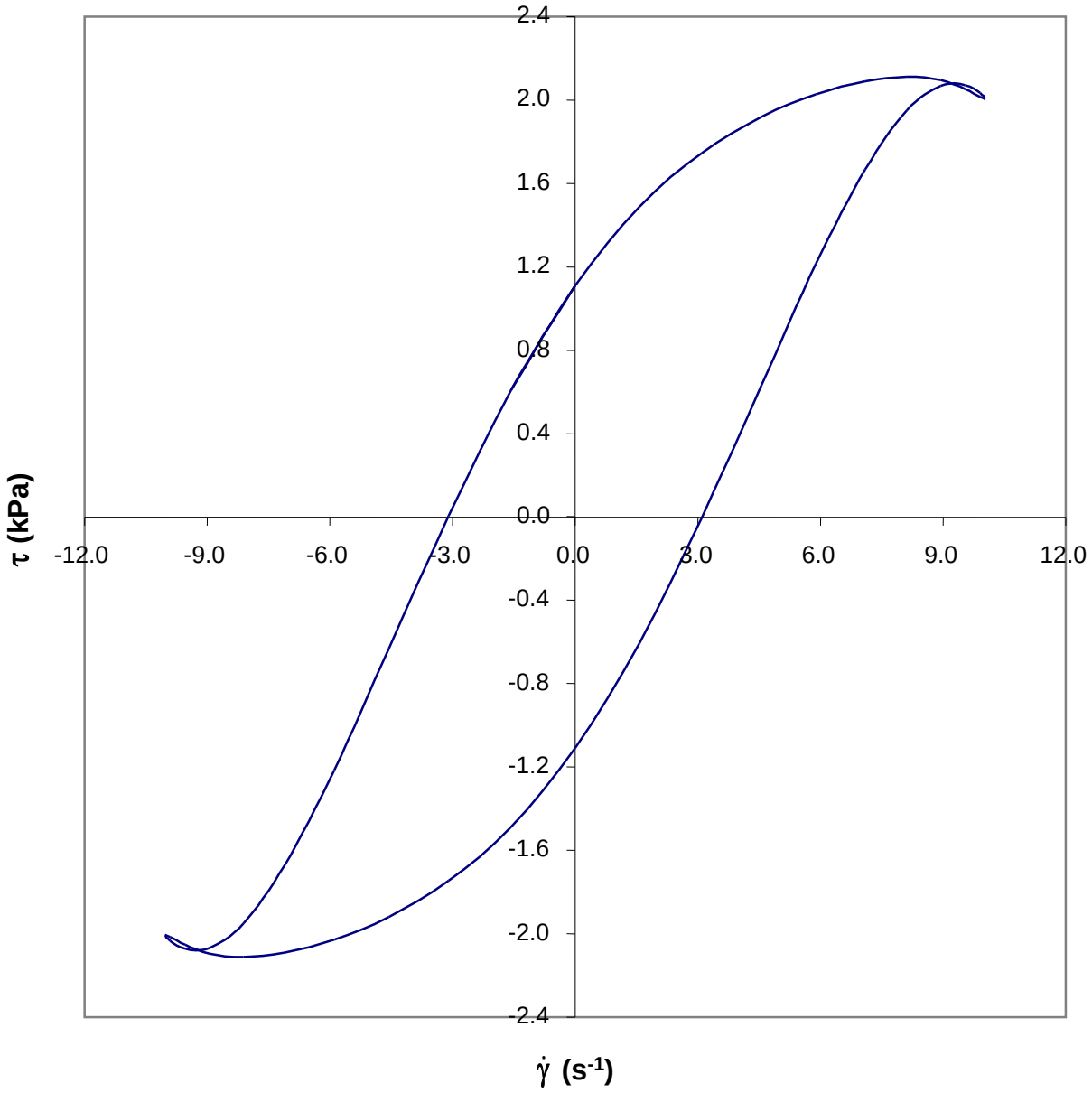

Figure 27 Shear stress *versus* shear rate loop at strain amplitude, γ_o = 4, for 6 week old full-fat pizza cheese at 40°C with f_o = 0.4 Hz. Slip causes twisting of the loop.

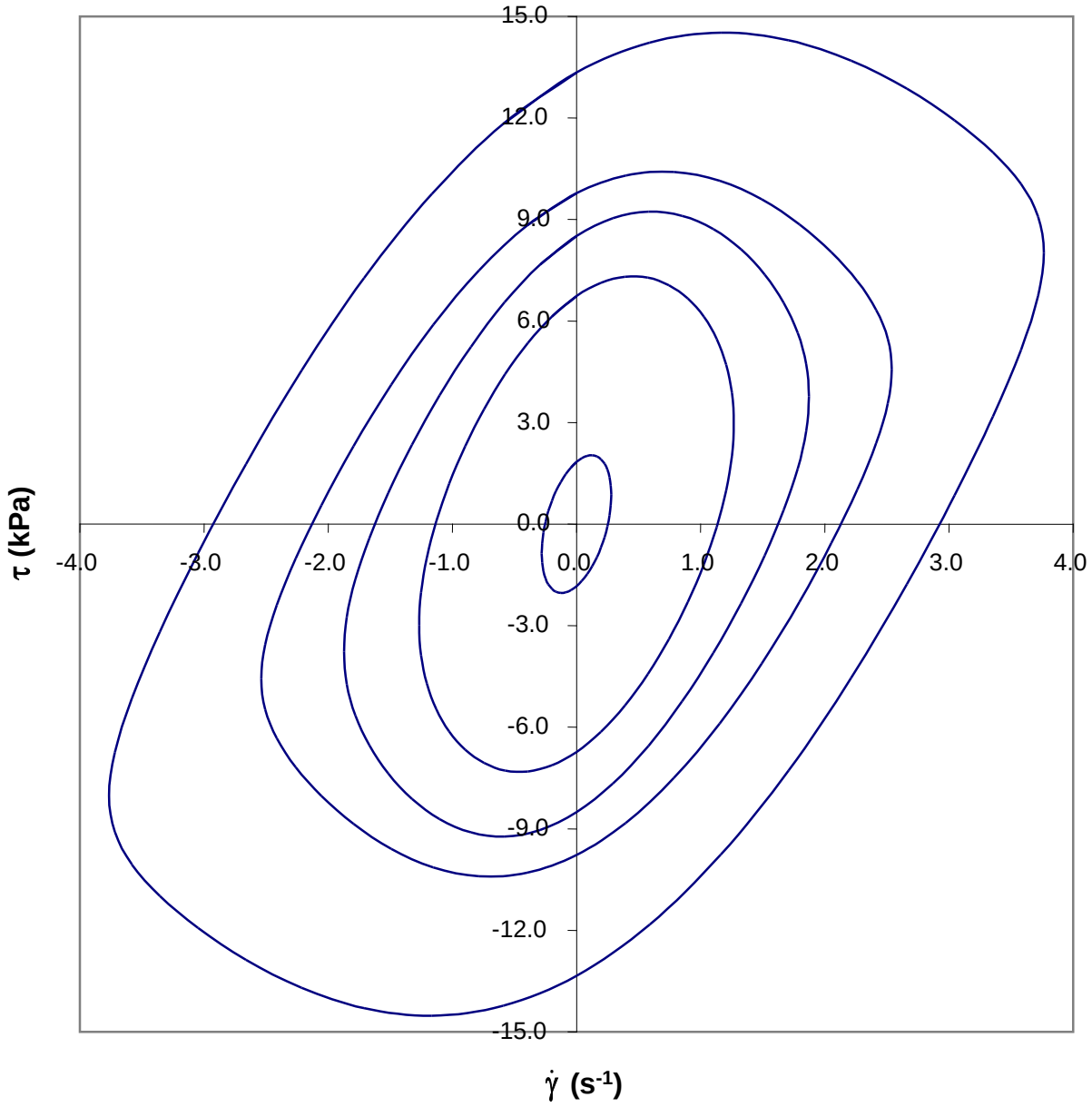

Figure 28 Shear stress *versus* shear rate loops for 1 week old reduced-fat mozzarella at 40°C with f_o = 0.4 Hz. Strain amplitudes are 0.1, 0.5, 0.75, 1, and 1.5.

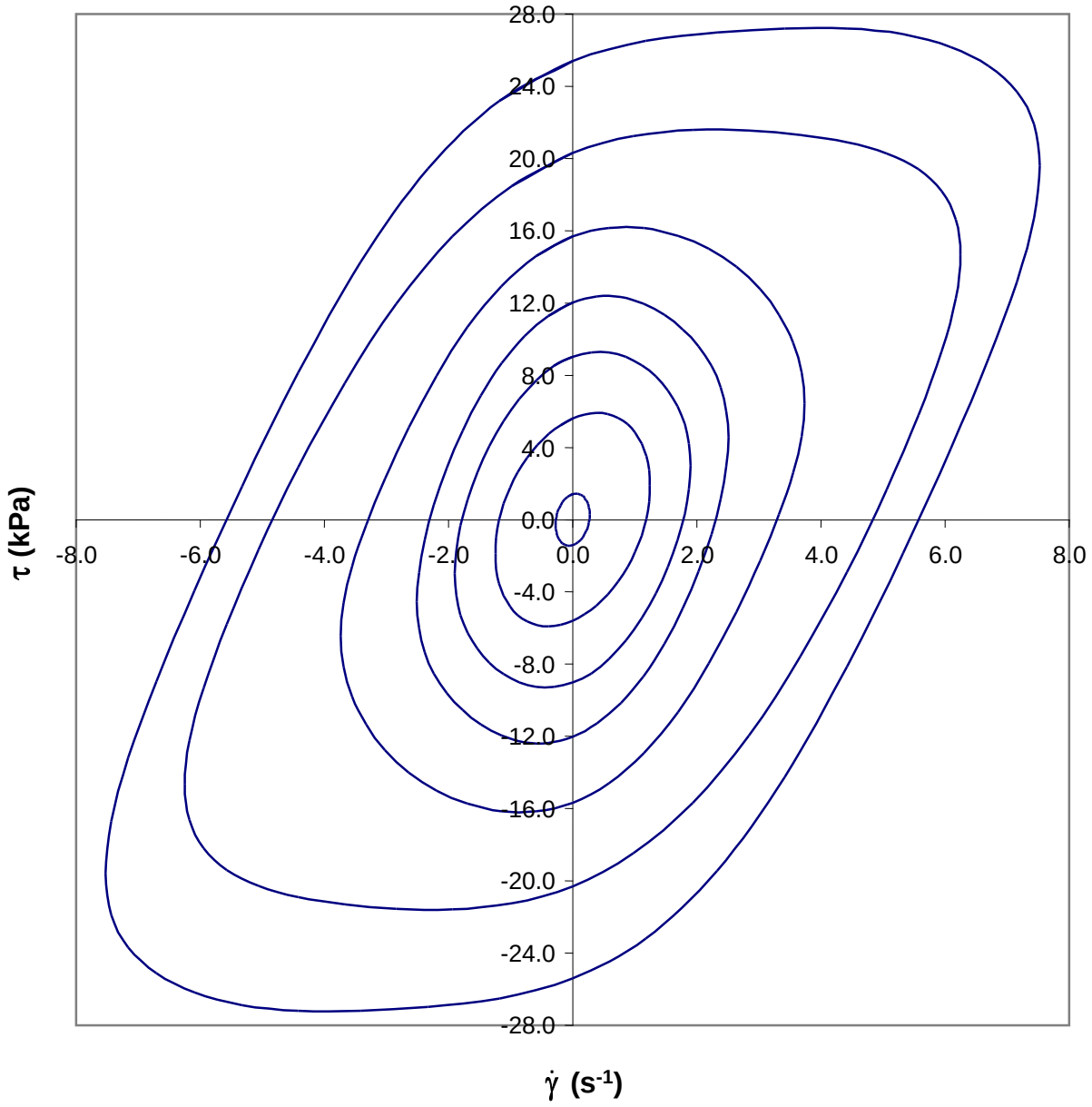

Figure 29 Shear stress *versus* shear rate loops for 4 week old reduced-fat mozzarella at 40°C with f_o = 0.4 Hz. Strain amplitudes are 0.1, 0.5, 0.75, 1, 1.5, 2.5, and 3.

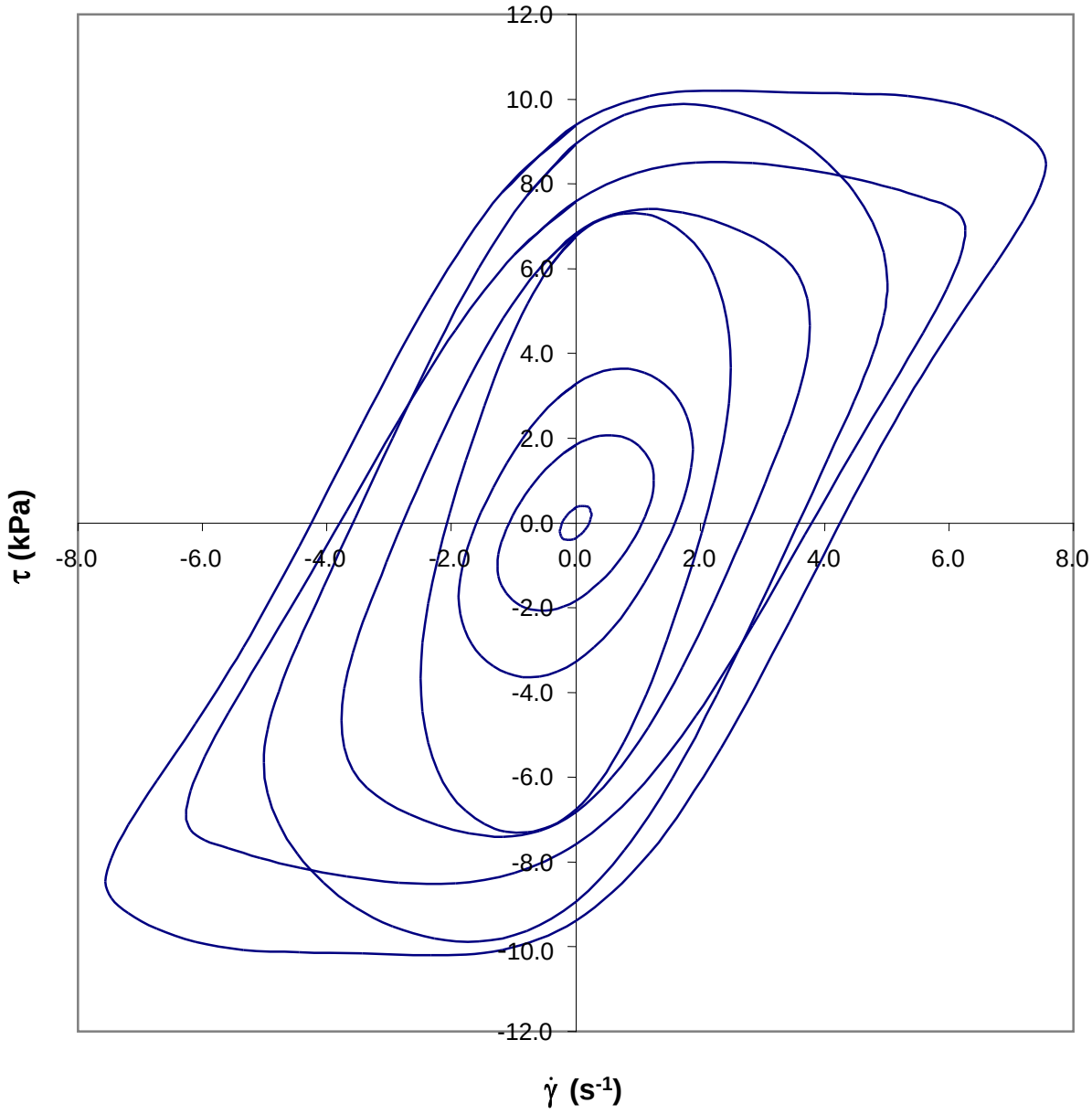

Figure 30 Shear stress *versus* shear rate loops for 6 week old reduced-fat mozzarella at 40°C with f_o = 0.4 Hz. Strain amplitudes are 0.1, 0.5, 0.75, 1, 1.5, 2, 2.5, and 3.

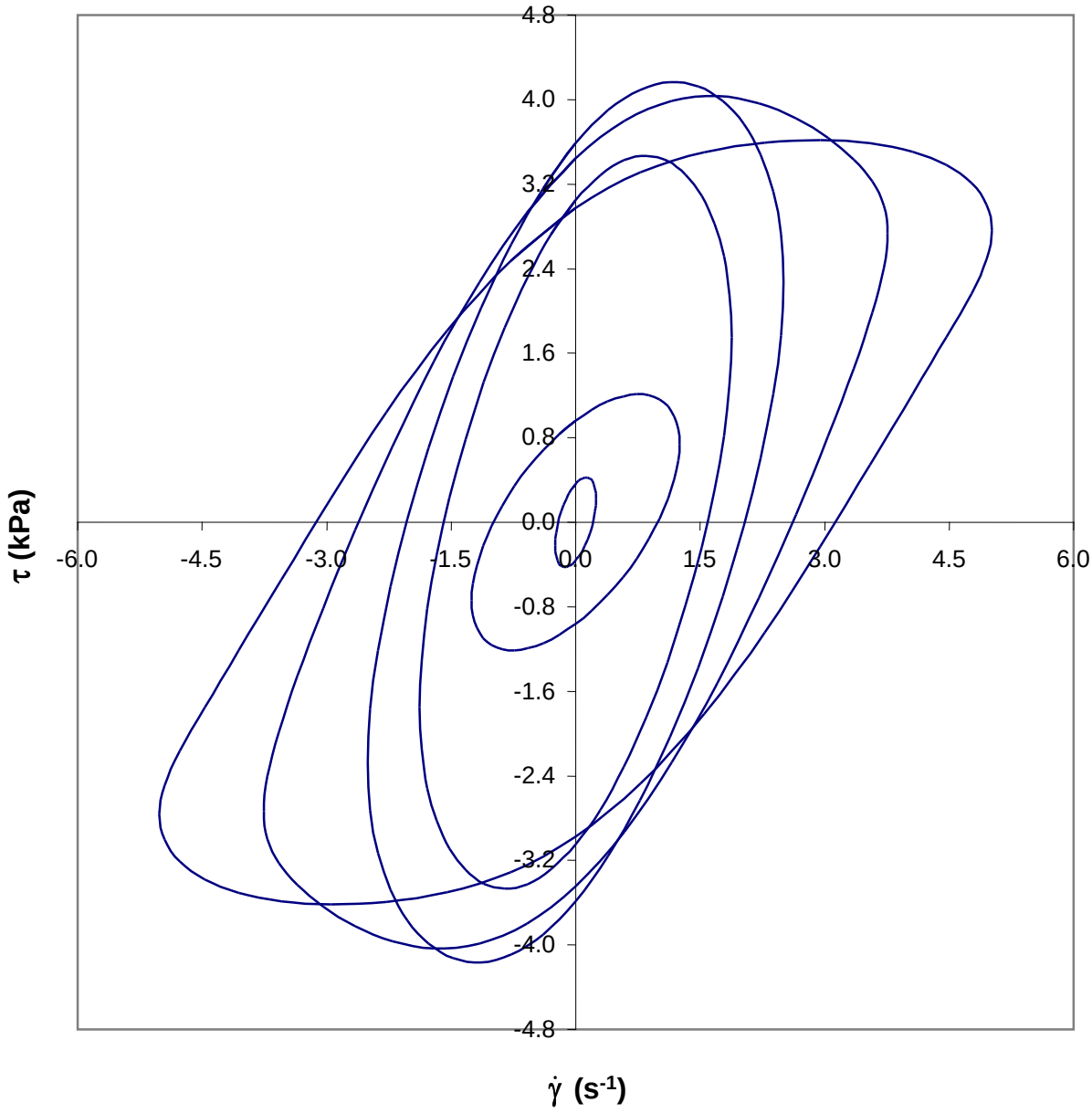

Figure 31 Shear stress *versus* shear rate loops for 12 week old reduced-fat mozzarella at 40°C with f_o = 0.4 Hz. Strain amplitudes are 0.1, 0.5, 0.75, 1, 1.5, and 2.

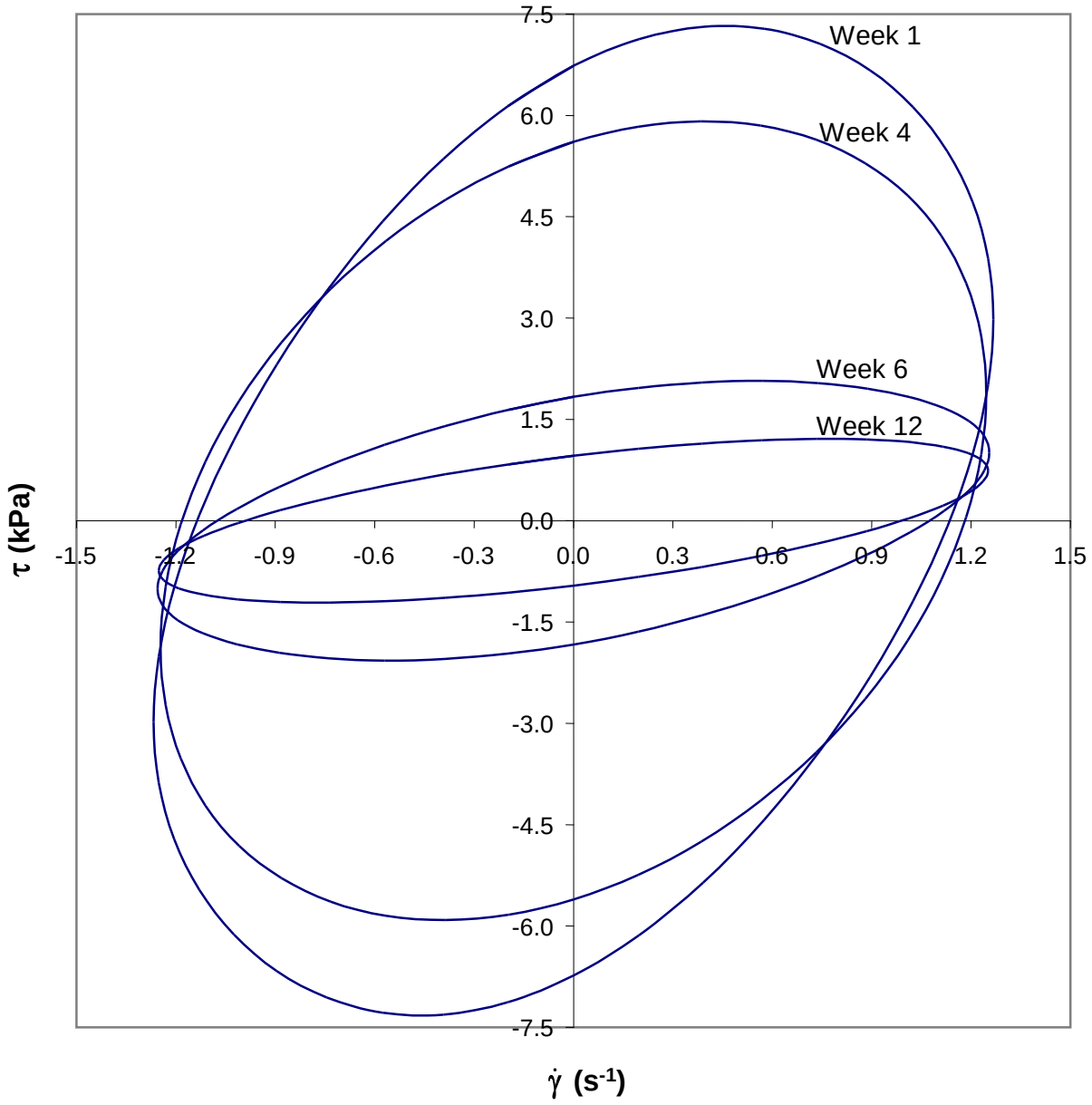

Figure 32 Effect of age on shear stress *versus* shear rate loops (γ_o = 0.5) for reduced-fat mozzarella at 40°C with f_o = 0.4 Hz. Mozzarella softens with age.

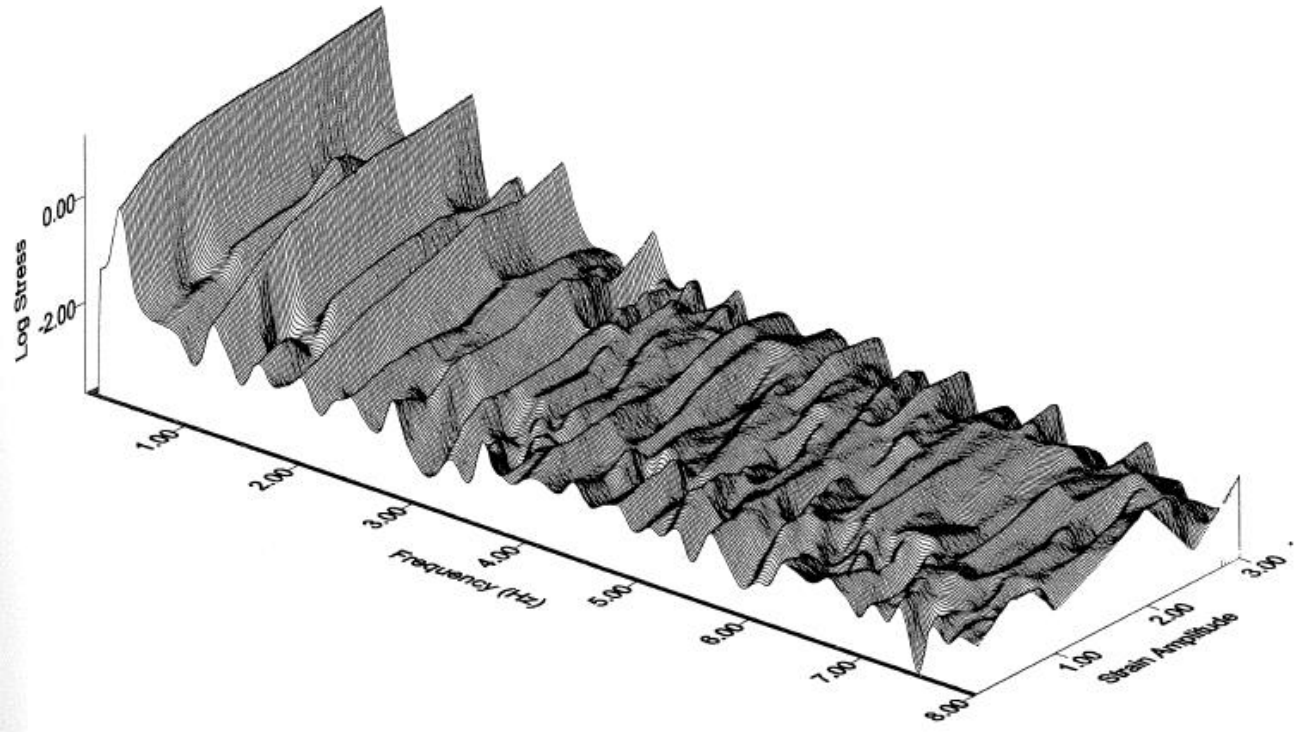

Figure 33 3D amplitude spectrum for 4 week old reduced-fat mozzarella at 40°C with f_o = 0.4 Hz. The higher, odd harmonics rise with strain amplitude.

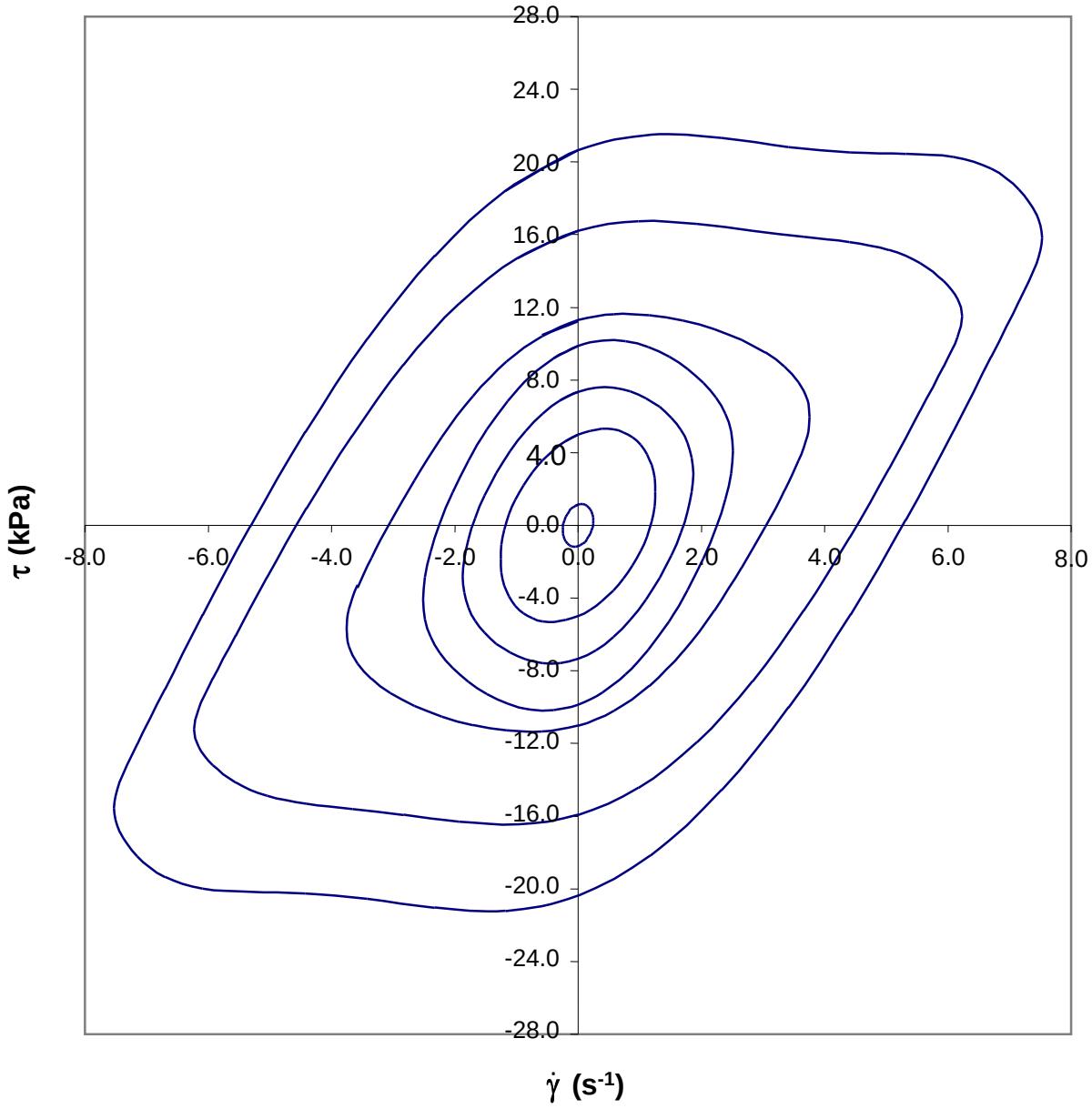

Figure 34 Shear stress *versus* shear rate loops for 4 week old reduced-fat mozzarella. Same samples repeated at 40°C with f_o = 0.4 Hz. Strain amplitudes are 0.1, 0.5, 0.75, 1, 1.5, 2.5, and 3. Mozzarella exhibits poor repeatability at 40°C.

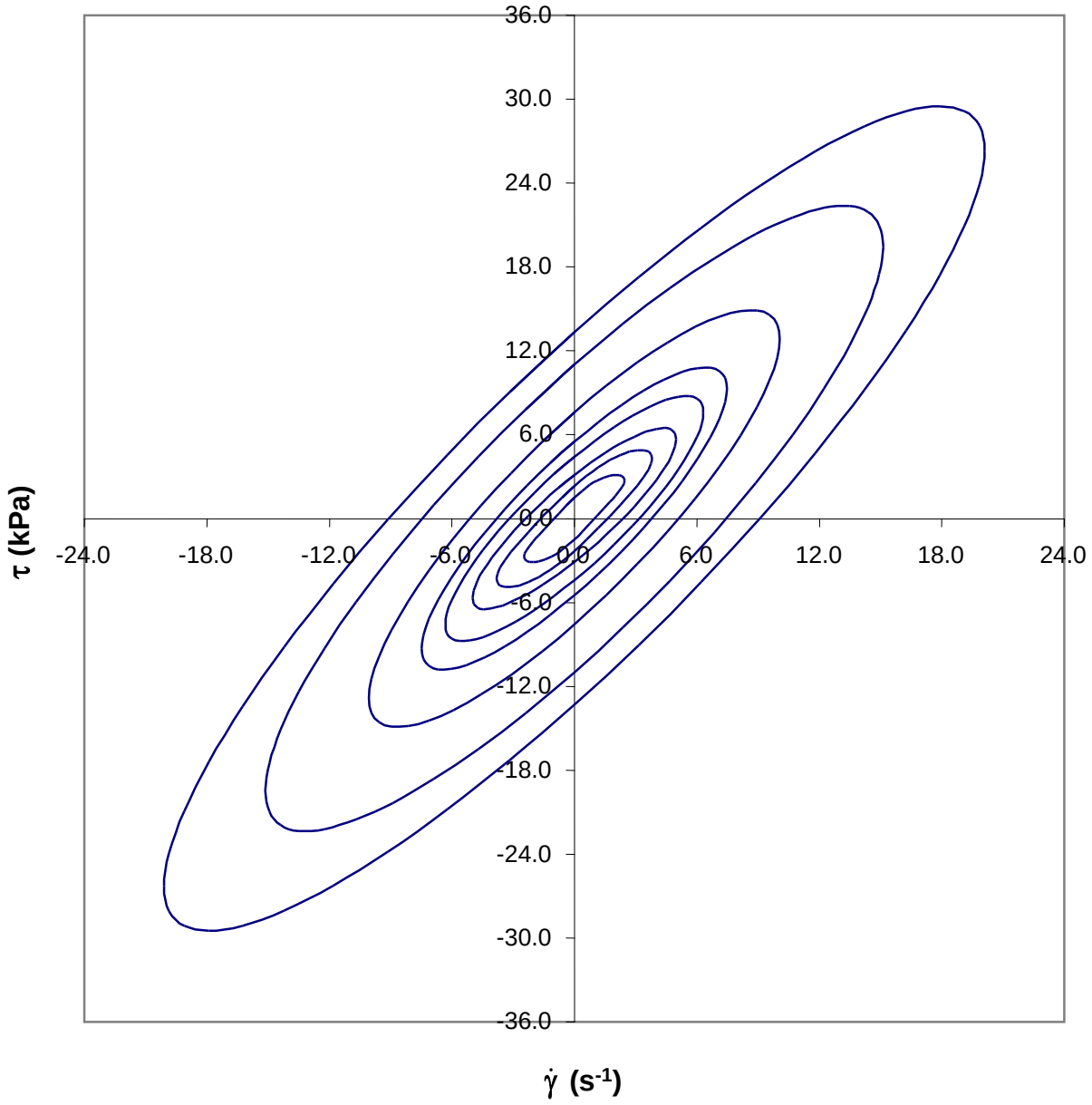

Figure 35 Shear stress *versus* shear rate loops for 1 week old reduced-fat mozzarella at 60°C with f_o = 0.4 Hz. Strain amplitudes are 1, 1.5, 2, 2.5, 3, 4, 6, and 8. All the loops are ellipses.

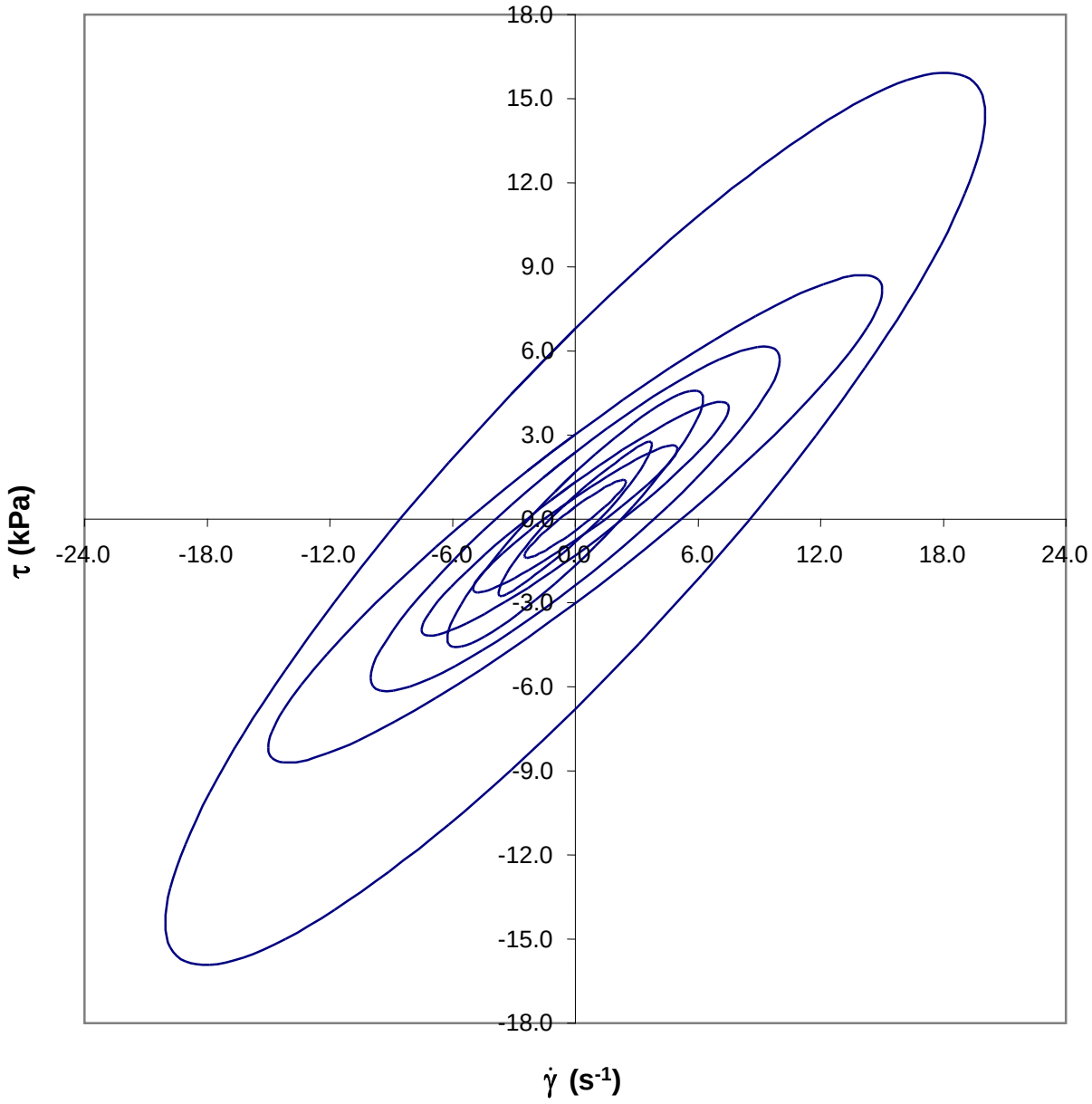

Figure 36 Shear stress *versus* shear rate loops for 4 week old reduced-fat mozzarella at 60°C with f_o = 0.4 Hz. Strain amplitudes are 1, 1.5, 2, 2.5, 3, 4, 6, and 8. All the loops are ellipses.

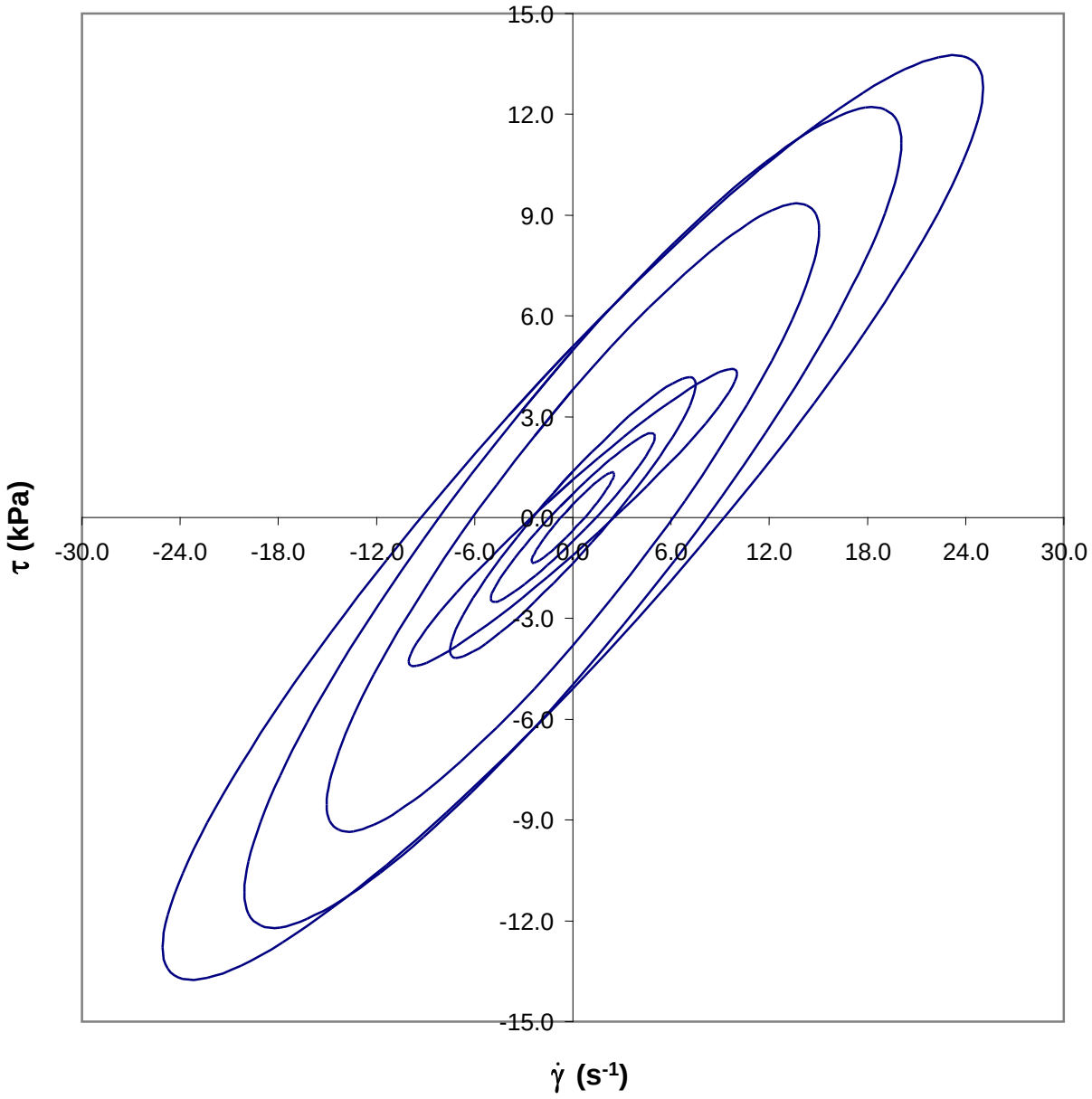

Figure 37 Shear stress *versus* shear rate loops for 6 week old reduced-fat mozzarella at 60°C with f_o = 0.4 Hz. Strain amplitudes are 1, 2, 3, 4, 6, 8, and 10. All the loops are ellipses.

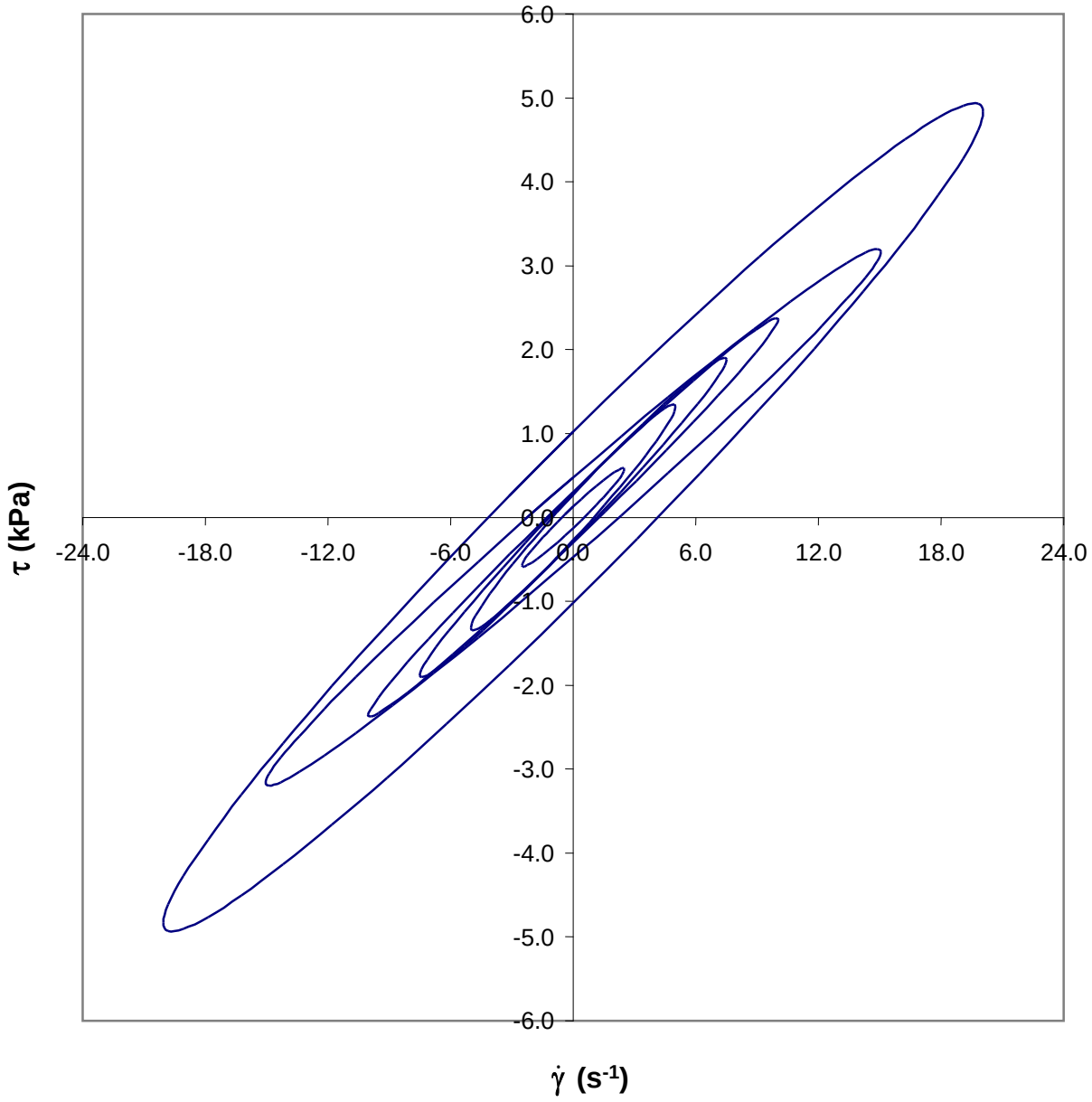

Figure 38 Shear stress *versus* shear rate loops for 12 week old reduced-fat mozzarella at 60°C with f_o = 0.4 Hz. Strain amplitudes are 1, 2, 3, 4, 6, and 8. All the loops are ellipses.

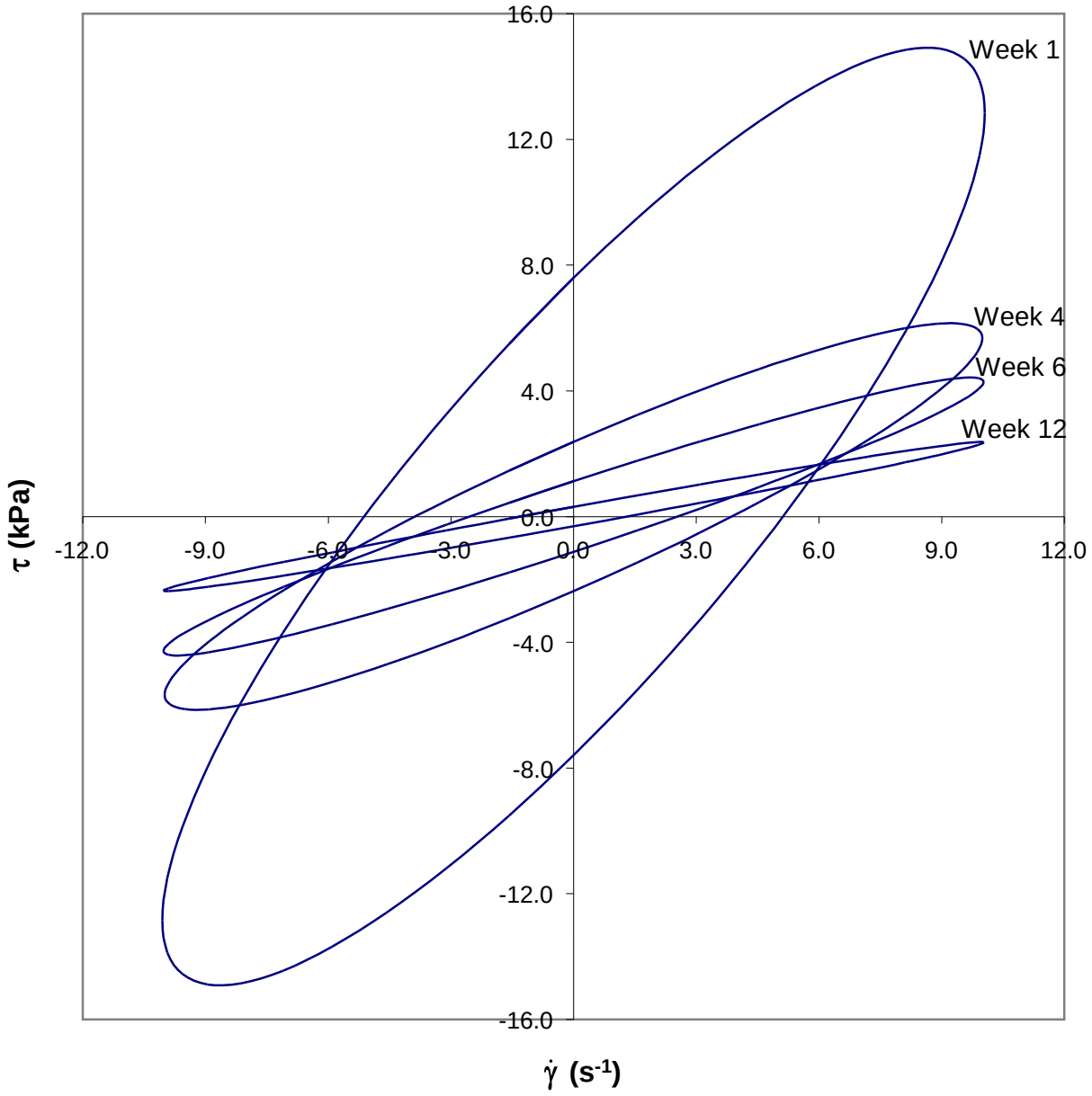

Figure 39 Effect of age on shear stress *versus* shear rate loops (γ_o = 4) for reduced-fat mozzarella at 60°C with f_o = 0.4 Hz. Mozzarella softens with age.

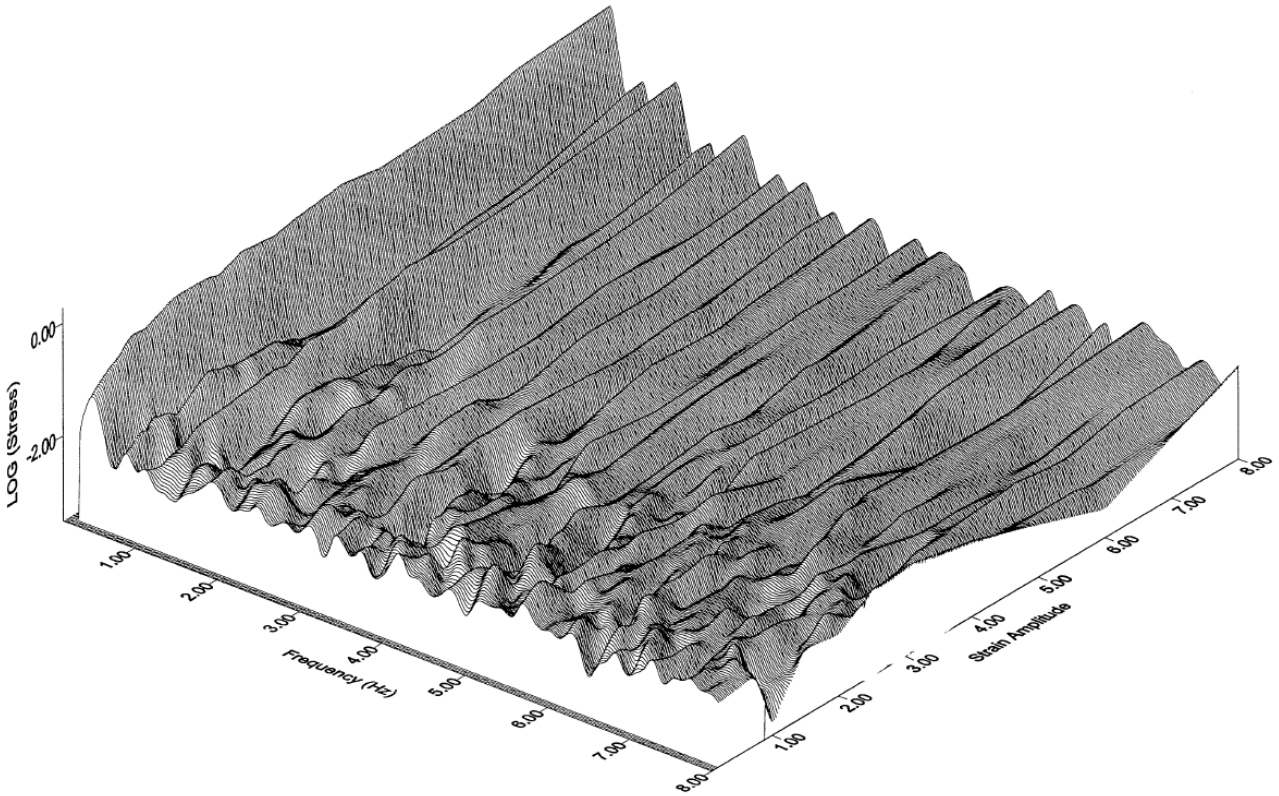

Figure 40 3D amplitude spectrum for 4 week old reduced-fat mozzarella at 60°C with f_o = 0.4 Hz. Although higher harmonics are detected, only the fundamental harmonic at 0.4 Hz matters.

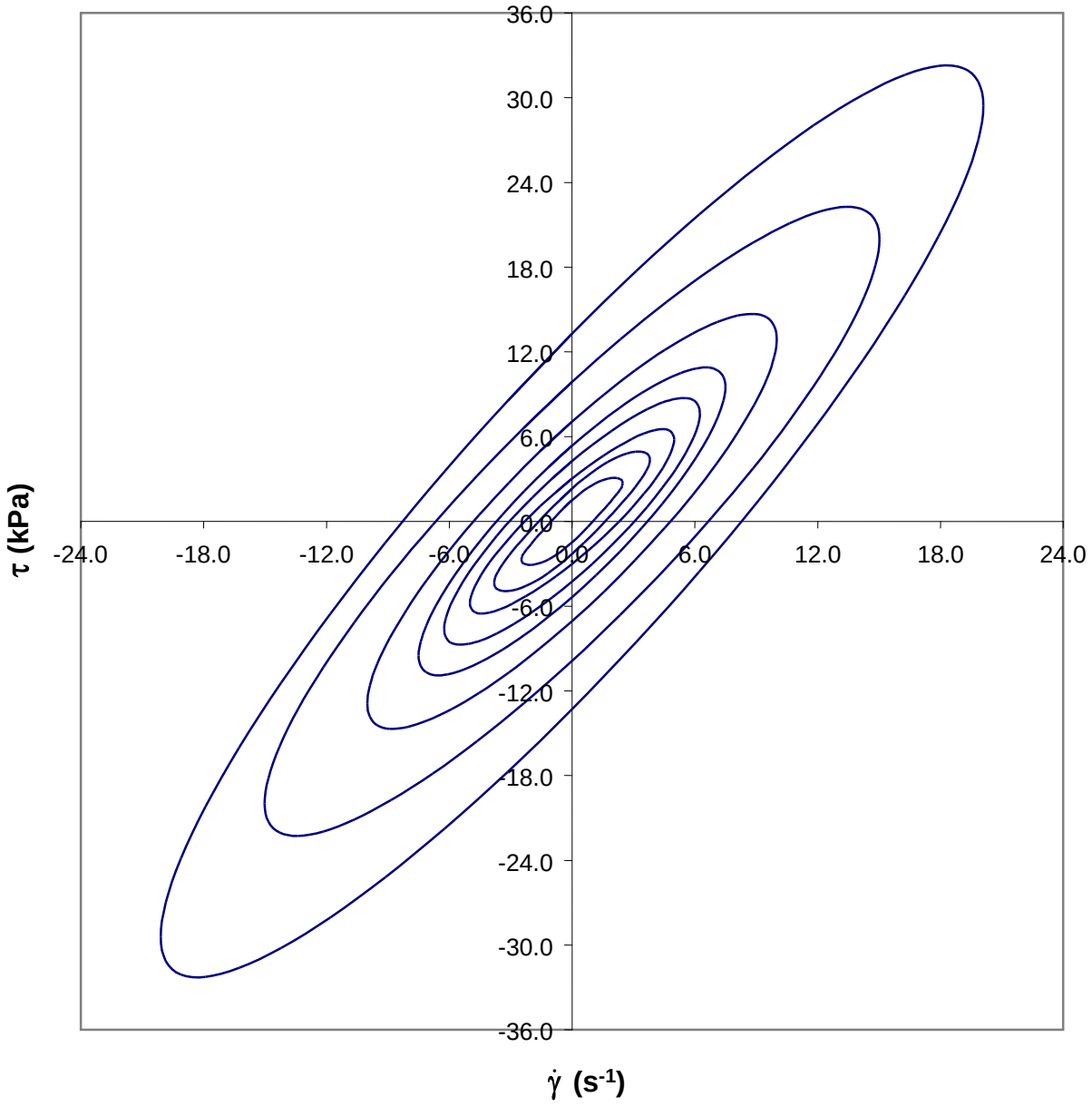

Figure 41 Shear stress *versus* shear rate loops for 1 week old reduced-fat mozzarella. Same samples repeated at 60°C with f_o = 0.4 Hz. Strain amplitudes are 1, 1.5, 2, 2.5, 3, 4, 6, and 8. Mozzarella exhibits good repeatability with slightly higher stresses.

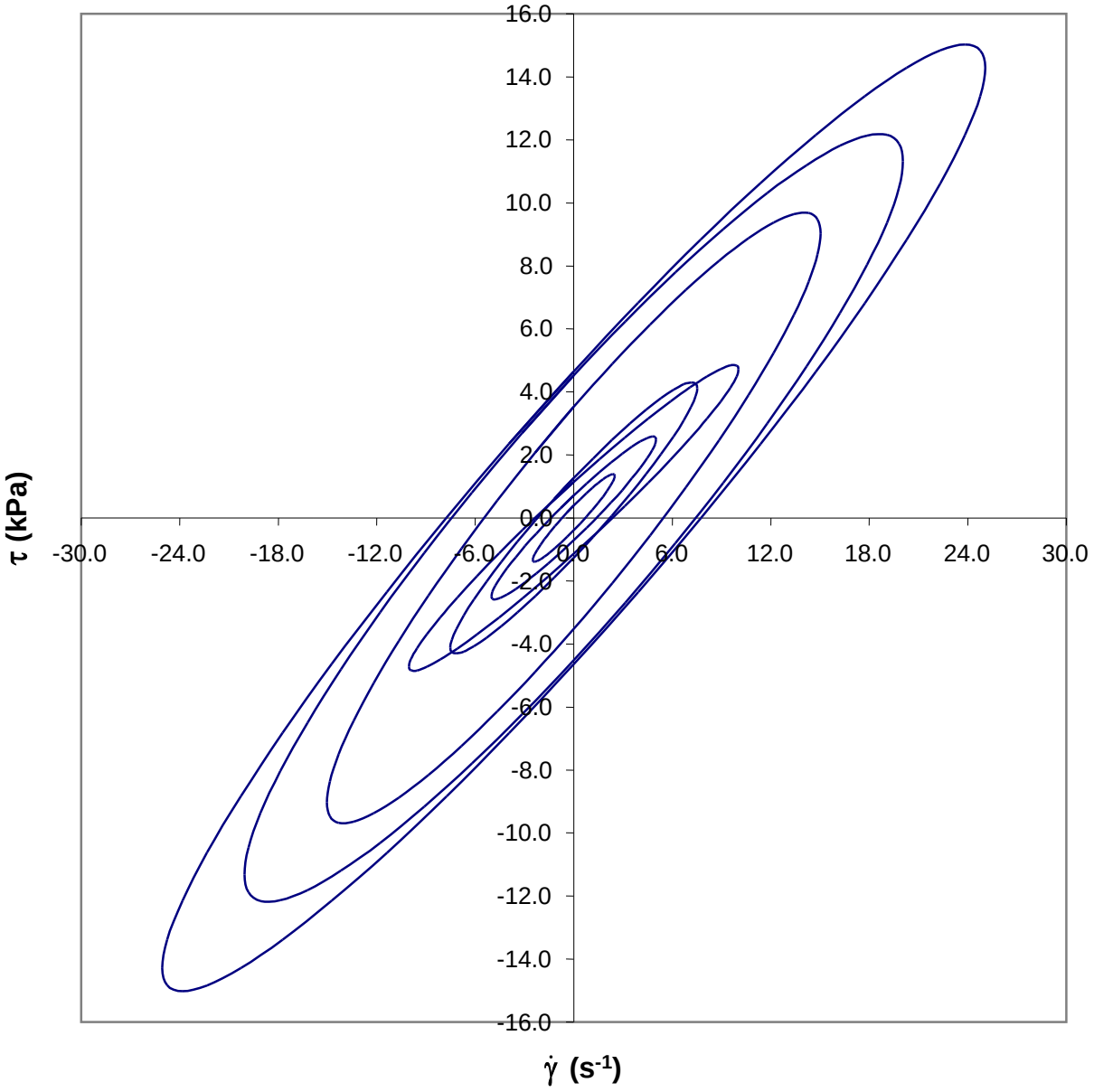

Figure 42 Shear stress *versus* shear rate loops for 6 week old reduced-fat mozzarella. Same samples repeated at 60°C with f_o = 0.4 Hz. Strain amplitudes are 1, 2, 3, 4, 6, 8, and 10. Mozzarella exhibits good repeatability with slightly higher stresses.

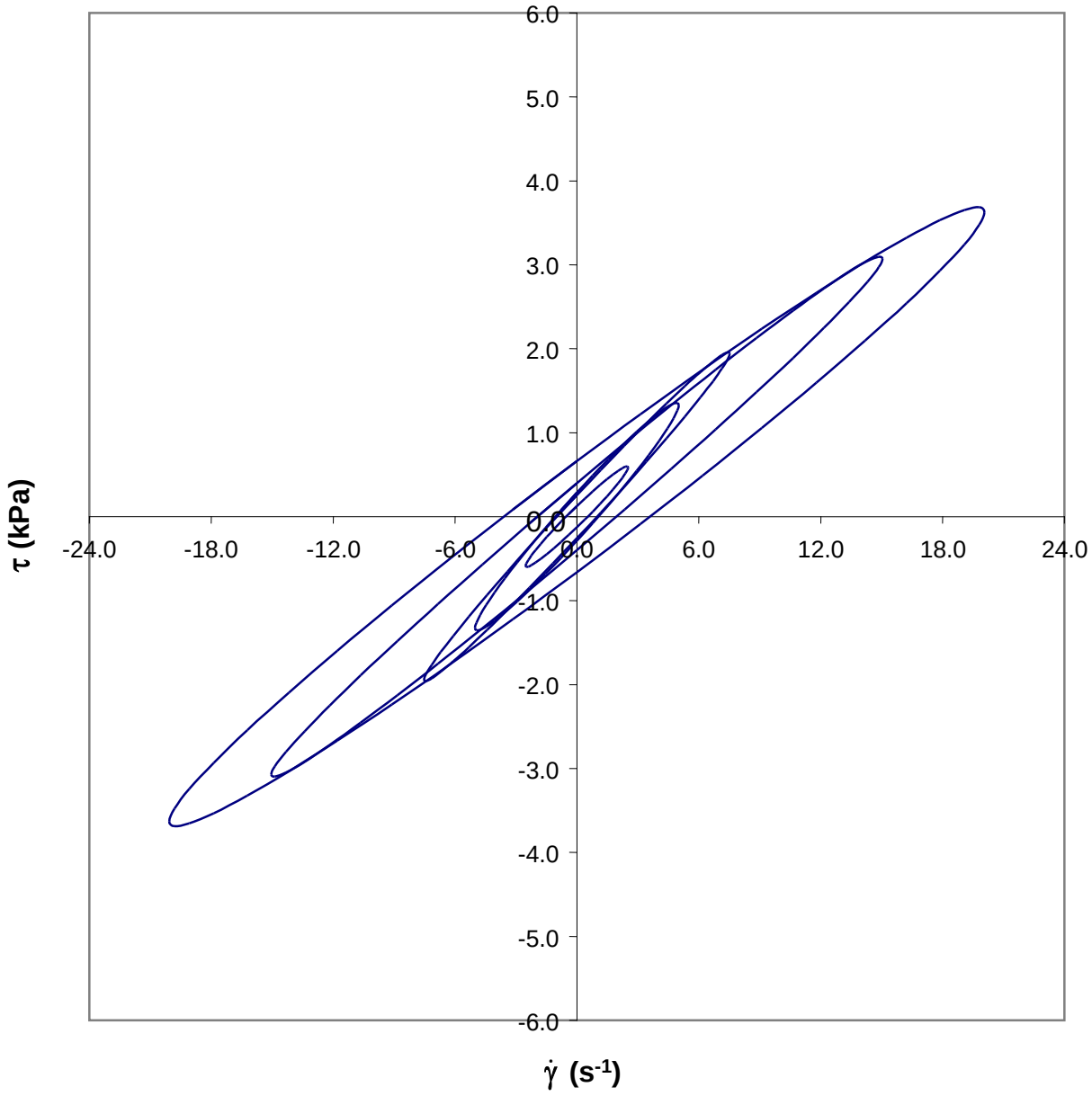

Figure 43 Shear stress *versus* shear rate loops for 12 week old reduced-fat mozzarella. Same samples repeated at 60°C with f_o = 0.4 Hz. Strain amplitudes are 1, 2, 3, 6, and 8. Repeatability worsens as mozzarella ages.

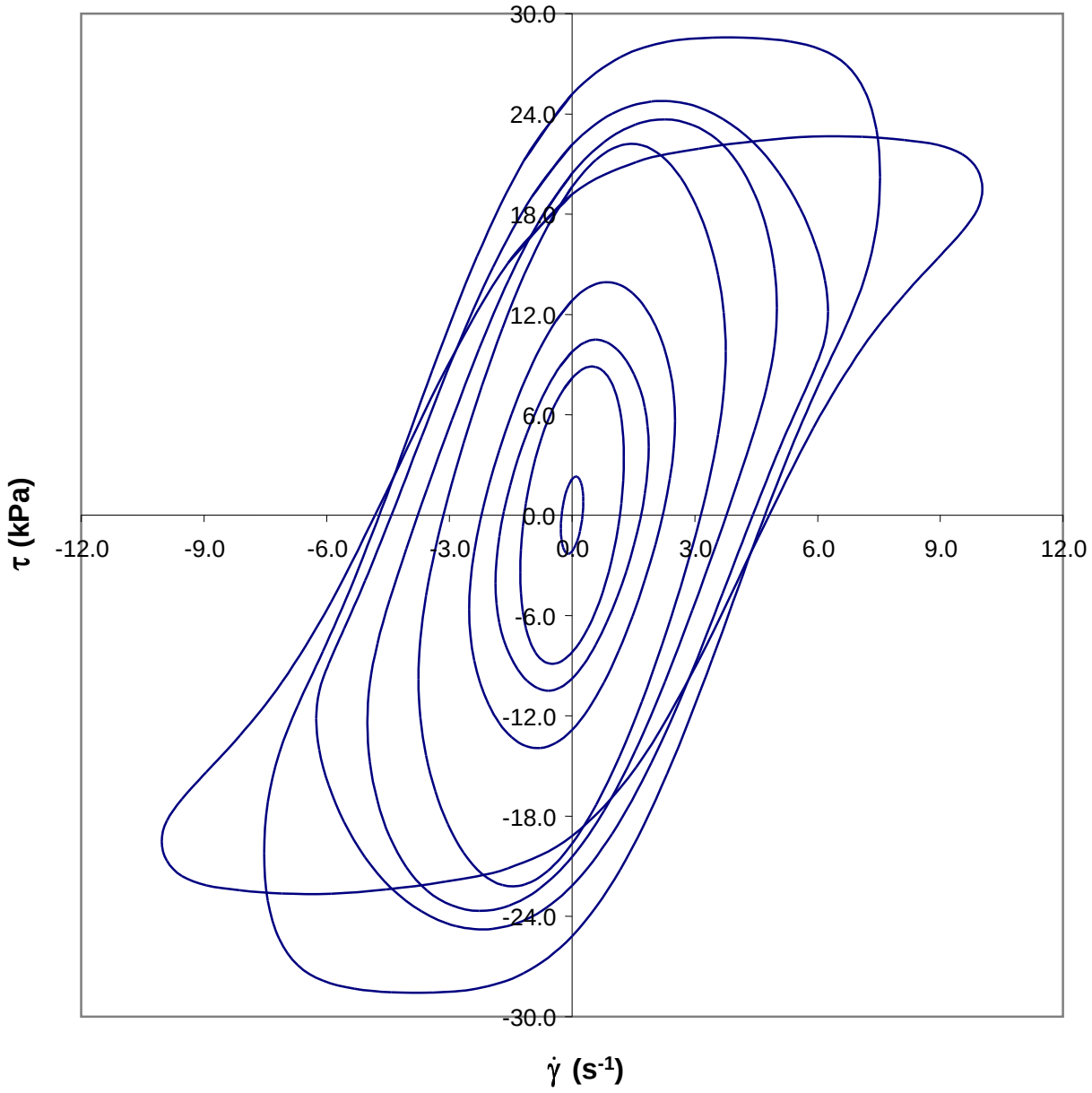

Figure 44 Shear stress *versus* shear rate loops for 1 week old reduced-fat cheddar at 40°C with f_o = 0.4 Hz. Strain amplitudes are 0.1, 0.5, 0.75, 1, 1.5, 2, 2.5, 3, and 4.

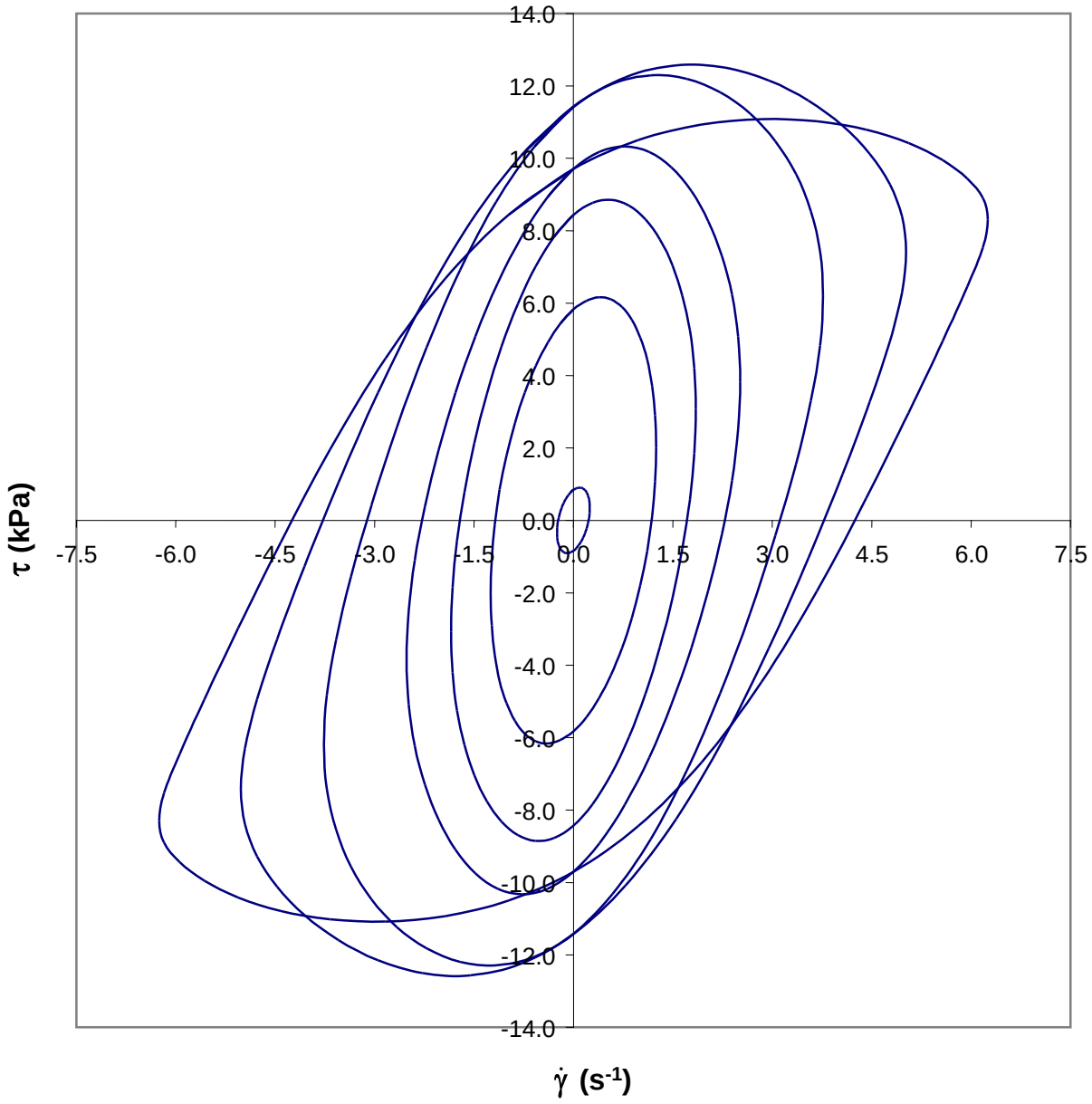

Figure 45 Shear stress *versus* shear rate loops for 4 week old reduced-fat cheddar at 40°C with f_o = 0.4 Hz. Strain amplitudes are 0.1, 0.5, 0.75, 1, 1.5, 2, and 2.5.

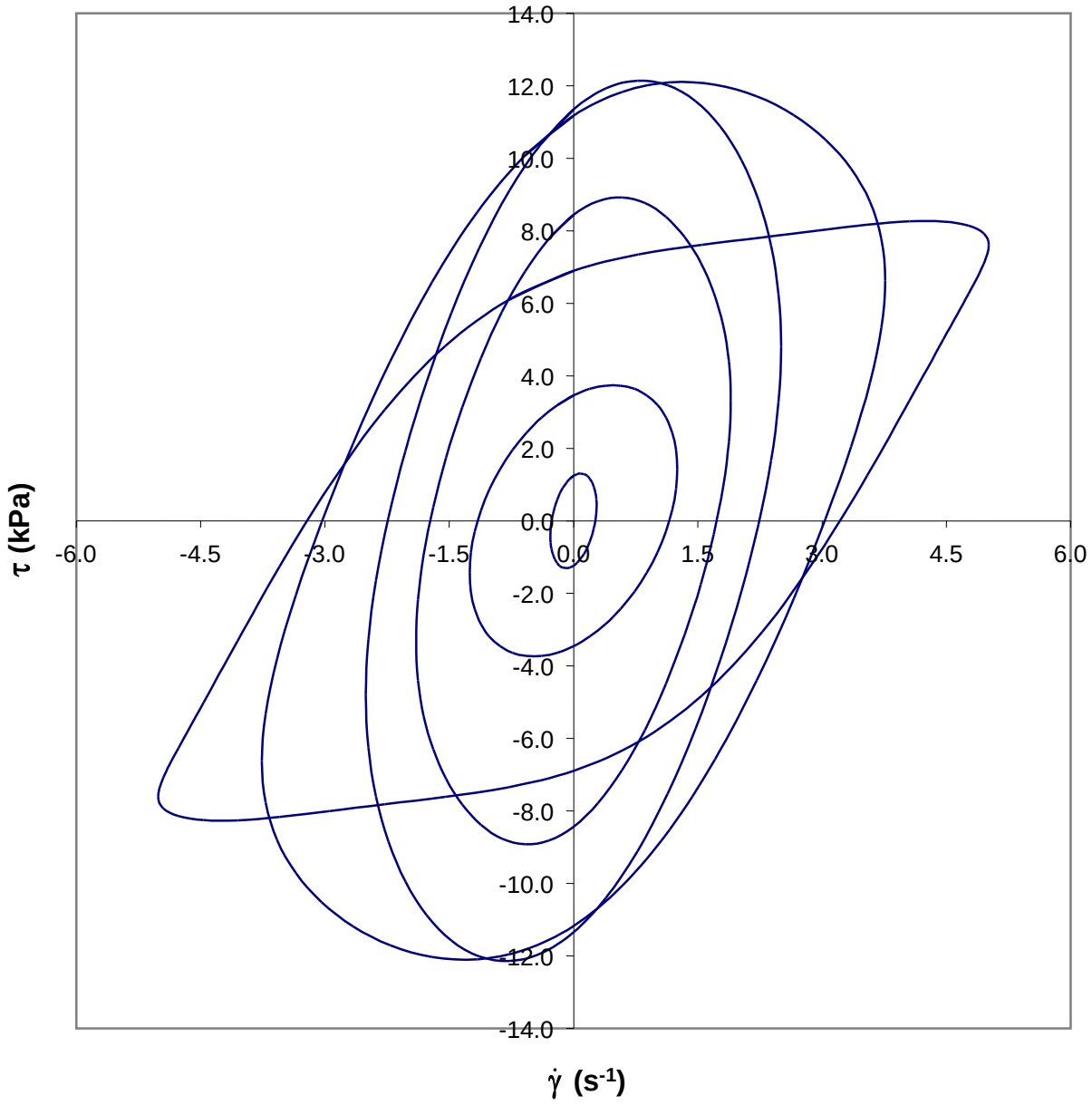

Figure 46 Shear stress *versus* shear rate loops for 6 week old reduced-fat cheddar at 40°C with f_o = 0.4 Hz. Strain amplitudes are 0.1, 0.5, 0.75, 1, 1.5, and 2.

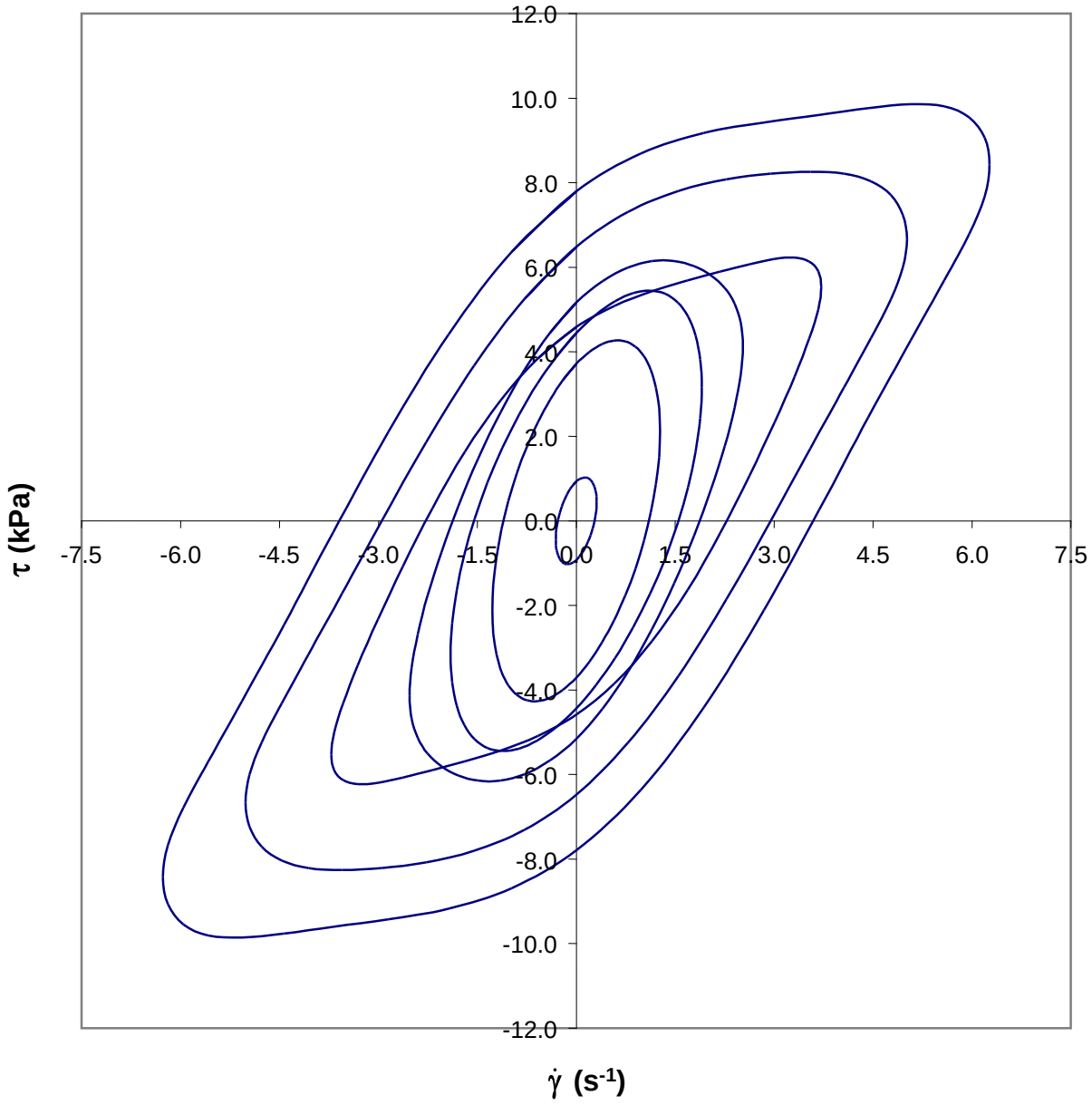

Figure 47 Shear stress *versus* shear rate loops for 12 week old reduced-fat cheddar at 40°C with f_o = 0.4 Hz. Strain amplitudes are 0.1, 0.5, 0.75, 1, 1.5, 2, and 2.5.

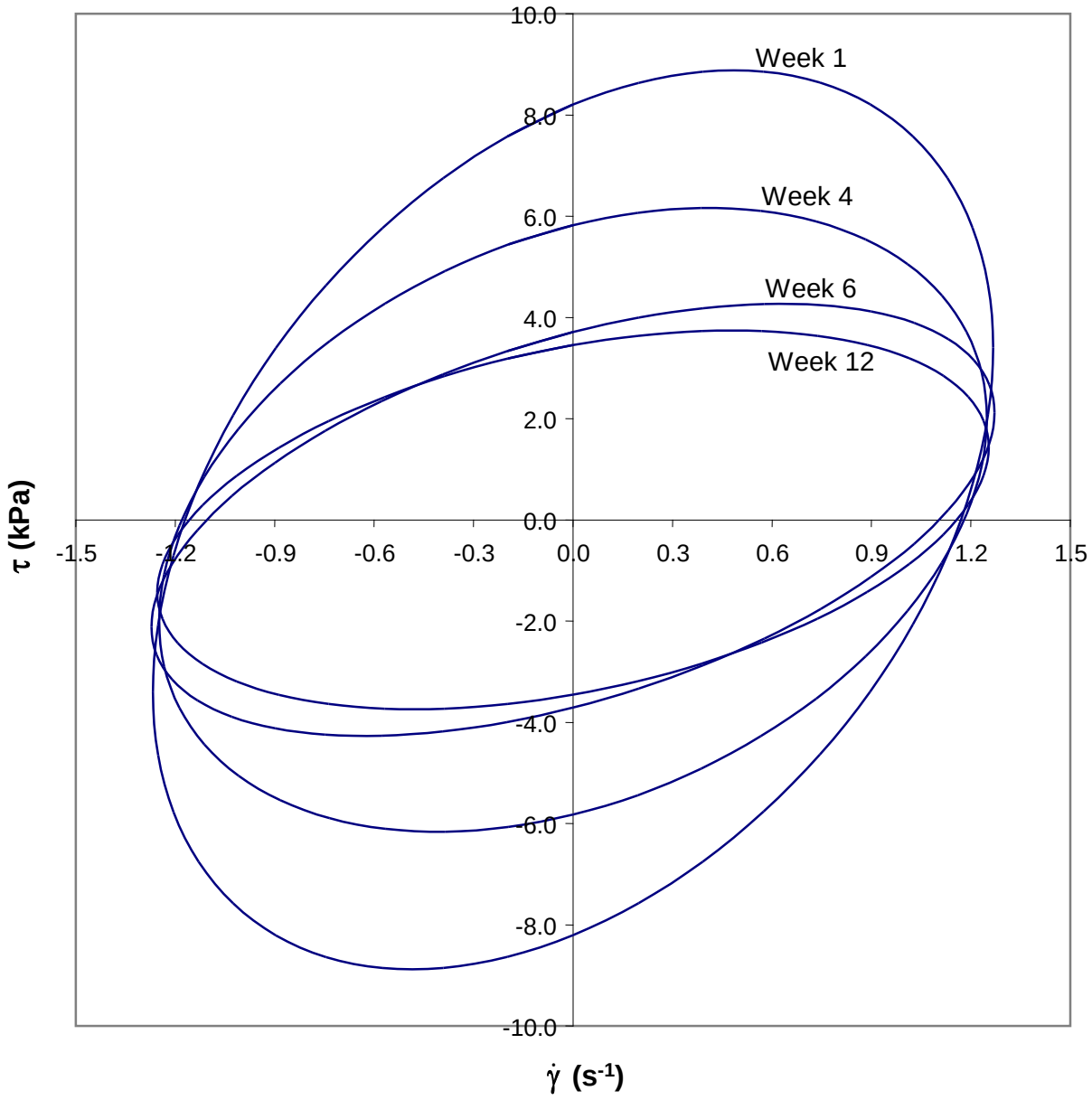

Figure 48 Effect of age on shear stress *versus* shear rate loops (γ_o = 0.5) for reduced-fat cheddar at 40°C with f_o = 0.4 Hz. Cheddar softens with age.

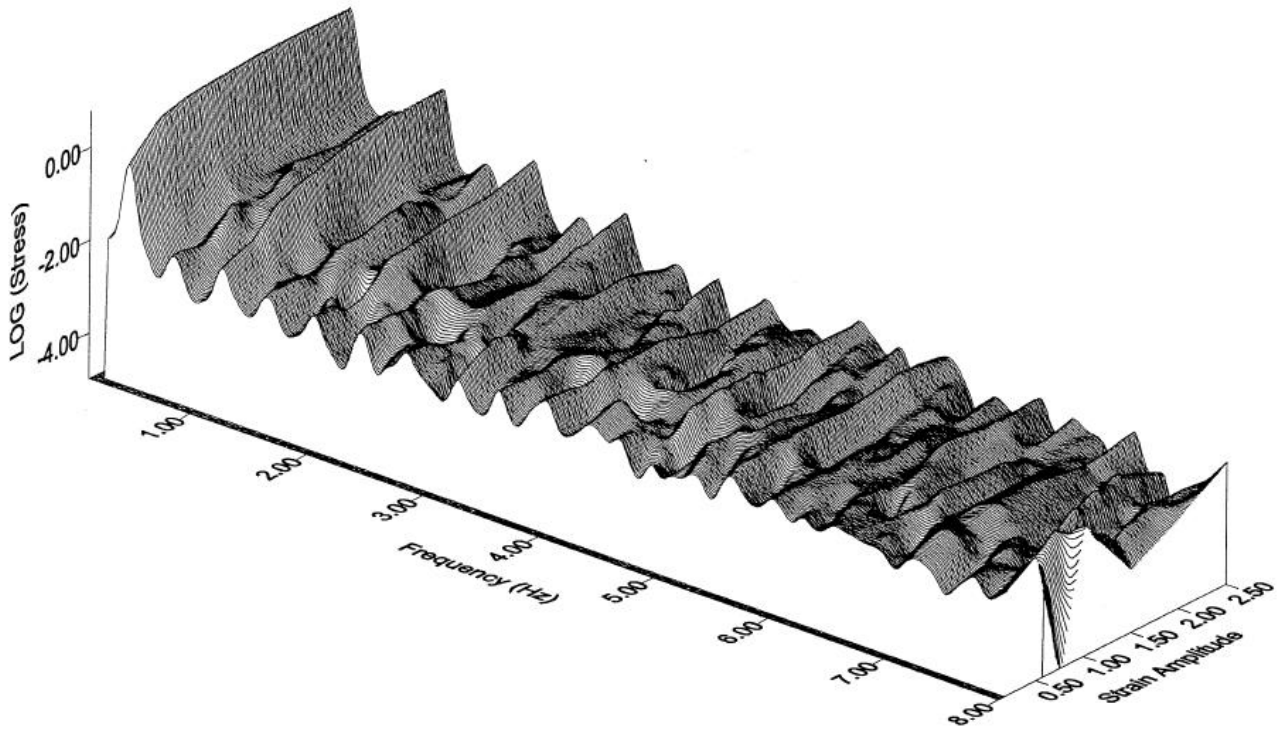

Figure 49 3D amplitude spectrum for 4 week old reduced-fat cheddar at 40°C with f_o = 0.4 Hz. The higher, odd harmonics rise with strain amplitude.

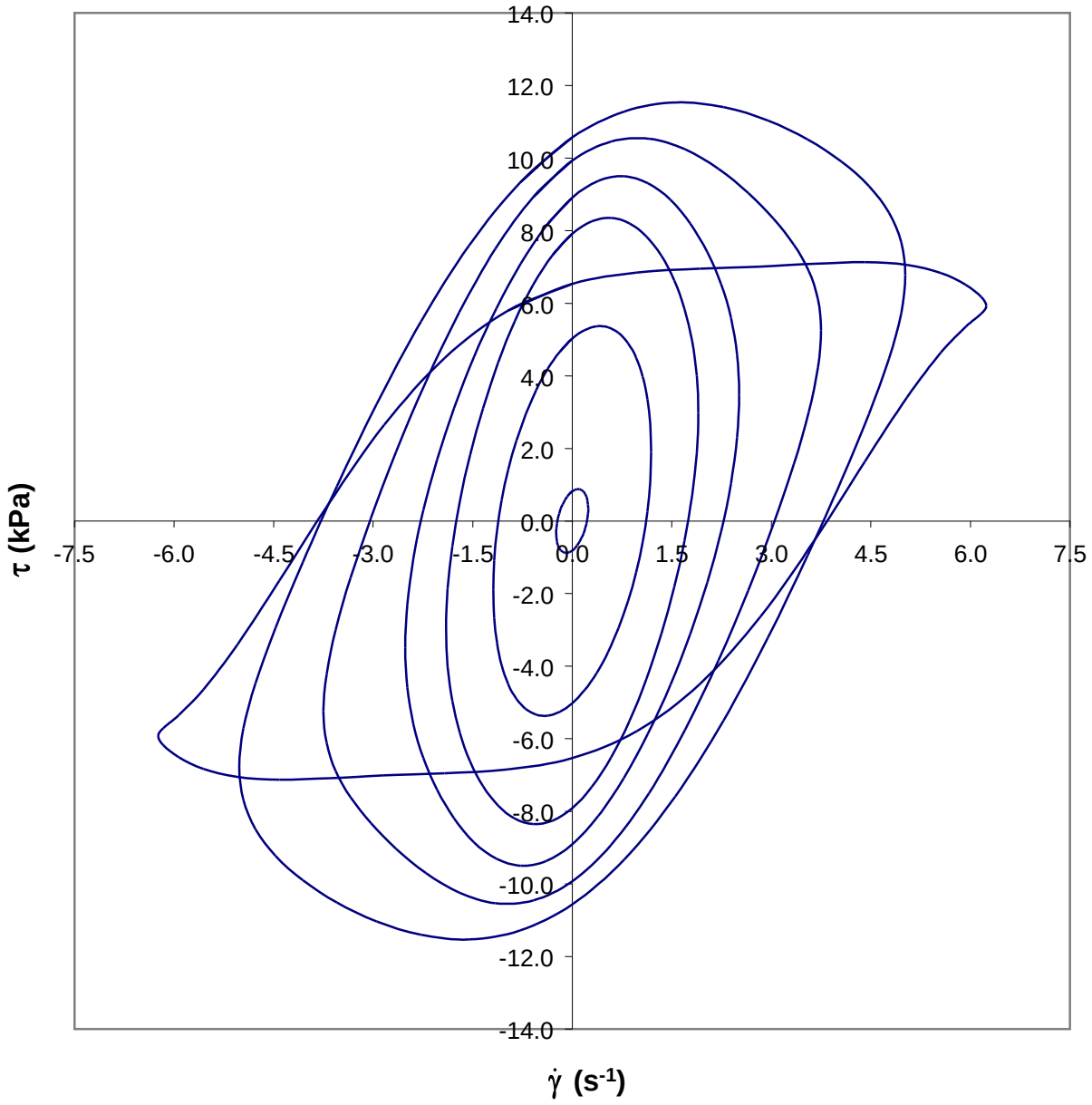

Figure 50 Shear stress *versus* shear rate loops for 4 week old reduced-fat cheddar. Same samples repeated at 40°C with f_o = 0.4 Hz. Strain amplitudes are 0.1, 0.5, 0.75, 1, 1.5, 2, and 2.5. Cheddar exhibits relatively good repeatability at $\gamma_o \leq 2$.

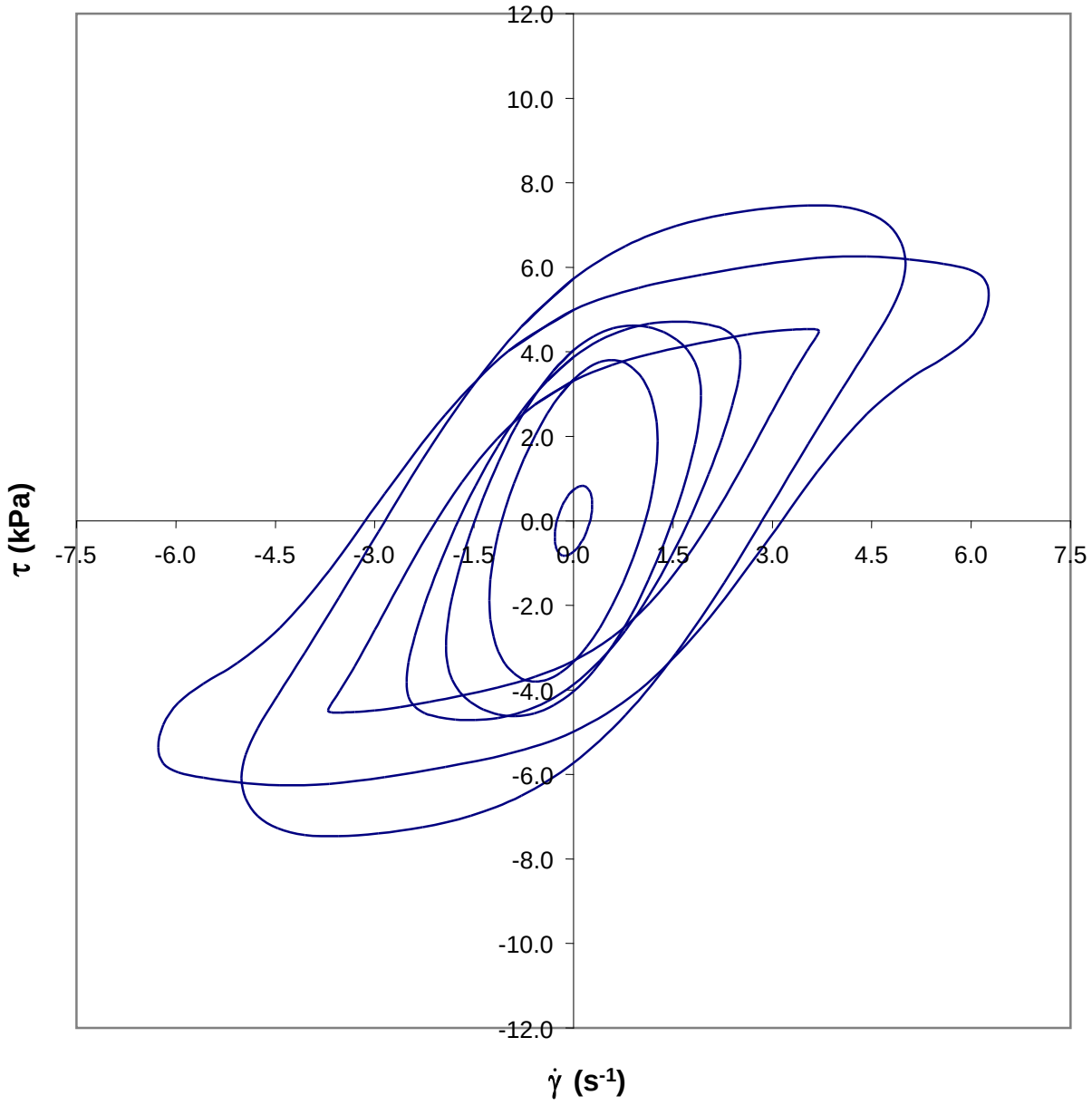

Figure 51 Shear stress *versus* shear rate loops for 12 week old reduced-fat cheddar. Same samples repeated at 40°C with f_o = 0.4 Hz. Strain amplitudes are 0.1, 0.5, 0.75, 1, 1.5, 2, and 2.5. Repeatability worsens as cheddar ages.

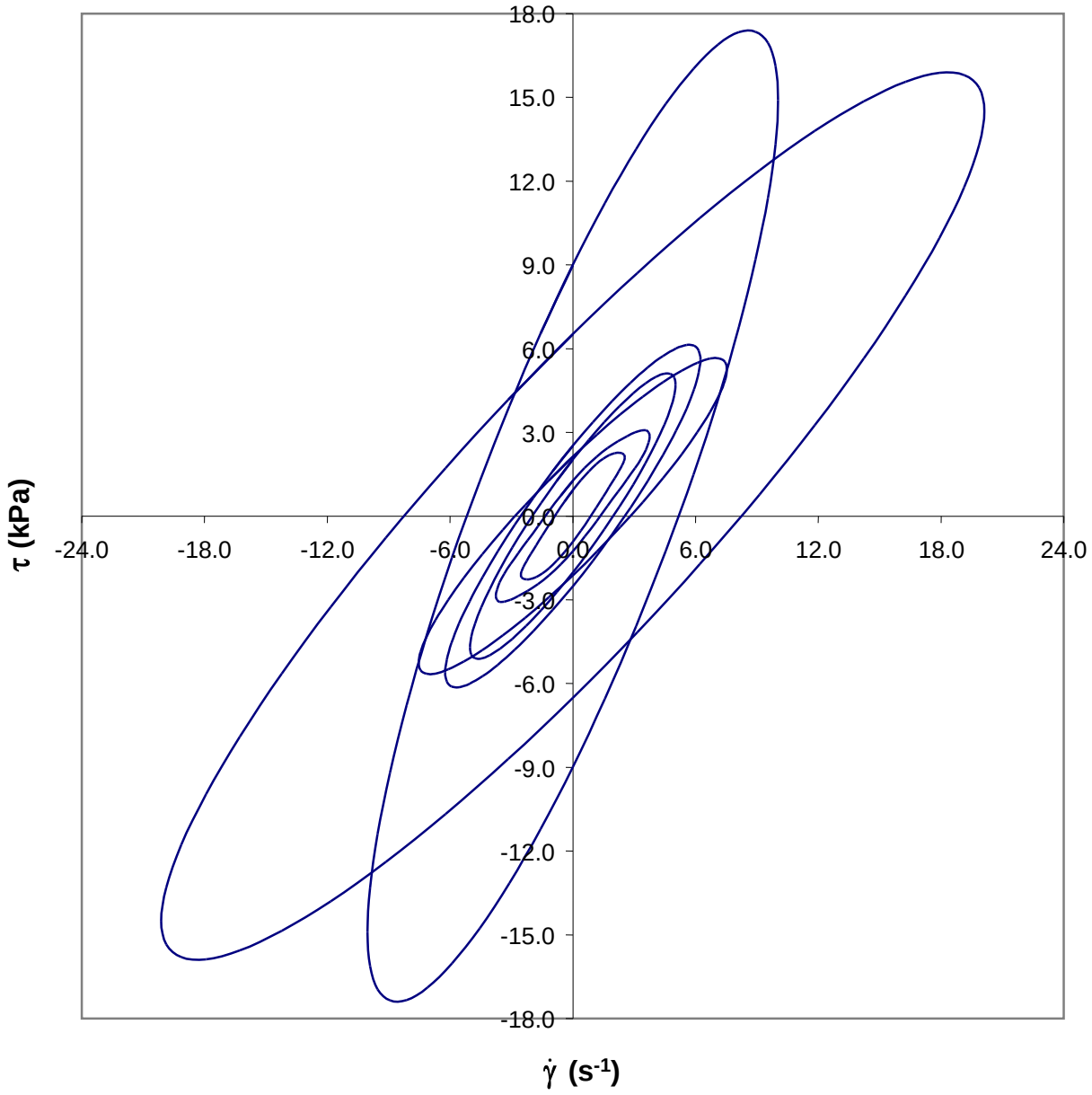

Figure 52 Shear stress *versus* shear rate loops for 1 week old reduced-fat cheddar at 60°C with f_o = 0.4 Hz. Strain amplitudes are 1, 1.5, 2, 2.5, 3, 4, and 8. All the loops are ellipses.

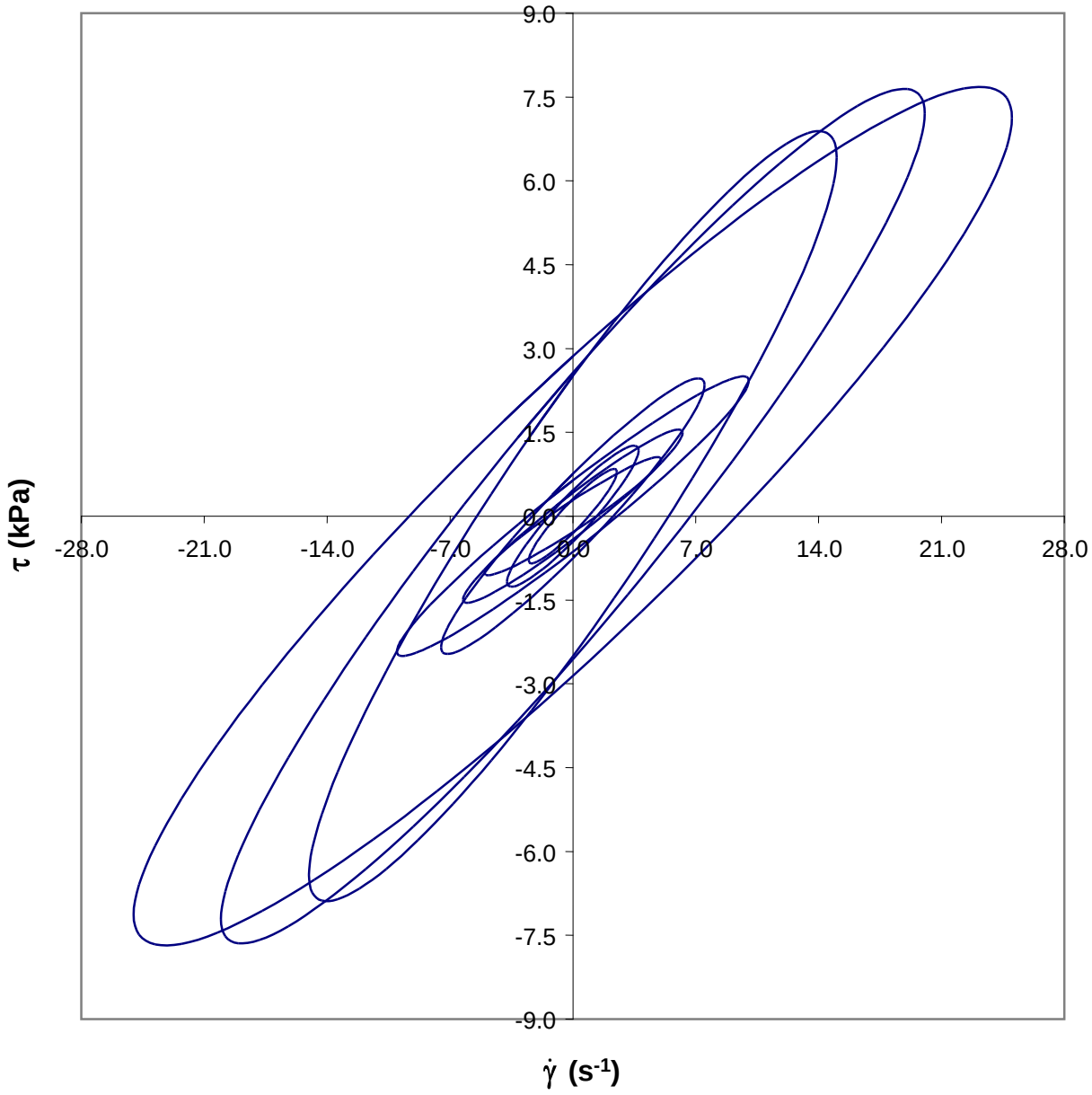

Figure 53 Shear stress *versus* shear rate loops for 4 week old reduced-fat cheddar at 60°C with f_o = 0.4 Hz. Strain amplitudes are 1, 1.5, 2, 2.5, 3, 4, 6, 8, and 10. All the loops are ellipses.

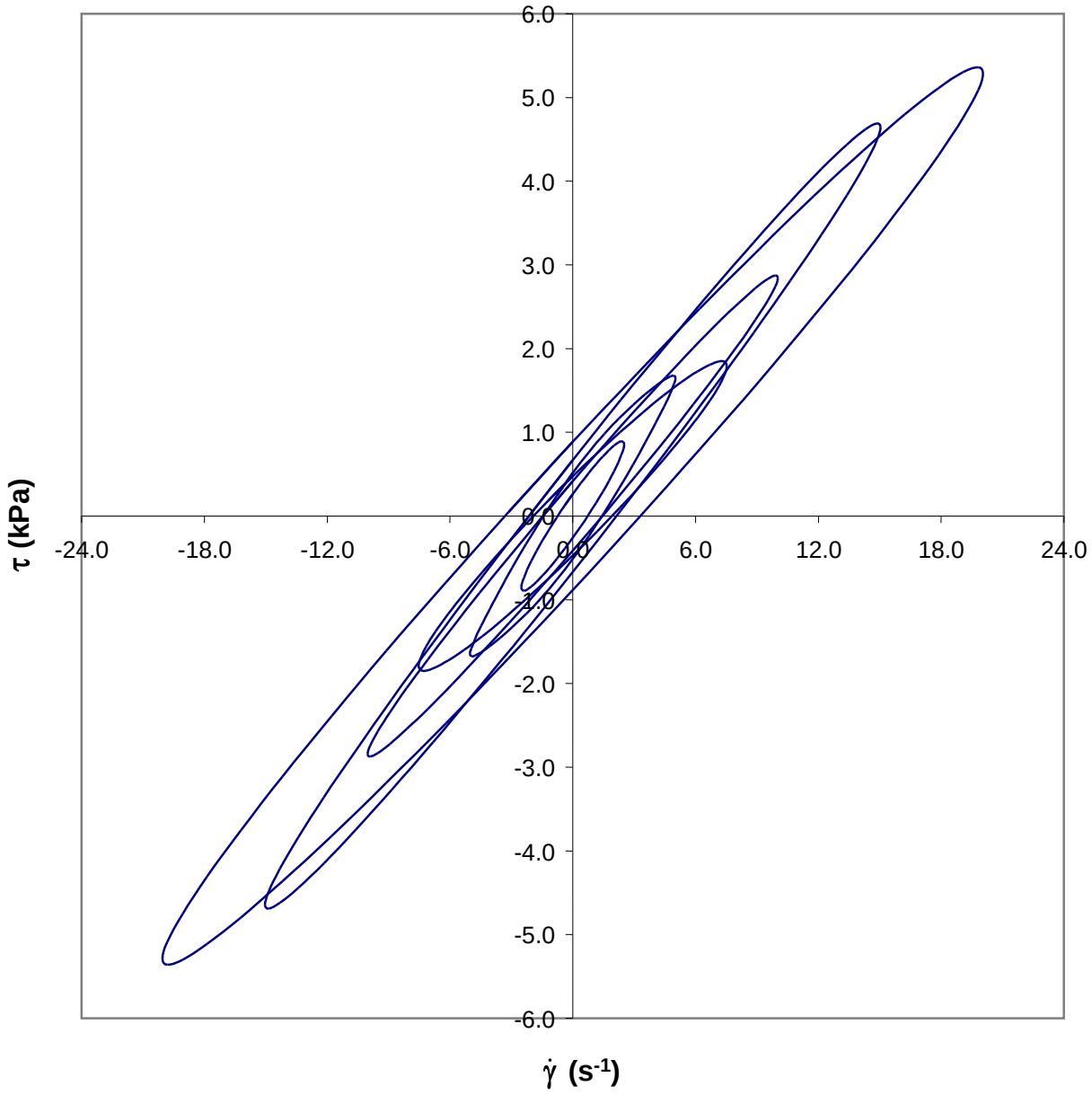

Figure 54 Shear stress *versus* shear rate loops for 6 week old reduced-fat cheddar at 60°C with f_o = 0.4 Hz. Strain amplitudes are 1, 2, 3, 4, 6, and 8. All the loops are ellipses.

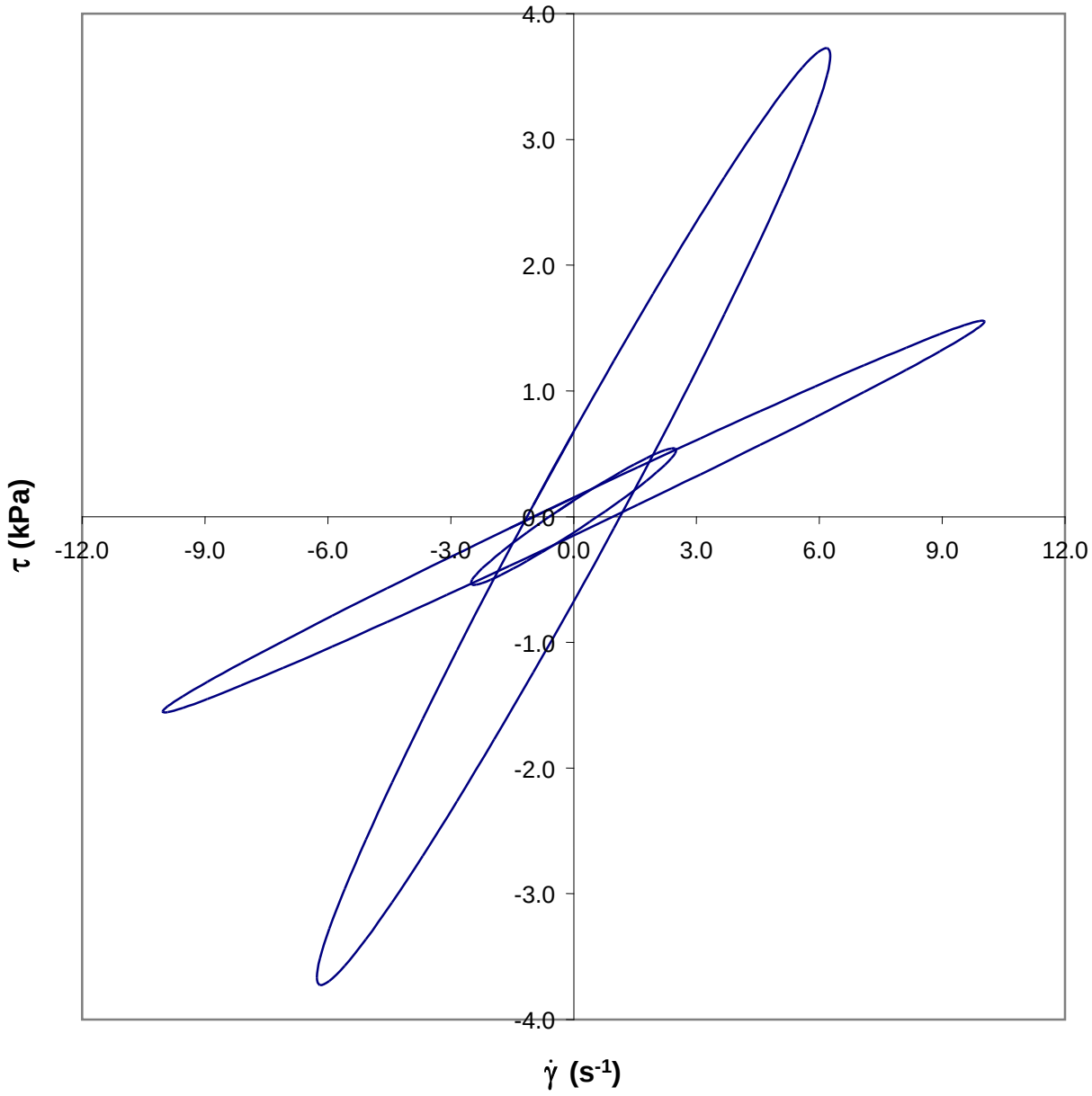

Figure 55 Shear stress *versus* shear rate loops for 12 week old reduced-fat cheddar at 60°C with f_o = 0.4 Hz. Strain amplitudes are 1, 2.5, and 4. All the loops are ellipses.

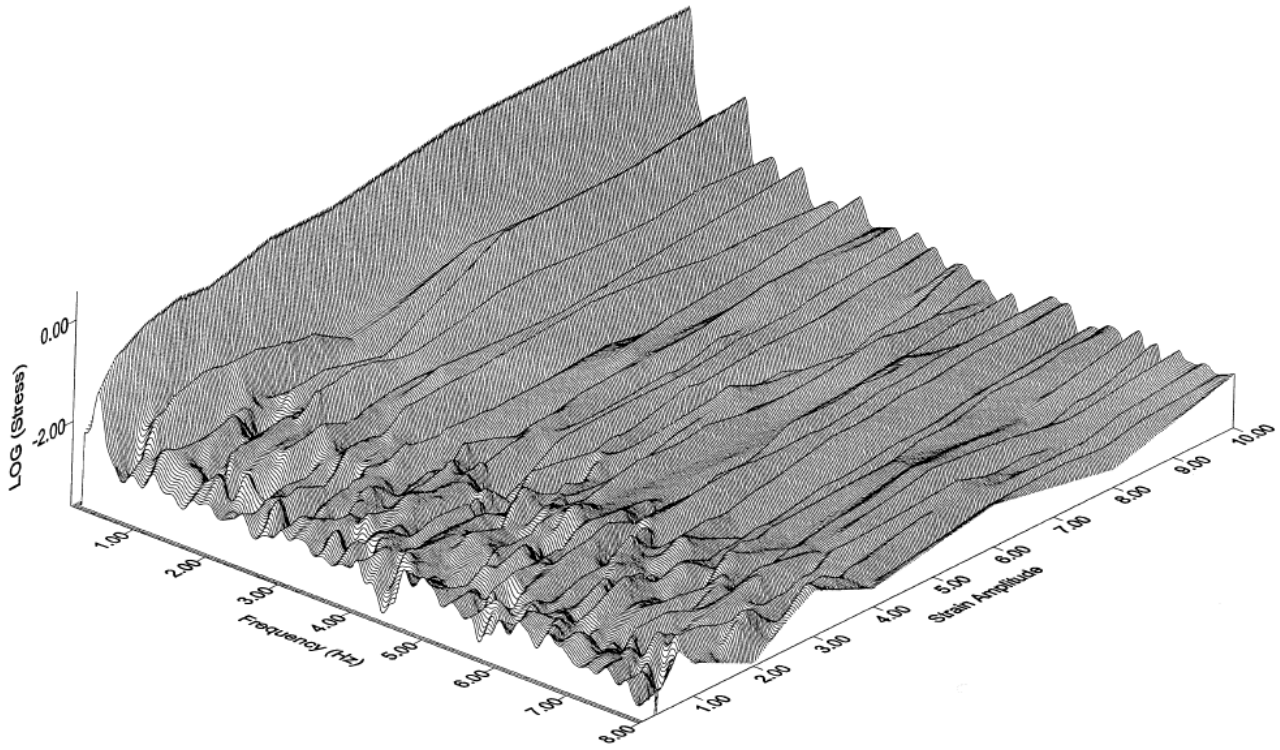

Figure 56 3D amplitude spectrum for 4 week old reduced-fat cheddar at 60°C with f_o = 0.4 Hz. Although higher harmonics are detected, only the fundamental harmonic at 0.4 Hz matters.

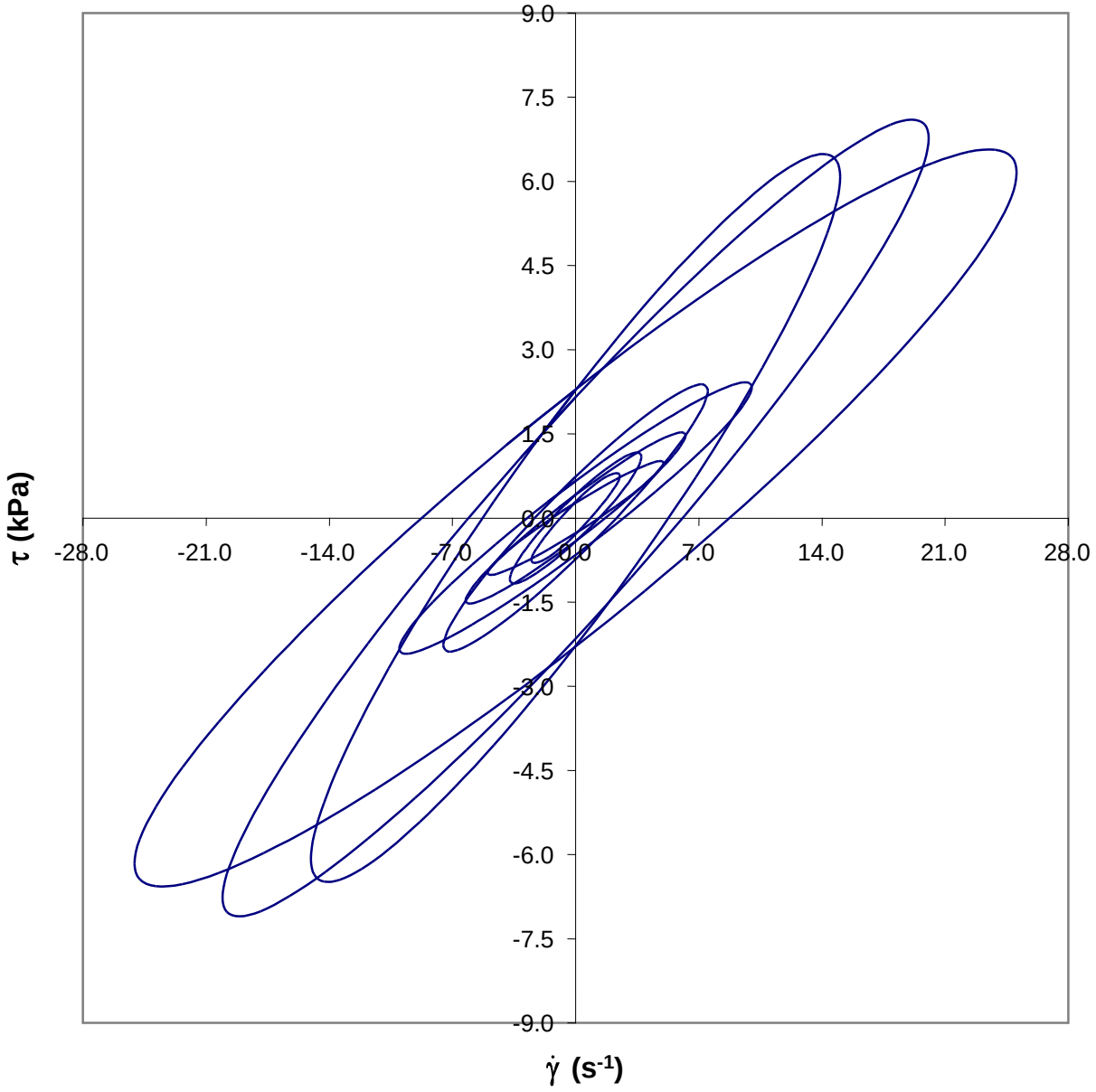

Figure 57 Shear stress *versus* shear rate loops for 4 week old reduced-fat cheddar. Same samples repeated at 60°C and test frequency of 0.4 Hz. Strain amplitudes are 1, 1.5, 2, 2.5, 3, 4, 6, and 8. Cheddar exhibits good repeatability.

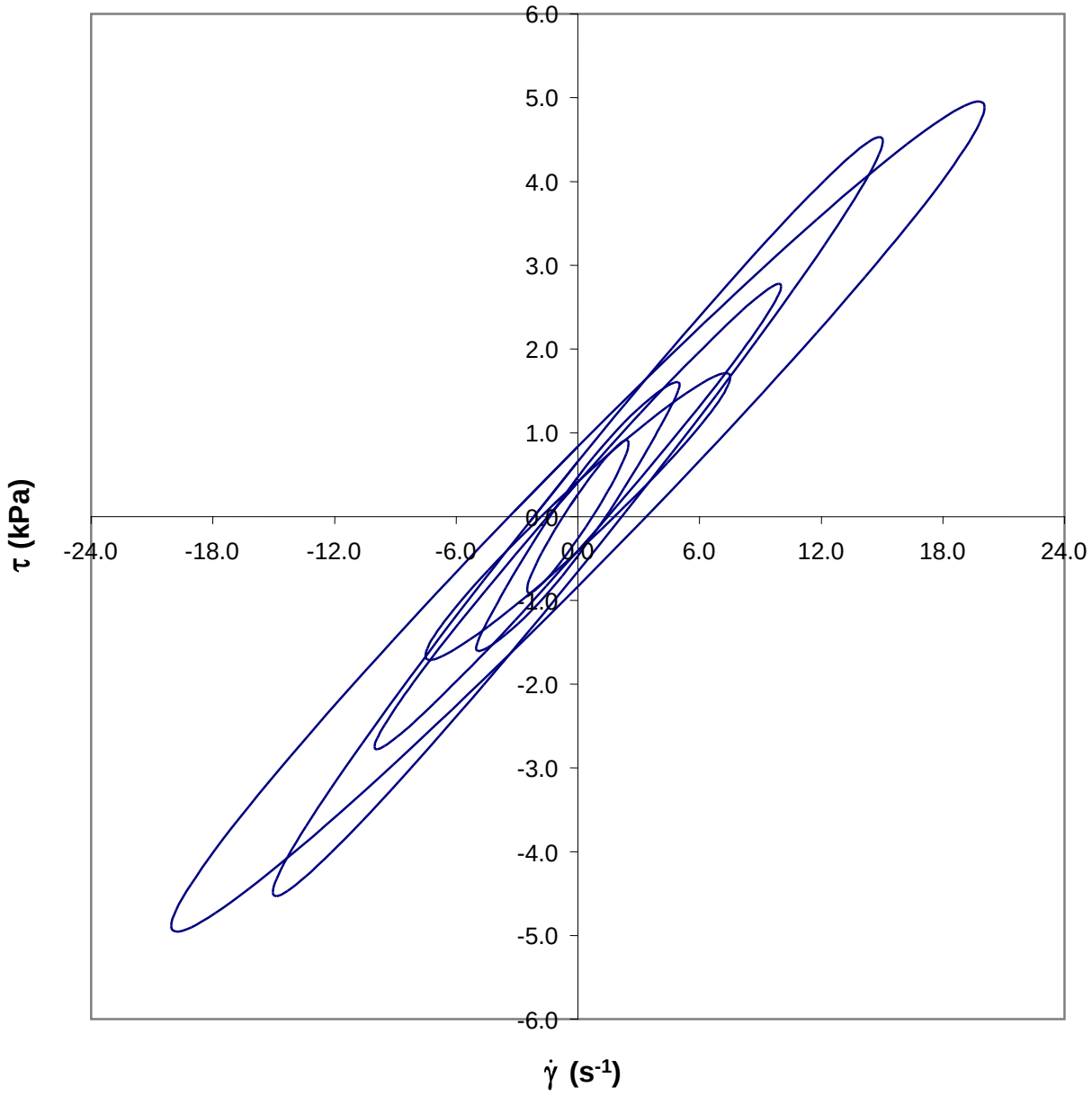

Figure 58 Shear stress *versus* shear rate loops for 6 week old reduced-fat cheddar. Same samples repeated at 60°C with f_o = 0.4 Hz. Strain amplitudes are 1, 2, 3, 4, 6, and 8. Cheddar exhibits good repeatability.

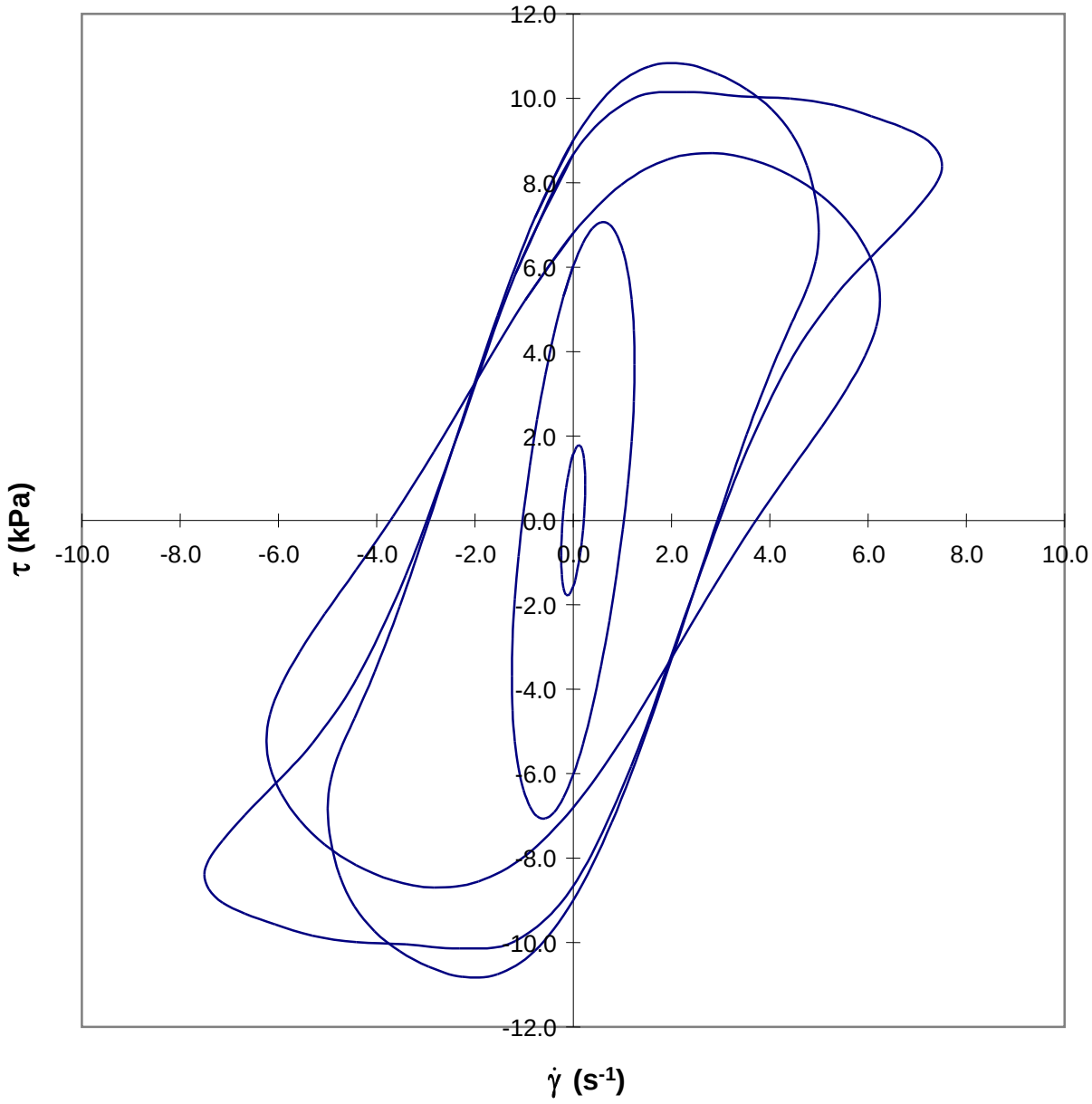

Figure 59 Shear stress *versus* shear rate loops for 1 week old reduced-fat pizza cheese at 40°C with f_o = 0.4 Hz. Strain amplitudes are 0.1, 0.5, 2, 2.5, and 3.

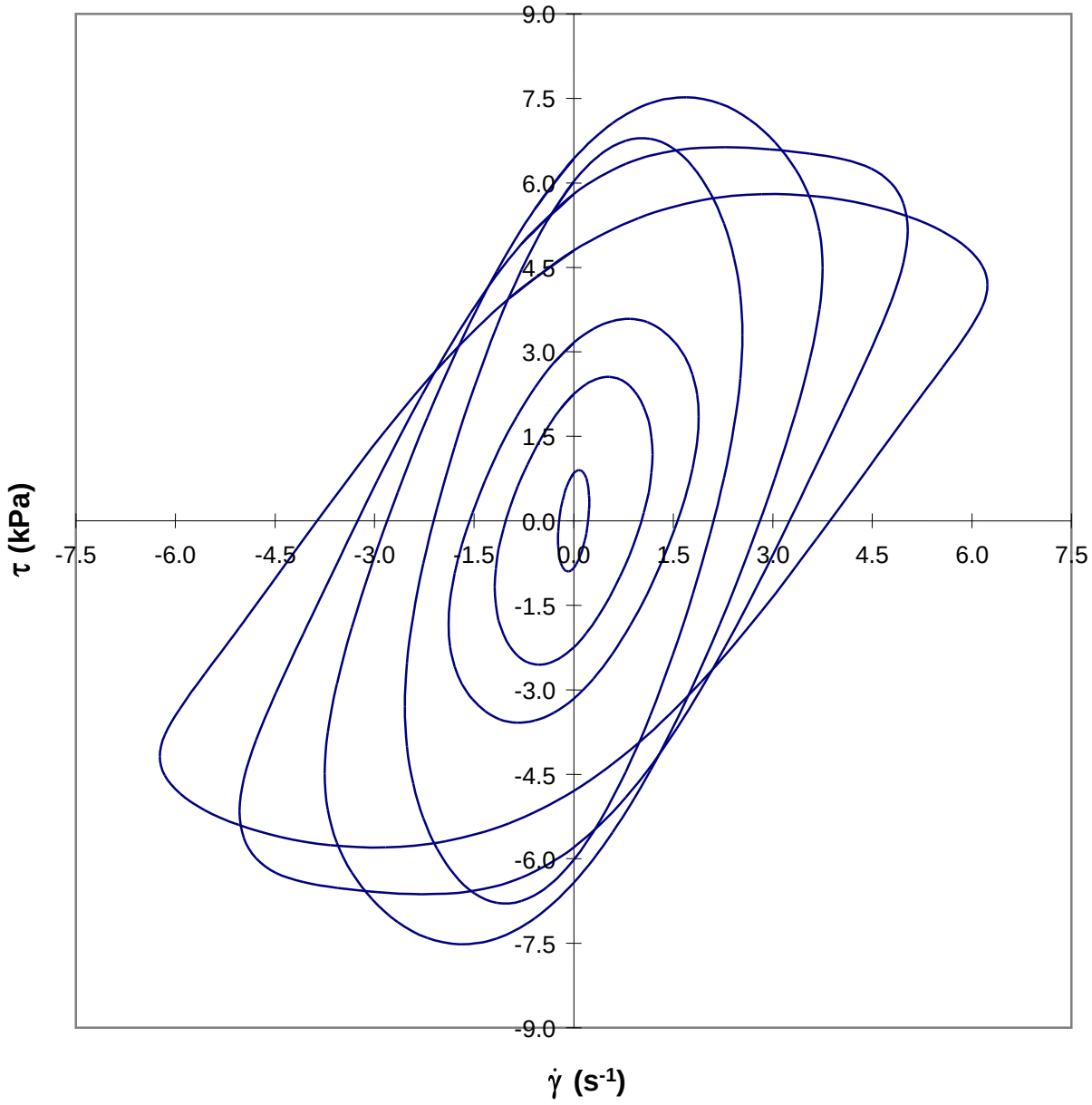

Figure 60 Shear stress *versus* shear rate loops for 4 week old reduced-fat pizza cheese at 40°C with f_o = 0.4 Hz. Strain amplitudes are 0.1, 0.5, 0.75, 1, 1.5, 2, and 2.5.

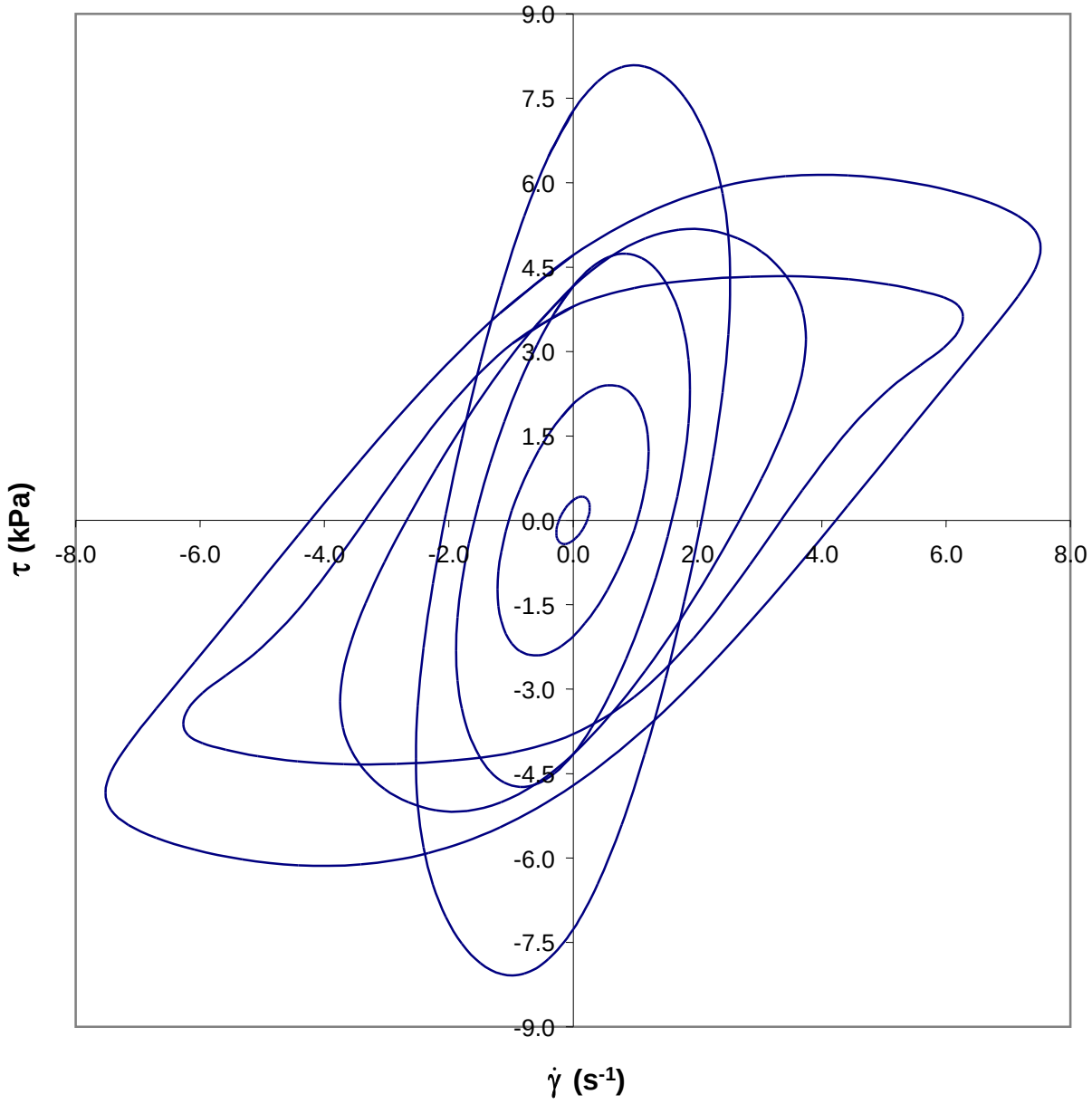

Figure 61 Shear stress *versus* shear rate loops for 6 week old reduced-fat pizza cheese at 40°C with f_o = 0.4 Hz. Strain amplitudes are 0.1, 0.5, 0.75, 1, 1.5, 2.5, and 3.

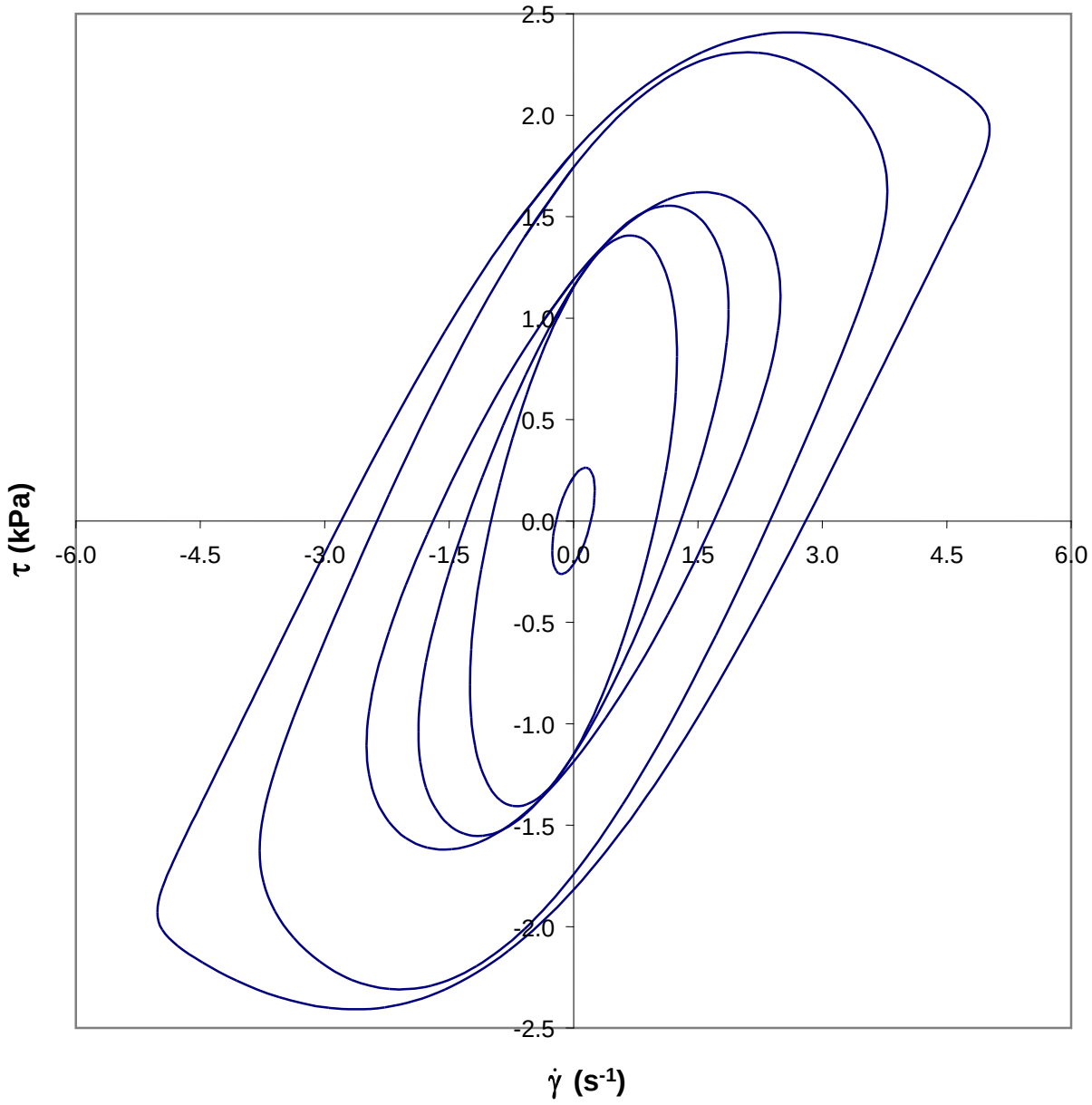

Figure 62 Shear stress *versus* shear rate loops for 12 week old reduced-fat pizza cheese at 40°C with f_o = 0.4 Hz. Strain amplitudes are 0.1, 0.5, 0.75, 1, 1.5, and 2.

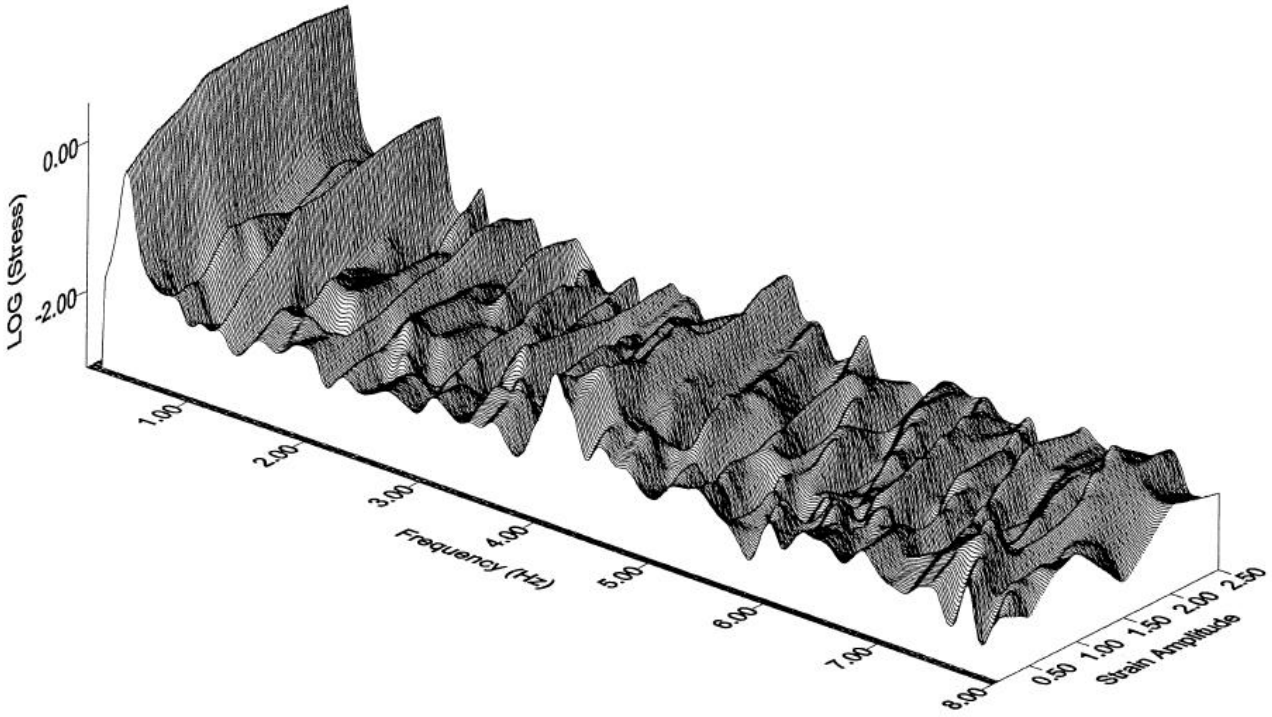

Figure 63 3D amplitude spectrum for 4 week old reduced-fat pizza cheese at 40°C with f_o = 0.4 Hz. The third harmonic rises with strain amplitude.

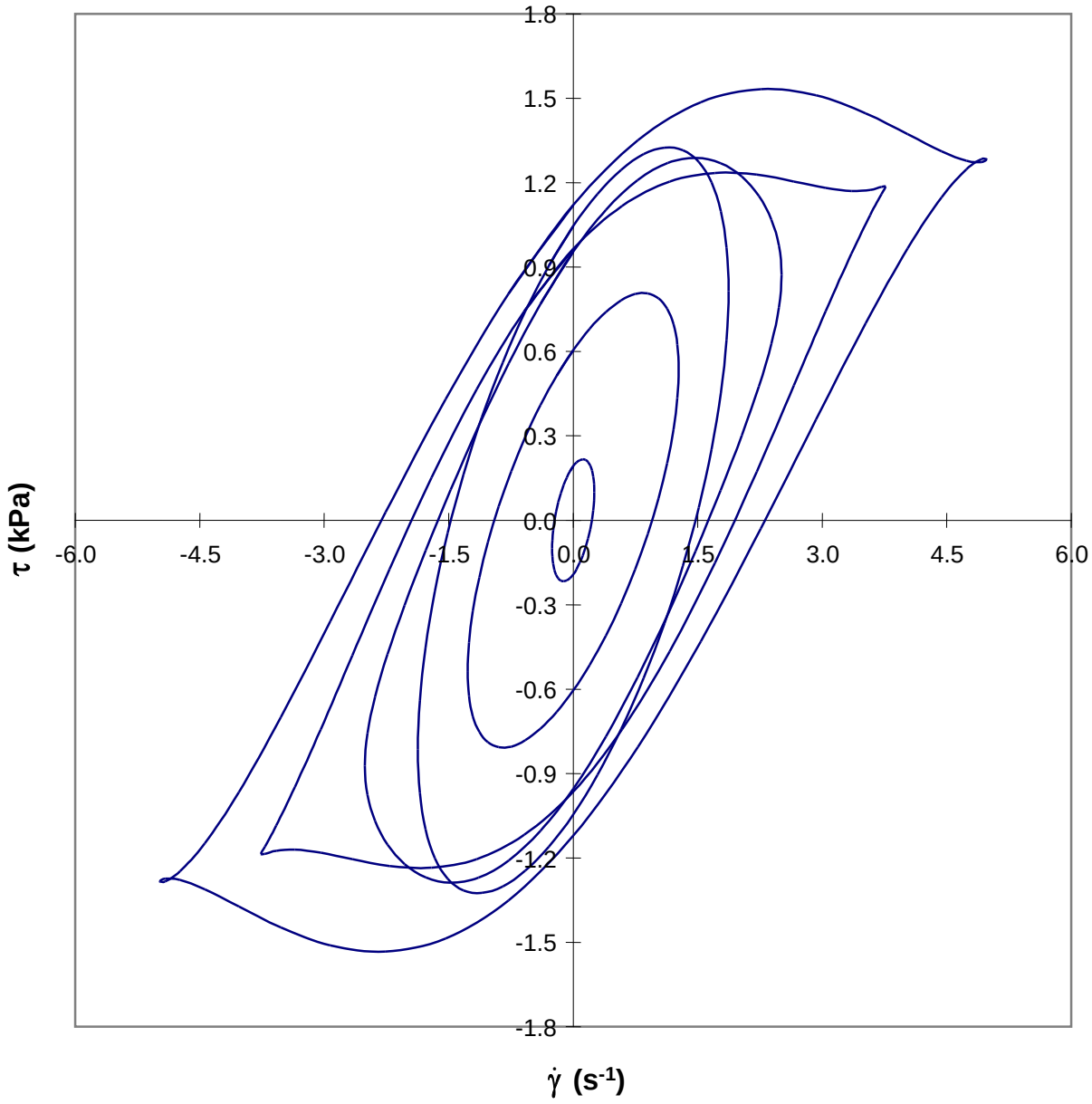

Figure 64 Shear stress *versus* shear rate loops for 4 week old full-fat pizza cheese at 40°C with f_o = 0.4 Hz. Strain amplitudes are 0.1, 0.5, 0.75, 1, 1.5, and 2.

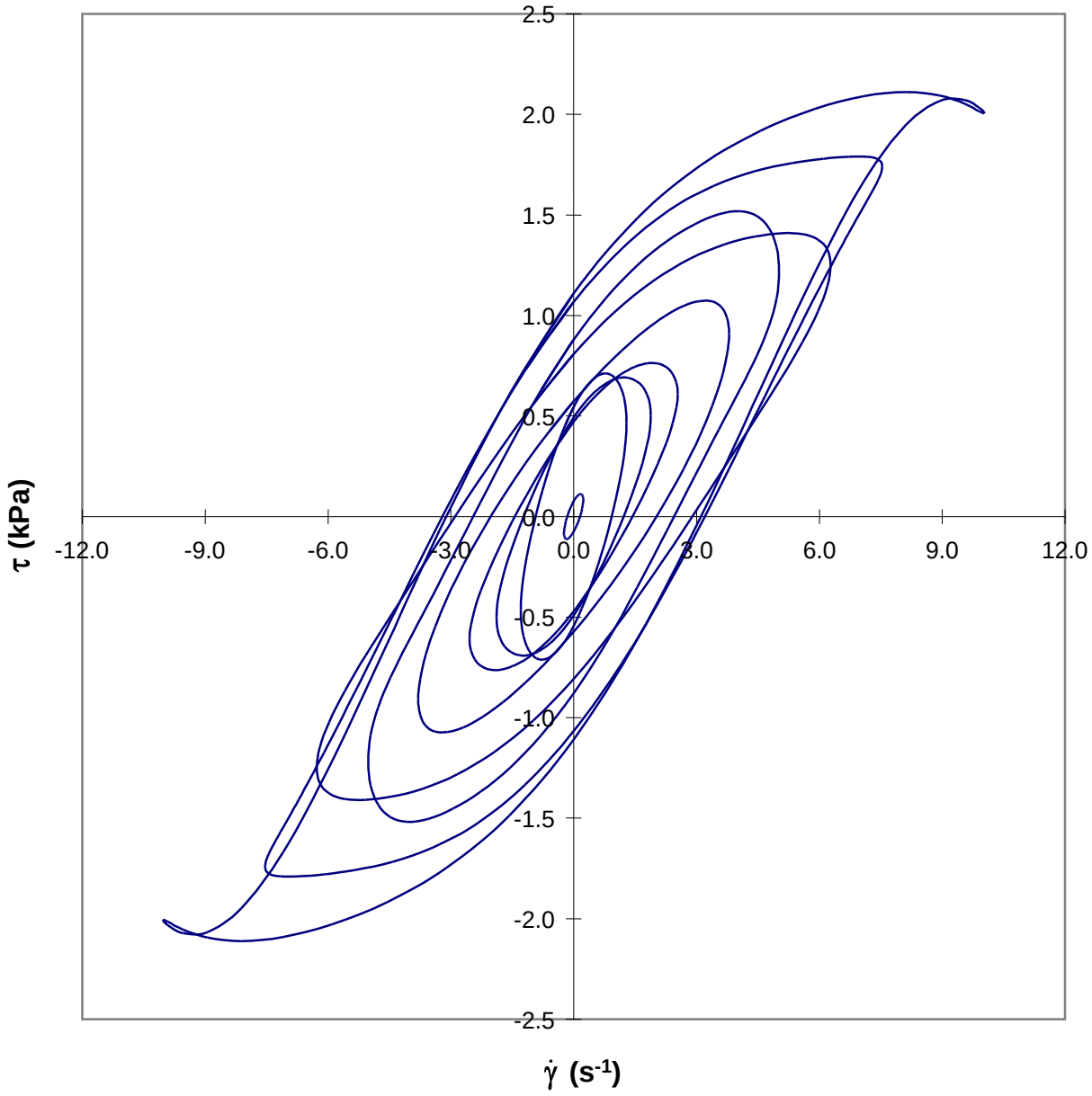

Figure 65 Shear stress *versus* shear rate loops for 6 week old full-fat pizza cheese at 40°C with f_o = 0.4 Hz. Strain amplitudes are 0.1, 0.5, 0.75, 1, 1.5, 2, 2.5, 3, and 4.

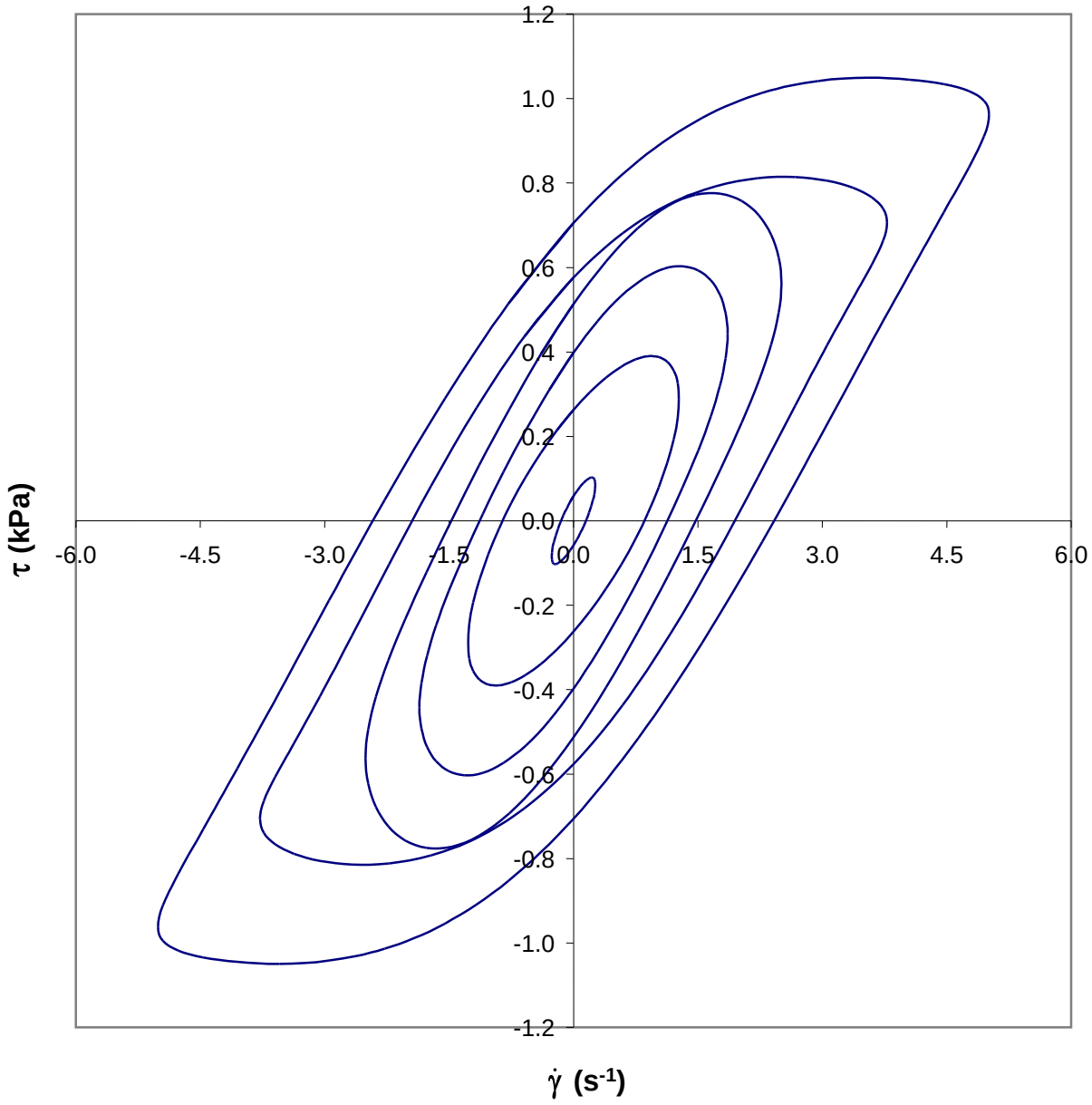

Figure 66 Shear stress *versus* shear rate loops for 12 week old full-fat pizza cheese at 40°C with f_o = 0.4 Hz. Strain amplitudes are 0.1, 0.5, 0.75, 1, 1.5, and 2.

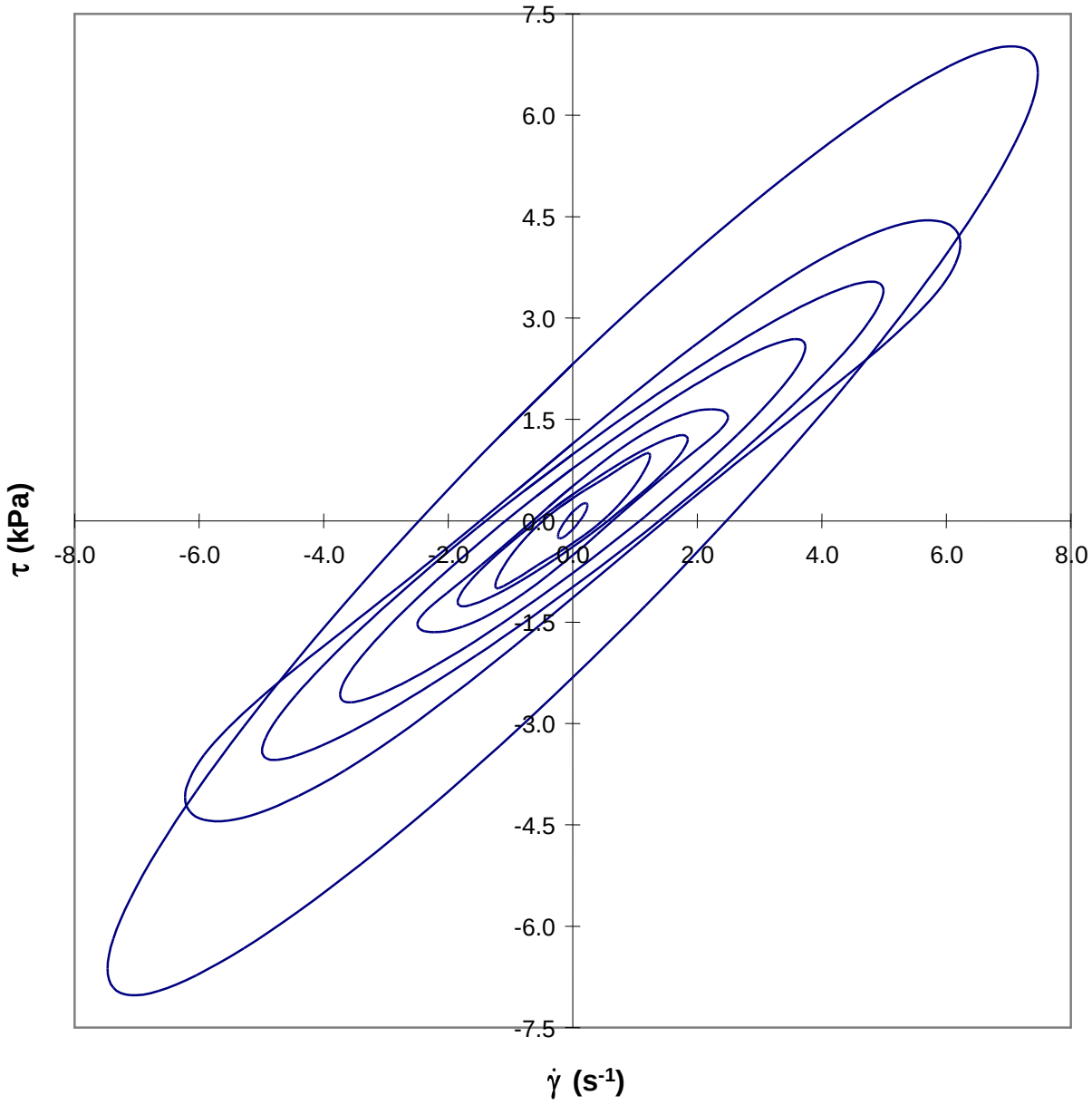

Figure 67 Shear stress *versus* shear rate loops for 1 week old reduced-fat pizza cheese at 60°C with f_o = 0.4 Hz. Strain amplitudes are 0.1, 0.5, 0.75, 1, 1.5, 2, 2.5, and 3.

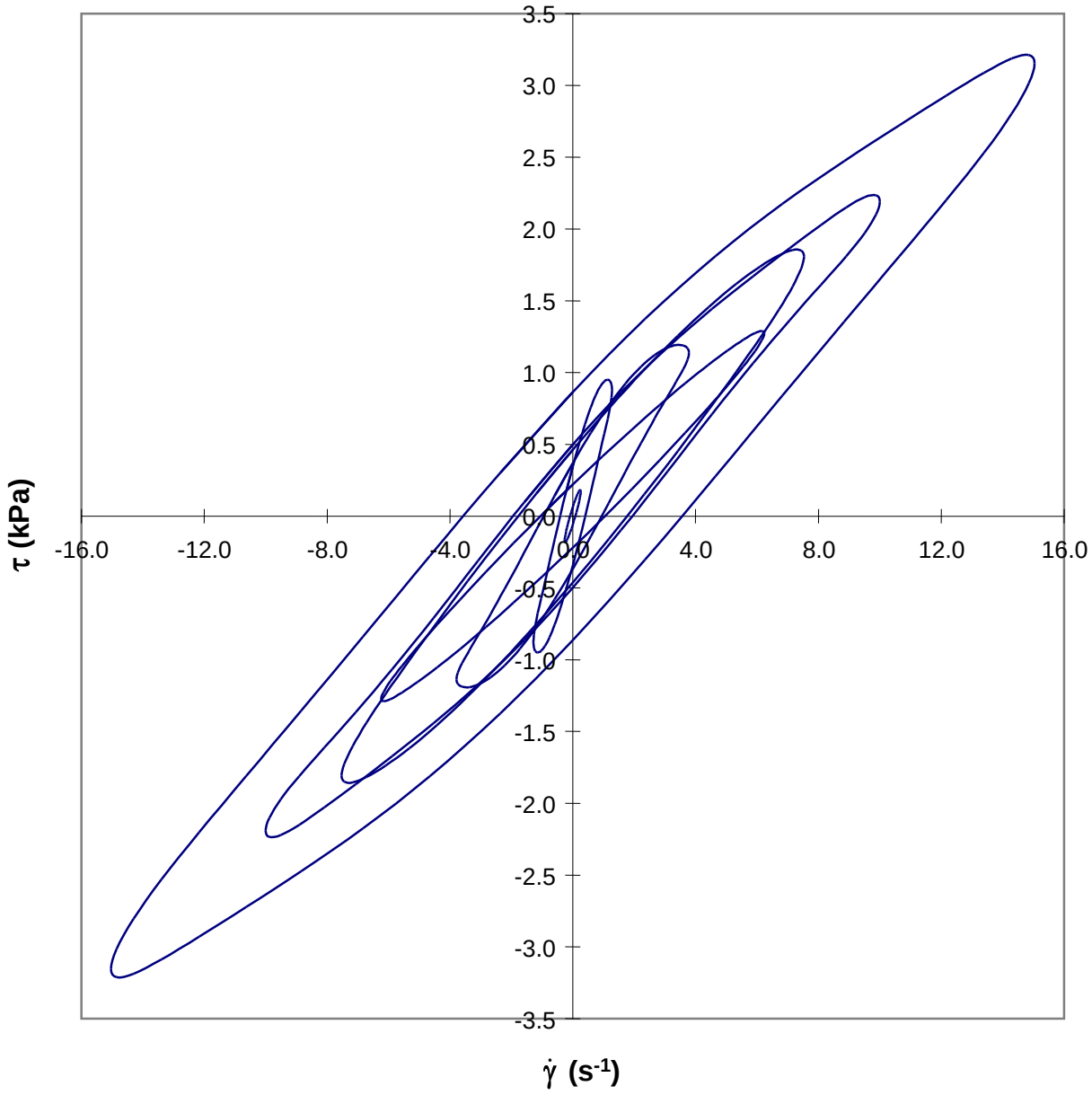

Figure 68 Shear stress *versus* shear rate loops for 4 week old reduced-fat pizza cheese at 60°C with f_o = 0.4 Hz. Strain amplitudes are 0.1, 0.5, 1.5, 2.5, 3, 4, and 6.

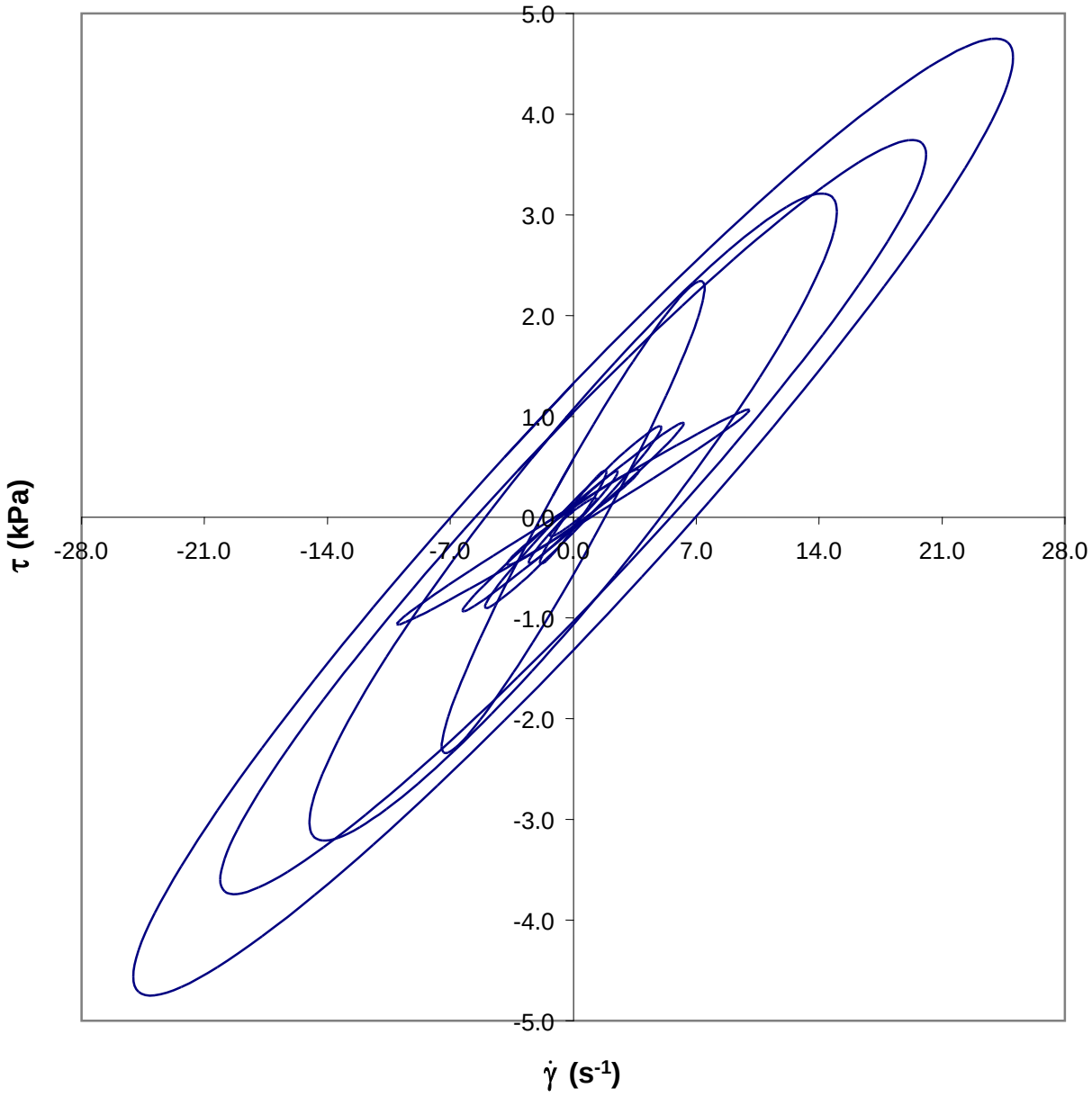

Figure 69 Shear stress *versus* shear rate loops for 6 week old reduced-fat pizza cheese at 60°C with f_o = 0.4 Hz. Strain amplitudes are 0.5, 0.75, 1, 1.5, 2, 2.5, 3, 4, 6, 8, and 10.

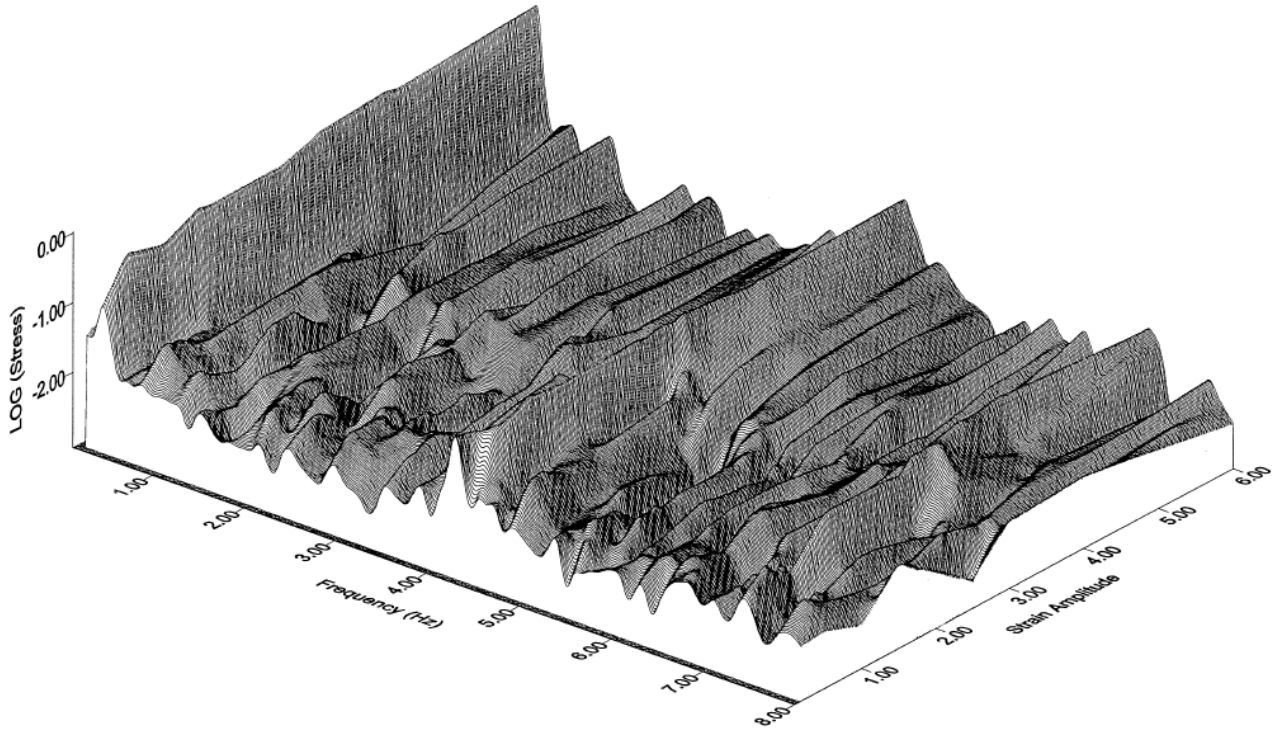

Figure 70 3D amplitude spectrum for 4 week old reduced-fat pizza cheese at 60ºC with f_o = 0.4 Hz. Although higher harmonics are detected, only the fundamental harmonic at 0.4 Hz matters.

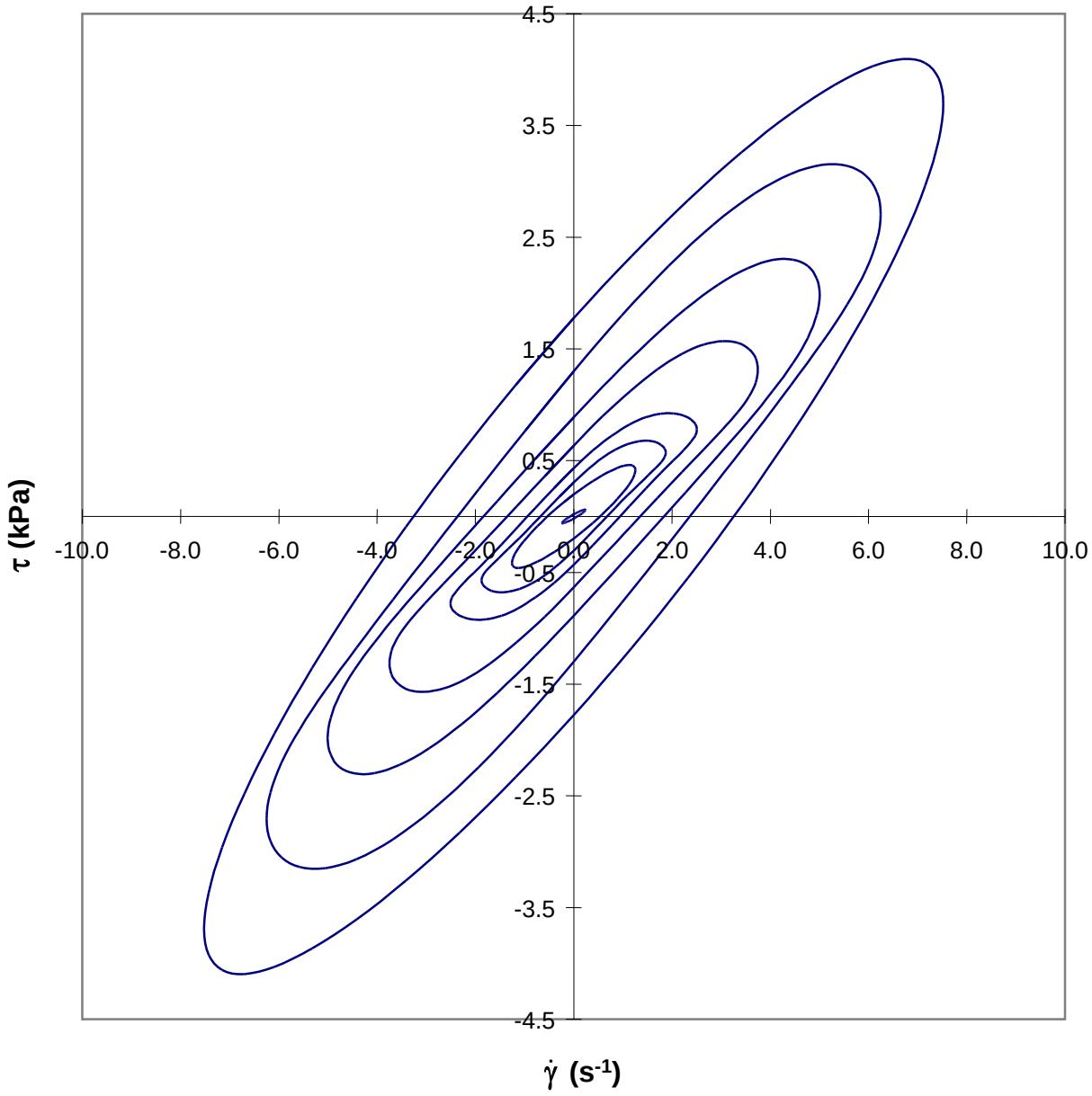

Figure 71 Shear stress *versus* shear rate loops for 1 week old full-fat pizza cheese at 60°C with f_o = 0.4 Hz. Strain amplitudes are 0.1, 0.5, 0.75, 1, 1.5, 2, 2.5, and 3.

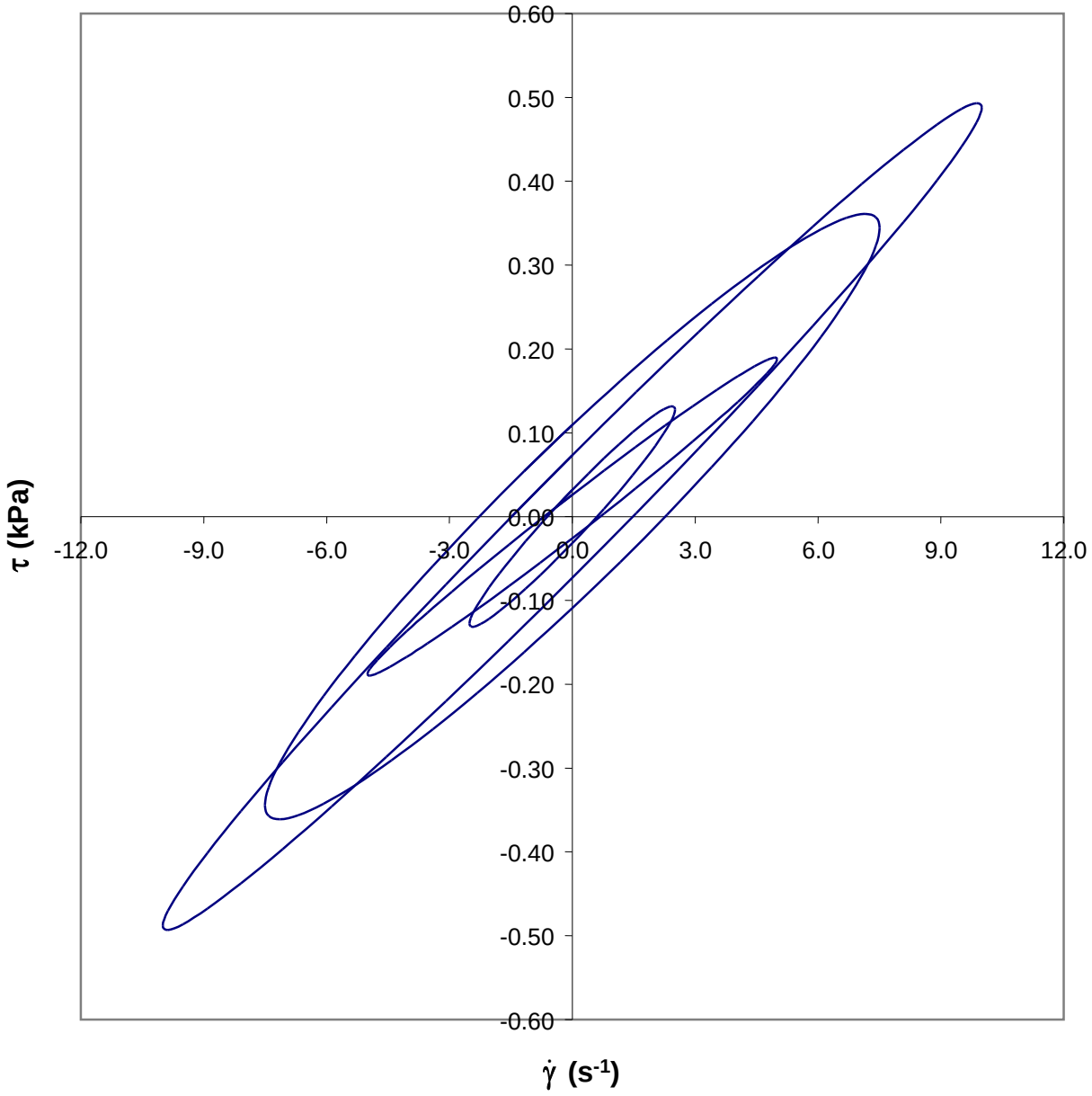

Figure 72 Shear stress *versus* shear rate loops for 6 week old full-fat pizza cheese at 60°C with f_o = 0.4 Hz. Strain amplitudes are 1, 2, 3, and 4.

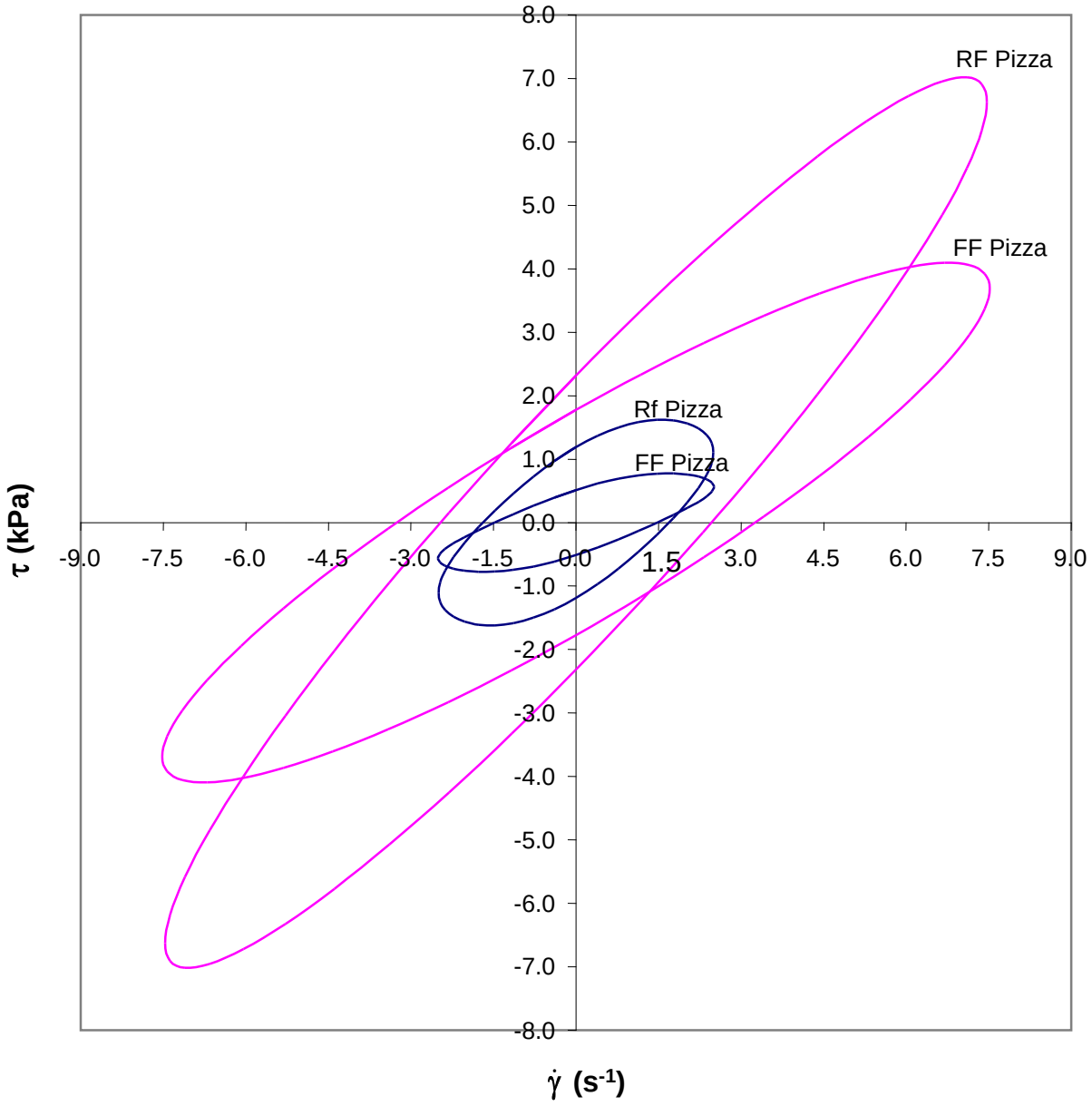

Figure 73 Effect of fat content on pizza cheese. Outer two loops are at 60°C and γ_o = 3, inner loops are at 40°C and γ_o = 1; with f_o = 0.4 Hz. Fat nearly halves the stresses.

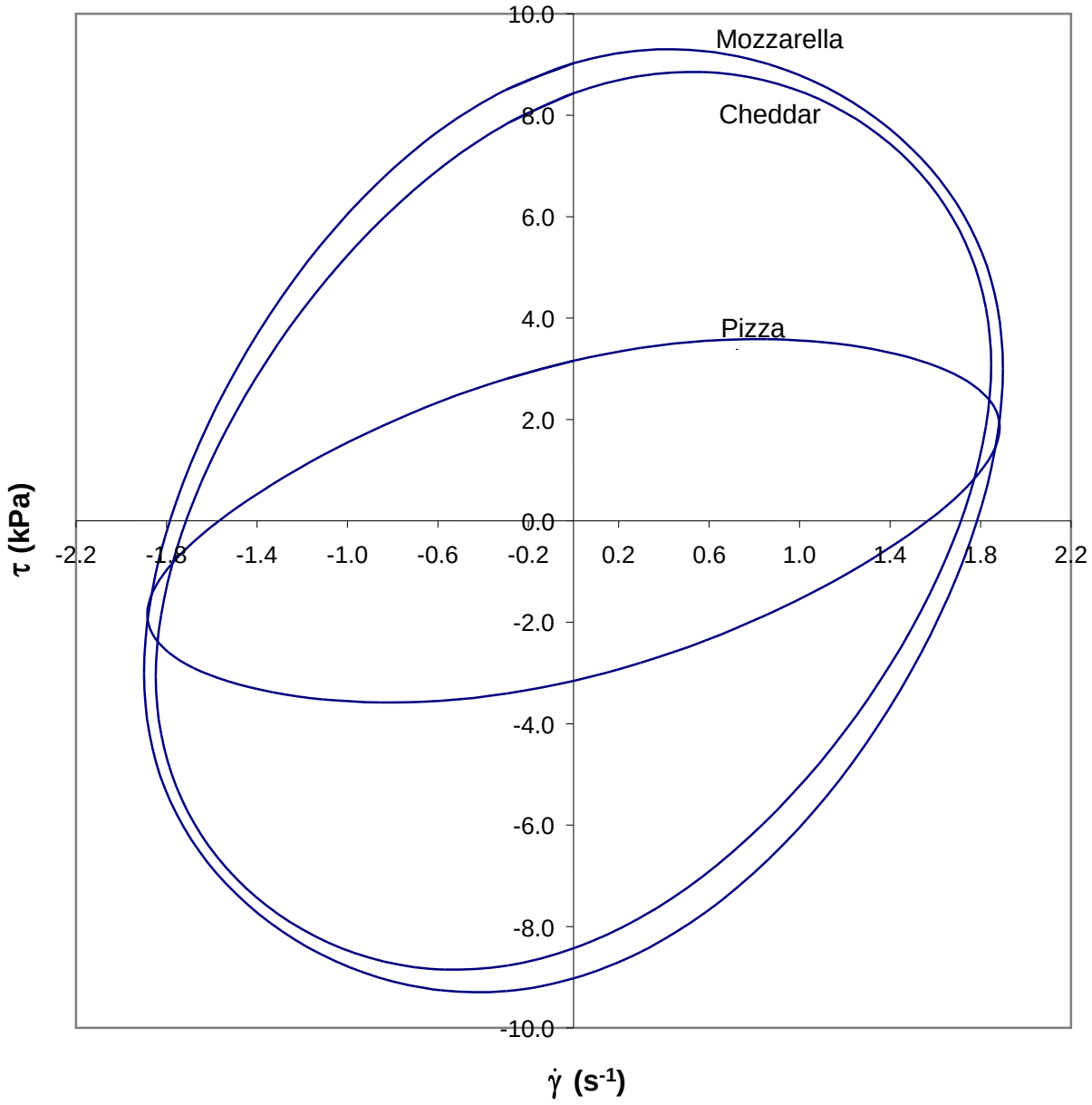

Figure 74 Comparing shear stress *versus* shear rate loops (γ_o = 0.75) for the reduced-fat, natural cheeses at 4 weeks and 40°C, with f_o = 0.4. Mozzarella and cheddar are similar; pizza cheese is much softer.

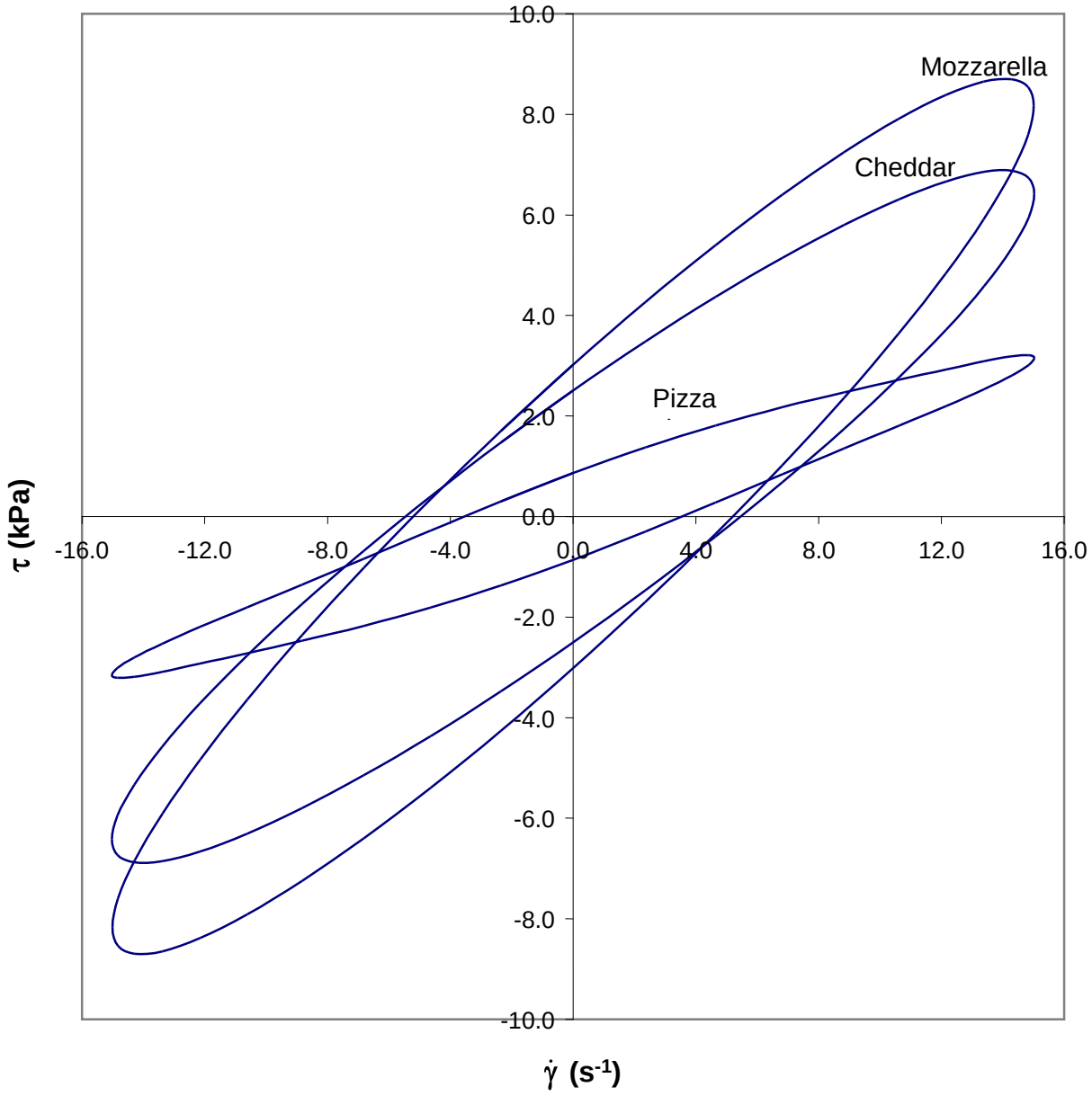

Figure 75 Comparing shear stress *versus* shear rate loops (γ_o = 0.75) for the reduced-fat, natural cheeses at 4 weeks and 60°C, with f_o = 0.4. Mozzarella and cheddar are similar; pizza cheese is much softer.

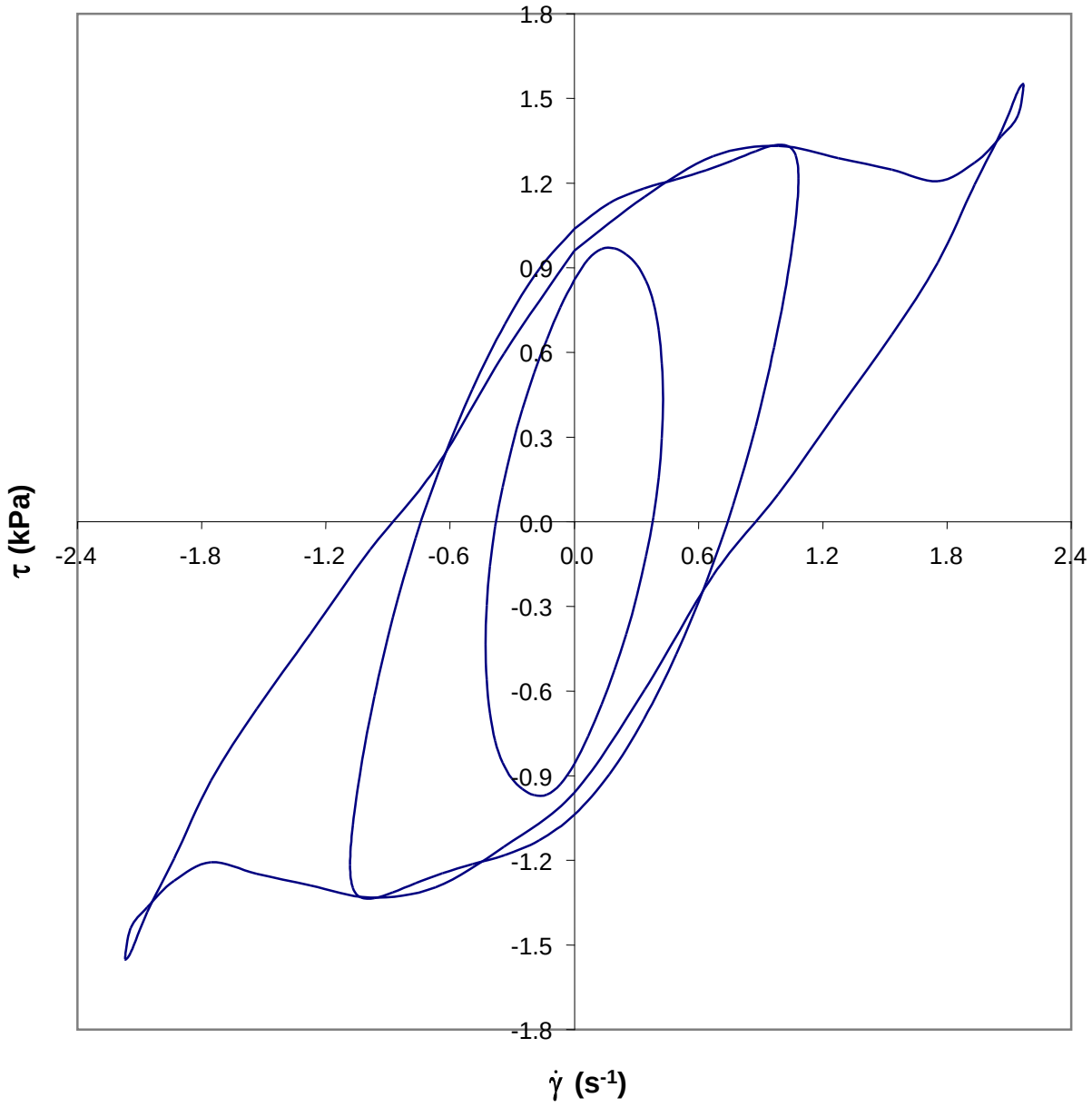

Figure 76 Shear stress *versus* shear rate loops for fat-free process mozzarella at 30°C with f_o = 0.25 Hz. Strain amplitudes are 0.3, 0.8, and 1.4.

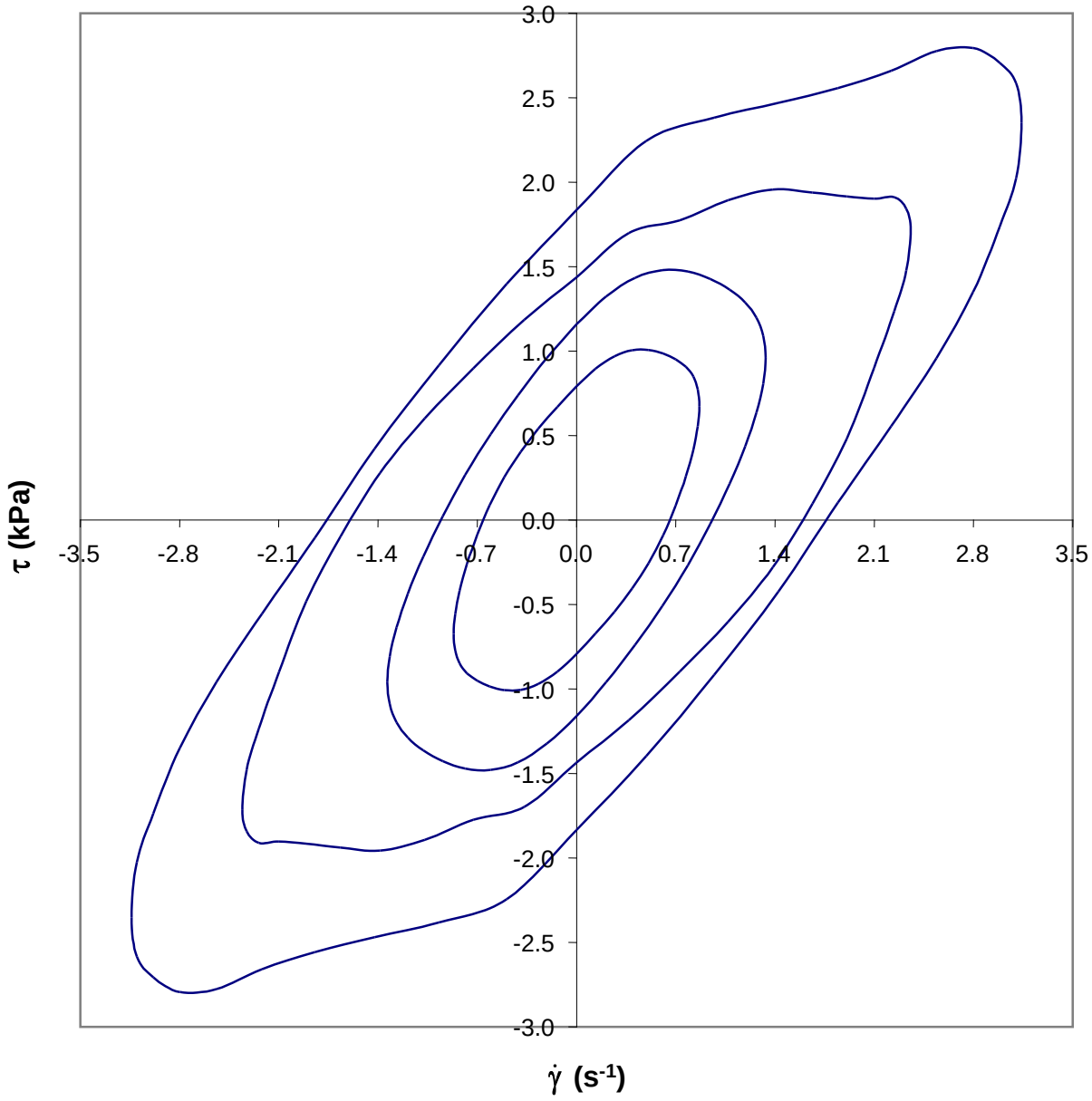

Figure 77 Shear stress *versus* shear rate loops for fat-free process mozzarella at 35°C with f_o = 0.25 Hz. Strain amplitudes are 0.55, 0.8, 1.4, and 2. Loops become concentric at the higher temperature.

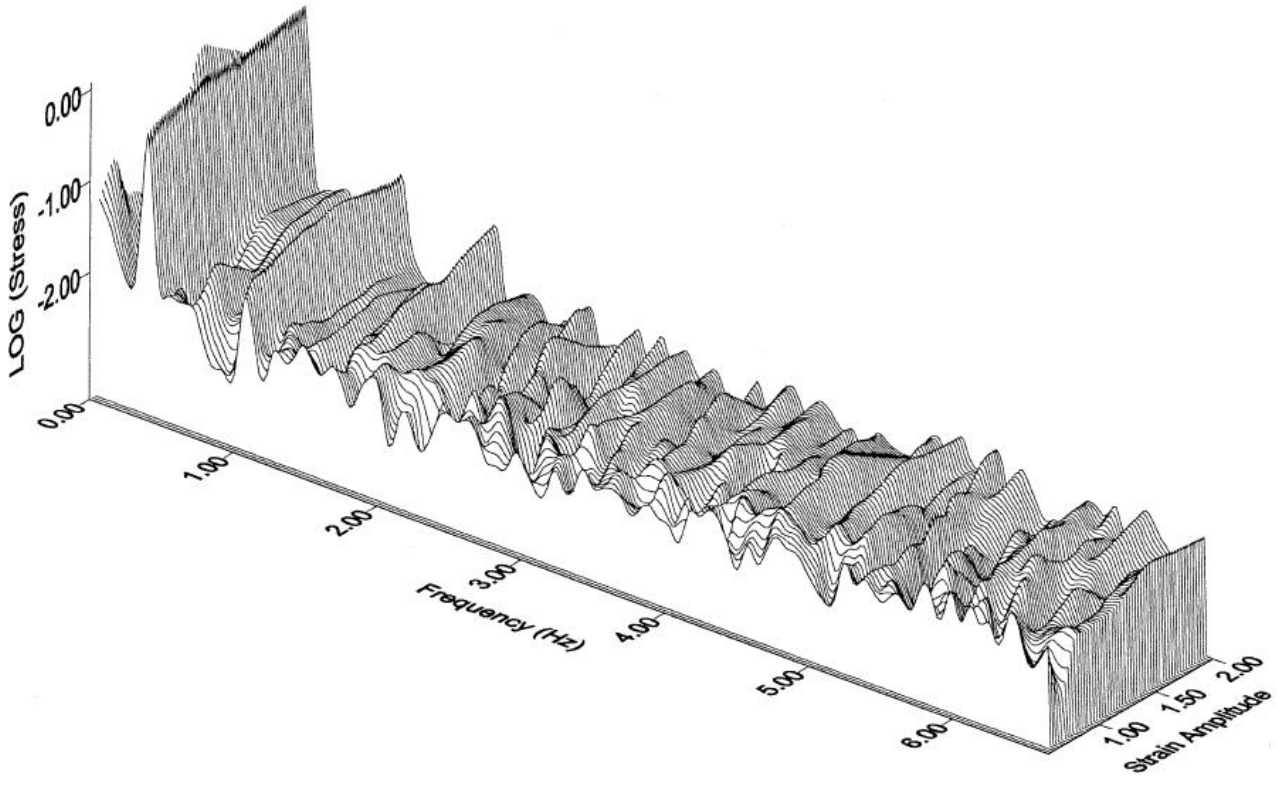

Figure 78 3D Amplitude spectrum for fat-free process mozzarella at 35ºC with f_o = 0.25 Hz. The higher, odd harmonics rise with strain amplitude.

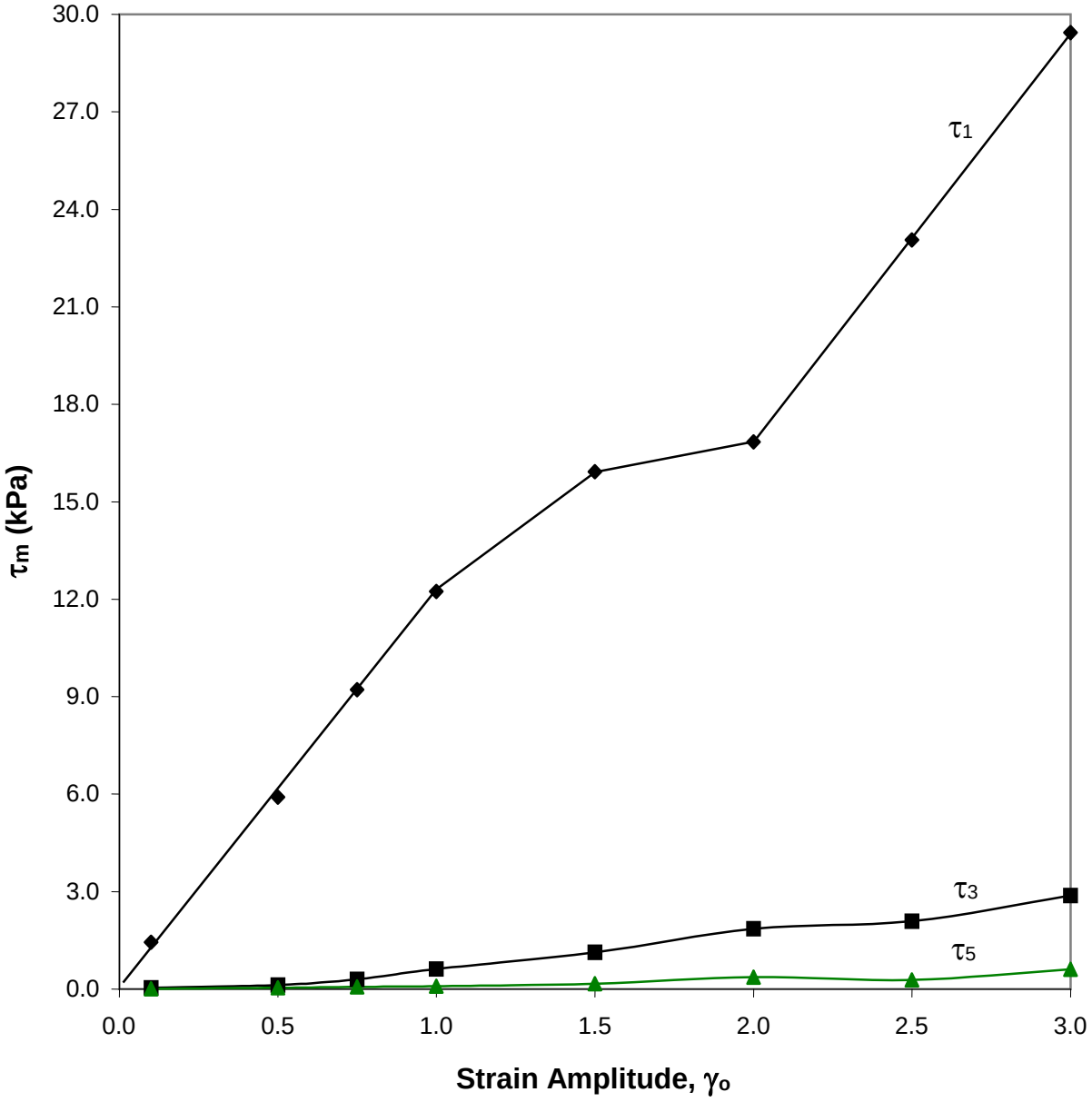

Figure 79 Effect of γ_o on fundamental, third and fifth harmonics of shear stress for reduced-fat mozzarella at 4 weeks and 40°C, with f_o = 0.4 Hz. The higher, odd harmonics rise with γ_o.

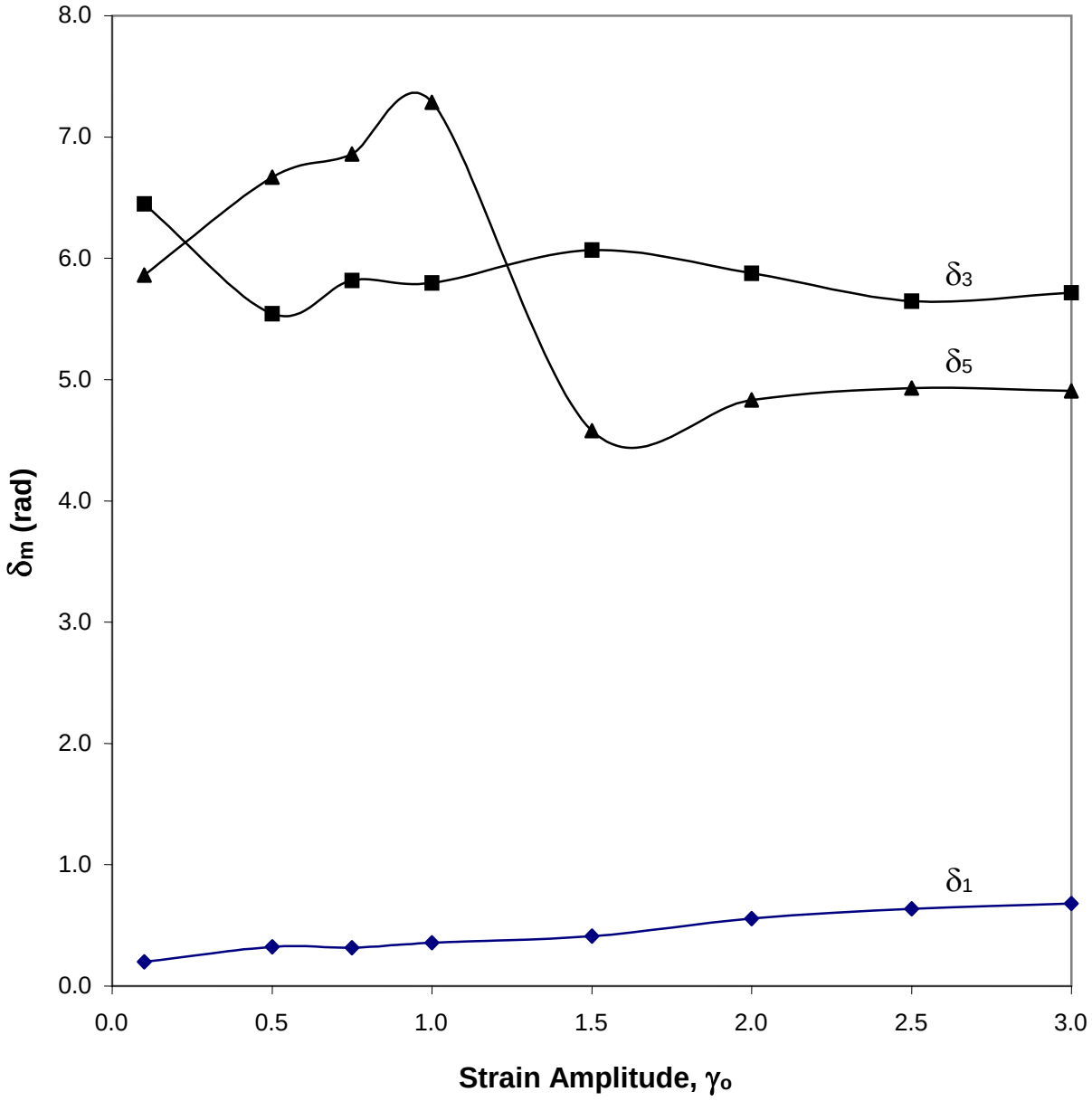

Figure 80 Effect of γ_o on the phase angles of the principal harmonics of shear stress for reduced-fat mozzarella at 4 weeks and 40°C, with f_o = 0.4 Hz. δ_1 rises with γ_o, while δ_3 and δ_5 are not monotonic with γ_o.

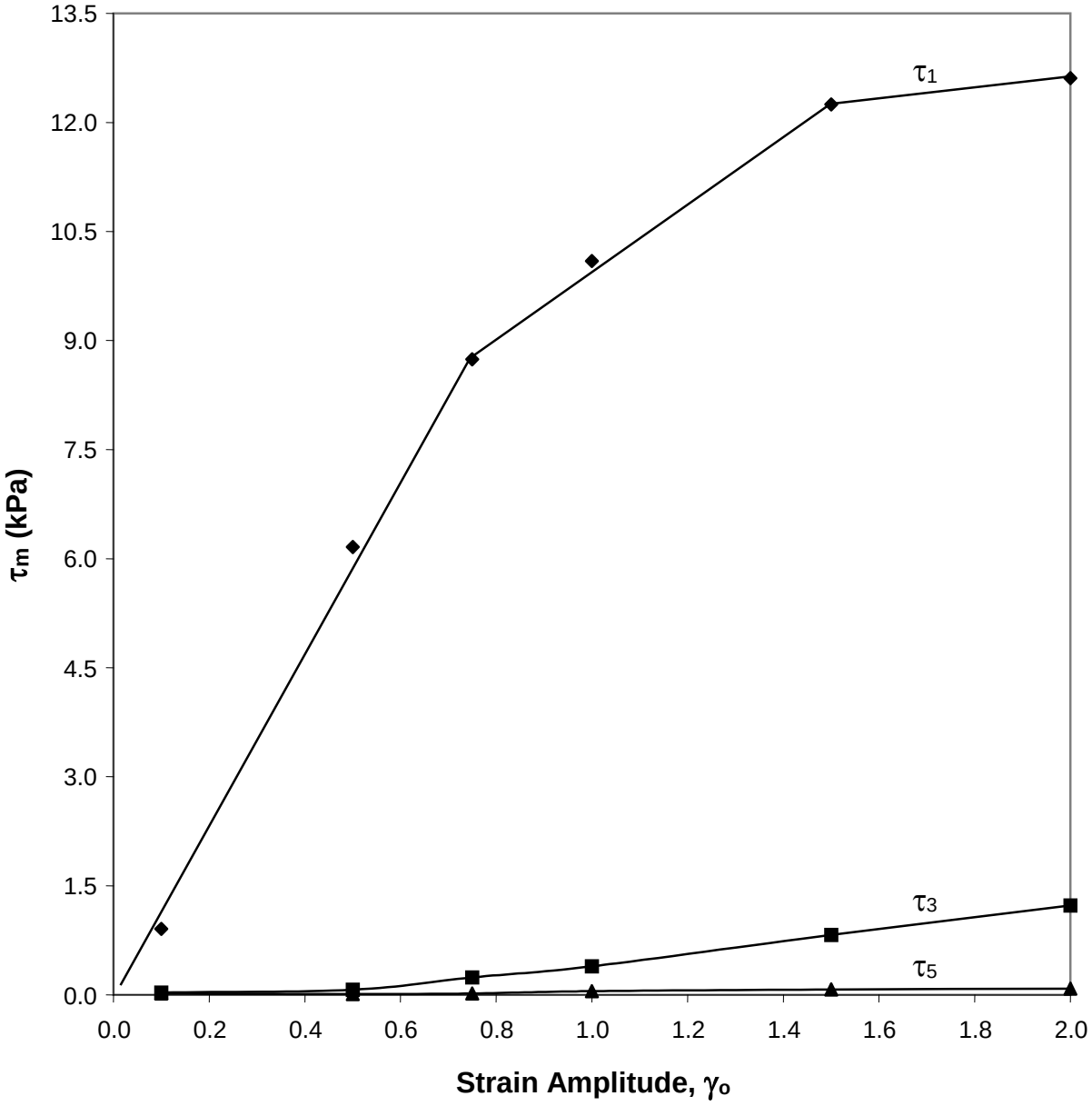

Figure 81 Effect of γ_o on fundamental, third and fifth harmonics of shear stress for reduced-fat cheddar at 4 weeks and 40°C, with f_o = 0.4 Hz. The higher, odd harmonics rise with γ_o.

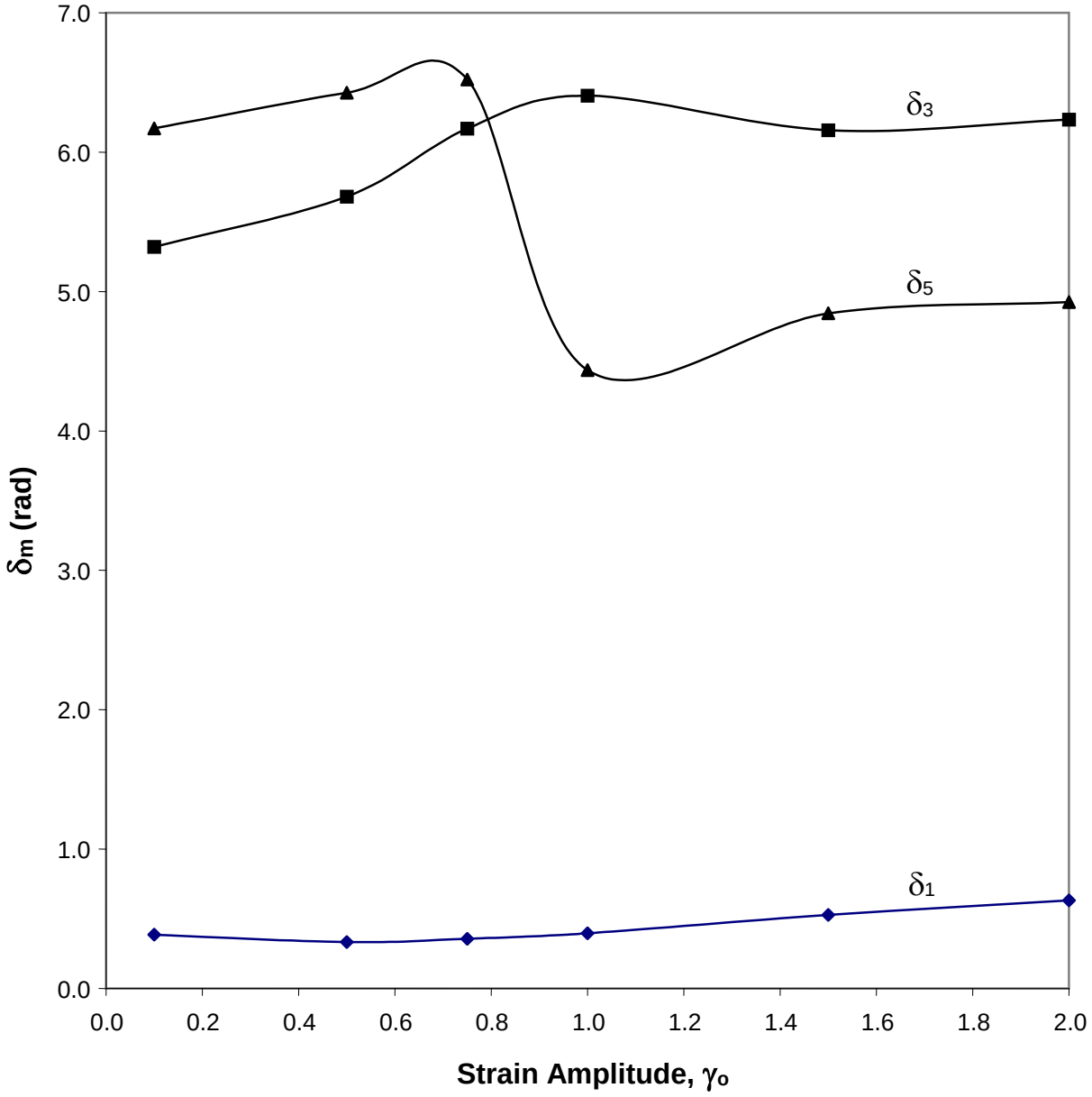

Figure 82 Effect of γ_o on the phase angles of the principal harmonics of shear stress for reduced-fat cheddar at 4 weeks and 40°C, with f_o = 0.4 Hz. δ_1 rises with increasing γ_o, while δ_3 and δ_5 are not monotonic with γ_o.

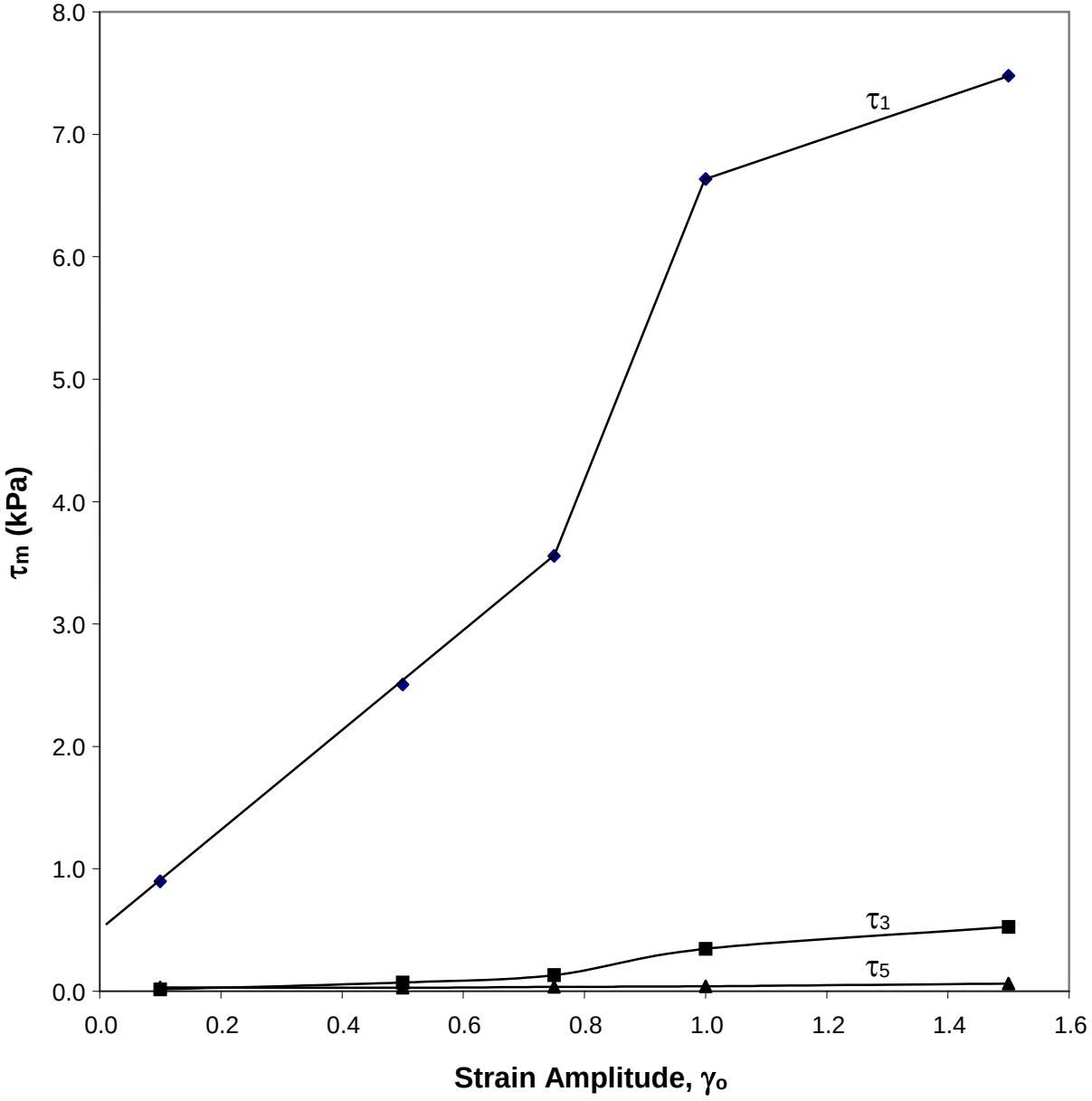

Figure 83 Effect of γ_o on fundamental, third and fifth harmonics of shear stress for reduced-fat pizza cheese at 4 weeks and 40°C, with f_o = 0.4 Hz. The higher, odd harmonics rise with γ_o, and pizza cheese appears to exhibit a yield stress.

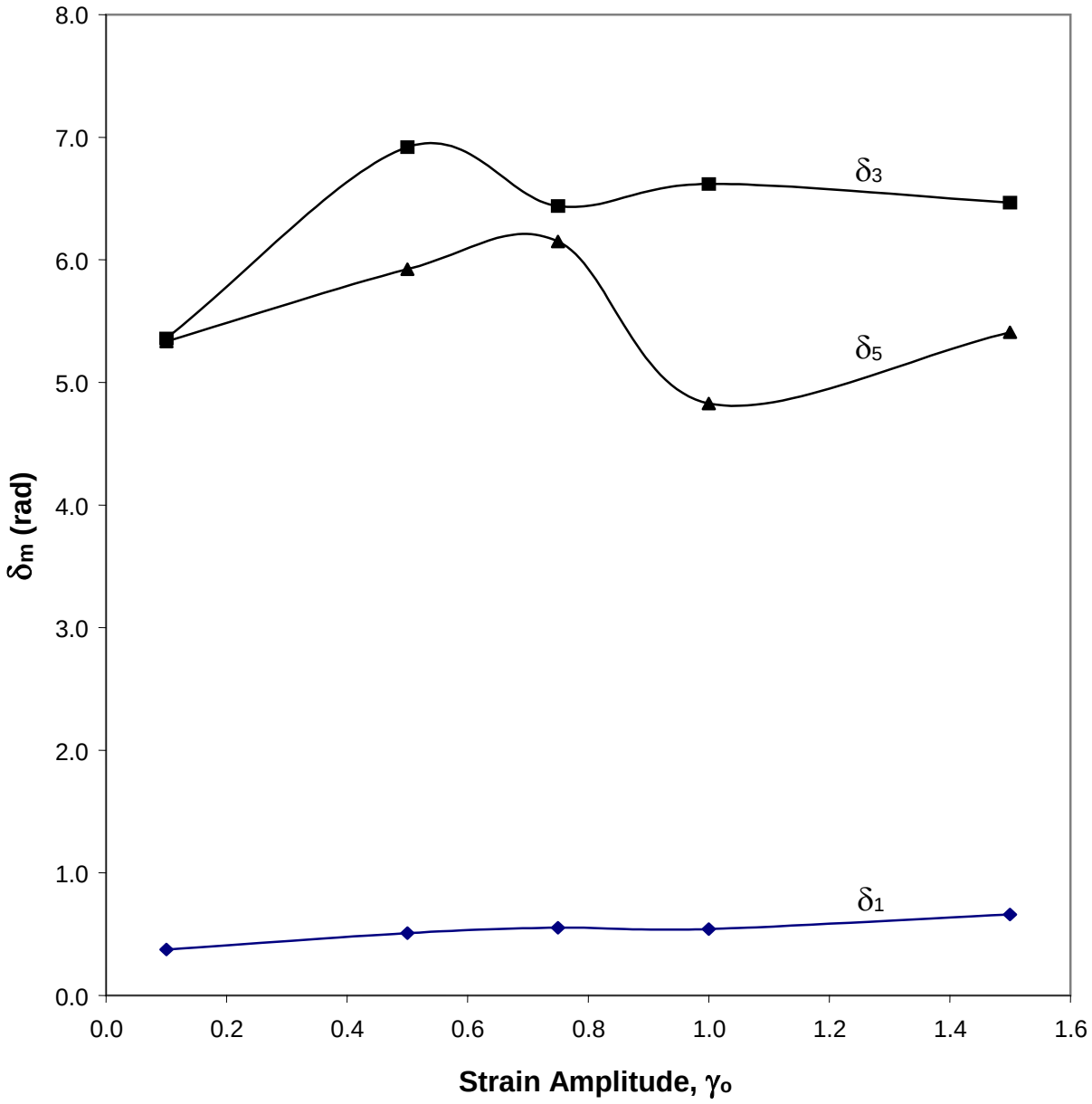

Figure 84 Effect of γ_o on the phase angles of the principal harmonics of shear stress for reduced-fat pizza cheese at 4 weeks and 40°C, with f_o = 0.4 Hz. δ_1 rises with γ_o, while δ_3 and δ_5 are not monotonic with γ_o.

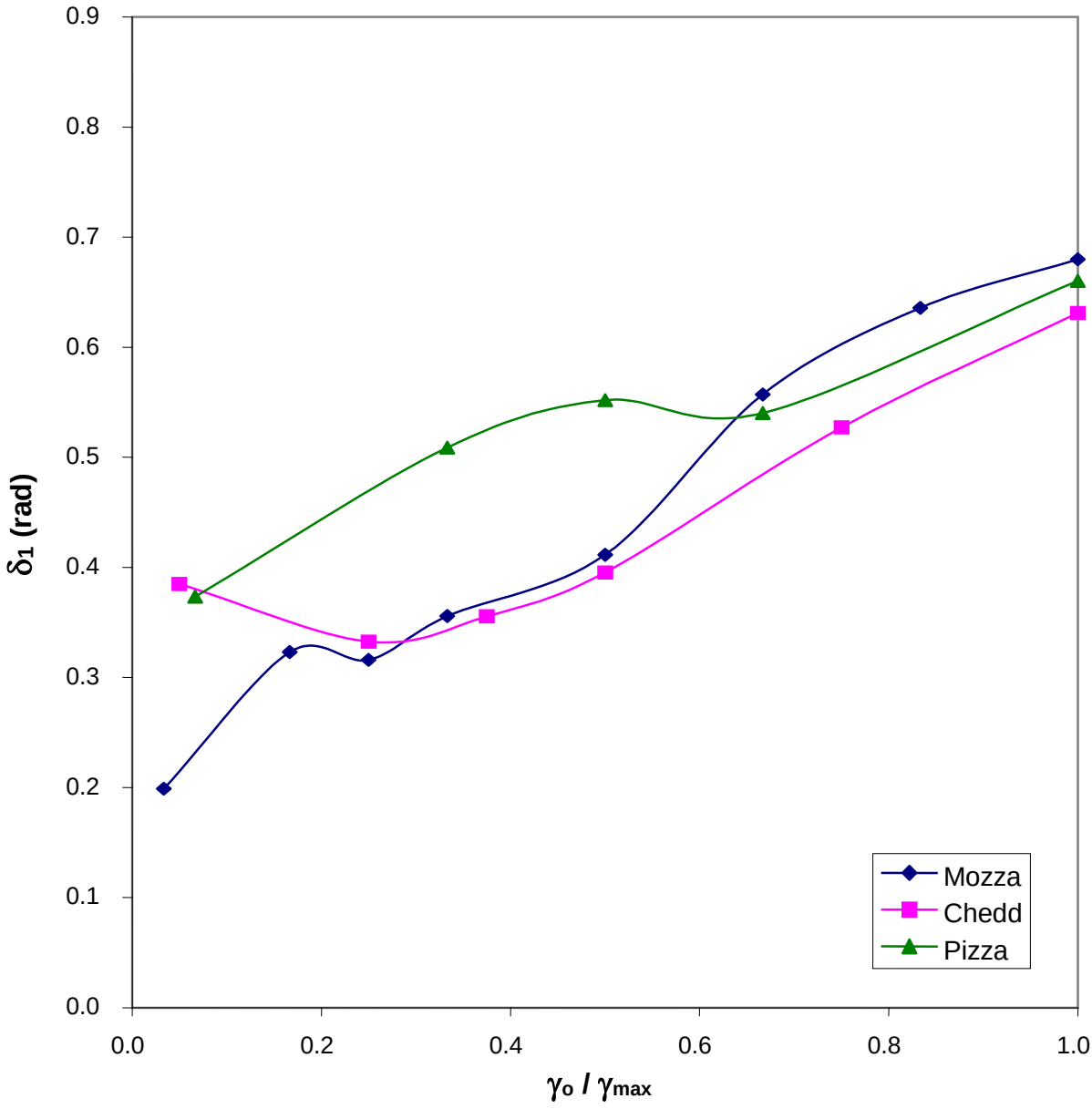

Figure 85 Comparing phase angles of the fundamental harmonic (δ_1) for the reduced-fat, natural cheeses at 4 weeks and 40°C, with f_o = 0.4 Hz. δ_1 for all cheeses increases with γ_o.

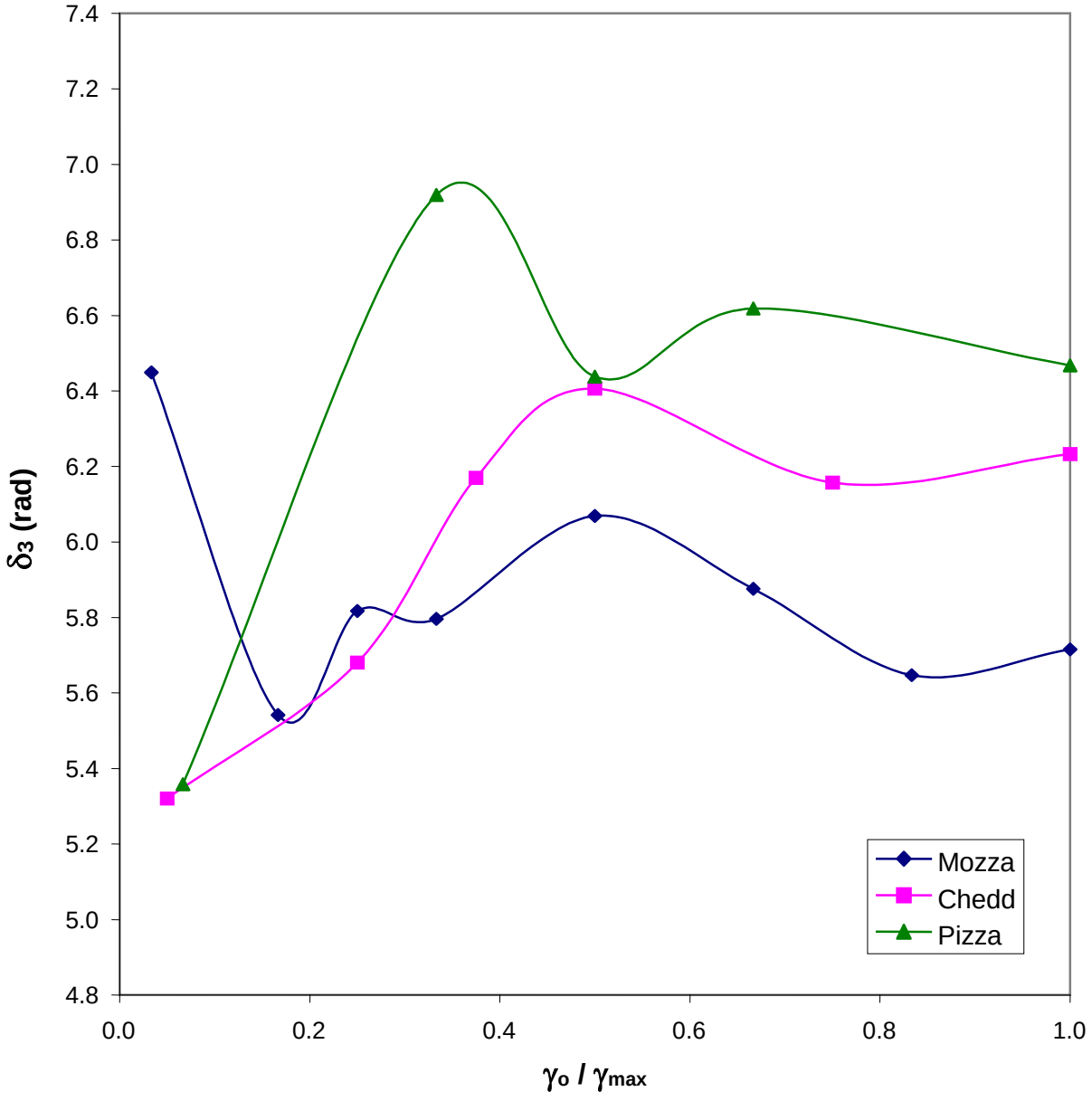

Figure 86 Comparing phase angles of the third harmonic (δ_3) for the reduced-fat, natural cheeses at 4 weeks and 40°C, with f_o = 0.4 Hz. δ_3 for all cheeses follow a similar trend.

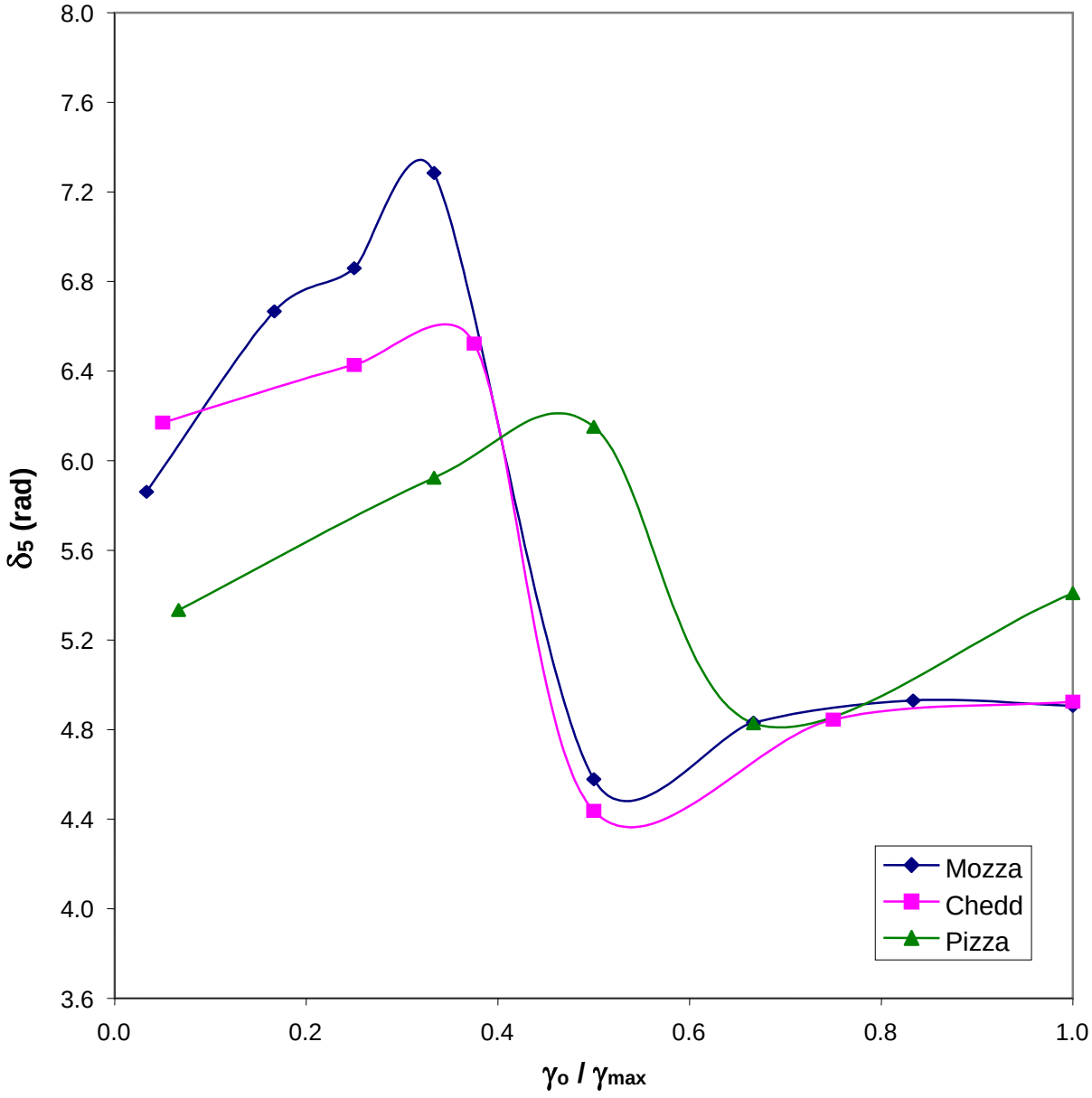

Figure 87 Comparing phase angles of the fifth harmonic (δ_5) for the reduced-fat, natural cheeses at 4 weeks and 40°C, with f_o = 0.4 Hz. δ_5 for all cheeses follow a similar trend, with mozzarella and cheddar almost overlapping at $\gamma_o / \gamma_{max} \geq 0.4$.

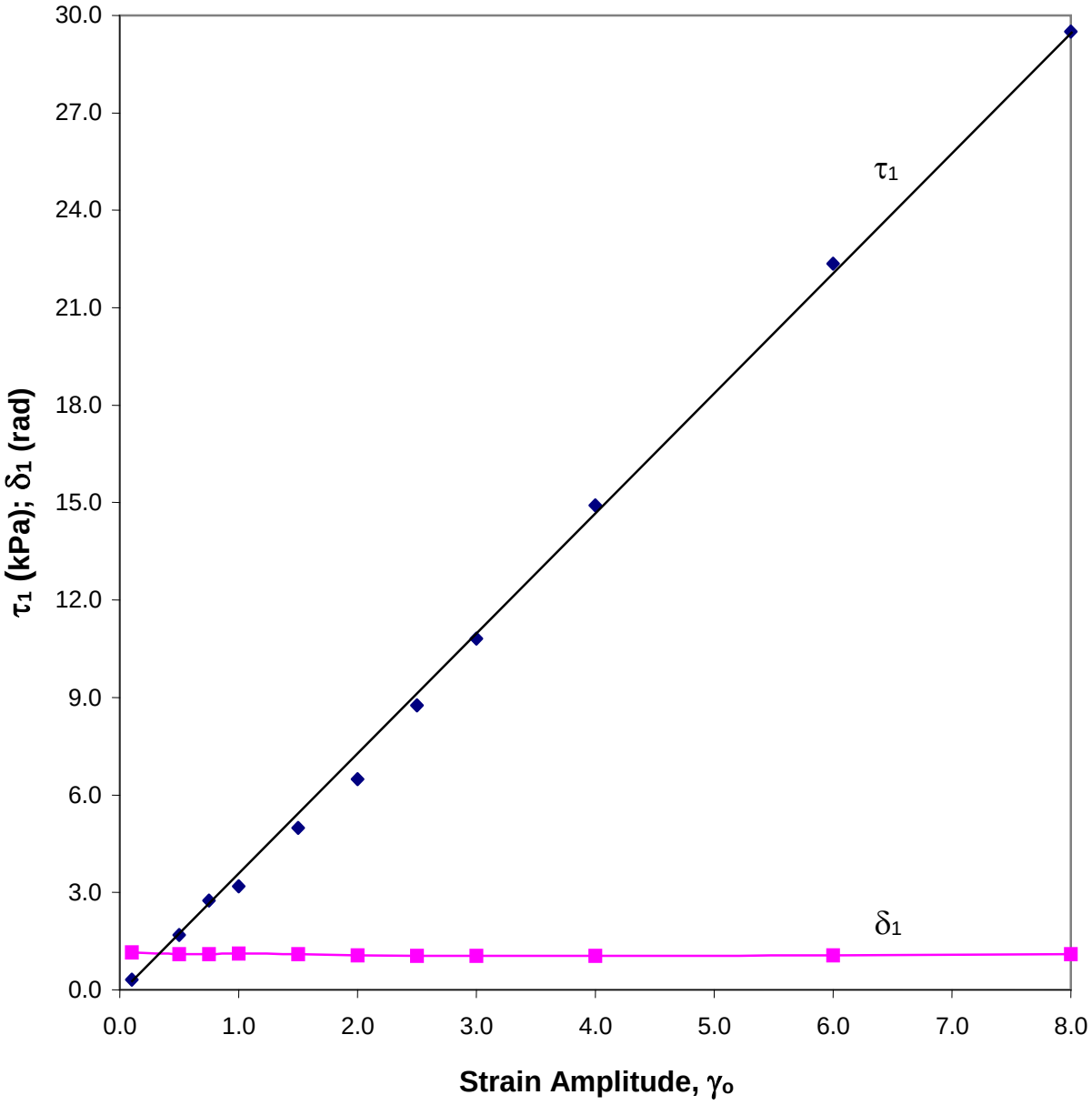

Figure 88 Effect of γ_o on fundamental harmonics τ_1 and δ_1 for reduced-fat mozzarella at 1 week and 60°C, with f_o = 0.4 Hz. δ_1 stays nearly constant with γ_o.

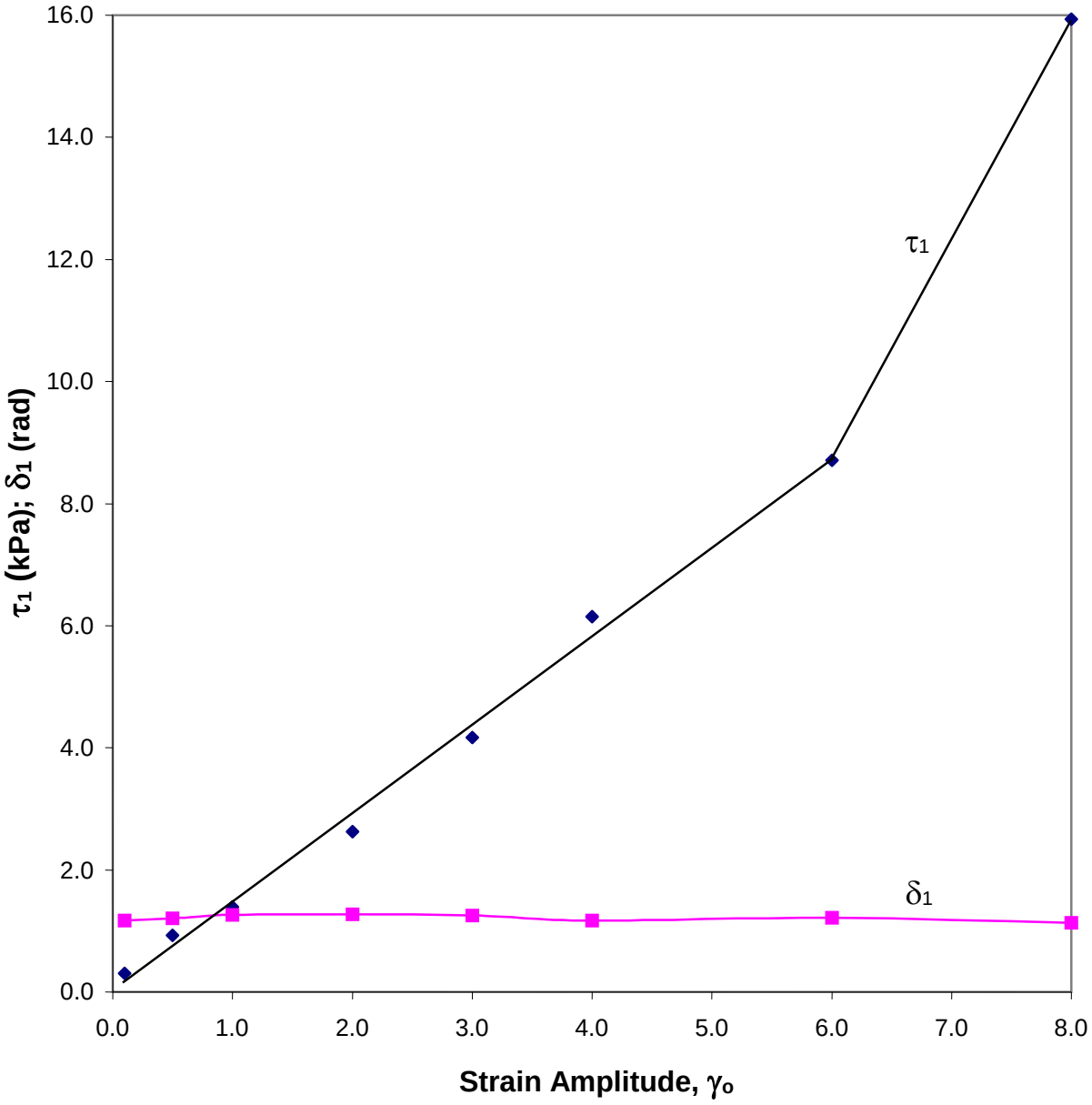

Figure 89 Effect of γ_o on fundamental harmonics τ_1 and δ_1 for reduced-fat mozzarella at 4 weeks and 60°C, with f_o = 0.4 Hz. δ_1 stays nearly constant with γ_o.

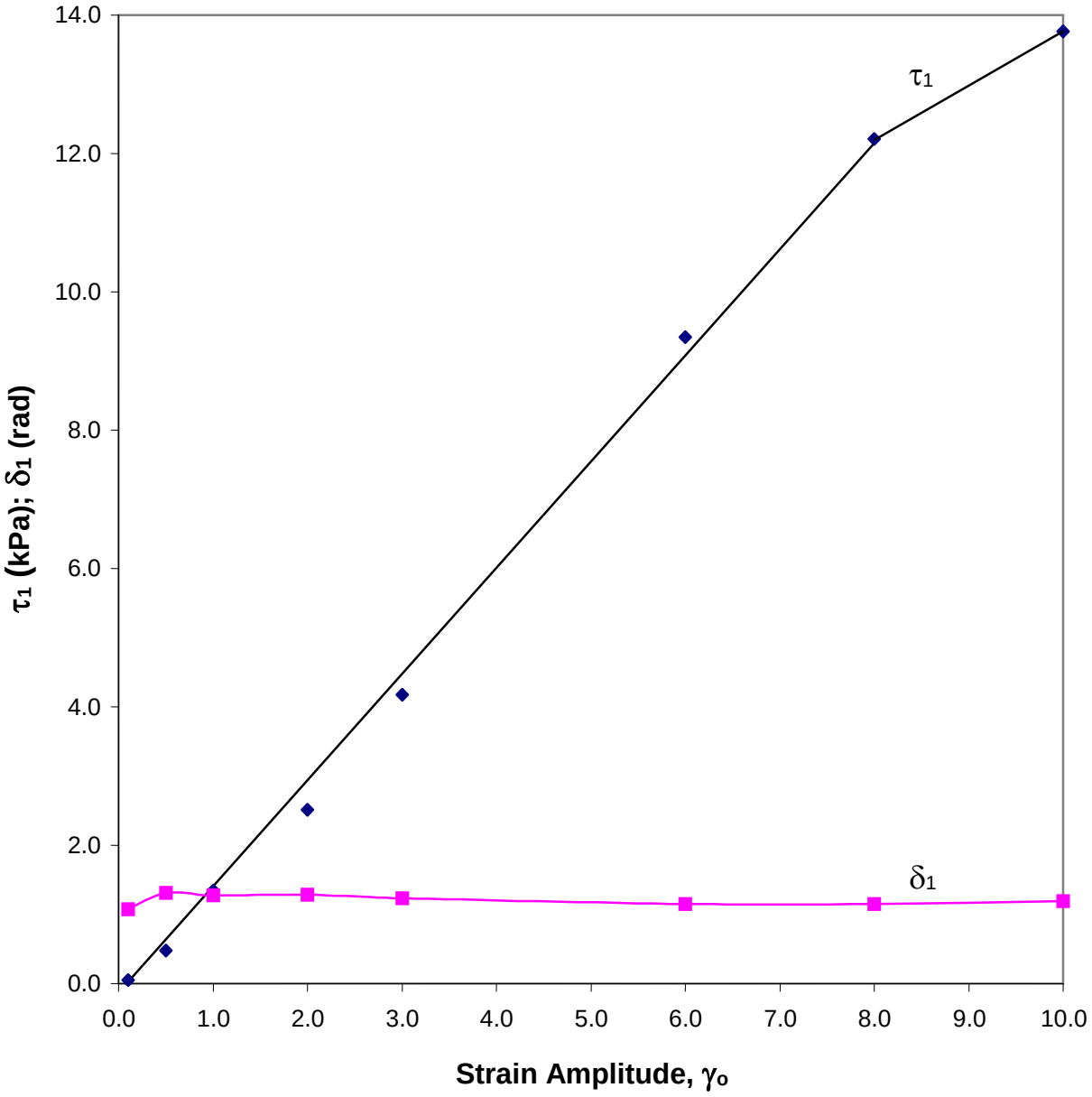

Figure 90 Effect of γ_o on fundamental harmonics τ_1 and δ_1 for reduced-fat mozzarella at 6 weeks and 60°C, with f_o = 0.4 Hz. δ_1 stays nearly constant with γ_o.

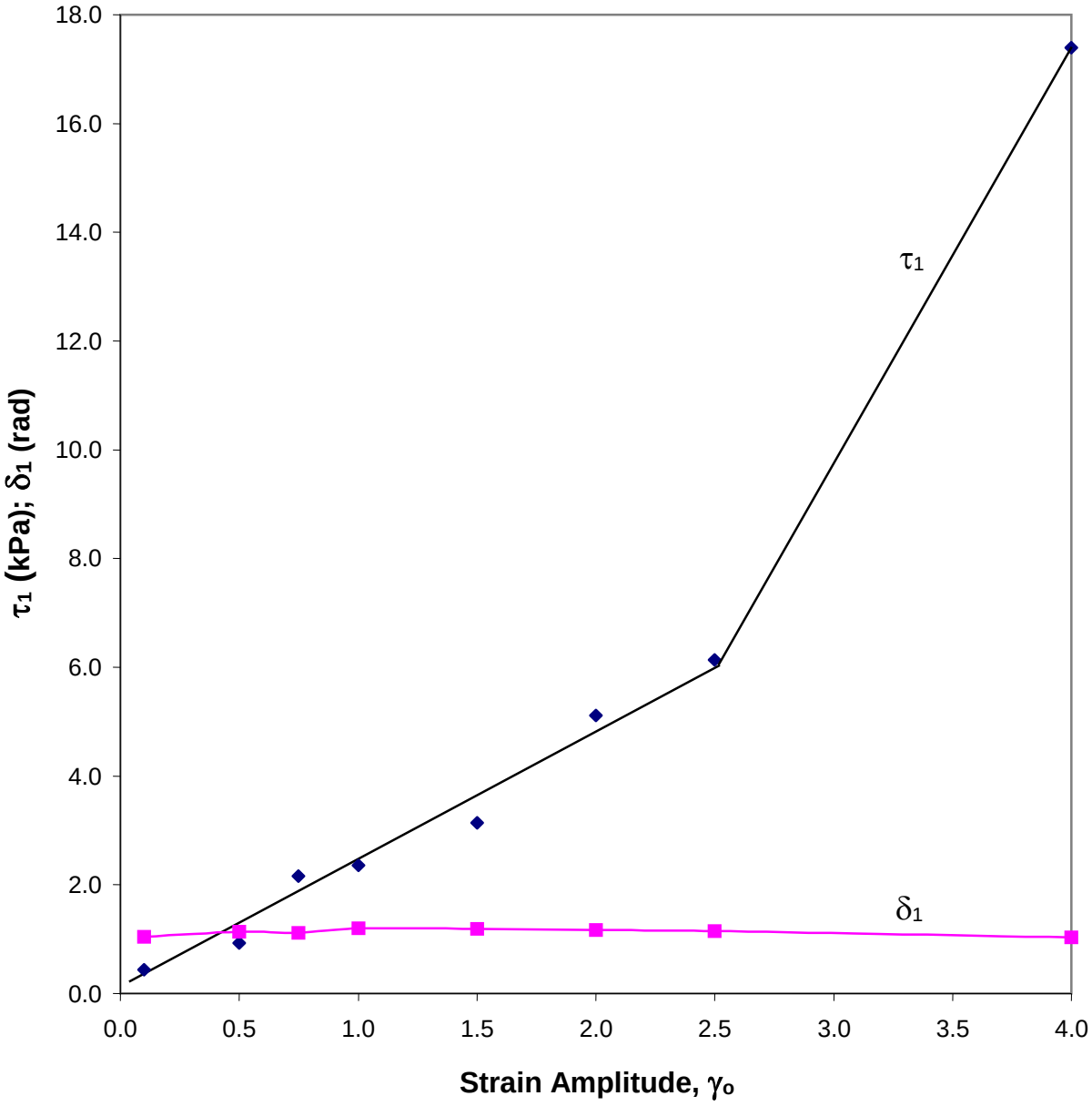

Figure 91 Effect of γ_o on fundamental harmonics τ_1 and δ_1 for reduced-fat cheddar at 1 week and 60°C, with f_o = 0.4 Hz. δ_1 stays nearly constant with γ_o.

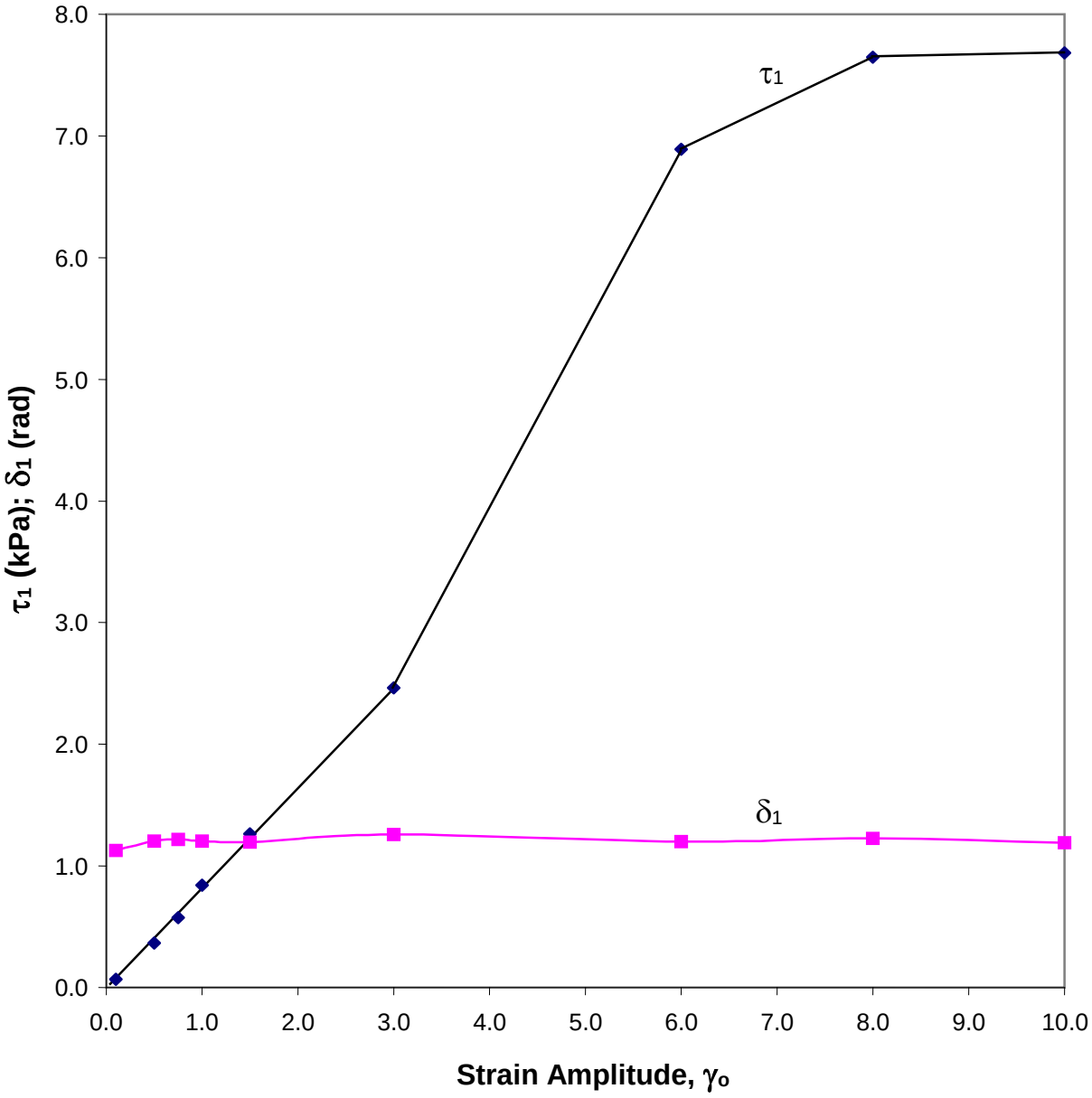

Figure 92 Effect of γ_o on fundamental harmonics τ_1 and δ_1 for reduced-fat cheddar at 4 weeks and 60°C, with f_o = 0.4 Hz. δ_1 stays nearly constant with γ_o.

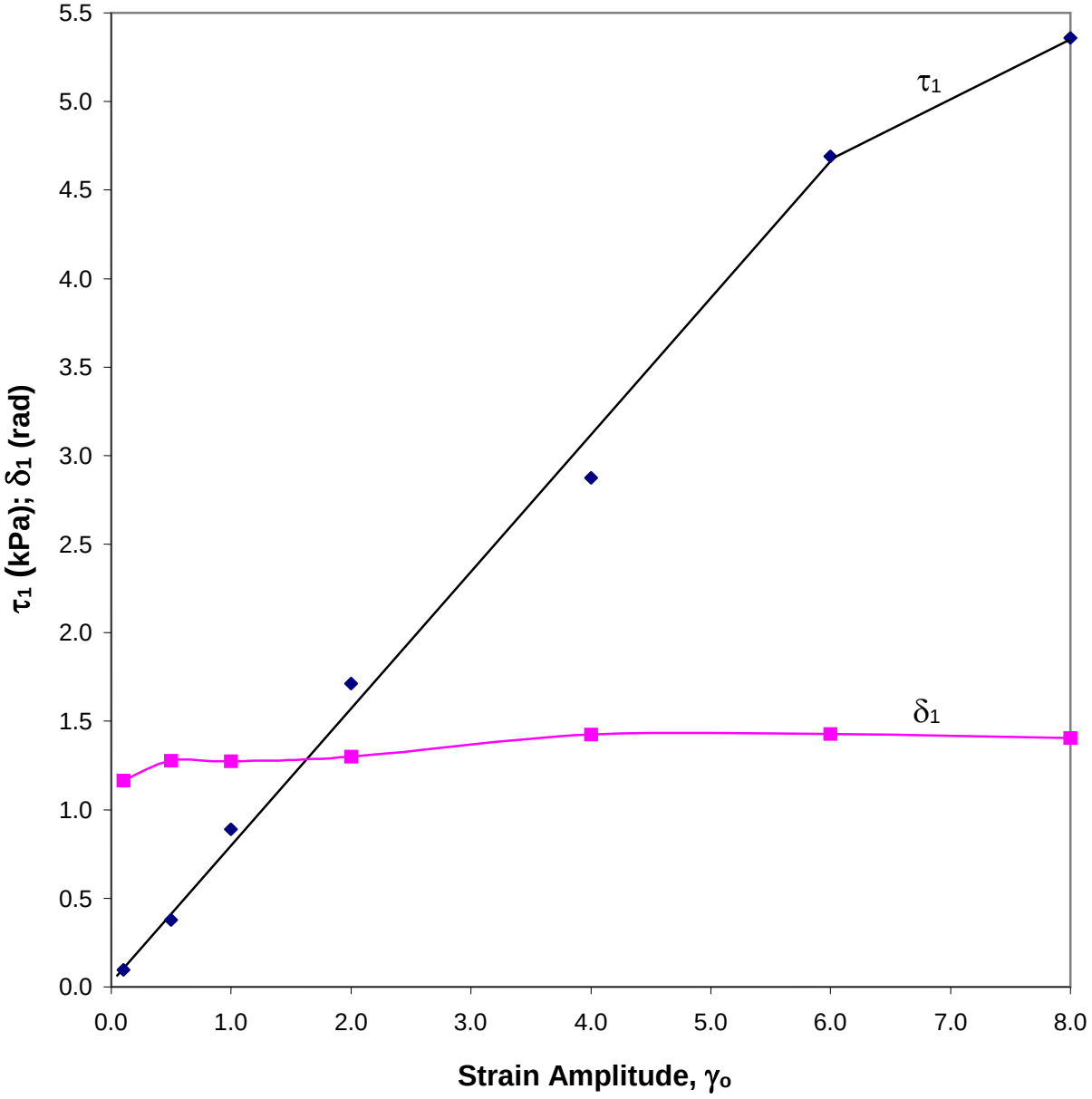

Figure 93 Effect of γ_o on fundamental harmonics τ_1 and δ_1 for reduced-fat cheddar at 6 weeks and 60°C, with f_o = 0.4 Hz. δ_1 stays nearly constant with γ_o.

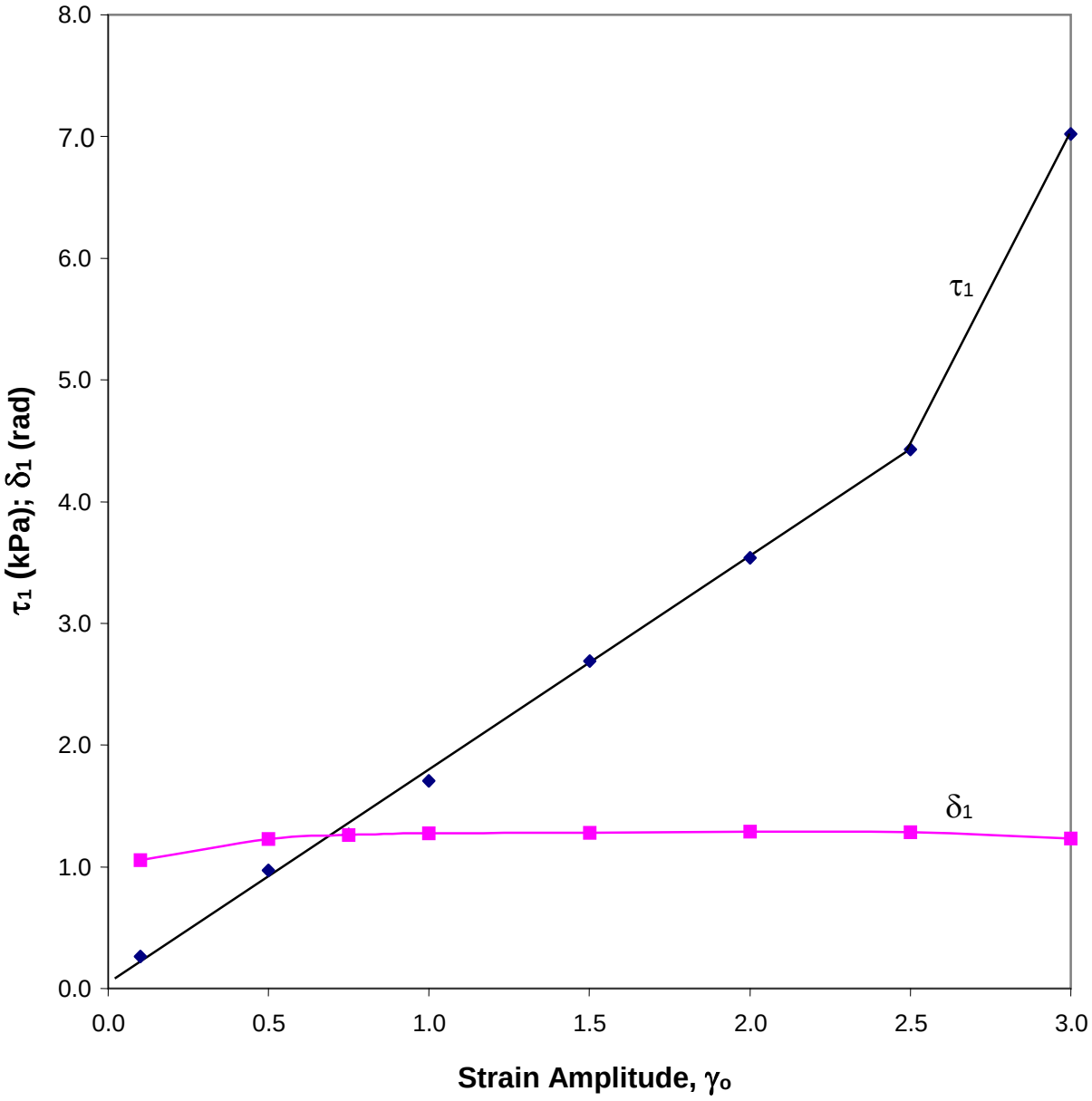

Figure 94 Effect of γ_o on fundamental harmonics τ_1 and δ_1 for reduced-fat pizza cheese at 1 week and 60°C, with f_o = 0.4 Hz. δ_1 stays nearly constant with γ_o.

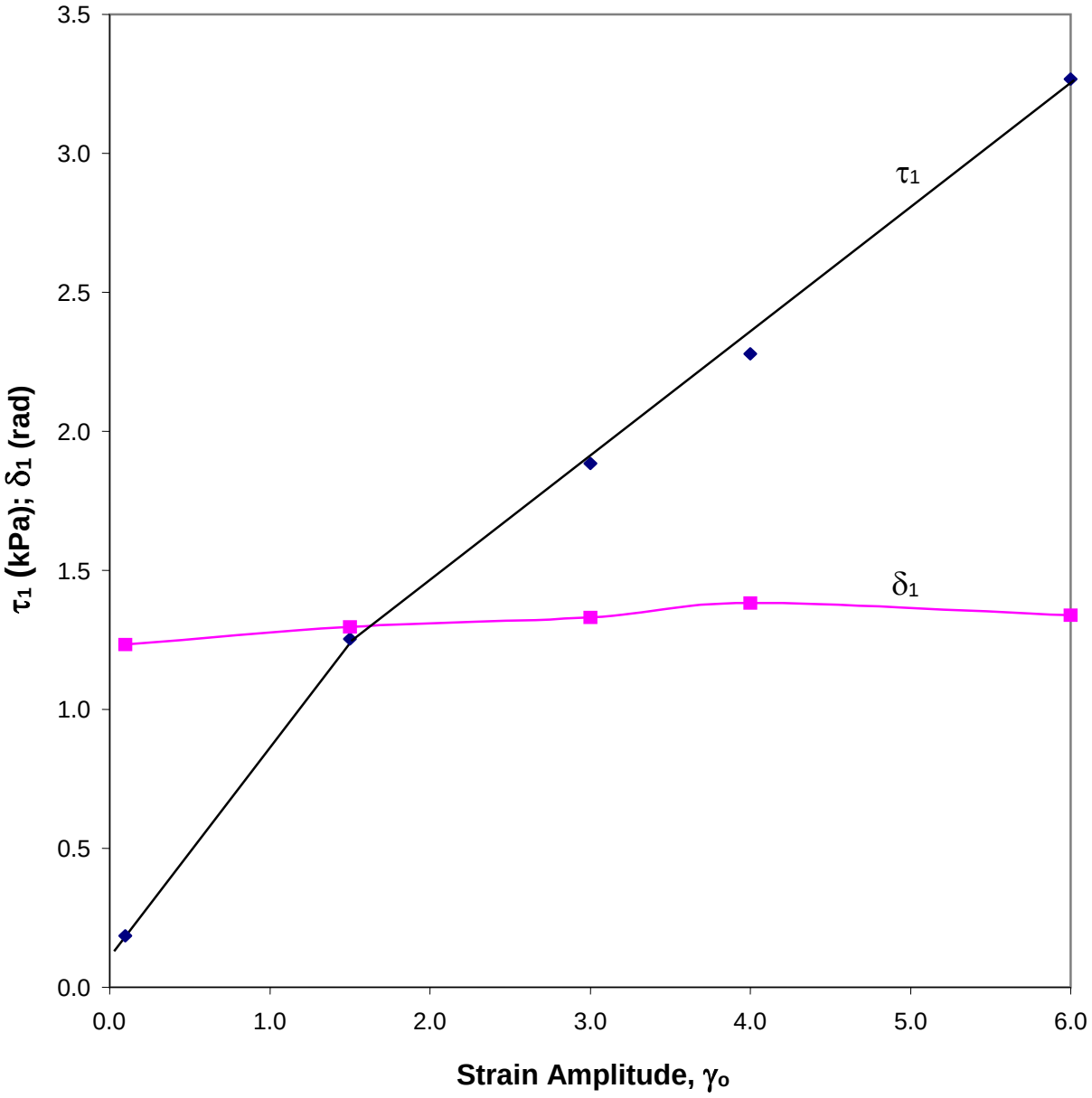

Figure 95 Effect of γ_o on fundamental harmonics τ_1 and δ_1 for reduced-fat pizza cheese at 4 weeks and 60°C, with f_o = 0.4 Hz. δ_1 stays nearly constant with γ_o, and pizza cheese appears to exhibit a yield stress.

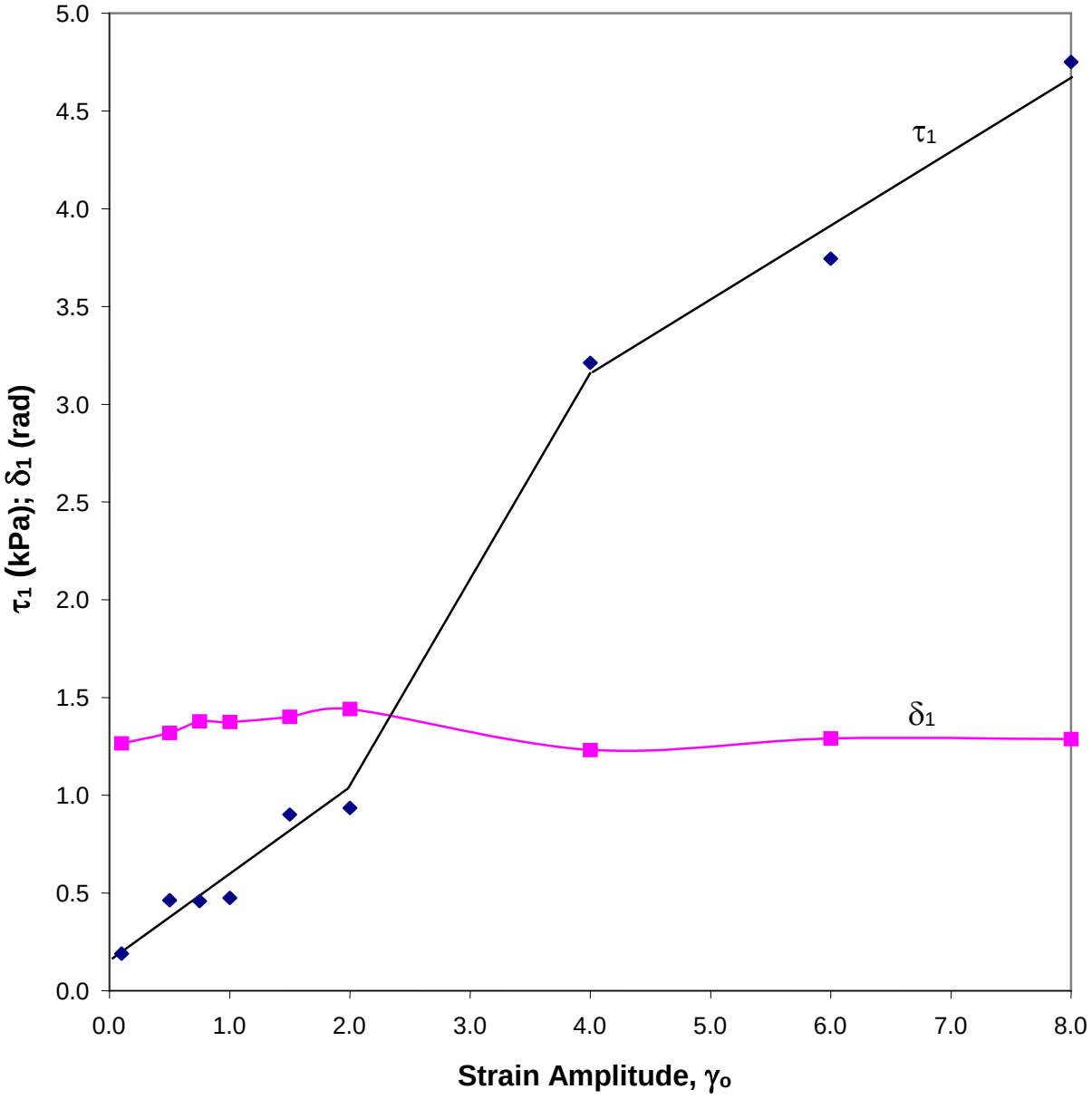

Figure 96 Effect of γ_o on fundamental harmonics τ_1 and δ_1 for reduced-fat pizza cheese at 6 weeks and 60°C, with f_o = 0.4 Hz. Pizza cheese appears to exhibit a yield stress.

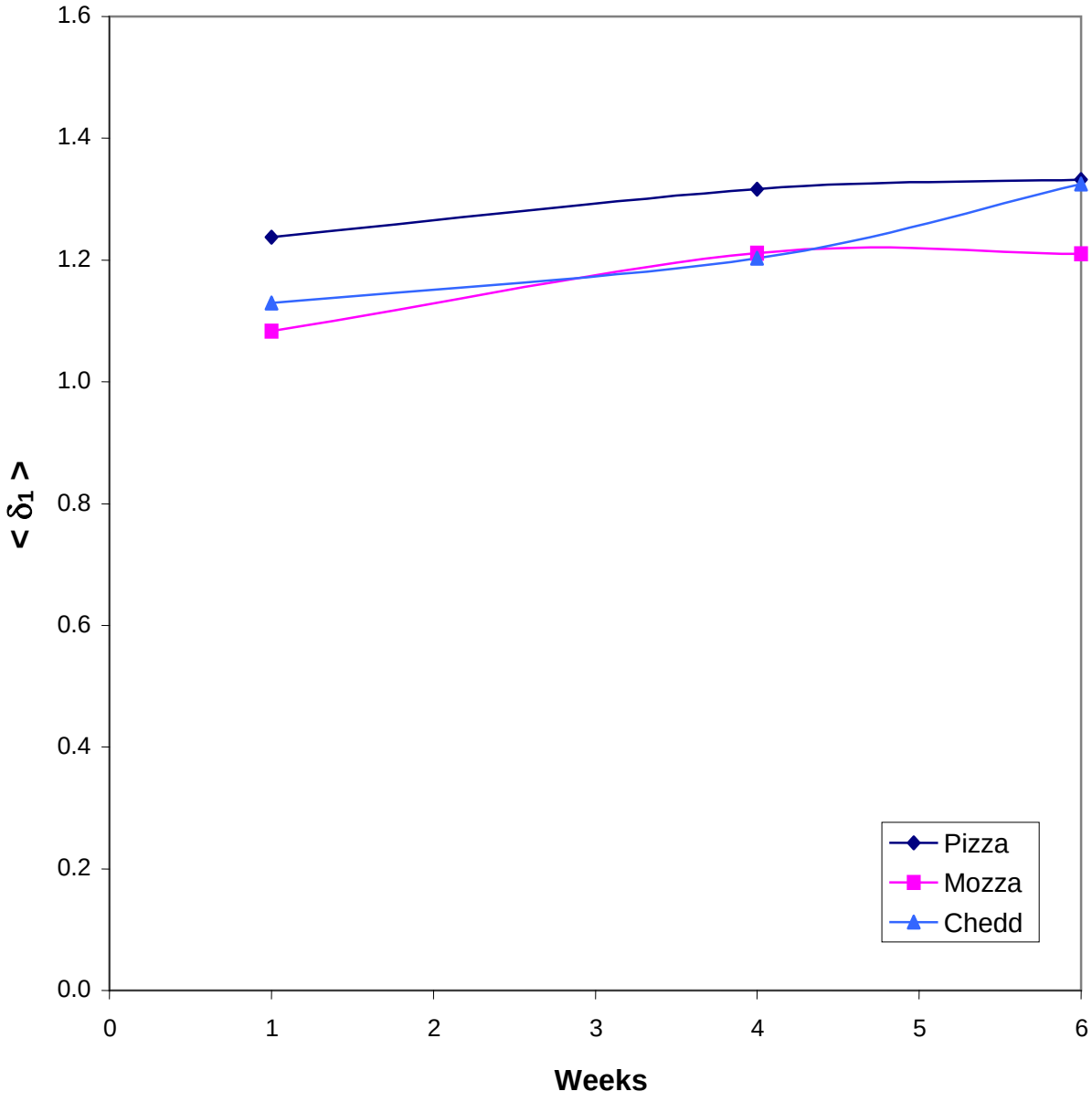

Figure 97 Effect of age on *average* fundamental phase angles ($< \delta_1 >$) for the reduced-fat, natural cheeses at 6 weeks and 60°C, with f_o = 0.4 Hz. $< \delta_1 >$ increases with age for the three cheeses.

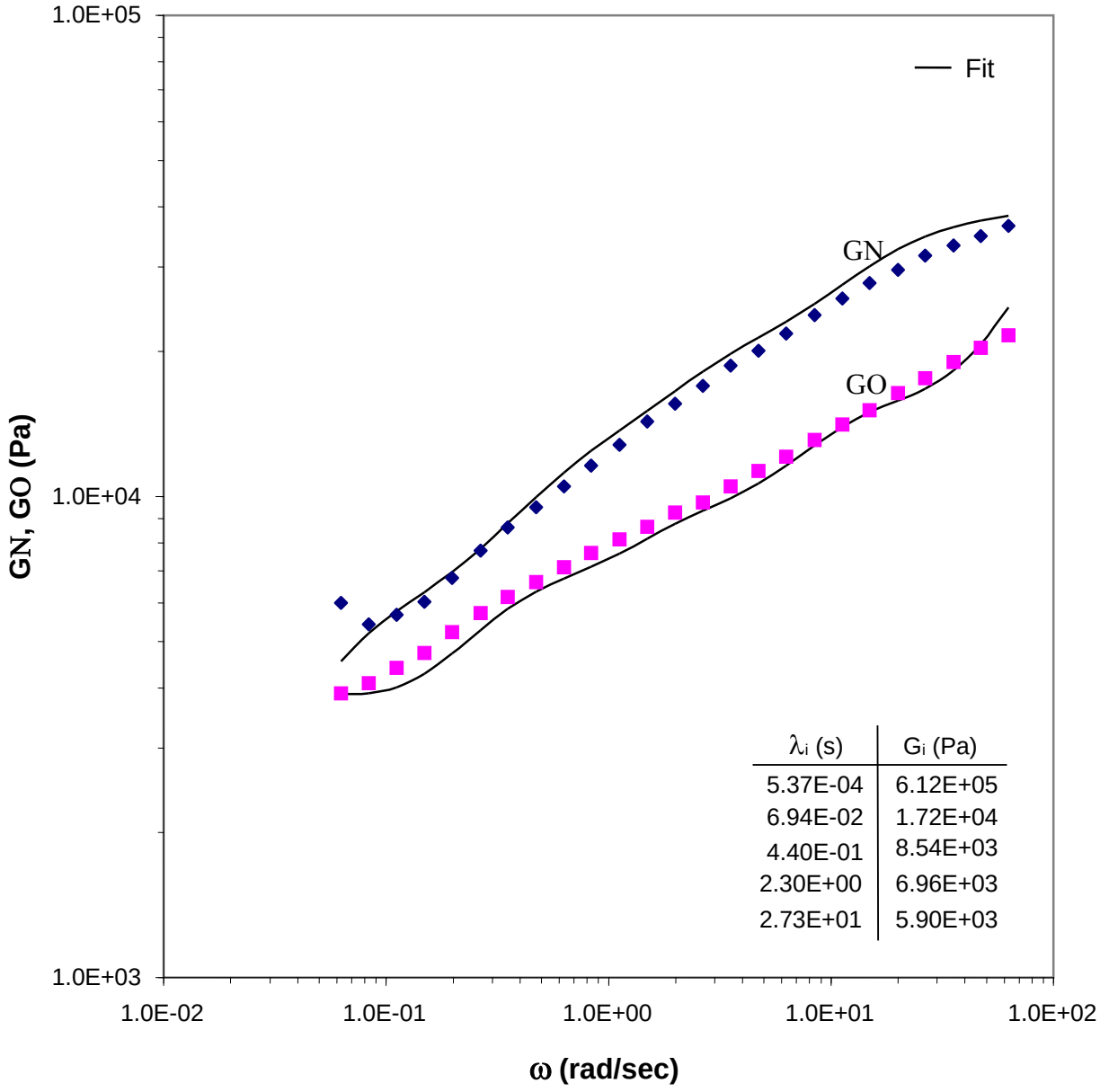

Figure 98 Discrete relaxation spectrum for reduced-fat mozzarella at 6 weeks and 40°C. Calculated by *parsimonious* modeling using IRIS.

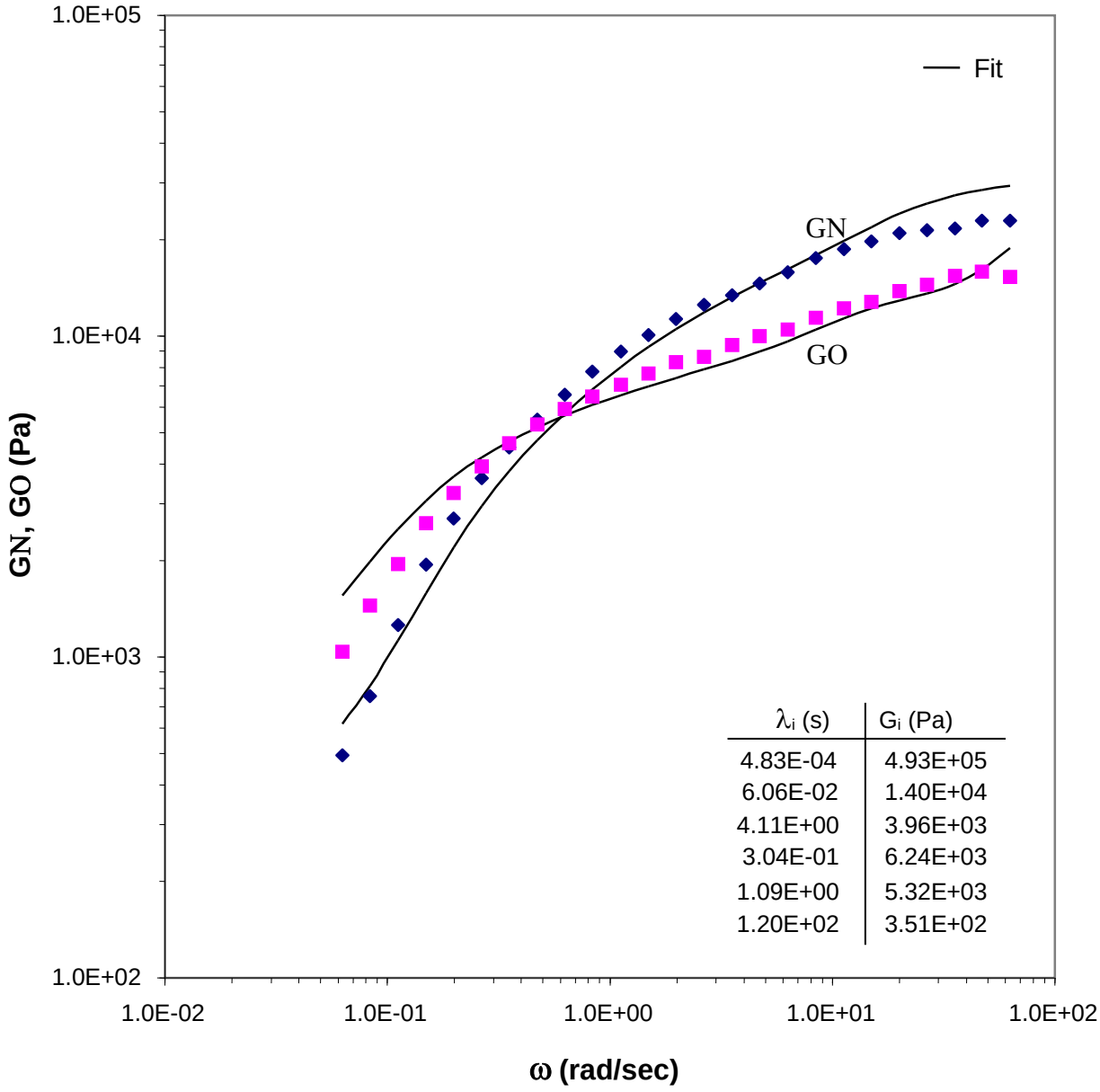

Figure 99 Discrete relaxation spectrum for reduced-fat mozzarella at 6 weeks and 60°C. Calculated by *parsimonious* modeling using IRIS.

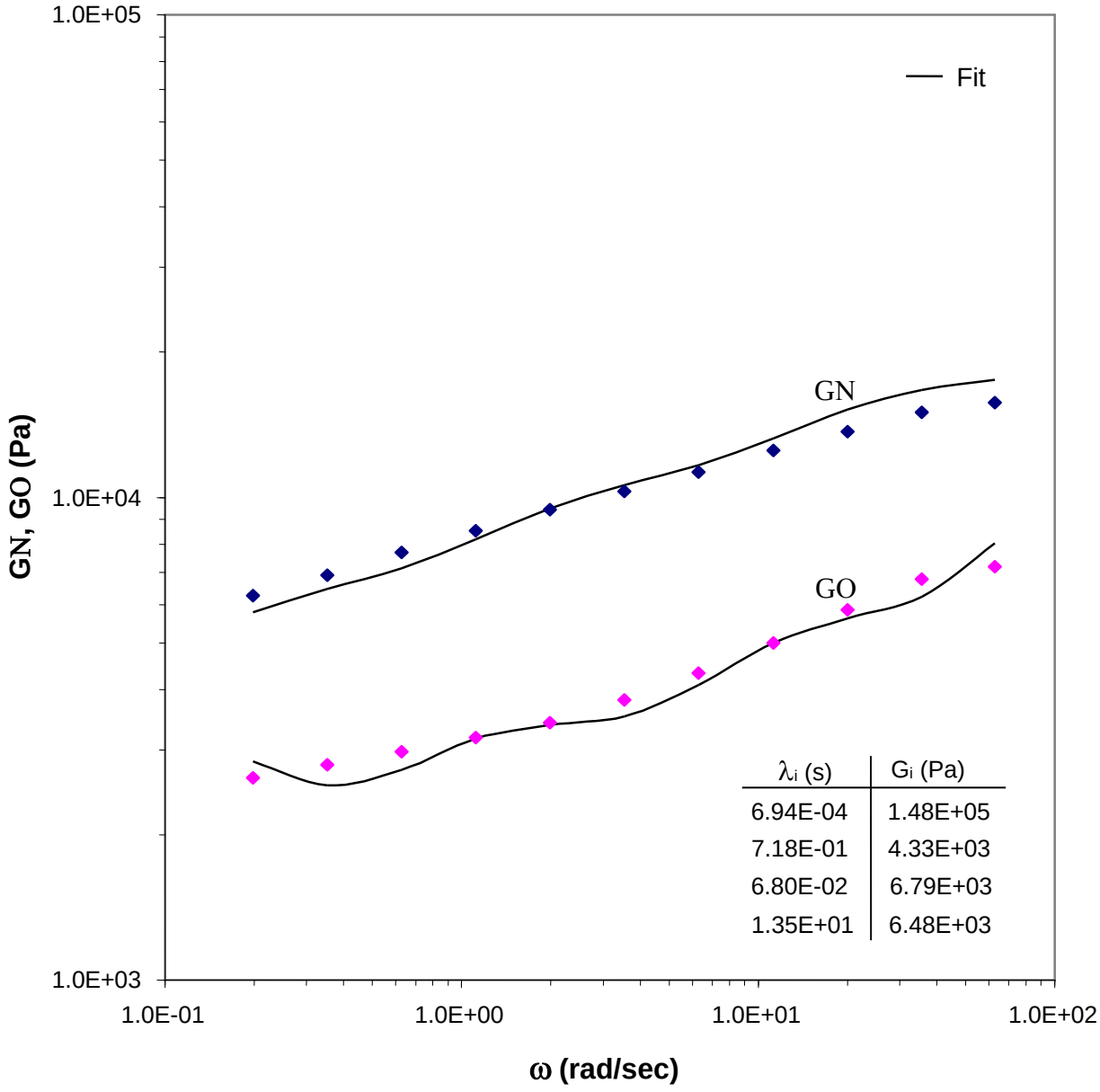

Figure 100 Discrete relaxation spectrum for reduced-fat cheddar at 6 weeks and 40°C. Calculated by *parsimonious* modeling using IRIS.

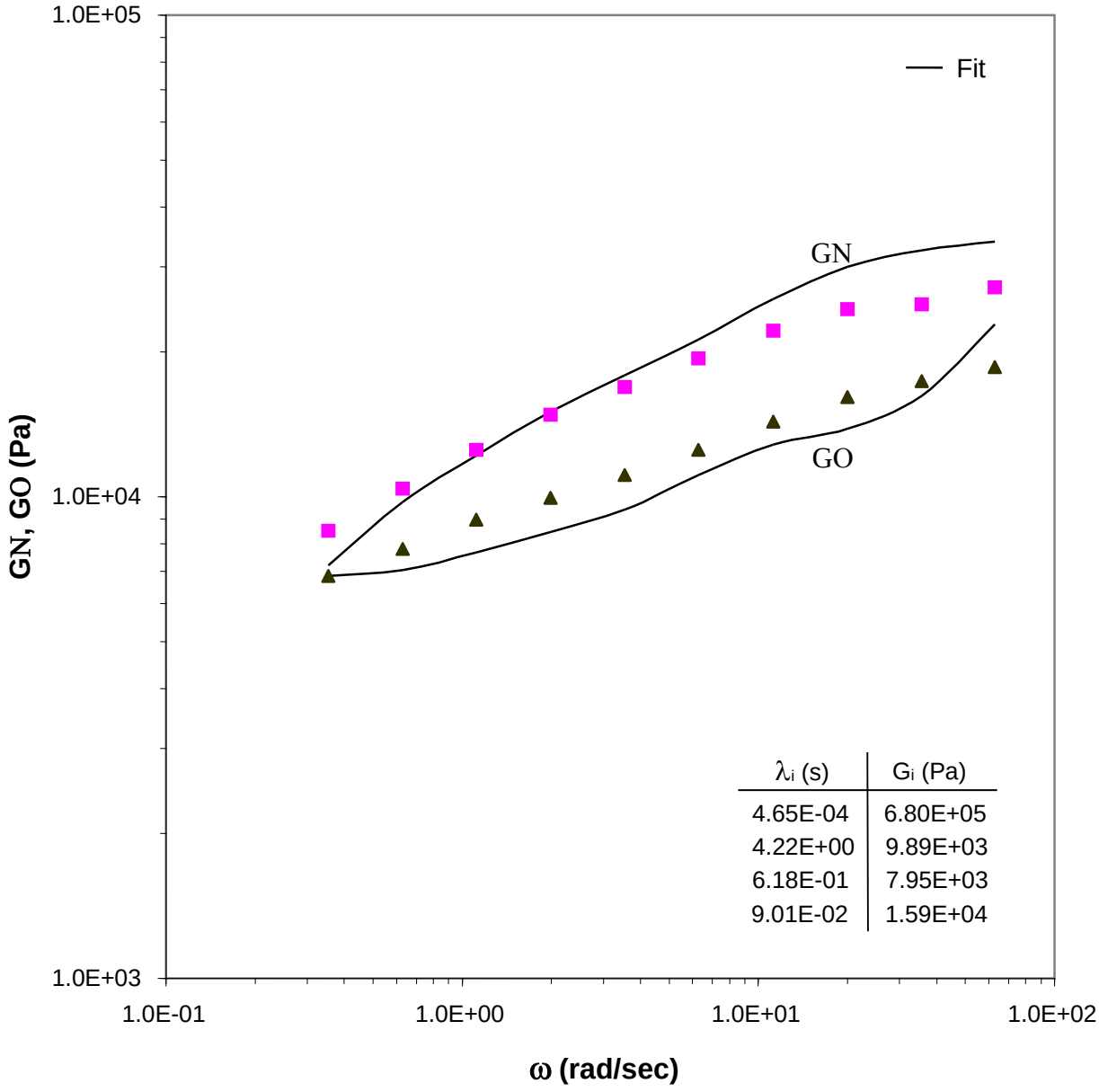

Figure 101 Discrete relaxation spectrum for reduced-fat cheddar at 6 weeks and 60°C. Calculated by *parsimonious* modeling using IRIS.

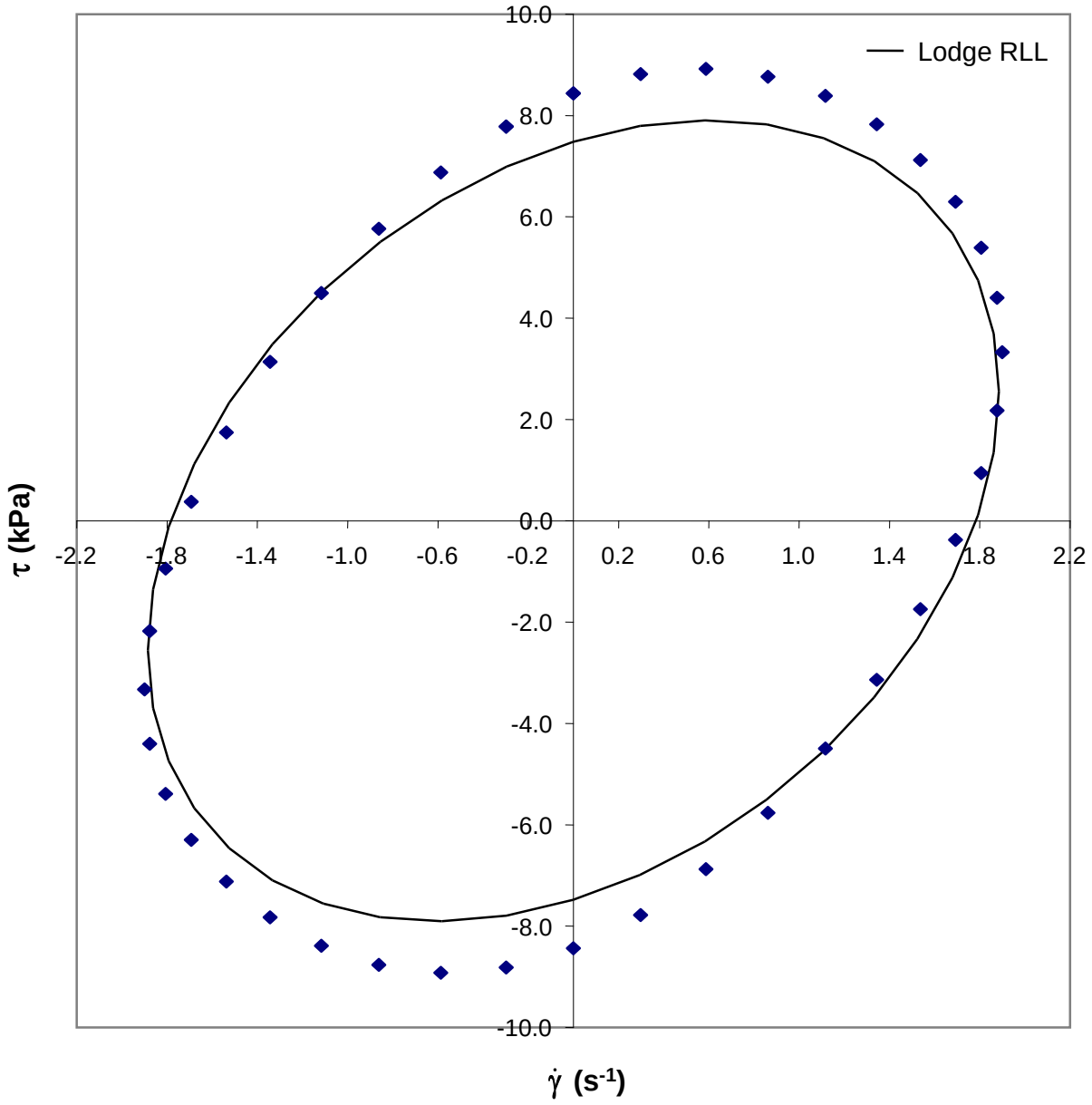

Figure 102 Comparing the Lodge rubberlike liquid to LAOS results for reduced-fat cheddar at 40°C with f_o = 0.4 Hz. Strain amplitude is 0.75. Cheddar slightly overpredicts the linear stresses.

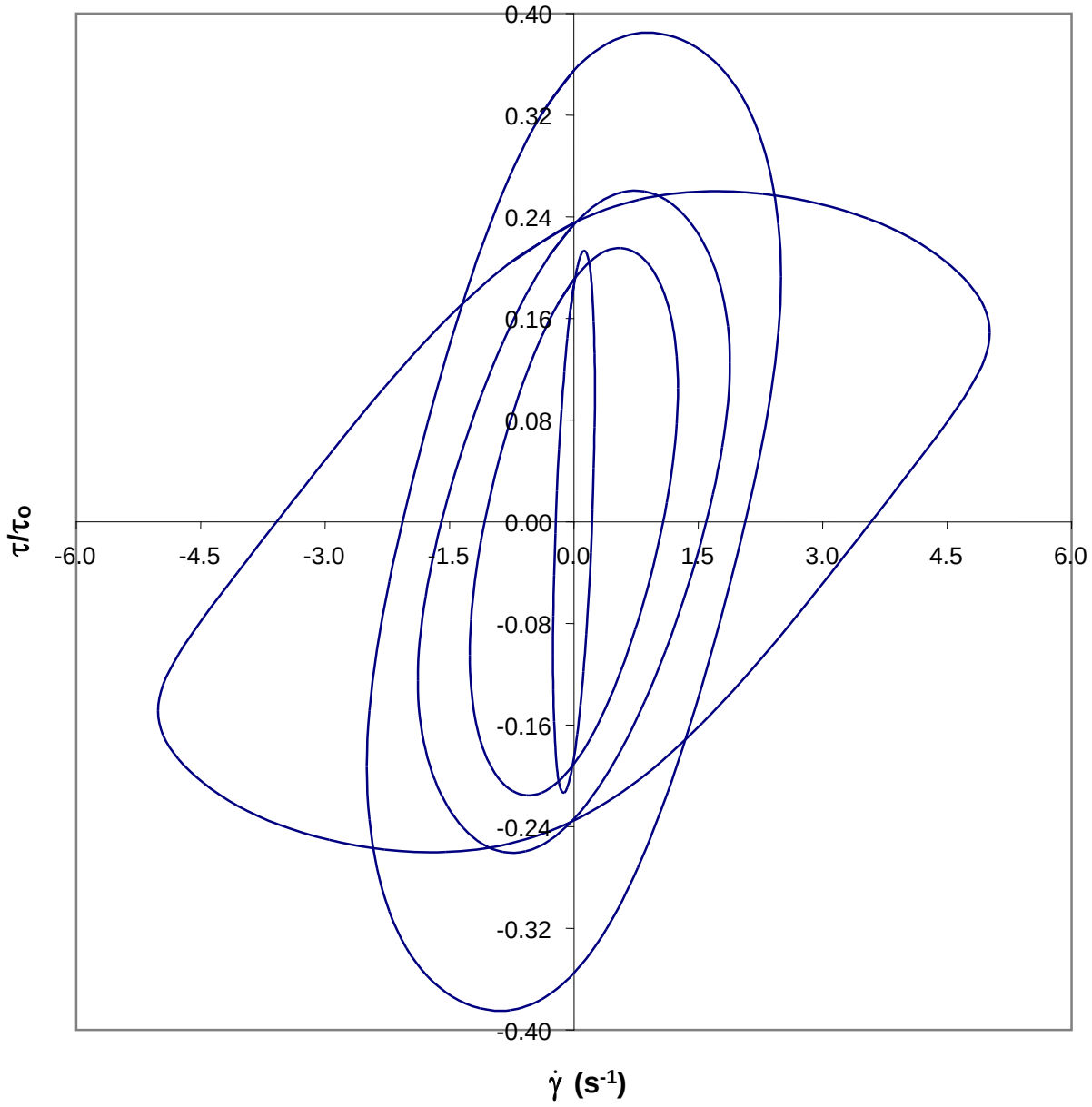

Figure 103 Departures from linearity for reduced-fat mozzarella at 6 weeks and 40°C with f_o = 0.4 Hz. Shear stress has been normalized with Lodge's rubberlike liquid theory. Strain amplitudes are 0.1, 0.5, 0.75, 1, and 2. Mozzarella is highly nonlinear.

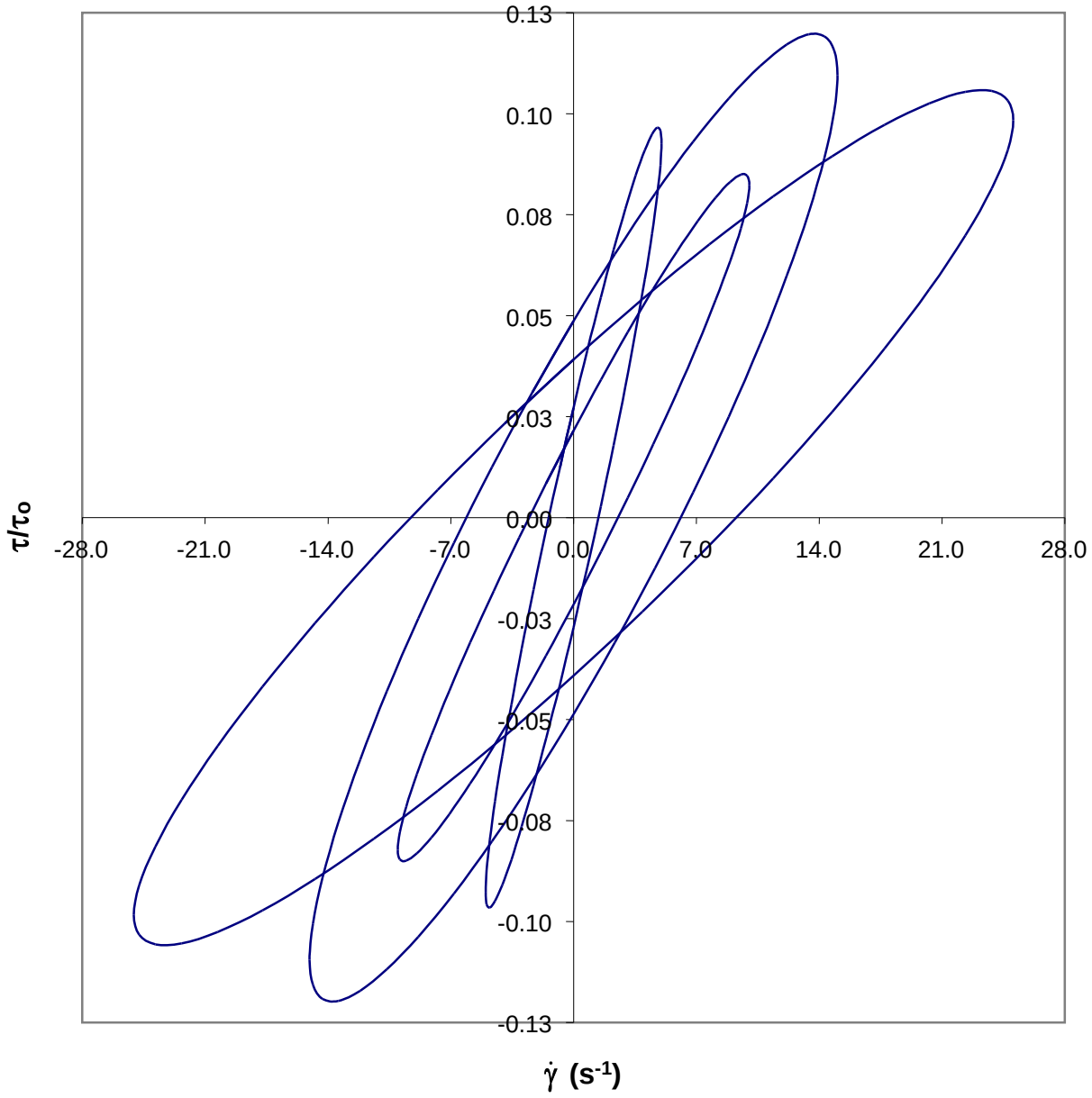

Figure 104 Departures from linearity for reduced-fat mozzarella at 6 weeks and 60°C with f_o = 0.4 Hz. Shear stress has been normalized with Lodge's rubberlike liquid theory. Strain amplitudes are 2, 4, 6, and 10. Mozzarella is highly nonlinear.

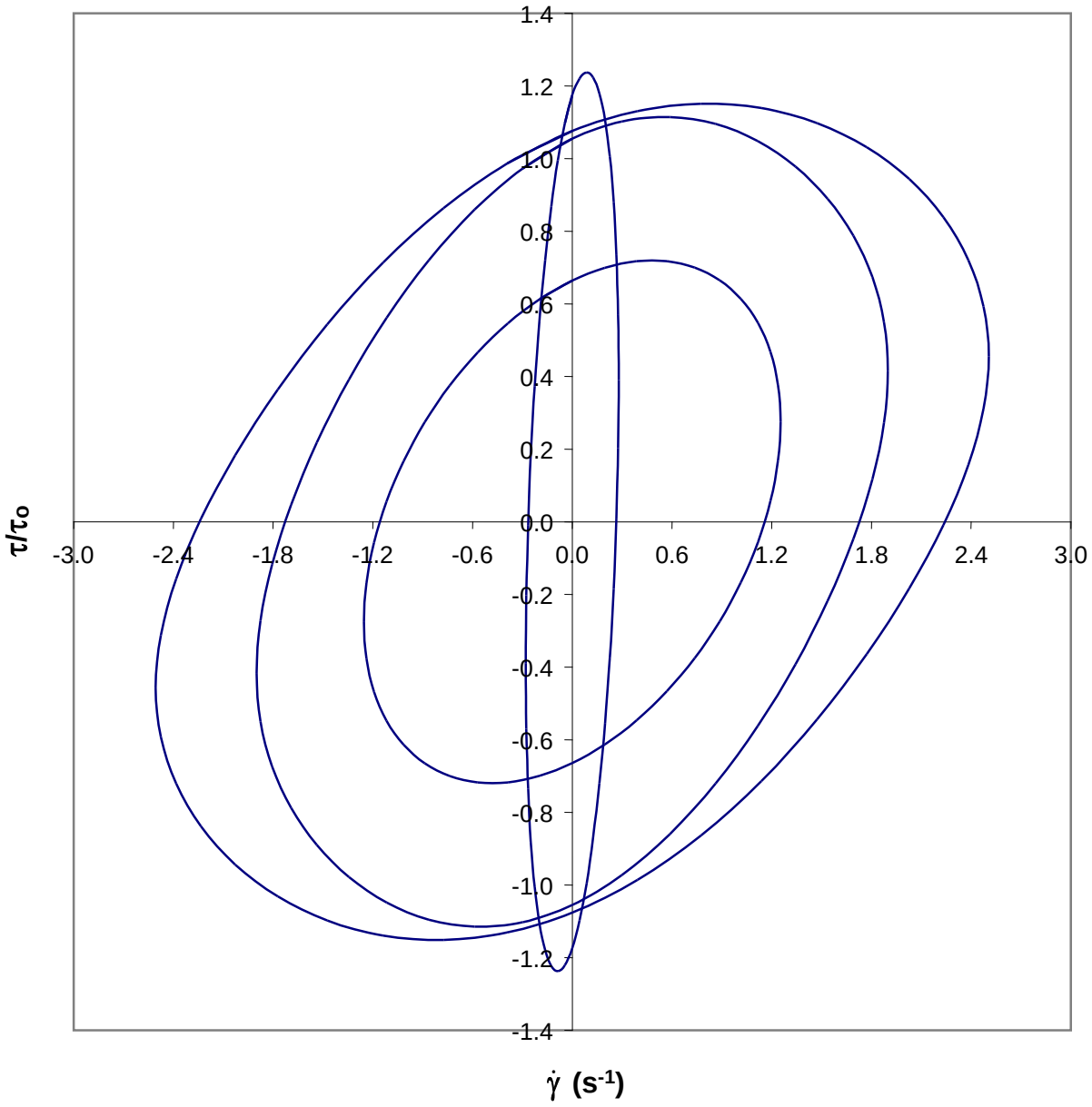

Figure 105 Departures from linearity for reduced-fat cheddar at 6 weeks and 40°C with f_o = 0.4 Hz. Shear stress has been normalized with Lodge's rubberlike liquid theory. Strain amplitudes are 0.1, 0.5, 0.75, and 1. Cheddar is almost linear.

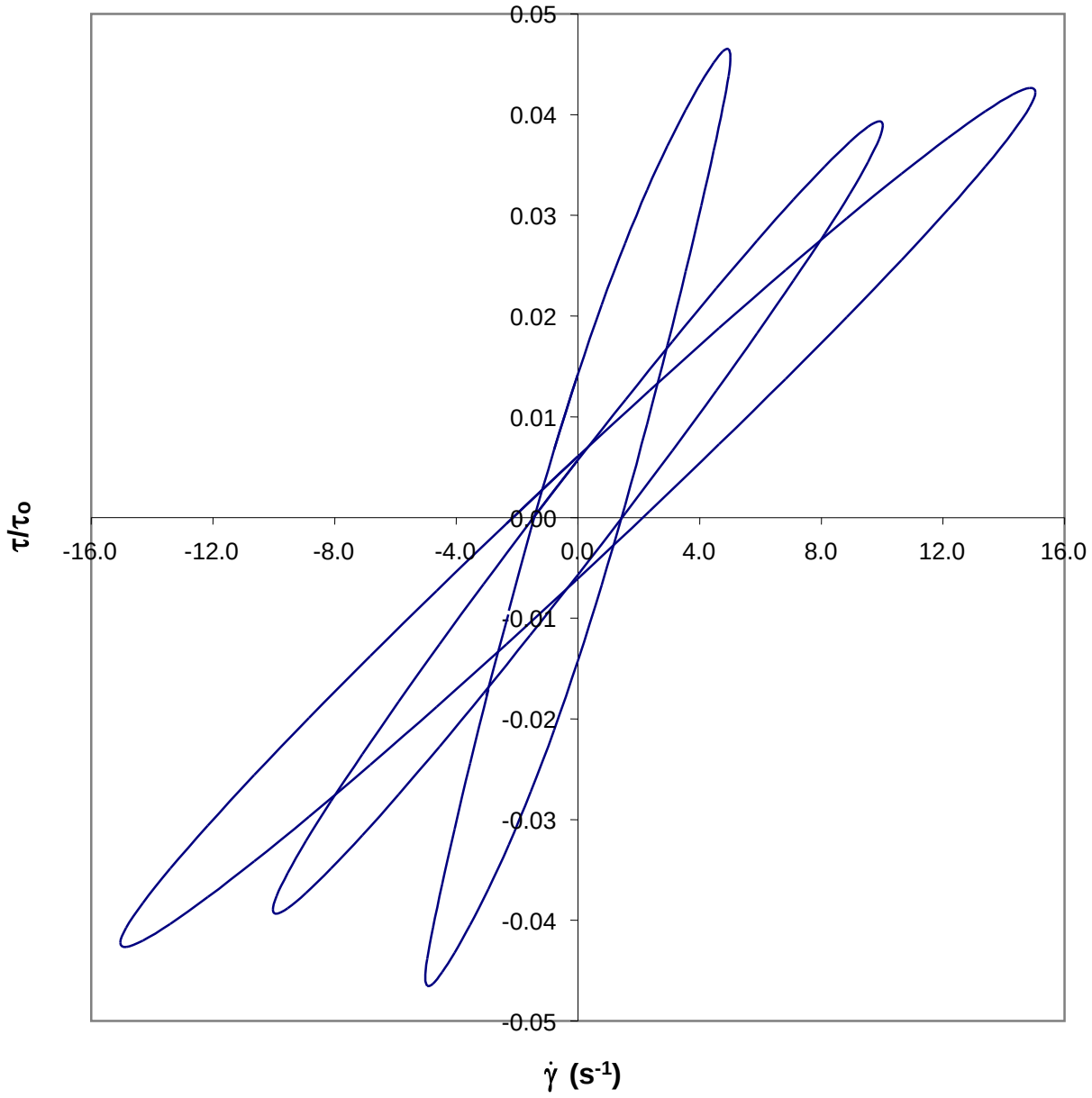

Figure 106 Departures from linearity for reduced-fat cheddar at 6 weeks and 60°C with f_o = 0.4 Hz. Shear stress has been normalized with Lodge's rubberlike liquid theory. Strain amplitudes are 2, 4, and 6. Cheddar is highly nonlinear.

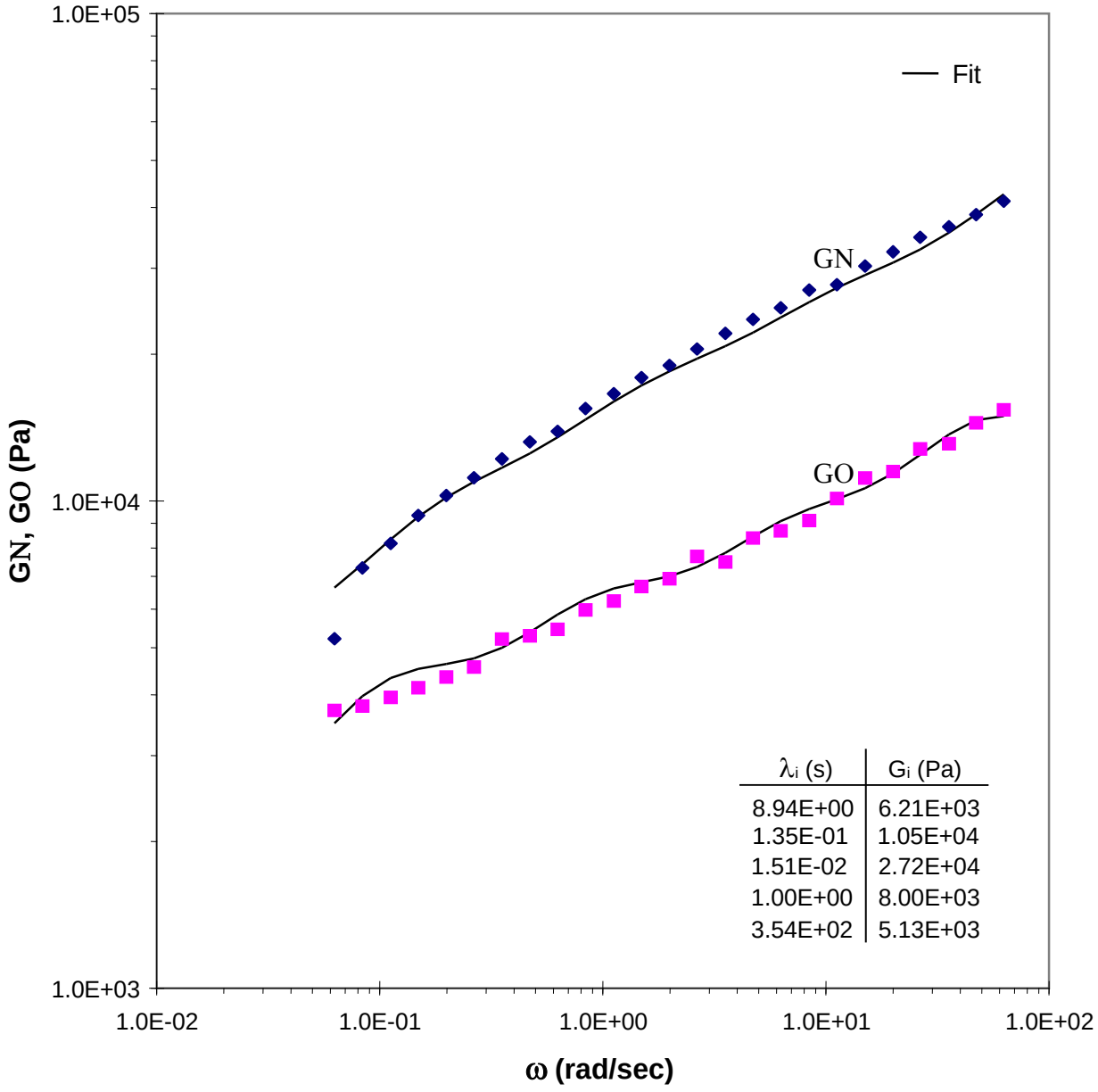

Figure 107 Discrete relaxation spectrum for fat-free process mozzarella at 30°C. Calculated by *parsimonious* modeling using IRIS.

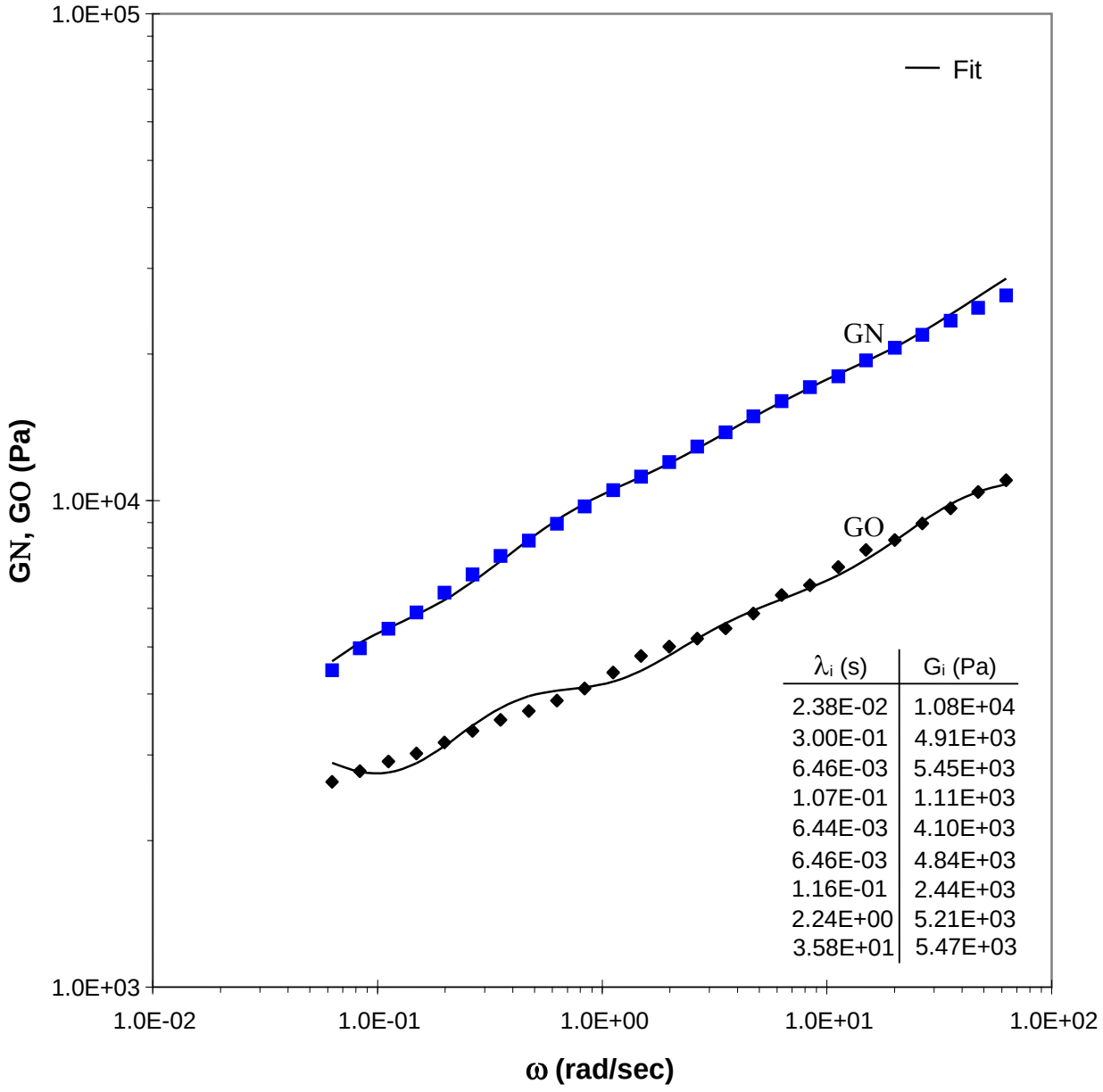

Figure 108 Discrete relaxation spectrum for fat-free process mozzarella at 35°C. Calculated by *parsimonious* modeling using IRIS.

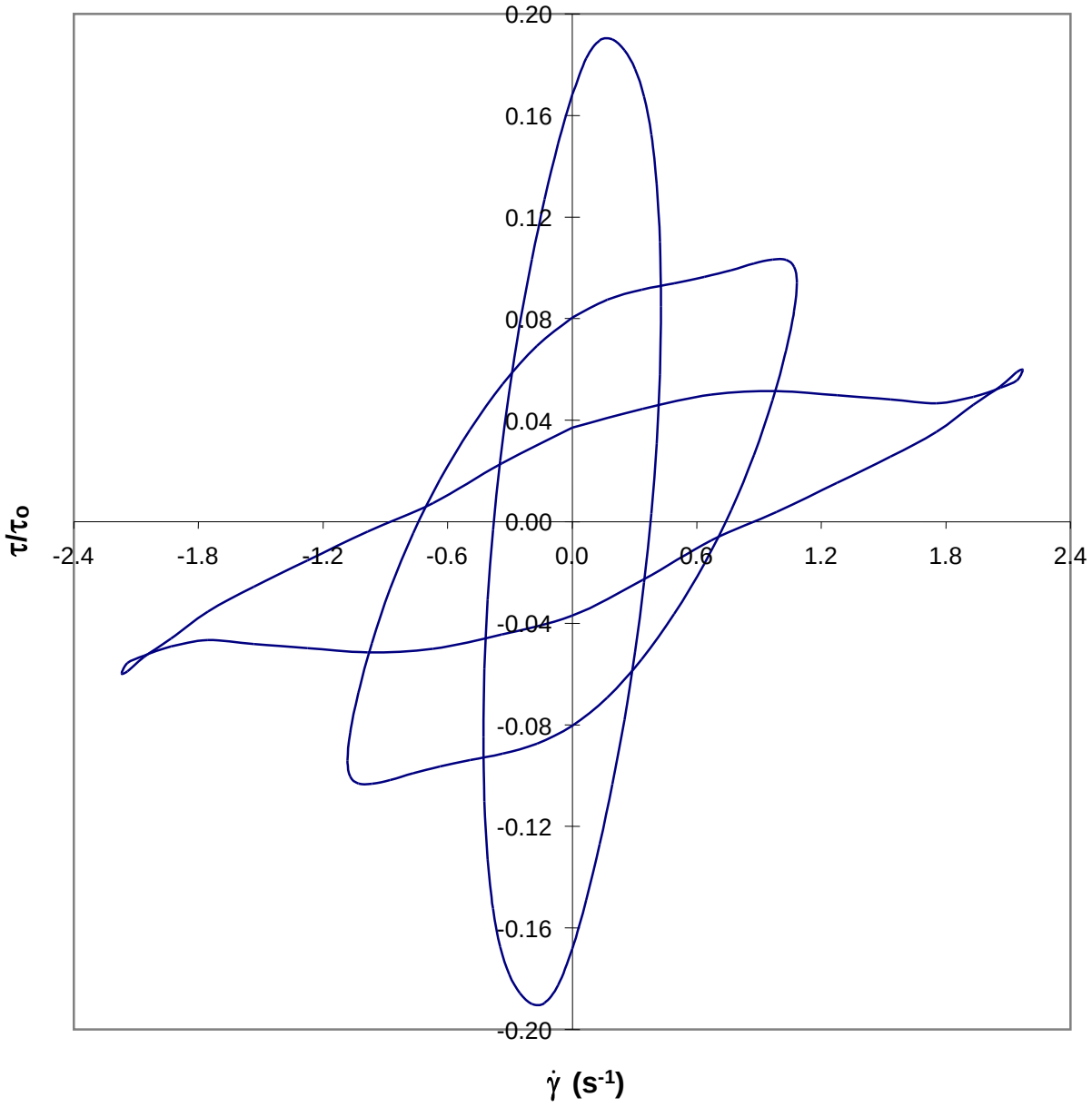

Figure 109 Departures from linearity for fat-free process mozzarella at 30°C with f_o = 0.25 Hz. Shear stress has been normalized with Lodge's rubberlike liquid theory. Strain amplitudes are 0.3, 0.8, and 1.4. Process mozzarella is highly nonlinear.

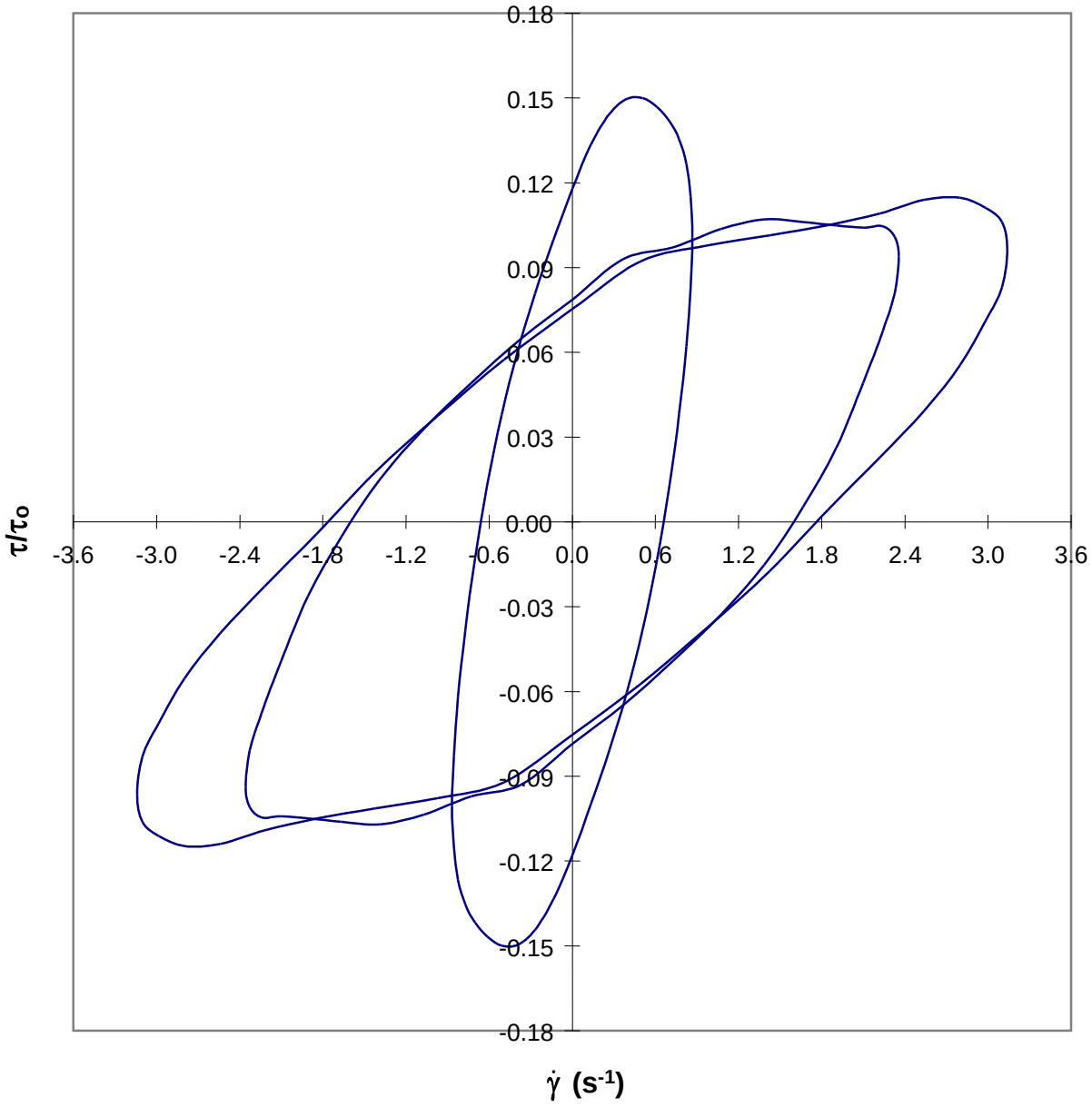

Figure 110 Departures from linearity for fat-free process mozzarella at 35°C with f_o = 0.25 Hz. Shear stress has been normalized with Lodge's rubberlike liquid theory. Strain amplitudes are 0.55, 1.4, and 2. Process mozzarella is highly nonlinear.

Appendix A Proximeter Setup and Transducer Calibration

The Interlaken procedures for proximeter setup and transducer calibration follow:

Proximeter Setup

1. Thread lock nut and proximeter housing onto proximeter.
2. Adjust the position of the proximeter protrusion in the housing to about 4 mm.
3. Tighten the lock nut against the proximeter housing.
4. With the amplifier off, insert the proximeter assembly into the transducer body until the proximeter tip contacts the target. Back the proximeter assembly away from the target approximately 0.5 mm. Tighten the clamp bolts on top of the housing to secure the proximeter assembly. The clamp bolts should be greased with a high temperature anti-seize compound.
5. Turn on amplifier and set the gain and offset to midrange.
6. Loosen clamp bolts and carefully move the proximeter toward the target until the amplifier display reads zero. Avoid touching the target with the proximeter.
7. Tighten the clamp bolts.

SST Calibration

1. Hang dead pan through the calibration port (see Fig. 11).
2. With no mass on the dead pan, turn the offset knob on the Capacitec amplifier until it reads 0.00 V and then tare (zero) the stress channel.

3. Place 1000 g on the dead pan. Record the current gain setting (from knob) and record the displayed stress value from the computer screen. Then calculate the desired gain as follows:

$$G_d = G_c \frac{\sigma_d}{\sigma_c} \tag{4. 2}$$

where G_d is the desired gain, G_c is the current gain, σ_d is the desired stress and σ_c is the current stress.

4. Remove mass from the dead pan and set the gain value on the screen to the desired value. Then adjust the offset until the display reads 0.00 V and tare the stress channel.
5. Verify the calibration by adding 1000 g mass to the dead pan again, and reading the displayed stress value.
6. Repeat steps 3 – 5 until the process converges.
7. Repeat with appropriate masses for other ranges.

Appendix B Calibration Constant Measurement

The McGill method for measuring the calibration constant follows:

1. Calibrate the SST using the method recommended by Interlaken (Appendix A) with a calibration constant of 130.2 kPa/kg.
2. Remove the transducer from the fixed plate and secure it with a clamp so that it remains horizontal.
3. Measure the circular active face diameter (Fig. 11) and calculate its surface area.
4. Hang a known mass directly on the active face. Knowing the area and the load, calculate the shear stress for this load (see below).
5. Check whether the stress readout on the computer matches the stress calculated in Step 4. If not, calculate the new calibration constant as follows:

$$C_n = C_i \frac{\sigma_{cal}}{\sigma_r} \tag{4. 3}$$

where C_n is the new calibration constant, C_i is the ideal calibration constant, σ_{cal} is the calculated stress, and σ_r is the readout stress.

Sample Calculation

To measure the calibration constant, two parameters must be known. First, the diameter of the SST active face (Fig. 11) must be measured to calculate its surface area. This is usually done with a digital micrometer for accuracy. Second, the applied load on the active face must be known in Newtons. Ideally, the calibration constant is the ratio of the force at

the active face to its surface area. Following is a sample calculation performed by Lan (1997) showing calculation of the SST calibration constant using the McGill method.

Diameter of active face, $D = 0.3855$ (in) $= 0.0097917$ (m)

Area of active face, $A = \frac{\pi D^2}{4} = 7.53019 \times 10^{-5}$ (m^2)

Mass used, $M = X$ (kg)

Force, $F = Mg = 9.81X$ (N)

Shear stress at active face, $\tau = \frac{F}{A} = \frac{9.81X}{7.53019 \times 10^{-5}} = 130.105X$ (kPa)

Therefore, for $X = 1$ (kg), calculated shear stress $\tau = 130.105$ (kPa)

Computer stress readout $= 11.20$ (kPa)

Original calibration constant $= 130.20$ (kPa/kg)

Therefore, new calibration constant $C_n = 130.20\left(\frac{130.105}{11.20}\right)$

$$\boxed{C_n = 150 \text{ (kPa/kg)}}$$

Appendix C Spectral Analysis Program

This FORTRAN program computes the material properties $\tau_m(f_o,\gamma_o)$ and $\delta_m(f_o,\gamma_o)$ from the stress and strain signals (time series) of a LAOS experiment, and plots the results as stress *versus* strain and stress *versus* shear rate loops. It also displays the amplitude spectrum showing the different harmonics, and sends all the loop and amplitude data to a file.

```
************************************************************************
*                                                                      *
*     SPECTRAL ANALYSIS OF LAOS DATA                                   *
*     USING DISCRETE FOURIER TRANSFORM (DFT)                           *
*                                                                      *
*     SALMAN TARIQ                                                     *
*     MAY 15TH, 1997                                                   *
*                                                                      *
************************************************************************
*                                                                      *
*    1)AN EVEN NUMBER OF CYCLES MUST BE SELECTED FOR ANALYSIS,         *
*      WITH EACH STRAIN CYCLE BEING COSINUSOIDAL                       *
*    2)THE INPUT FILES MUST BE NAMED 'strain.dat' AND 'stress.dat',    *
*      AND THE DATA MUST BE FORMATTED CORRECTLY (XX.XXXXXEXXX)         *
*    3)THE DFT RESULTS ARE GIVEN IN 'strain.out' AND 'stress.out'      *
*    4)THE STRESS VS SHEAR RATE DATA IS IN FILE 'loop1.out'            *
*    5)THE STRESS VS STRAIN DATA IS IN FILE 'loop2.out'                *
*    6)THE AMPLITUDE SPECTRUM IS IN FILE 'ampl.out'                    *
*                                                                      *
************************************************************************

      PROGRAM DFT

      INTEGER DATAPTS,DATAPTSMAX,NUMCYC,MMAX,MREQ,DATCYC

      REAL PI,F,DELT,DELF,OMEGA,AG,GAMMA(0:50000),GAMMAO,DELGAMMA,
     +SIGMA(0:50000),SIGMAD(0:50000),DELSIGMAD(0:50000),SIGMAM(99),
     +DELSIGMAM(99),GAMMADOT(0:50000),KDELF(0:50000),NYQUIST
      REAL XS(0:99999),XSR(0:99999),XSI(0:99999)
      REAL XSS(0:99999),XSSR(0:99999),XSSI(0:99999)

      OPEN(10,FILE='strain.dat',STATUS ='UNKNOWN')
      OPEN(11,FILE='stress.dat',STATUS ='UNKNOWN')
      OPEN(12,FILE='strain.out',STATUS='UNKNOWN')
      OPEN(13,FILE='stress.out',STATUS='UNKNOWN')
      OPEN(14,FILE='ampl.out',STATUS='UNKNOWN')
      OPEN(15,FILE='loop1.out',STATUS='UNKNOWN')
      OPEN(16,FILE='loop2.out',STATUS='UNKNOWN')
      OPEN(17,FILE='loop3.out',STATUS='UNKNOWN')

      PI=3.141593
```

```
      PRINT*
      PRINT*,'PLEASE ENTER NUMBER OF CYCLES FOR ANALYSIS (MUST BE AN
     +INTEGER):'
        READ*, NUMCYC
        PRINT*,'PLEASE ENTER TOTAL NUMBER OF DATA POINTS FOR ANALYSIS:'
      READ*, DATAPTS
      PRINT*,'PLEASE ENTER TEST FREQUENCY IN Hz:'
      READ*, F

*     CALCULATE TIME INTERVAL BETWEEN POINTS AND FREQUENCY RESOLUTION
      DELT=NUMCYC/(F*DATAPTS)
      DELF=F/NUMCYC

*     CALCULATE DATA POINTS PER CYCLE
      DATCYC=DATAPTS/NUMCYC

*     CALCULATE ANGULAR FREQUENCY
      OMEGA=2.*PI*F

*     CALCULATE NYQUIST FREQUENCY
      NYQUIST=1/(2.*DELT)

*-----------------------------------------------------------------------
*     DFT ON STRAIN DATA TO COMPUTE AMPLITUDE AND PHASE CONTENT
*-----------------------------------------------------------------------

*     READ IN DATA FOR STRAIN
        DO 5 I=0,DATAPTS-1
         READ(10,10) XS(I)
5       CONTINUE

10      FORMAT(1E12.5)

*     COMPUTE DFT
        XSR=0
        XSI=0
        DO 30 K=0, DATAPTS-1
          DO 20 N=0, DATAPTS-1
           AG=2.*PI*K*N/DATAPTS
           XSR(K)=XSR(K)+XS(N)*COS(AG)/DATAPTS
           XSI(K)=XSI(K)-XS(N)*SIN(AG)/DATAPTS
20        CONTINUE
30      CONTINUE

*     WRITE RESULTS TO FILE
        DO 40 I=0,DATAPTS-1
          WRITE(12,50) XSR(I), XSI(I)
40    CONTINUE

50      FORMAT(1X,1E14.5,2X,1E14.5)

*     CALCULATE STRAIN AMPLITUDE AND PHASE ANGLE FOR 1ST HARMONIC
      GAMMAO=2.*ABS(SQRT((XSR(NUMCYC))**2+(XSI(NUMCYC))**2))
      DELGAMMA=ATAN(XSI(NUMCYC)/XSR(NUMCYC))

*     PRINT RESULTS ON SCREEN
      PRINT*
      PRINT*, '-------------------------------------------------'
```

```
      PRINT*, 'STRAIN DATA RESULTS'
      PRINT*, '-------------------------------------------------'
      PRINT*
      PRINT*, 'THE STRAIN AMPLITUDE AND PHASE ANGLE ARE:'
      PRINT*, 'STRAIN AMPLITUDE:', GAMMAO
      PRINT*, 'PHASE ANGLE (RADIANS):', DELGAMMA
      PRINT*
      PRINT*

*-----------------------------------------------------------------------
*     DFT ON STRESS DATA TO COMPUTE FREQUENCY SPECTRA
*       AND STRESS RESPONSE
*-----------------------------------------------------------------------

*     READ IN DATA FOR STRESS
      DO 55 I=0,DATAPTS-1
        READ(11,60) XSS(I)
55      CONTINUE

60    FORMAT(1E12.5)

*     COMPUTE DFT
      XSSR=0
      XSSI=0
      DO 80 K=0, DATAPTS-1
        DO 70 N=0, DATAPTS-1
         AG=2.*PI*K*N/DATAPTS
         XSSR(K)=XSSR(K)+XSS(N)*COS(AG)/DATAPTS
         XSSI(K)=XSSI(K)-XSS(N)*SIN(AG)/DATAPTS
70      CONTINUE
80    CONTINUE

*     WRITE RESULTS TO FILE
        DO 85 I=0,DATAPTS-1
          WRITE(13,50) XSR(I), XSI(I)
85      CONTINUE

*     COMPUTE AMPLITUDE SPECTRA
      DATAPTSMAX=DATAPTS/2
      DO 90 K=0,DATAPTSMAX
        KDELF(K)=K*DELF
        SIGMAD(K)=ABS(SQRT((XSSR(K))**2+(XSSI(K))**2))
90    CONTINUE

*     WRITE SPECTRA TO FILE
      DO 100 K=0,DATAPTSMAX
        WRITE(14,110) KDELF(K), SIGMAD(K)
100   CONTINUE

110   FORMAT(1X,F6.3,2X,1E14.5)

*     COMPUTE AMPLITUDES AND PHASE ANGLES
      MMAX=0
      DO 115 M=1,99,2
        SIGMAM(M)=2.*ABS(SQRT((XSSR(M*NUMCYC))**2+(XSSI(M*NUMCYC))**2))
        DELSIGMAD(M)=ATAN(XSSI(M*NUMCYC)/XSSR(M*NUMCYC))
        DELSIGMAM(M)=DELSIGMAD(M)-M*DELGAMMA
          IF (M*NUMCYC.GT.DATAPTSMAX) THEN
            MMAX=M-2
```

```
            GO TO 116
          ENDIF
115   CONTINUE

*     PRINT RESULTS ON SCREEN
116   PRINT*, '-------------------------------------------------'
      PRINT*, 'STRESS DATA RESULTS'
      PRINT*, '-------------------------------------------------'
      PRINT*
      PRINT*, ' M       SIGMA(M)       DELSIGMA(M)'

      DO 120 M=1,MMAX,2
      PRINT 125, M, SIGMAM(M), DELSIGMAM(M)
120   CONTINUE

125   FORMAT(I3,4X,1F11.6,7X,1F11.6)

      PRINT*
130   PRINT*, 'THE NYQUIST FREQUENCY IS:', NYQUIST, 'Hz'
      PRINT*
      PRINT*, 'THE MAXIMUM HARMONIC IS:', MMAX
      PRINT*
      PRINT*, 'WHAT IS THE HIGHEST HARMONIC YOU WANT INCLUDED IN THE
     +STRESS'
      PRINT*, 'RESPONSE (MUST BE BELOW MAXIMUM HARMONIC)?'
      READ*, MREQ
      PRINT*

*     COMPUTE STRESS, STRAIN, AND SHEAR RATE
      SIGMA=0
      DO 150 NT=0, DATCYC+1
        DO 140 M=1, MREQ, 2
         SIGMA(NT)=SIGMA(NT)+SIGMAM(M)*COS(M*OMEGA*(NT*DELT)+
     +DELSIGMAM(M))
         GAMMA(NT)=GAMMAO*COS(OMEGA*(NT*DELT))
         GAMMADOT(NT)=-GAMMAO*OMEGA*SIN(OMEGA*(NT*DELT))
140     CONTINUE
150   CONTINUE

*     WRITE RESULTS TO FILE
      DO 160 NT=0, DATCYC+1
        TIME=NT*DELT
        WRITE(15,170) GAMMADOT(NT), SIGMA(NT)
        WRITE(16,170) GAMMA(NT), SIGMA(NT)
160   CONTINUE

*     WRITE EXPERIMENTAL STRESS-STRAIN DATA TO FILE
      DO 165 NT=1, DATAPTS
        WRITE(17,170) XS(NT), XSS(NT)
165   CONTINUE

170   FORMAT(1X,1E14.5,2X,1E14.5)

*-----------------------------------------------------------------------
*     PLOT RESULTS  (IF ON AN HP-UNIX MACHINE)
*-----------------------------------------------------------------------

*     1)STRESS VS SHEAR RATE PLOT
      REWIND(15)
```

```
      READ(15,170) (GAMMADOT(NT), SIGMA(NT), NT=1, DATCYC+2)
      CALL EZCURV(GAMMADOT,SIGMA,DATCYC+2,' ',' ')
      CALL EZSPLOT('plot1.ps','STRESS VS STRAIN RATE',
     +'STRAIN RATE  /sec', 'STRESS  kPa',.TRUE.,.TRUE.)

*     2)AMPLITUDE SPECTRUM
      REWIND(14)
      READ(14,110) (KDELF(K), SIGMAD(K), K=1, DATAPTSMAX+1)
      CALL EZCURV(KDELF,SIGMAD,DATAPTSMAX+1,' ',' ')
      CALL EZSPLOT('plot3.ps','AMPLITUDE SPECTRUM',
     +'FREQUENCY  Hz','STRESS AMPLITUDE   kPa',.TRUE.,.FALSE.)

*     3)STRESS VS STRAIN PLOT
      REWIND(16)
      REWIND(17)
      READ(16,170) (GAMMA(NT), SIGMA(NT), NT=1, DATCYC+2)
      READ(17,170) (XS(NT), XSS(NT), NT=1, DATAPTS)
      CALL EZCURV(GAMMA,SIGMA,DATCYC+2,'DFT','x')
      CALL EZCURV(XS,XSS,DATAPTS,'RAW',' ')
      CALL EZSPLOT('plot2.ps','STRESS VS STRAIN','STRAIN',
     +'STRESS  kPa',.TRUE.,.TRUE.)

      STOP

      END

*-------------------------------------------------------------------------
*-------------------------------------------------------------------------
```

Appendix D Numerical Differentiation Program

This FORTRAN program computes the numerical derivative of a time series using the parabolic least squares method and sends the data to a file.

```
************************************************************************
*                                                                      *
*     NUMERICAL DERIVATIVE OF A TIME SERIES                            *
*     USING THE PARABOLIC LEAST SQUARES METHOD                         *
*                                                                      *
*     SALMAN TARIQ                                                     *
*     JANUARY 15TH, 1997                                               *
*                                                                      *
************************************************************************

      PROGRAM DIFF

      REAL Y(40), YP(40)

      OPEN(10,FILE='DATA',STATUS ='UNKNOWN')
      OPEN(11,FILE='DATA1',STATUS ='UNKNOWN')

      N=40

      TIME=4.D0

      DT=TIME/N

*     READ IN TIME SERIES
      DO I=1,N
      READ(10,100) Y(I)
      ENDDO

100   FORMAT(1E12.5)

*     COMPUTE NUMERICAL DERIVATIVE
      YP(1)=(1-21*Y(1)+13*Y(2)+17*Y(3)-9*Y(4))/(20*DT)
      YP(2)=(-11*Y(1)+3*Y(2)+7*Y(3)+Y(4))/(20*DT)

      DO I=3, N-2
      YP(I)=(-2*Y(I-2)-Y(I-1)+Y(I+1)+2*Y(I+2))/(10*DT)
      ENDDO

      YP(N-1)=(11*Y(N)-3*Y(N-1)-7*Y(N-2)-Y(N-3))/(20*DT)

      YP(N)=(21*Y(N)-13*Y(N-1)-17*Y(N-2)+9*Y(N-3))/(20*DT)

*     WRITE RESULTS TO FILE
      DO I=1, N
      WRITE(*,110) YP(I)
      ENDDO
```

```
110   FORMAT(1E12.5)
      STOP
      END
*-------------------------------------------------------------------------
*-------------------------------------------------------------------------
```

References

Ak, M.M., "Rheological Measurements on Mozzarella Cheese," Ph.D. Thesis, University of Wisconsin-Madison (1993)

Astarita, G. and R.J.J. Jongschaap, *J. of Non-Newtonian Fluid Mech.*, **3**:281 (1977-78)

Bagley, E.B. and D.D. Christianson, *Food Technol.*, **41**(3):96 (1987)

Baird, D.G. and D.I. Collias, Polymer Processing: Principles and Design, Butterworth-Heinemann, Newton, MA, 1995

Baumgaertel, M. and H.H. Winter, *Rheol. Acta*, **28**:511 (1989)

Baumgaertel, M., P.R. Soskey, M. Mours, and H.H. Winter, "Innovative Rheological Interface Software," Version 5.1, IRIS Development, Amherst, MA (1987-97)

Bourne, M.C., *J. Food Sci.*, **33**:223 (1968)

Bourne, M.C., *Food Technol.*, **32**:62 (1978)

Bird, R.B., O. Hassager, R.C. Armstrong, and C.F. Curtis, Dynamics of Polymeric Liquids, Volume 2: Kinetic Theory, 2nd Ed., John Wiley & Sons, New York, 1987

Bland, D.R., The Theory of Linear Viscoelasticity, Pergamon Press, London, 1960

Caric, M. and M. Kalab, "Processed Cheese Products," in: Ch.15, Cheese: Chemistry, Physics and Microbiology, Vol. 2, ed. P.F. Fox, Chapman & Hall, London, p. 467 (1993)

Casiraghi, E.M., E.B. Bagley, and D.D. Christianson, *J. Texture Studies*, **16**:281 (1985)

Chang, Y.S., J.S. Guo, Y.P. Lee, and L.H. Sperling, *J. Chem. Educ.*, **63**:1077 (1986)

Cheese Links, "The Basics of Making Cheese," http://www.wgx.com/cheesenet/links/right.html

Chen, A.H., J.W. Larkin, C.J. Clark, and W.E. Irwin, *J. Dairy Sci.*, **62**(6):901 (1979)

Darby, R., Viscoelastic Fluids- An Introduction to Their Properties and Behavior, Marcel Dekker, Inc., New York, 1976

Davis, J.G., *J. Dairy Res.*, **8**:245 (1937)

Dealy, J.M., J.F. Petersen, and T.-T. Tee, *Rheol. Acta*, **12**:550 (1973)

Dealy, J.M., US Patent No. 4 464 928, August 14, 1984

Dealy, J.M. and K.F. Wissbrun, Melt Rheology and Its Role in Plastics Processing, Van Nostrand Reinhold, New York, 1990

Farkye, N.Y. and P.F. Fox, *Trends in Food Sci. Technol.*, **1**:37 (1990)

Ferry, J.D., Viscoelastic Properties of Polymers, John Wiley, New York, 1980

Fox, P.F., "Cheese: An Overview," in: Ch.1, Cheese: Chemistry, Physics and Microbiology, Vol. 1, ed. P.F. Fox, Chapman & Hall, London, pp. 1 (1993)

Friedrich, G. and B. Hoffmann, *Rheol. Acta*, **22**:425 (1983)

Giacomin, A.J., "A Sliding Plate Melt Rheometer Incorporating a Shear Stress Transducer," Ph.D. Thesis, McGill University (1987)

Giacomin, A.J. and J.M. Dealy, "Large–Amplitude Oscillatory Shear," in: Ch.4, Techniques in Rheological Measurement, ed. A.A. Collyer, Chapman and Hall, London & New York, pp. 99-121 (1993)

Giacomin, A.J. and J.M. Dealy, Paper G3, 58th Annual Meeting Soc. Rheol., Tulsa, OK, USA, October, 1986

Giacomin, A.J., T. Samurkas, and J.M. Dealy, *Pol. Eng. Sci.*, **29**:499 (1989)

Graham, M. D., *J. Rheol.* **39**(4):697 (1995)

Hatzikiriakos, S.G. and J.M. Dealy, *J. Rheol.*, **35**:497 (1991)

Hibberd, G.E., W.J. Wallace, and K.A. Wyatt, *J. Sci. Instrum.*, **43**:84 (February 1966)

Holsinger, V.H., P.W. Smith, and M.H. Tunick, "Overview: Cheese Chemistry and Rheology," in: Chemistry of Structure-Function Relationships in Cheese, ed. E.L. Malin and M.H. Tunick, Plenum Press, New York, p. 1 (1995)

Kindstedt, P.S., *Cult. Dairy Prod. J.*, **26**(3):27 (1991)

Kindstedt, P.S., "Mozzarella and Pizza Cheese," in: Ch.12, Cheese: Chemistry, Physics and Microbiology, Vol. 2, ed. P.F. Fox, Chapman & Hall, London, p. 337 (1993)

Lan, S.K., "The Role of Dynamic Slip in Extrusion Melt Fracture," M.S. Thesis, University of Wisconsin-Madison (1997)

Larson, R., Constitutive Equations for Polymer Melts and Solutions, Buttersworths, Boston, MA, 1988

Lawrence, R.C., J. Gilles, and L.K. Creamer, "Cheddar Cheese and Related Dry-Salted Cheese Varieties," in: Ch.1, Cheese: Chemistry, Physics and Microbiology, Vol. 2, ed. P.F. Fox, Chapman & Hall, London, p. 1 (1993)

Lee, C.H, E.M. Imoto, and C. Rha, J. Food Sci., **43**(5):1600 (1978)

Liu, T.Y., D.S. Soong, and M.C. Williams, *J. Polym. Sci.: Pol. Phys. Ed.*, **2**:1561 (1984)

Liu, T.Y., D.W. Mead, D.S. Soong, and M.C. Williams, *Rheol. Acta*, **22**:81 (1983)

Lodge, A.S., Elastic Liquids, Academic Press, New York, 1964

Lathi, B.P., Linear Systems and Signals, Berkeley-Cambridge Press, Carmichael, 1992

Ma, L., M.A. Drake, G.V. Barbosa-Canovas, and B.G. Swanson, *J. Food Sc.*, **61**(4):821 (1996)

MacSporran, W.C. and R.P. Spiers, *Rheol. Acta*, **23**:90 (1984)

Matsumoto, T., Y. Segawa, Y. Warashina, and S. Onogi, *Trans. Soc. Rheol.*, **17**:47 (1973)

McCarthy, R.V., *J. Rheol.*, **22**:623 (1978)

Nelson, D.L., N.F. Olson, and A.S. Lodge, "Application of the Weissenberg Effect in Predicting Physical Characteristics of Mozzarella Cheese on Pizza," Internal Report: Department of Food Science & Rheology Research Center, University of Wisconsin-Madison (1983)

Olson, N.F., "Cheese," in: Biotechnology, 2nd Ed., Vol. 9: Enzymes, Biomass, Food and Feed, ed. H.-J. Rehm and G. Reed, VCH, Weinheim, p. 353 (1995)

Olson, N.F., meeting at Department of Food Science, University of Wisconsin-Madison, June, 1997

Olson, N.F., S. Gunasekaran, and D.D. Bogenrief, *Neth. Milk Dairy J.*, **50**:279 (1996)

Onogi, S., T. Masuda, and T. Matsumoto, *Trans. Soc. Rheol.*, **14**:275 (1970)

Onogi, S. and T. Matsumoto, *Polym. Eng. Revs*, **1**:45 (1981)

Pearson, D.S. and W.E. Rochefort, *J. Polym. Sci.: Pol. Phys. Ed.*, **20**:83 (1982)

Perry, R.H, D.W. Green, and J.O. Maloney, Perry's Chemical Engineers Handbook, McGraw Hill, New York, 1997

Pipkin, A.C., Lectures in Viscoelastic Theory, Springer-Verlag, New York, 1972

Powell, R.L. and Schwarz, *J. Polym. Sci.: Pol. Phys. Ed.*, **17**:969 (1979)

Powell, R.L. and Schwarz, *J. Rheol.*, **23**:323 (1979)

Ramirez, R.W., The FFT: Fundamentals and Concepts, Prentice-Hall, Inc., Englewoods Cliffs, NJ, 1985

Rao, M.A.,"Viscoelastic Properties of Cheeses," in Ch.6: Viscoelastic Properties of Foods, ed. M.A. Rao and J.F. Steffe, Elsevier Applied Science, London & New York, p. 173 (1992)

Ruegg, M., P. Eberhard, L.M. Popplewell, and M. Peleg, "Melting Properties of Cheese," Bull. 268, *Internat. Dairy Fed.*, Brussels, Belgium, p. 36 (1991)

Schapery, R.A. and D.E. Cantey, AIAA J., **4**:255 (February 1966)

Scott Blair, G.W., *Adv. Foods Res.*, **8**:1 (1958)

Scott Blair, G.W. and M. Baron, *Proc. 12th Int. Dairy Congr.*, **2**:49 (1949)

Sivashinsky, N., A.T. Tsai, T.J. Moon, and D.S. Soong, *J. Rheol.*, **28**:287 (1984)

Spiers, R.P., PhD Thesis, University of Bradford (1977)

Steffe, J.F., Rheological Methods in Food Process Engineering, 2nd Ed., Freeman Press, East Lansing, MI, 1996

Szczesniak, A.S., "Physical Properties of Foods: What they are and their relation to other food properties," in: Physical Properties of Foods, ed. M. Peleg and E.B. Bagley, Avi Publishing Co., Inc., Westport, CT (1983)

Tanner, R.I., Engineering Rheology, Oxford University Press, Oxford, 1985

Tee, T.T. and J.M. Dealy, *Trans. Soc. Rheol.*, **19**:595 (1975)

Tsai, A.T. and D.S. Soong, *J. Rheol.*, **29**:1 (1985)

Tunick, M.H. and E.J. Nolan, "Rheology of Cheese," in: Physical Chemistry of Food Processes, Vol. I: Fundamental Aspects, ed. I.C. Baianu, Van Nostrand Reinhold Co., New York, p. 273 (1992)

Whitaker, S. and R.L. Pigford, *I&EC*, **52**(2):185 (February, 1960)

Volodkevich, N.N., *Food Res.*, **3**:221 (1938)

Weissenberg, K., *Nature*, **159**:310 (1947)

Winter, H.H., M. Baumgartel, and P.R. Soskey, "A Parsimonious Model for Viscoelastic Liquids and Solids," in: Ch.5, Techniques in Rheological Measurement, ed. A.A. Collyer, Chapman and Hall, London & New York, pp. 99-121 (1993)

Zehren, V.L. and D.D Nusbaum, Process Cheese, Cheese Reporter Publishing Company, Madison, WI, 1992